

VOLUME 10  
FEBRUARY 1911

# JOURNAL OF THE

*Engineering*

*Mechanics*

*Division*

PROCEEDINGS OF THE

AMERICAN SOCIETY

OF CIVIL ENGINEERS





---

Journal of the  
ENGINEERING MECHANICS DIVISION  
Proceedings of the American Society of Civil Engineers

---

ENGINEERING MECHANICS DIVISION  
EXECUTIVE COMMITTEE

Egor P. Popov, Chairman; Bruce G. Johnston, Vice-Chairman;  
John W. Clark; Merit P. White; Edward Wenk, Jr., Secretary  
Elmer K. Timby, Board Contact Member

COMMITTEE ON PUBLICATIONS

Bruce G. Johnston, Chairman; Hans H. Bleich; Jack E. Cermak;  
Donald L. Dean; John E. Goldberg; William J. Hall; John D. Haltiwanger;  
Herbert S. Suer; Joseph F. Throop

CONTENTS

February, 1961

Papers

	Page
Spherical Waves in a Plastic Locking Medium by Mario G. Salvadori, Richard Skalak, and Paul Weidlinger . . . . .	1
Vibration of Shear Buildings by Flexibility Method by Ming L. Pei . . . . .	13
Dynamic Elastic-Plastic Analysis of Structures by Melvin L. Baron, Hans H. Bleich, and Paul Weidlinger . . . . .	23
Viscoelastic Plate on a Viscoelastic Foundation by Karl S. Pister . . . . .	43
Moire Fringes as a Means of Analyzing Strains by C. A. Sciammerella and A. J. Durelli . . . . .	55
Minimum-Weight Design of Beams for Deflections by Ralph L. Barnett . . . . .	75
Stress Analysis of Translational Shells by Kristoffer Apeland . . . . .	111
Wind-Induced Vibrations in Antenna Members by William Weaver, Jr. . . . .	141
(over)	

Copyright 1961 by the American Society of Civil Engineers.

---

## DISCUSSION

---

	Page
The Neutral Axis in Plastic Bending of Beams, by Aris Phillips. (October, 1959. Prior discussion: April, 1960. Discussion closed.) by Aris Phillips (Closure) . . . . .	169
Experimental Studies of Beams on Elastic Foundations, by Robert L. Thoms. (June, 1960. Prior discussion: December, 1960. Discussion closed.) by M. T. Davisson . . . . .	171
Underground Structures Subject to Air Overpressure, by E. T. Selig, K. E. McKee, and E. Vey. (August, 1960. Prior discussion: None. Discussion closed.) by Paul I. Rongved . . . . .	173
by G. S. Kovacs and R. T. Frankian . . . . .	175
Arch Dam Analysis with an Electric Analog Computer, by Richard H. MacNeal. (August, 1960. Prior discussion: None. Discussion closed.) by Paul Baumann . . . . .	177
by Maurice L. Dickinson . . . . .	179
Restrained Columns, by Morris Ojalvo. (October, 1960. Prior discussion: None. Discussion closes: March 1, 1961.) by Donald S. Mansell . . . . .	181
Bearing Capacity of Floating Ice Sheets, by G. G. Meyerhof. (October, 1960. Prior discussion: None. Discussion closes: March 1, 1961.) by H. G. Hopkins . . . . .	185

---

Journal of the  
ENGINEERING MECHANICS DIVISION  
Proceedings of the American Society of Civil Engineers

---

SPHERICAL WAVES IN A PLASTIC LOCKING MEDIUM

By Mario G. Salvadori,<sup>1</sup> F. ASCE, Richard Skalak,<sup>2</sup> M. ASCE, and  
Paul Weidlinger,<sup>3</sup> F. ASCE

---

SYNOPSIS

Asymptotic short-time and long-time solutions are derived in closed form for the spherical wave propagation in an infinite, plastic locking medium due to various types of time-varying pressures applied to the surface of a spherical cavity. Among these are: (a) a constant pressure; (b) a center of dilatation; (c) an adiabatic gas expansion; and (d) an energy input due to an exploding point mass.

---

INTRODUCTION

The propagation of plane waves in various types of locking media has been considered by several authors.<sup>4,5,6</sup> Spherical waves in plastic locking media

---

Note.—Discussion open until July 1, 1961. To extend the closing date one month, a written request must be filed with the Executive Secretary, ASCE. This paper is part of the copyrighted Journal of the Engineering Mechanics Division, Proceedings of the American Society of Civil Engineers, Vol. 87, No. EM 1, February, 1961.

<sup>1</sup> Prof. of Civ. Engrg., Columbia Univ., New York, N. Y.

<sup>2</sup> Assoc. Prof. of Civ. Engrg., Columbia Univ., New York, N. Y.

<sup>3</sup> Cons. Engr., New York, N. Y.

<sup>4</sup> "Stress Waves in Dissipative Media," by M. G. Salvadori, R. Skalak, and P. Weidlinger, Transactions, New York Academy of Science, Ser. II, Vol. 21, No. 5, 1959, pp. 427-434.

<sup>5</sup> "Waves and Shocks in Locking and Dissipative Media," by M. G. Salvadori, R. Skalak, and P. Weidlinger, Journal Engrg. Mechanics Div., ASCE, Vol. 86, April, 1960.

<sup>6</sup> "On the Plane Motion of Sand," by A. I. Ishlinskii, Ukr. Math. Journal, Vol. 6, No. 4, 1954.

were investigated by A. S. Kompaneets<sup>7</sup> and more recently (1960) by N. V. Zvolinskii who derived the wave equations for an elasto-plastic medium of limited compressibility.<sup>8</sup>

Since, in general, closed-form solutions of this type of problem cannot be obtained, asymptotic closed-form solutions are given in this paper for an infinite ideal locking medium. An equation of motion is first derived for large strains and displacements when a variable pressure is applied to the surface of a spherical cavity. It is then shown that its early time asymptotic solution is the rigorous solution of the same problem when small strains and displacements are considered. The long time asymptotic solution of the same equation is then shown to be the rigorous solution for a point source pressure when large strains and displacements are again considered.

The behavior of a three-dimensional plastic locking medium with Coulomb friction under compressive stresses is characterized as follows:

1. At first the material of initial density  $\rho_0$  does not offer resistance to compression, but, once a critical value of the dilatation is reached, such that the density reaches the value  $\rho_1$  and a constant value of the dilatation

$$\xi = 1 - \rho_0/\rho_1 < 1 \dots\dots\dots (1)$$

is maintained from then on (Fig. 1).

2. During the subsequent motion with a constant density  $\rho_1$  the material satisfies the three-dimensional yield condition derivable from Coulomb's law of failure<sup>9</sup>

$$\sigma_r - \sigma_\theta = -c + \frac{1-k}{1+k} (\sigma_r + \sigma_\theta) \dots\dots\dots (2)$$

in which, due to symmetry, the radial and tangential stresses  $\sigma_r$ ,  $\sigma_\theta$  are principal stresses, the constant  $c$  is proportional to the cohesion, and  $k$  is a function of the coefficient of internal friction.

The previously described behavior is typical of certain cohesive granular soils under high compressive stresses. Since under such stresses the effect of cohesion becomes negligible as compared to that of friction, Eq. 2 becomes

$$\sigma_\theta = k \sigma_r \dots\dots\dots (3)$$

with

$$0 \leq k \leq 1$$

<sup>7</sup> "Shock Waves in Plastic Compacting Media," by A. S. Kompaneets, Proceedings, Academy of Science, USSR, Vol. 106, No. 1, 1956, pp. 49-52.

<sup>8</sup> "On the Emission of an Elastic Wave from a Spherical Explosion in the Ground," by N. V. Zvolinskii, P. M. M., Vol. 24, No. 1, 1960, pp. 126-133.

<sup>9</sup> "On Coulomb's Law of Failure in Soils," by R. T. Shield, Journal Mech. Physical Solids, 4(1955), May 1960, pp. 10-16.

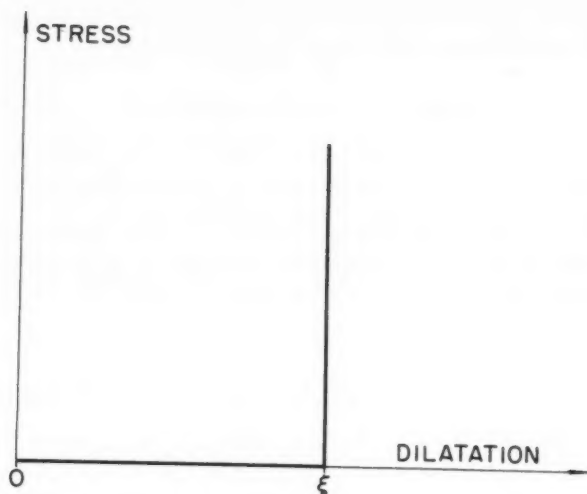


FIG. 1

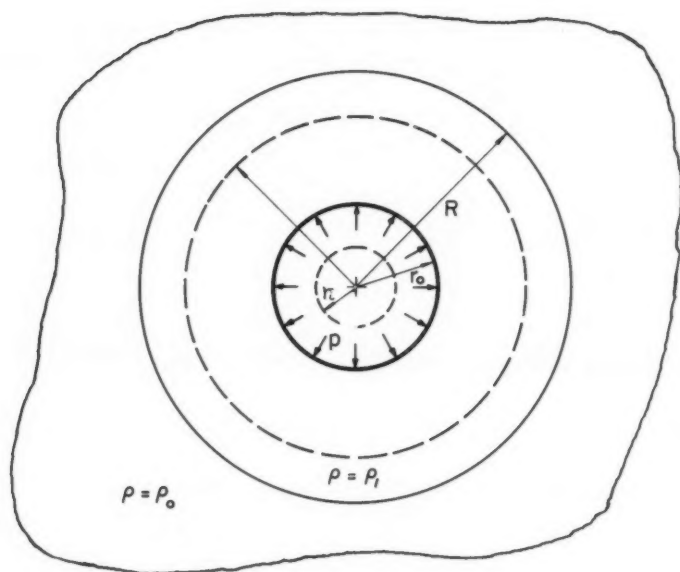


FIG. 2

*Notation.*—The letter symbols adopted for use in this paper are defined where they first appear, in the illustrations or in the text, and are arranged alphabetically, for convenience of reference, in the Appendix.

### SPHERICAL WAVE EQUATIONS

Consider a spherical cavity of initial radius  $r_i$  in an infinite ideal locking medium. From  $t = 0$  on, the cavity boundary is subjected to a uniform pressure of intensity  $p$ , which is a function of the expanding cavity radius  $r_0$ . Let  $r$  be the Lagrangian coordinate of a particle, and  $w$  its radial displacement at a time  $t$ , when the medium has been compacted to a density  $\rho_1$  up to a distance  $R$  from the cavity center, while beyond  $R$ , the medium is at rest with a density  $\rho_0$  (Fig. 2).

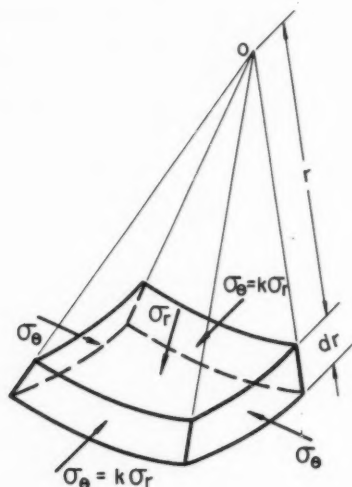


FIG. 3

Under these assumptions conservation of mass requires that

$$(r - w)^3 = \frac{1}{1 - \xi} r^3 - \frac{\xi}{1 - \xi} R^3 \dots \dots \dots (4)$$

and, in particular, that at the cavity boundary, in which  $r = r_i + w_0 = r_0$ ,

$$x \equiv \frac{R}{r_0} = \left[ \xi + (1 - \xi) \left( \frac{r_i}{R} \right)^3 \right]^{-1/3} \dots \dots \dots (5)$$

For  $\xi \ll 1$ , and at an early time when the change in the cavity radius is negligible, so that  $r_0 \approx r_i$ , the ratio  $x$  approaches the value

$$x_S = \frac{R}{r_i} \dots \dots \dots (6)$$

At late times when  $R$  is large enough for  $(1 - \xi)(r_i/R)^3$  to be much less than  $\xi$ , the ratio  $x$  approaches the constant value

$$x_L = \xi^{-1/3} \dots \dots \dots (7)$$

Denoting time derivatives by dots, the particle velocity at  $r$  ( $\dot{w} = \dot{r}$ ) becomes, by Eq. 4,

$$\dot{w} = \left(\frac{R}{r}\right)^2 \xi \dot{R} \dots \dots \dots (8)$$

and at the wave front ( $r = R$ )

$$\dot{w} \Big|_{r=R} = \xi \dot{R} \dots \dots \dots (9)$$

The particle acceleration, by Eq. 8, becomes

$$\ddot{w} = \xi (R^2 \ddot{R} + 2 R \dot{R}^2) r^{-2} - 2 \xi^2 R^4 \dot{R}^2 r^{-5} \dots \dots (10)$$

The equation of motion for an elementary volume of soil in spherical coordinates (Fig. 3) is given by

$$\frac{\partial \sigma_r}{\partial r} + \frac{2(1-k)}{r} \sigma_r = -\rho_1 \ddot{w} \dots \dots \dots (11)$$

in which  $w$  is defined by Eq. 10, and its particular solution satisfying the boundary condition;

$$\sigma_r \Big|_{r=r_0} = p(r_0) \dots \dots \dots (12)$$

is, for  $k \neq 1/2$ ,

$$\begin{aligned} \sigma_r = p(r_0) \left(\frac{r}{r_0}\right)^{-2+2k} &+ \frac{\rho_1 \xi}{(1-2k)r_0} (R^2 \ddot{R} + 2 R \dot{R}^2) \left[ \left(\frac{r}{r_0}\right)^{-2+2k} \right. \\ &\left. - \left(\frac{r}{r_0}\right)^{-1} \right] + \frac{\rho_1 \xi^2}{(1+k)r_0^4} R^4 \dot{R}^2 \left[ \left(\frac{r}{r_0}\right)^{-2+2k} - \left(\frac{r}{r_0}\right)^{-4} \right] \dots \dots \dots (13a) \end{aligned}$$

and, for  $k = 1/2$ ,

$$\begin{aligned} \sigma_r = p(r_0) \left(\frac{r}{r_0}\right)^{-1} &- \frac{\rho_1 \xi}{r_0} (R^2 \ddot{R} + 2 R \dot{R}^2) \left(\frac{r}{r_0}\right)^{-1} \ln \left(\frac{r}{r_0}\right) \\ &+ \frac{2}{3} \frac{\rho_1 \xi^2}{r_0^4} R^4 \dot{R}^2 \left[ \left(\frac{r}{r_0}\right)^{-1} - \left(\frac{r}{r_0}\right)^{-4} \right] \quad (k = 1/2) \dots \dots (13b) \end{aligned}$$



Conservation of momentum across the wave front ( $r = R$ ) requires, by Eq. 9, that

$$\sigma_r \Big|_{r=R} = \rho_1 \xi (1 - \xi) \dot{R}^2 \dots\dots\dots (14)$$

Setting this value of  $\sigma_r$  in Eqs. 13a, and 13b, and making use of Eq. 5, the equation governing the motion of the wave front becomes

$$\alpha R \frac{d\dot{R}^2}{dR} + \beta \dot{R}^2 = \frac{2p}{\rho_1 \xi (1 - \xi)} \dots\dots\dots (15)$$

in which the variable coefficients  $\alpha$  and  $\beta$  are given for  $k \neq 1/2$  by

$$\left. \begin{aligned} \alpha &= \frac{1}{(2k-1)(1-\xi)} (x - x^{2-2k}) \\ \beta &= 2 \left[ x^{2-2k} + \frac{2}{(2k-1)(1-\xi)} (x - x^{2-2k}) \right. \\ &\quad \left. - \frac{\xi}{(1+k)(1-\xi)} (x^4 - x^{2-2k}) \right] \end{aligned} \right\} (k \neq 1/2) \dots (16a)$$

and for  $k = 1/2$  by

$$\alpha = \frac{1}{1-\xi} x \ln x$$

(k = 1/2) ... (16b)

and

$$\beta = 2 \left[ x + \frac{2}{1-\xi} x \ln x - \frac{2}{3} \frac{\xi}{1-\xi} (x^4 - x) \right]$$

*Short Time Asymptotic Solution (Finite cavity, small strain, small displacement solution).*—Substituting  $x = x_s$  from Eq. 6 into Eq. 16a and b, one obtains the differential equation valid for small displacements. A further simplification is obtained by considering the strains to be small, that is, neglecting terms in  $\xi^2$  and, hence, the third term at the right hand member of  $\beta$  in Eqs. 16a or 16b. Since Eq. 6 is valid when the expansion of the cavity is negligible, and the pressure  $p$  is considered a function of the cavity radius  $r_0$ , the pressure is to be assumed constant

$$p(r_0) = p_0 \dots\dots\dots (17a)$$

For an explosion<sup>10</sup> of yield  $W$  and gas constant  $\gamma$

$$p_0 = (\gamma - 1) \frac{W}{4/3 \pi r_i^3} \dots\dots\dots (17b)$$

The solution of Eq. 15 in terms of the non-dimensional wave front radius;

$$x_s = \frac{R}{r_i} \dots\dots\dots (6)$$

<sup>10</sup> "A Method of Concealing Underground Nuclear Explosions," by A. L. Latter, R. E. LeLevier, E. A. Martinelli, and W. G. McMillan, R-348, The RAND Corp., March 30, 1959.

thus becomes

$$\dot{x}_s^2 = \frac{2(2k-1)p_0}{\rho_1 \xi r_1^2} \frac{1}{x_s^4 (1-x_s^{1-2k})^2} \left[ \frac{1}{3} (x_s^3 - 1) - \frac{1}{4-2k} (x_s^{4-2k} - 1) \right] \dots (18a)$$

The corresponding solution for  $k = 1/2$  is

$$x_s^2 = \frac{2}{9} \frac{p_0}{\rho_1 \xi r_1^2} \frac{1}{x_s^4 \ln^2 x_s} \left[ x_s^3 (3 \ln x_s - 1) + 1 \right] \dots (18b)$$

*Long Time Asymptotic Solution (Point Source, finite strain, large displacement solution).*—Assuming for  $x$  the value  $\xi^{-1/3}$  given by Eq. 7, the coefficients  $\alpha$  and  $\beta$  of Eq. 15 become constant, and depend on  $\xi$  and  $k$  only. This equation, rigorously valid for  $r_1 = 0$ , coincides with the equation derived by Kompaneets.<sup>7</sup>

The following particular solutions of this equation are of interest:

*Center of Dilatation.*—The magnitude  $P_0$  of the total force exerted on the cavity surface is constant in time so that, letting

$$P_0 = \lim_{r_1 \rightarrow 0} 4 \pi p(r_1) r_1^2 \dots (19)$$

the variable pressure  $p$ , by Eqs. 4 and 9, becomes

$$p(R) = \frac{P_0}{4 \pi \xi^{2/3}} R^{-2} \dots (20)$$

The corresponding solution of Eq. 15 is

$$\dot{R}^2 = \frac{P_0}{\rho_1 \xi} \frac{1}{2 \pi \xi^{2/3} (\beta - 2\alpha)(1-\xi)} R^{-2} \dots (21)$$

If at a time  $t = t_1$ , when  $R = R_1$ ,  $P_0$  becomes zero, the wave front propagates with a velocity

$$\dot{R}^2 = \frac{P_0}{\rho_1 \xi} \frac{R_1^2}{2 \pi \xi^{2/3} (\beta - 2\alpha)(1-\xi)} \left( \frac{R}{R_1} \right)^{-\beta/\alpha} (R \geq R_1) \dots (22)$$

Since  $\beta/\alpha > 2$  for all values of  $\xi$  and  $k$ ,  $\dot{R}^2$  approaches zero asymptotically and the wave front never stops. This result stems from the neglect of the cohesion  $c$  in Eq. 2: a finite value of  $c$  gives a finite time at which the motion stops.

*Expansion of An Ideal Gas.*—In the expansion of an ideal gas the pressure  $p$  follows the law

$$\lim_{r_1 \rightarrow 0} p(r_1) r_1^{3\gamma} = p(r_0) r_0^{3\gamma} = K \dots (23)$$

in which  $\gamma$  and  $K$  are constant characteristics of the gas and of the energy of the explosion.

The solution of Eq. 15 when the pressure  $p_{r_0}$  is defined by Eq. 23 and  $\beta/\alpha > 3\gamma$ , is

$$\dot{R}^2 = \frac{2K}{\rho_1 \xi} \frac{\xi^{-\gamma}}{(\beta - 3\alpha\gamma)(1-\xi)} R^{-3\gamma} \dots\dots\dots (24)$$

(For  $\beta/\alpha < 3\gamma$  there are no solutions of the point source equation.) In this case also, the introduction of a finite value for the cohesion introduces a finite stopping time, as shown by Kompaneets.<sup>7</sup>

**Exploding Point Mass.**—Consider a point mass  $M$  located in the medium at  $r = 0$ , which at  $t = 0$  explodes so that its particles acquire a radial velocity  $\dot{r}_0$ .

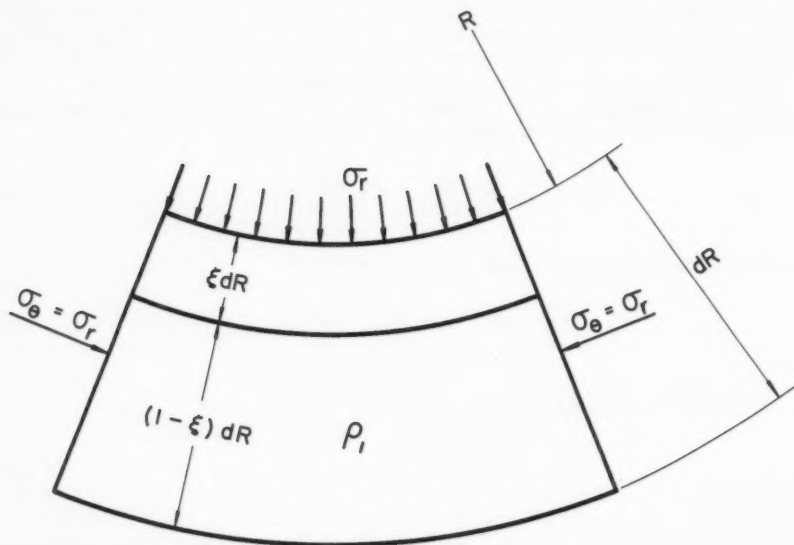


FIG. 4

Assuming that these particles remain on the boundary surface of an expanding spherical cavity of radius  $r_0$ , the total kinetic energy at a time  $t$  is

$$T = \frac{1}{2} \int_{r_0}^R 4 \pi \rho_1 r^2 \dot{r}^2 dr + \frac{1}{2} M \dot{r}_0^2 \dots\dots\dots (25)$$

and, by Eqs. 7, 8, and 25, the rate of increase of this energy is

$$\begin{aligned} \frac{dT}{dR} = & \left[ 4 \pi \rho_1 (\xi^{-1/3} - 1) R^3 + M \xi^{-4/3} \right] \xi^2 \dot{R} \frac{dR}{dR} \\ & + 6 \pi \rho_1 \xi^2 (\xi^{-1/3} - 1) R^2 \dot{R}^2 \dots\dots\dots (26) \end{aligned}$$

The rate of energy loss across the shock front is (Fig. 4)

$$\frac{dE}{dR} = - \frac{1}{2} \sigma_r \Big|_{r=R}^{\xi} \dots \dots \dots (27)$$

In the particular case of  $k = 1$  no other energy loss can occur within the medium so that

$$\frac{dT}{dR} + \frac{dE}{dR} = 0 \dots \dots \dots (28)$$

Hence, by Eqs. 26 and 27

$$\left( R^3 + r_m^3 \right) \frac{d\dot{R}}{dR} + 3 \mu R^2 \dot{R} = 0 \dots \dots \dots (29)$$

in which

$$r_m^3 = \frac{M}{4 \pi \rho_1 (\xi^{-1} - \xi^{-2/3}) \xi^2} \quad \mu = \frac{1}{2} + \frac{1 - \xi}{6(\xi^{-1/3} - 1)} \dots \dots \dots (30)$$

The solution of Eq. 29 with  $\dot{R}(0) = \dot{R}_0$ , and hence an energy input  $\frac{1}{2} M \dot{R}_0^2$ , is

$$\frac{\dot{R}}{\dot{R}_0} = \left[ 1 + \left( \frac{R}{r_m} \right)^3 \right]^{-\mu} \dots \dots \dots (31)$$

in which  $1/2 < \mu < 1$  for  $0 < \xi < 1$ .

*Intermediate Range Solutions.*—The variable coefficients  $\alpha$  and  $\beta$  of Eq. 15 approach their asymptotic values for  $R \rightarrow \infty$ , but become practically constant at finite values of  $R$  depending on  $k$  and  $\xi$ . For example, the behavior of  $\alpha$  and  $\beta$  versus  $x_s = R/r_i$  is given in Figs. 5(a) and 5(b) for  $k = 1, 1/2$ , and 0 when  $\xi = 0.1$ .

The solution of Eq. 15 in the intermediate range between the two asymptotic short-time and long-time solutions may be obtained by numerical means starting at the limit of the range of validity for either solution and integrating forward or backward, respectively.

The constant  $K$ , needed to continue the intermediate time solution for an explosion is obtained by Eq. 23. Table 1 shows the range of validity of the two asymptotic solutions.

TABLE 1

( $\xi = 0.1$ )

	Short Time								Long Time		
$\frac{R}{r_i}$	1.00	1.02	1.04	1.06	1.08	1.10	1.25	1.50	10	20	$\infty$
$x_s$	1.00	1.02	1.04	1.06	1.08	1.10	1.25	1.50	--	--	--
$x$	1.00	1.02	1.04	1.05	1.07	1.09	1.21	1.40	2.14	2.15	2.15
$x_L$	--	--	--	--	--	--	--	--	2.15	2.15	2.15

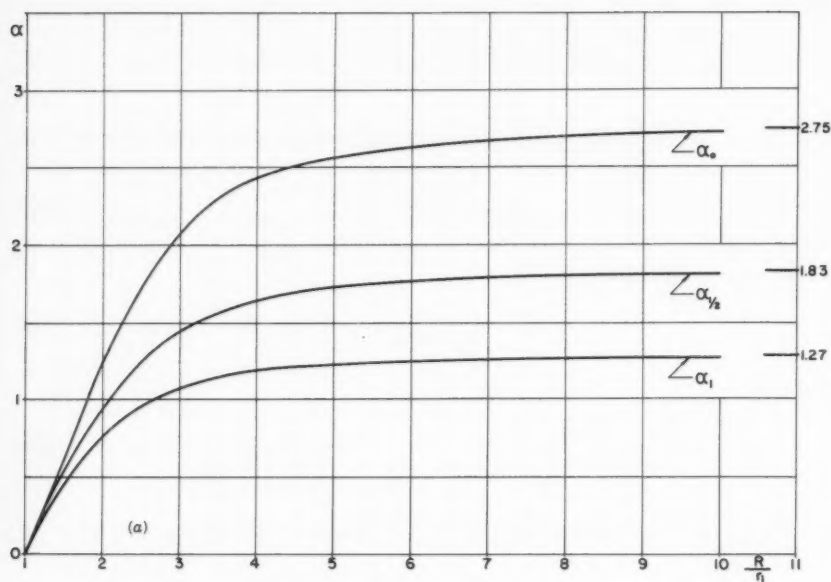


FIG. 5a

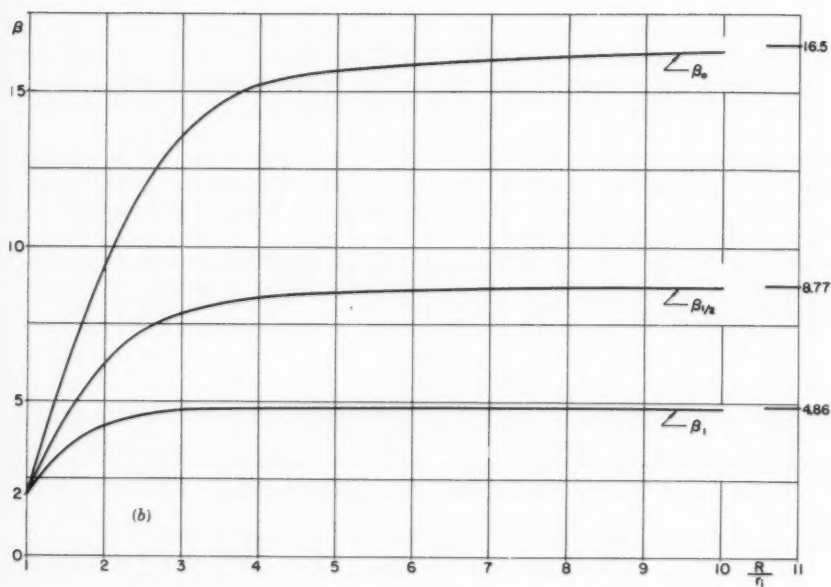


FIG. 5b

## ACKNOWLEDGMENTS

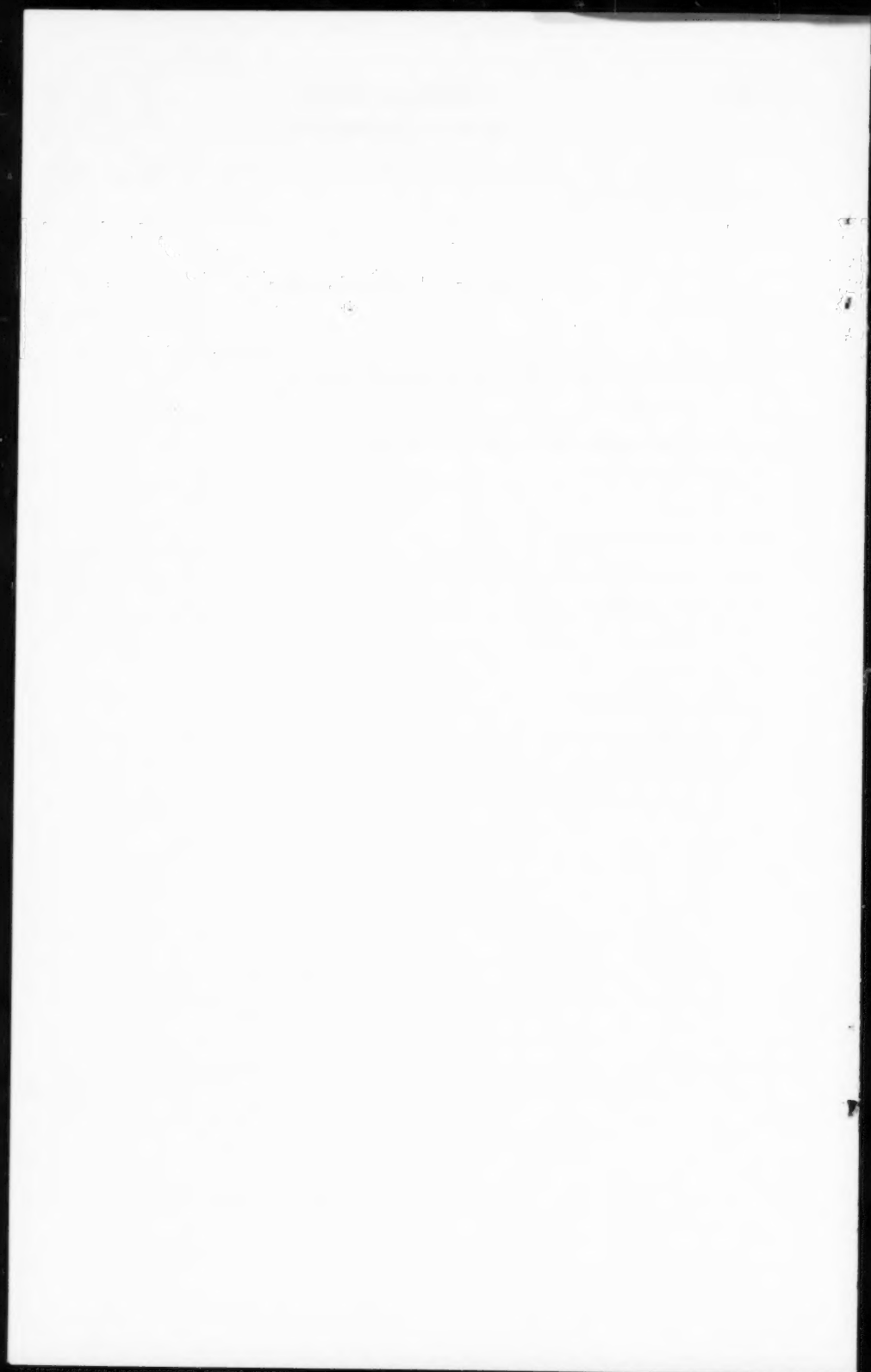
The authors are indebted to Hans H. Bleich, F. ASCE for the solution of the exploding point mass.

---

APPENDIX.—NOTATION

---

- $k$  = function of the coefficient of internal friction  
 $p$  = unit pressure  
 $r$  = Lagrangian coordinate of a particle  
 $r_0$  = cavity radius  
 $t$  = time  
 $W$  = explosion yield  
 $w$  = radial displacement of a particle  
 $\gamma$  = gas constant  
 $\xi$  = dilatation  
 $\rho$  = density  
 $\sigma_r$  = radial stress  
 $\sigma_\theta$  = tangential stress





---

Journal of the  
ENGINEERING MECHANICS DIVISION  
Proceedings of the American Society of Civil Engineers

---

VIBRATION OF SHEAR BUILDINGS BY FLEXIBILITY METHOD

Ming L. Pei,<sup>1</sup> M. ASCE

---

SYNOPSIS

The dynamic response of tall buildings caused by earthquake or blast loadings is usually analyzed with "shear building" assumption and the use of normal modes as generalized coordinates. For this purpose, it is frequently sufficient to use the first few frequencies and normal modes of the building. The standard matrix iteration method is not suitable for this purpose because it yields the highest mode first. A modified matrix iteration method using the inverse of the stiffness matrix is described. This will obtain the fundamental frequency and normal mode as the first result. The exact inverse of the stiffness matrix of any shear building is given by a formula and is easily obtained directly from the given physical data of the building. A numerical example illustrates the method.

---

SHEAR BUILDING

The numerical analysis of the dynamic response of an elastic rigid frame building to earthquake or blast loads presents difficulties due to the great complexity of the building itself. This may be considerably simplified by the introduction of "shear building" assumption, first proposed by M. P. White,<sup>2</sup> M.

---

Note.—Discussion open until July 1, 1961. To extend the closing date one month, a written request must be filed with the Executive Secretary, ASCE. This paper is part of the copyrighted Journal of the Engineering Mechanics Division, Proceedings of the American Society of Civil Engineers, Vol. 87, No. EM 1, February, 1961.

<sup>1</sup> Assoc. Prof., City College of New York, New York, N. Y.

<sup>2</sup> Discussion by M. P. White of "Natural Periods of Uniform Cantilever Beam," by L. S. Jacobsen, *Transactions*, ASCE, Vol. 104, 1939, p. 433.

ASCE. By the "shear building" assumption, we mean the following simplifications:

1. All floors are assumed to be rigid. As a direct consequence of this, all joint rotations are zero.
2. All columns are assumed to be inextensible.
3. The mass of the building is lumped at floor levels. This reduces an N-story building to an N lumped mass, N degrees-of-freedom problem.
4. The effect of direct stresses in columns on their flexural rigidities is neglected.

Generally speaking, the first step in a dynamic-response analysis is the calculation of undamped natural frequencies and normal modes of the buildings. This paper deals with a method of computing normal modes and natural frequencies of undamped shear buildings. There are many methods available for the determination of natural frequencies and normal modes, including the well-known Stodola-Vianello method,<sup>3</sup> Holzer method,<sup>4</sup> and matrix-iteration method.<sup>5,6,7</sup> The matrix iteration method is convenient in some instances, particularly if the work is carried out on electronic computers. The drawback of the standard matrix-iteration method is that we obtain successively the highest, the next highest, etc., frequency and normal mode. The fundamental frequency and lowest mode is obtained last of all, and is the least accurate of all results. Whereas in some engineering analysis, the lower frequencies are usually more important. Adequate results can sometimes be obtained without using all of the higher frequencies and modes. We show here that by using the flexibility matrix of the shear building, we may obtain the lowest frequency and normal mode first.

### FLEXIBILITY METHOD

An N-story tall building is shown schematically in Fig. 1. In accordance with the shear building assumption, all masses of columns are either neglected or lumped with the masses of the girders at the floor levels. The moment of inertia of girders is assumed to be infinite.

The spring constant,  $k_1$ , is the shear force necessary to produce a unit relative horizontal displacement between the ends of all the columns of the  $i^{\text{th}}$  story. Because the rotations of the ends of these columns are not permitted, due to the infinite rigidity of the girders, we have

$$k_1 = \frac{12 E I_1}{L_1^3} \dots \dots \dots (1)$$

<sup>3</sup> "Earthquake Stresses in Shear Buildings," by M. G. Salvadori, *Transactions*, ASCE, Vol. 119, 1954, p. 171.

<sup>4</sup> Discussion by J. A. Blume of "Earthquake Stresses in Shear Buildings," by M. G. Salvadori, *Transactions*, ASCE, Vol. 119, 1954, p. 171.

<sup>5</sup> "Dynamics of Framed Structures," by G. L. Rogers, John Wiley and Sons, Inc., New York, Chapters 3 and 4, 1959.

<sup>6</sup> "Engineering Analysis," by S. H. Crandall, McGraw-Hill Book Co., Inc., New York, Chapter 2, 1956.

<sup>7</sup> "Elementary Matrices," by B. A. Frazer, W. J. Duncan, and M. A. Collar, Cambridge Univ. Press, 1950, pp. 140-145, 308-316.

in which  $E$  is the modulus of elasticity, in pounds per square inch;  $I_i$  denotes the sum of moments of inertia of all columns of the  $i^{\text{th}}$  story, in inches to the fourth; and  $L_i$  refers to the length of columns of the  $i^{\text{th}}$  story in inches.

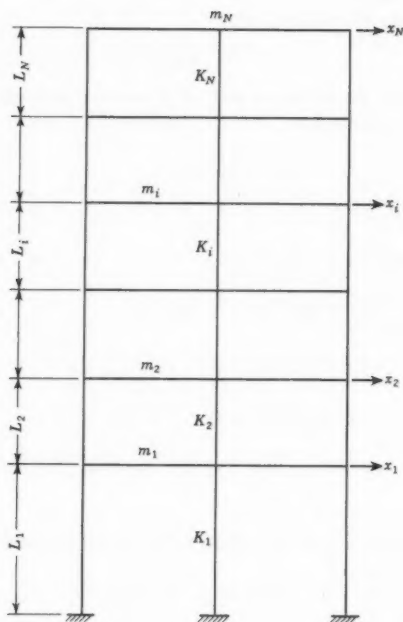


FIG. 1.— $N$ -STORY SHEAR BUILDING

The equation of motion for the mass on the  $i^{\text{th}}$  floor is

$$k_i(x_i - x_{i-1}) + k_{i+1}(x_{i+1} - x_i) = m_i \ddot{x}_i \dots \dots \dots (2a)$$

or,

$$-k_i x_{i-1} + (k_i + k_{i+1})x_i - k_{i+1} x_{i+1} = m_i \ddot{x}_i \dots \dots \dots (2b)$$

in which  $m_i$  is the mass at the  $i^{\text{th}}$  floor in pounds-seconds squared per inch; and  $x_i$  denotes the horizontal displacement of the  $i^{\text{th}}$  floor.

The equation of motion for the top floor is,

$$-k_{N-1} x_{N-1} + k_N x_N = m_N \ddot{x}_N \dots \dots \dots (2c)$$

It is noted that each of Eqs. 2 contains three terms on the lefthand-side, except the first and the last equation, which contain two terms. Eqs. 2 are used

by most writers<sup>8,9</sup> as the equation of motion in dynamic analysis of buildings. It should be pointed out that this equation is a direct consequence of the shear building assumption (infinite rigidity of floor girders), and is not valid for elastic rigid frame buildings, in general. If the moments of inertia of floor girders are not infinite, then each of Eqs. 2 will have  $N$  lefthand-side terms. Furthermore, the coefficients of these terms are no longer known, but must be obtained by lengthy calculations.<sup>10,11</sup>

For undamped, free vibration, let

$$x_i = \delta_i \sin t \dots\dots\dots (3)$$

Substituting into Eq. 2, we obtain a set of  $N$  simultaneous homogeneous equations for an  $N$ -story building.

$$\left. \begin{aligned} (k_1 + k_2) \delta_1 - k_2 \delta_2 &= \omega^2 m_1 \delta_1 \\ -k_2 \delta_1 + (k_2 + k_3) \delta_2 - k_3 \delta_3 &= \omega^2 m_2 \delta_2 \\ -k_3 \delta_2 + (k_3 + k_4) \delta_3 - k_4 \delta_4 &= \omega^2 m_3 \delta_3 \\ \dots\dots\dots &\dots\dots\dots \\ \dots\dots\dots &\dots\dots\dots \\ -k_N \delta_{N-1} + k_N \delta_N &= \omega^2 m_N \delta_N \end{aligned} \right\} \dots\dots (4)$$

It is convenient to write Eq. 4 as one matrix equation as follows:

$$[K] [\delta] = \omega^2 [M] [\delta] \dots\dots\dots (5)$$

in which  $[M]$ ,  $[K]$  and  $[\delta]$  are matrices defined as follows:

$$\text{Displacement matrix } [\delta] = \begin{bmatrix} \delta_1 \\ \delta_2 \\ \vdots \\ \delta_N \end{bmatrix} \dots\dots\dots (6)$$

<sup>8</sup> "Earthquake Forces on Systems with Several Degrees of Freedom," by B. Hojlund Rasmussen, Bulletin of the Seismological Society of America, Vol. 45, October, 1955, p. 269.

<sup>9</sup> "Response of Tall Buildings to Random Earthquakes," by A. C. Eringen, Proceedings of the 3rd United States Natl. Congress of Applied Mechanics, 1958, p. 141-151.

<sup>10</sup> "Stiffness Method of Rigid Frame Analysis," by M. L. Pei, Proceedings of the 2nd ASCE Conference on Electronic Computation, September, 1960.

<sup>11</sup> "The Dynamic Response of Tall Structures to Lateral Loads," by L. Schenker, Proceedings Paper No. 994, ASCE, 1956.

$$\text{Mass matrix } [M] = \begin{bmatrix} m_1 & & & & \\ & m_2 & & & \\ & & m_3 & & \\ & & & \ddots & \\ & & & & m_i \\ & & & & & \ddots \\ & & & & & & m_N \end{bmatrix} \quad (\text{diagonal}) \dots (7)$$

and

$$\text{Stiffness matrix } [K] = \begin{bmatrix} k_1 + k_2 & -k_2 & & & \\ & -k_2 & k_2 + k_3 & -k_3 & \\ & & & -k_3 & k_3 + k_4 & -k_5 \\ & & & & \dots & \\ & & & & & -k_{N-1} & k_N \end{bmatrix} \dots (8)$$

Premultiplying Eq. 5 by the inverse of  $[K]$ , yields

$$\begin{aligned} [\delta] &= \omega^2 [K]^{-1} [M][\delta] = \omega^2 [F][M][\delta] \\ &= \omega^2 [H][\delta] \dots \dots \dots (9) \end{aligned}$$

in which, for simplicity, we denote  $[F] = [K]^{-1}$ , and  $[H] = [F][M]$ . If matrix iteration procedure is carried out with Eq. 9, we shall obtain the fundamental mode and natural frequency of the shear building. Usually, matrix inversion is a lengthy process, and it is not too practical to calculate Eq. 9 for a general building. However, for shear buildings, the exact inverse of  $K$  is given by the formula

$$f_{ij} = \begin{cases} \sum_{r=1}^i f_r & i > j \\ \sum_{r=1}^j f_r & i < j \end{cases} \dots \dots \dots (10a)$$

in which  $f_i$  is the reciprocal of  $k_i$ . Or, written out in full,

$$[F] = \begin{bmatrix} f_1 & f_1 & f_1 & \dots & f_1 \\ f_1 & f_1+f_2 & f_1+f_2 & & f_1+f_2 \\ \dots & & & & \\ \dots & & & & \\ f_1 & f_1+f_2 & f_1+f_2+f_3 & \dots & f_r \end{bmatrix} \dots \dots \dots (10b)$$

The proof of Eq. 10 is fairly simple, since the elements in the flexibility matrix are the displacement influence coefficients of the shear building. That is,  $f_{ij}$  is the displacement of the  $i$ th floor due to a unit load applied at the  $j$ th floor level. With the unit load applied at the first floor of the building, shown in Fig. 2, the displacements of all floors are the same and equal to  $L_1^3/12 E I_1$ . Hence, every element in the first column of the flexibility matrix is equal to  $f_1$ .

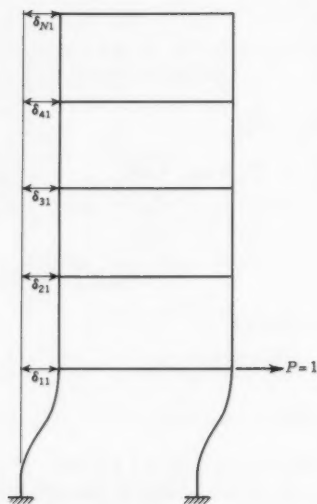


FIG. 2.—DISPLACEMENTS OF SHEAR BUILDING DUE TO A UNIT LOAD AT THE FIRST FLOOR LEVEL

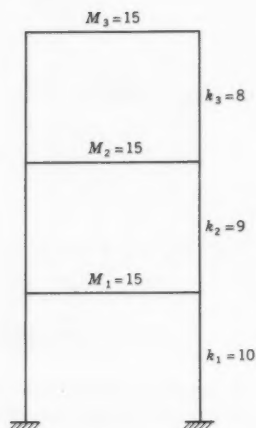


FIG. 3.—THREE-STORY BUILDING

Next, with the unit load applied at the second floor level, the displacement of the first floor is equal to  $f_1$ ; and the displacements of all upper floors are equal to  $f_1 + f_2$ . Thus, the second column of the flexibility matrix is,

$$\begin{bmatrix} f_{21} \\ f_{22} \\ \vdots \\ f_{2N} \end{bmatrix} = \begin{bmatrix} f_1 \\ f_1 + f_2 \\ \vdots \\ f_1 + f_2 \end{bmatrix}$$

The remaining columns of the flexibility matrix can be derived in the same way. Briefly, the iteration procedure is as follows:

1. Compute the flexibility matrix directly from given data by means of Eq. 10.
2. Assume arbitrarily a column vector  $[\delta]_0$ , as the initial approximation of the normal mode. Compute, an improved approximation by

$$[\delta]_1 = [H] [\delta]_0 \dots\dots\dots (11)$$

3. Repeat step 2 until convergence. The final  $[\delta]$  is the normal mode.
4. The natural frequency is computed from

$$\omega = \sqrt{\frac{\delta_r}{\delta_{r+1}}} \dots\dots\dots (12)$$

in which  $\delta_r$  and  $\delta_{r+1}$  are the corresponding values of  $\delta$  of the same floor in the  $r$ th and  $(r+1)$ th iteration. Usually, we may use the  $\delta$  having the largest absolute magnitude for this calculation. Some idea of the accuracy of the result may be obtained by means of the enclosure theorem,<sup>6</sup> which gives the upper and lower limit of the true frequency as,

$$\left(\frac{\delta_r}{\delta_{r+1}}\right)_{\min} \leq \omega^2 \leq \left(\frac{\delta_r}{\delta_{r+1}}\right)_{\max} \dots\dots\dots (13)$$

Alternatively, a better estimate of the frequency may be obtained<sup>3</sup> by taking the ratio of the weighted average of  $\delta_r$  and  $\delta_{r+1}$ .

$$\omega^4 = \frac{\sum_{i=1}^N m_i \delta_{i,r}^2}{\sum_{i=1}^N m_i \delta_{i,r+1}^2} \dots\dots\dots (14)$$

### ILLUSTRATIVE EXAMPLE

*First Mode.*—Although the method is particularly useful for tall buildings, we shall for simplicity's sake use a three-story building analyzed by Rogers<sup>5</sup>

TABLE 1.—ANALYSIS DATA

1 (1)	Mass, in lb-sec <sup>2</sup> per in. (2)	Spring constant k, in kips per inch (3)
3	15	8
2	15	9
1	15	10



as an illustration. The building is shown in Fig. 3, and its masses and spring constants are given in Table 1. The mass matrix is a diagonal matrix.

$$[M] = \begin{bmatrix} 15 & 0 & 0 \\ 0 & 15 & 0 \\ 0 & 0 & 15 \end{bmatrix}$$

The flexibility matrix is computed by means of Eq. 10.

$$[F] = \begin{bmatrix} 1/10 & 1/10 & 1/10 \\ 1/10 & 1/10+1/9 & 1/10+1/9 \\ 1/10 & 1/10+1/9 & 1/10+1/9+1/8 \end{bmatrix} = \frac{1}{360} \begin{bmatrix} 36 & 36 & 36 \\ 36 & 76 & 76 \\ 36 & 76 & 121 \end{bmatrix} \text{ in. per kip}$$

and

$$[H] = [F][M] = \frac{15}{360,000} \begin{bmatrix} 36 & 36 & 36 \\ 36 & 76 & 76 \\ 36 & 76 & 121 \end{bmatrix} \text{ sec}^2$$

Since we are concerned with the relative magnitudes of the displacements of the normal mode, we may discard the numerical factor from  $H$  to simplify calculations. To begin the calculations, we assume

$$[\delta]_0 = \begin{bmatrix} 1 \\ 2 \\ 2 \end{bmatrix}$$

First cycle.—Applying Eq. 11, we have

$$[\delta]_1 = [H][\delta]_0 = \begin{bmatrix} 36 & 36 & 36 \\ 36 & 76 & 76 \\ 36 & 76 & 121 \end{bmatrix} \begin{bmatrix} 1 \\ 2 \\ 2 \end{bmatrix} = \begin{bmatrix} 180 \\ 340 \\ 430 \end{bmatrix}$$

Second cycle.—Applying Eq. 11 again. Discard a factor of 10.

$$[\delta]_2 = [H][\delta]_1 = \begin{bmatrix} 36 & 36 & 36 \\ 36 & 76 & 76 \\ 36 & 76 & 121 \end{bmatrix} \begin{bmatrix} 18 \\ 34 \\ 43 \end{bmatrix} = \begin{bmatrix} 3420 \\ 6500 \\ 8435 \end{bmatrix} = 3,420 \begin{bmatrix} 1 \\ 1.90 \\ 2.47 \end{bmatrix}$$

Third cycle.—

$$[\delta]_3 = [H][\delta]_2 = \begin{bmatrix} 660,780 \\ 1,258,180 \\ 1,637,755 \end{bmatrix} = 660,780 \begin{bmatrix} 1 \\ 1.904 \\ 2.479 \end{bmatrix}$$

Fourth cycle.—

$$[\delta]_4 = [H][\delta]_3 = 128,041,740 \begin{bmatrix} 1 \\ 1.90468 \\ 2.48027 \end{bmatrix}$$

This may be taken as the first normal mode of the shear building. The natural frequency is obtained from Eq. 12.

$$\omega_1 = \sqrt{\delta_0 / \delta_1} = \sqrt{\frac{360,000}{15}} \sqrt{\frac{2}{430}} = 10.56 \text{ radians per sec}$$

$$\omega_2 = 11.06 \text{ radians per sec}$$

$$\omega_3 = 11.12 \text{ radians per sec}$$

and

$$\omega_4 = 11.13 \text{ radians per sec}$$

Alternatively, the fundamental frequency may be obtained by Eq. 13. Using, for example, the results of the first and second cycle, we have

$$\omega = \sqrt[4]{\frac{18^2 + 34^2 + 43^2}{(3420^2 + 6500^2 + 8435^2)(15/360,000)^2}} = 11.13 \text{ radians per sec}$$

*Higher modes.*—Having obtained the first mode, we may proceed to calculate the next higher mode. The general procedure is well known<sup>6,7,12</sup> and will not be discussed here. In this manner, one may calculate as many, or as few, normal modes as necessary.

#### ADDITIONAL REFERENCES

1. "A Method for the Solution of Oscillation Problems by Matrices," Phil. Magazine, Vol. 7, No. 17, 1934, pp. 865-909.
2. "Numerical Analysis of Earthquake Response of a Tall Building," by T. P. Tung and N. M. Newmark, Bulletin of the Seismological Society of America, Vol. 45, October, 1955, p. 269.

<sup>12</sup> "Notes on the Determination of Higher Modes of Vibration by the Stodola or Matrix Iteration Method," by H. E. Fetti, Journal of Aeronautical Science, Vol. 26, No. 5, May, 1959, p. 317.



---

Journal of the  
ENGINEERING MECHANICS DIVISION  
Proceedings of the American Society of Civil Engineers

---

DYNAMIC ELASTIC-PLASTIC ANALYSIS OF STRUCTURES

By Melvin L. Baron,<sup>1</sup> A. M. ASCE, Hans H. Bleich,<sup>2</sup> F. ASCE, and  
Paul Weidlinger,<sup>3</sup> F. ASCE

---

SYNOPSIS

The objective of this paper is the presentation of the finite difference method for the elastic-plastic analysis of structures and a comparison of its results with simpler theories.

---

INTRODUCTION

One of the major problems facing structural and mechanical engineers is the design of structures which are capable of withstanding high pressure loadings of a transient or time dependent nature. For example, in the rapidly growing field of protective construction, the design requirement that structures should withstand high intensity overpressures produced by nuclear blasts, may lead for economic and other practical reasons to the necessity of abandoning the conventional requirement of limiting stresses to some value below the elastic limit (the working stress concept). Instead, plastic flow at various locations in the structure is permitted, but the total deflection must be kept within acceptable limits. An elastic-plastic analysis of such structures under transient pressure loading is required to determine two major design parameters:

1. The maximum permanent deflections produced in the structure due to its plastic behavior.

---

Note.—Discussion open until July 1, 1961. To extend the closing date one month, a written request must be filed with the Executive Secretary, ASCE. This paper is part of the copyrighted Journal of the Engineering Mechanics Division, Proceedings of the American Society of Civil Engineers, Vol. 87, No. EM 1, February, 1961.

<sup>1</sup> Assoc., Paul Weidlinger, Cons. Engr., New York, and Adjunct Assoc. Prof. of Civ. Engrg., Columbia Univ.

<sup>2</sup> Dir., Inst. of Flight Structures, Columbia Univ., N. Y.

<sup>3</sup> Cons. Engr., New York, N. Y.

2. The dynamic reactions and the load transmission through the structure onto its supporting foundation may in many cases be a controlling factor in the design.

Consider an initially elastic beam or frame structure which is subjected to time-dependent loads. Fundamentally the problem of finding the response of the structure could be formulated by writing the differential equations of motion for a three-dimensional elastic-plastic continuum. The complexity of the resulting equations for the complicated geometric shapes involved would obviously make their solution a major problem; even in the simple elastic problem, the treatment as a continuum is only manageable in a few simple cases. As a result, the beam concept has been introduced, replacing the structure by a center line with stiffness properties (that is, a linear relation between the bending moment and curvature). This approach gives good results in the elastic case as long as the length of the structural member is sufficiently greater than the transverse dimensions of the member.

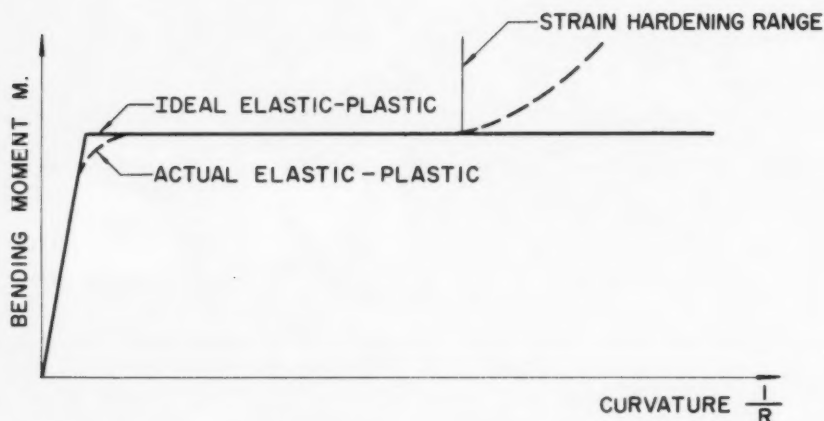


FIG. 1.—ELASTIC-PLASTIC MOMENT-CURVATURE RELATIONSHIP

A similar approach is used in the treatment of elastic-plastic beam and frame structures. A relation, which can be verified experimentally, between the bending moment  $M$  and the curvature of the deflected center line  $1/R$  is the basis for all current elastic-plastic analytical methods. This relation has the character shown in Fig. 1 and consists first of a linear portion followed by a transition to a nearly horizontal line. For the sake of simplicity the actual bending moment-curvature relation is replaced by an idealized curve consisting of the two straight lines shown in Fig. 1. This implies that the curvature is restricted to those values for which the strain hardening range is not entered. It also means that some detail near the knee of the  $M - 1/R$  diagram is lost, however, for members of structural steel, the ideal diagram is quite close to the actual one and the differences in the result must therefore be small. It should also be noted that the effects of shear yielding are neglected in the following treatment.

Further simplifying assumptions may be useful and appropriate for special cases:

1. In structures subjected to loads which produce large permanent deformations (in comparison with the elastic deformations), the elastic strain energy is small compared to the energy absorbed in the plastic stage and consequently the elastic response of the structure might be entirely neglected, leading to a rigid-plastic theory.
2. In structures for which the location of yield hinges can be clearly predicted for given pressure loadings, an analysis with plastic hinge locations which are assumed a priori can be performed.

Both assumptions result in attractive analytical simplifications, but the appropriateness of these methods, with the exception of certain trivial cases, remains somewhat in doubt unless they can be compared with more general procedures which do not put undue restrictions on the location of the plastic hinges or on the duration of the successive plastic and elastic stages at the points of hinge formation on the structure. In recent years, several less restrictive theories of dynamic elastic-plastic analysis have been formulated, but practical applications have been limited to simple structures, due to both mathematical and computational difficulties.

A theory was presented<sup>4</sup> in 1959 which permits a general analysis in sufficient detail for most practical problems, and its application by finite difference methods has been found to be ideally suited for high speed electronic computing equipment.

The purpose of this paper is twofold:

1. To present in detail the finite difference method for the elastic-plastic analysis of structures.
2. To clarify the appropriateness and range of validity of the simpler theories by comparing the results obtained from these theories with the more precise results of the finite difference method.

For purposes of numerical comparison, a loading of the form

$$p(t) = n p_0 e^{-t/t_0} \dots\dots\dots (1)$$

is used, in which  $p_0$  represents the static capacity load which will produce yielding in the structure under consideration;  $n p_0$  is the initial value of the dynamic load at the time  $t = 0$ ; and  $t_0$  is the decay constant. While the finite difference method can be generalized for application to complex-frame type structures, a form particularly suited for the analysis of statically determinate structures is given in this paper and numerical examples will be presented for a simply supported beam only. The range of validity of the simplified theories will be generally defined by the intensity of the initial value of the load in terms of the amplification factor  $n$ , while using the value of the maximum permanent deflection of the beam as a comparison criterion.

<sup>4</sup> "Dynamic Design in the Plastic Range," by H. H. Bleich and M. L. Baron, presented at the February 1959 ASCE Meeting, Engrg. Mechanics Div., Los Angeles, Calif.

*Notation.*—The letter symbols adopted for use in this paper are defined where they first appear, in the illustrations or in the text, and are arranged alphabetically, for convenience of reference, in Appendix II.

## FINITE DIFFERENCE METHOD FOR THE RESPONSE OF ELASTIC-PLASTIC STRUCTURES TO TRANSIENT LOADINGS

A method of analysis involving an expansion of the response of the structure into a series of normal modes of vibration was presented by Hans H. Bleich,<sup>5</sup> F. ASCE. In this analysis, the original modes of the elastic system were utilized throughout the elastic and plastic stages, and provision was made for the possibility of the formation of multiple plastic hinges (hinges at various points on the structure) and for the re-elasticizing and re-plasticizing of these points. Utilization of some of the general principles presented by Bleich<sup>5</sup> led to the development of the method of analysis of this section.<sup>4</sup> The method which employs a finite difference approach is presented in detail for application to statically determinate structures and is particularly well suited for use on high speed computers such as the IBM 704 which was used in the solution of the present problem and other problems.<sup>6</sup>

At this point, one may consider the type of problem which can be treated by a normal mode, or by a finite difference approach in general, with or without plasticity. In structural problems, the designer is usually satisfied with a knowledge of data on a beam at points where the spacing is of the order of the beam depth or perhaps at the most half of the beam depth, and both modal and finite difference analyses are suitable for such problems. Mode methods are useful because the computations can be restricted to a relatively small number of modes and, similarly, finite difference methods are permissible since the computations can be restricted to a relatively small number of mass points, leading to sufficiently accurate, physically, meaningful results. The elements of the structure will be assumed to be ideally elastic-plastic. They will exhibit the conventional elastic-plastic behavior of bending, that is to act elastically up to a certain capacity moment  $M_c$  and to become fully plastic when this moment is reached (Fig. 1). When the capacity moment  $M_c$  is maintained at a particular section, curvatures of arbitrarily large magnitude can occur there, and plastic-hinge action takes place.

Since the curvature at a section theoretically approaches infinity as the moment at the section approaches  $M_c$ , one may postulate that the attainment of the fully-plastic moment at a section allows finite changes of slope to occur at that section while the moment remains constant and equal to  $M_c$ . This corresponds to inserting a physical hinge which can only transmit a constant moment  $M_c$  at that section, hence, the concept of a plastic hinge. The capacity moment  $M_c$  of a member may be selected to allow for direct stresses which occur simultaneously with the moments, if these stresses are large.

*Equations of Motion-Elastic Stages.*—Consider a simply supported beam of length  $L$  (Fig. 2) which can be replaced by a continuous chain of equally or unequally spaced lumped rigid masses connected by inextensible bars with moment springs at each joint. Let  $E$  refer to the modulus of elasticity of beam

<sup>5</sup> "Response of Elastoplastic Structures to Transient Loads," by H. H. Bleich, Proceedings, New York Academy of Sciences, November, 1955.

<sup>6</sup> "On a Method of Amplification of the Dynamic Strength of Structures," by P. Weidlinger, M. L. Baron, and R. Skalak, (U), Air Force Special Weapons Center, Report No. AFSWC-TR-59-10, October, 1958.



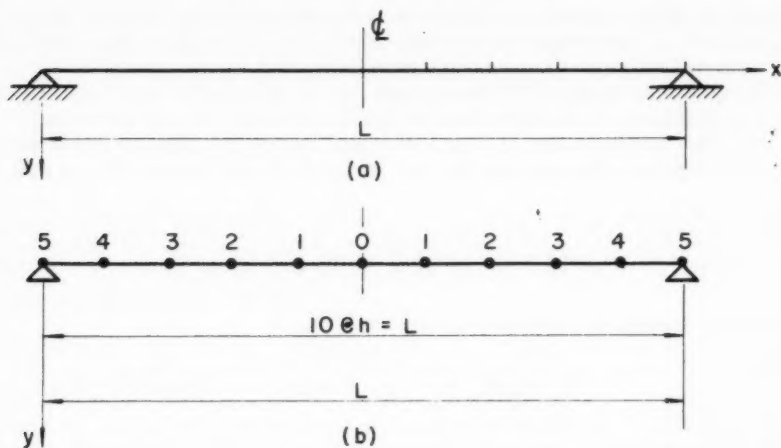


FIG. 2.—BEAM MODEL

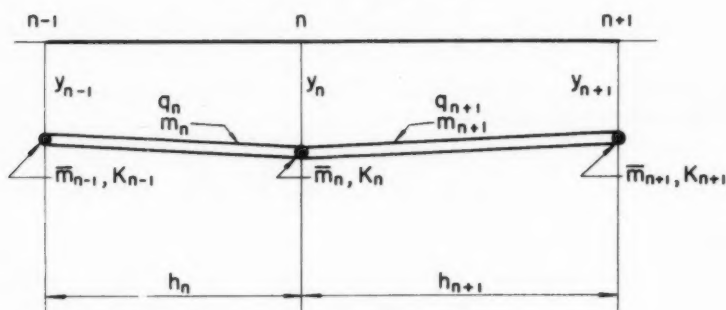
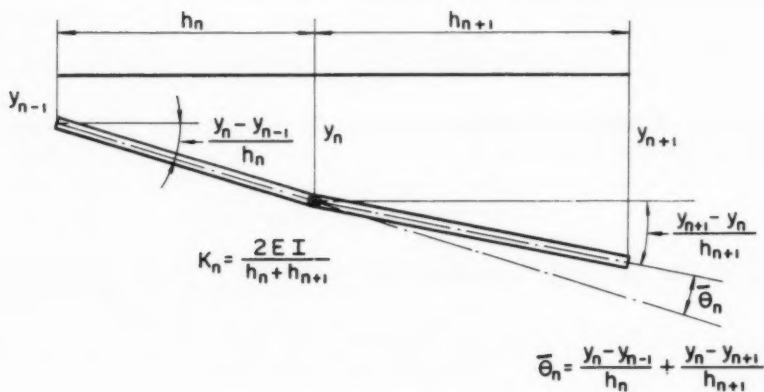


FIG. 3.—NOMENCLATURE FOR MODEL

FIG. 4.—DETERMINATION OF  $\bar{\theta}_n$

material,  $I$  be the moment of inertia of cross section of the beam (constant at all sections),  $m$  denote the mass of the beam per unit length of span, and  $y$  refer to the deflection of the beam, positive downward.

The equations of motion of the masses during the elastic stage may be derived by utilization of Hamilton's principle and the calculus of variations.

Using the nomenclature of Fig. 3, in which  $m_n$  is the mass of the structure per unit of length in the span  $h_n$ , the lumped mass at the point  $n$ ,  $\bar{m}_n$ , is defined as

$$\bar{m}_n = \frac{1}{2} \left[ m_n h_n + m_{n+1} h_{n+1} \right] \dots\dots\dots (2)$$

The kinetic energy associated with the mass  $\bar{m}_n$  is

$$\bar{T}_n = \frac{1}{2} \bar{m}_n \dot{y}_n^2 = \frac{1}{2} \left[ \frac{m_n h_n + m_{n+1} h_{n+1}}{2} \right] \dot{y}_n^2 \dots (3)$$

and the total kinetic energy of all the mass points of the model is obtained by summing the individual  $\bar{T}_n$ ,

$$\bar{T} = \sum_n \bar{T}_n = \frac{1}{2} \sum_n \left[ \frac{m_n h_n + m_{n+1} h_{n+1}}{2} \right] \dot{y}_n^2 \dots\dots\dots (4)$$

The potential energy of the structure, that is, the strain energy of the support beam, can be expressed as

$$\bar{V} = \sum_n \frac{1}{2} M_n \bar{\theta}_n = \sum_n \frac{1}{2} K_n \bar{\theta}_n^2 \dots\dots\dots (5)$$

in which

$$M_n = K_n \bar{\theta}_n \dots\dots\dots (6)$$

is the moment at the joint  $n$ , and quantity

$$K_n = \frac{2EI}{h_n + h_{n+1}} \dots\dots\dots (7)$$

is the moment required to produce a unit-angle rotation at the joint  $n$ . The angle  $\bar{\theta}_n$  is obtained from Fig. 4.

$$\bar{\theta}_n = - \left[ \frac{y_{n+1} - y_n}{h_{n+1}} - \left( \frac{y_n - y_{n-1}}{h_n} \right) \right] \dots\dots\dots (8)$$

Using Eqs. 7 and 8, Eqs. 5 and 6 become;

$$\bar{V} = \frac{1}{2} \sum_n K_n \left[ \left( \frac{y_n - y_{n-1}}{h_n} \right) - \left( \frac{y_{n+1} - y_n}{h_{n+1}} \right) \right]^2 \dots\dots\dots (9)$$

and

$$M_n = - \frac{2EI}{h_n + h_{n+1}} \left[ \frac{y_{n+1} - y_n}{h_{n+1}} - \left( \frac{y_n - y_{n-1}}{h_n} \right) \right] \dots (10)$$

Forming the function  $\bar{T} - \bar{V}$ ,

$$\bar{T} - \bar{V} = \sum_n \left\{ \left[ \frac{m_n h_n + m_{n+1} h_{n+1}}{4} \right] \dot{y}_n^2 - \frac{1}{2} K_n \left[ \frac{y_n - y_{n-1}}{h_n} - \left( \frac{y_{n+1} - y_n}{h_{n+1}} \right) \right]^2 \right\} \dots (11)$$

and applying Hamilton's Principle,

$$\delta (\bar{T} - \bar{V}) = 0 \dots (12)$$

we obtain, by means of the calculus of variations, the equation of motion for the free vibrations of the  $n^{\text{th}}$  concentrated mass

$$\begin{aligned} & \left[ \frac{m_n h_n + m_{n+1} h_{n+1}}{2} \right] \ddot{y}_n + \frac{K_{n-1}}{h_n h_{n-1}} y_{n-2} \\ & - \left[ \frac{K_{n-1}}{h_n} \left( \frac{1}{h_{n-1}} + \frac{1}{h_n} \right) + \frac{K_n}{h_n} \left( \frac{1}{h_{n+1}} + \frac{1}{h_n} \right) \right] y_{n-1} \\ & + \left[ \frac{K_{n-1}}{h_n^2} + \frac{K_{n+1}}{h_{n+1}^2} + K_n \left( \frac{1}{h_n} + \frac{1}{h_{n+1}} \right)^2 \right] y_n \\ & - \left[ \frac{K_{n+1}}{h_{n+1}} \left( \frac{1}{h_{n+1}} + \frac{1}{h_{n+2}} \right) + \frac{K_n}{h_{n+1}} \left( \frac{1}{h_{n+1}} + \frac{1}{h_n} \right) \right] y_{n+1} \\ & + \frac{K_{n+1}}{h_{n+1} h_{n+2}} y_{n+2} = 0 \dots (13) \end{aligned}$$

If the structure is subjected to uniform loadings  $q_n(t)$  on each sub-span  $h_n$ , the right-hand side of Eq. 13 is set equal to

$$\frac{q_n h_n + q_{n+1} h_{n+1}}{2} \dots (14)$$

(Note that  $q_n$  is the uniform load per unit length of span in the span  $h_n$ . In the notation of this section, the subscript  $n$  refers to the span to the left of the mass  $\bar{m}_n$ ; the subscript  $n+1$  refers to the span to the right of the mass point.)

For the simply supported beam under consideration, for which the mass points are equally spaced on either side of  $\bar{m}_n$ , that is  $h_n \pm k = h$  ( $k = 0, 1, 2$ ), the equation of motion for the concentrated mass  $\bar{m}_n$  becomes

$$\left( \frac{m_n + m_{n+1}}{2} \right) \ddot{y}_n + \frac{EI}{h^4} \delta^4 y_n = \frac{q_n + q_{n+1}}{2} \dots (15)$$

in which

$$\delta^4 y_n = y_{n-2} - 4y_{n-1} + 6y_n - 4y_{n+1} + y_{n+2} \dots (16)$$

For a constant moment of inertia, the equations for  $K_n$  and  $M_n$  become, respectively,

$$K_n = \frac{EI}{h} \dots (17)$$

and

$$M_n = -\frac{EI}{h^2} \delta^2 y_n \dots (18)$$

in which

$$\delta^2 y_n = y_{n+1} - 2y_n + y_{n-1} \dots (19)$$

Noting that

$$\delta^4 y_n = \delta^2 (\delta^2 y_n) \dots (20)$$

and using Eq. 18, Eq. 15 is written in a more convenient form

$$\left[ \frac{m_n + m_{n+1}}{2} \right] \ddot{y}_n = \frac{q_n + q_{n+1}}{2} + \frac{\delta^2 M_n}{h^2} \dots (21)$$

Referring to the beam in Fig. 2 (b) where it is broken into ten equal intervals of length  $h = L/10$ , the structure is analyzed as a continuous chain of eleven lumped mass points located at the positions 0, 1, 2, 3, 4, and 5. As the loading on the structure will be symmetrical with respect to the center line, in the present example, only the equations of motion for six of the masses will be required. Eqs. 18 and 21 may be used for the concentrated masses at the points 0, 1, 2, 3 and 4.

A summary of the equations of motion in the elastic range for the model of Fig. 2 (b) is as follows

$$\left[ \frac{m_0 + m_1}{2} \right] \ddot{y}_0 = \frac{q_0 + q_1}{2} + \frac{1}{h^2} [2 M_1 - 2 M_0] ; n = 0 \dots (22a)$$

and

$$\left[ \frac{m_n + m_{n+1}}{2} \right] \ddot{y}_n = \frac{q_n + q_{n+1}}{2} + \frac{1}{h^2} [M_{n+1} - 2 M_n + M_{n-1}] ; n = 1, 2, 3, 4, \dots (22b)$$

in which the moment-displacement equations are given by

$$M_0 = - \frac{EI}{h^2} [2 y_1 - 2 y_0] ; n = 0 \dots \dots \dots (23a)$$

$$M_n = - \frac{EI}{h^2} (y_{n-1} - 2 y_n + y_{n+1}) ; n = 1, 2, 3, 4 \dots \dots \dots (23b)$$

and

$$M_5 = 0 \text{ simple support } \dots \dots \dots (23c)$$

Eqs. 22a and 22b are integrated by a numerical forward-step integration in time. Replacing the function  $\ddot{y}_n(t)$  by the first term of its finite difference expansion in central differences,

$$\ddot{y}_n = \frac{y_n(t+k) - 2 y_n(t) + y_n(t-k)}{k^2} \dots \dots \dots (24)$$

in which  $k$  is the interval of the time steps, recurrence equations for the deflection  $y_n(t+k)$  are obtained in terms of the moments, loads and displacements at the times  $t$  and  $t-k$

$$y_0(t+k) = \frac{[q_0(t) + q_1(t)] k^2}{m_0 + m_1} + \frac{4 [M_1(t) - M_0(t)] k^2}{h^2 (m_0 + m_1)} + 2 y_0(t) - y_0(t-k) ; n = 0 \dots \dots \dots (25a)$$

$$y_n(t+k) = \frac{[q_n(t) + q_{n+1}(t)] k^2}{m_n + m_{n+1}} + \frac{2 [M_{n-1}(t) - 2 M_n(t) + M_{n+1}(t)] k^2}{h^2 (m_n + m_{n+1})} + 2 y_n(t) - y_n(t-k) \dots \dots \dots (25b)$$

and

$$y_5 = 0 \text{ simple support} \dots\dots\dots (25c)$$

The initial conditions of zero displacement and zero velocity

$$y_n(0) = \dot{y}_n(0) = 0 \dots\dots\dots (26)$$

lead to the conditions

$$y_n(0) = 0, y_n(k) = y_n(-k) \dots\dots\dots (27)$$

and to the starting formulas

$$y_n(0) = 0$$

$$y_n(k) = \frac{1}{2} \left[ \frac{q_n(0) + q_{n+1}(0)}{m_n + m_{n+1}} \right] k^2 \dots\dots\dots (28)$$

The question of the stability of the numerical integration of Eqs. 25 which controls the choice of the time step "k" is examined in Appendix I.

*Plastic Stages.*—For sufficiently large pressure loadings,  $q_n(t)$ , plastic deformations may start at a time  $t = t_1$  at any of the various points  $n$ , on the beam. Thereafter, the deformation curve of the structure will no longer be smooth, but will show "kinks" at points where the plastic hinges occurred at any time during the loading history. Considering such a point on the beam,  $n = j$ , at the time  $t = t_1$ , the moment  $M_j$  computed from Eqs. 23 will be larger than the capacity moment of the beam,  $M_c$ . This is physically impossible and so a corrective displacement must be introduced at each point on the beam in which  $M_c < M_j$ , such that the condition  $M_n \leq M_c$  is enforced at every point on the beam. Such a corrective displacement due to plasticity at the joint  $j$  only is given by

$$y_n^c = \theta_j \Psi_{jn} \dots\dots\dots (29)$$

in which  $y_n^c$  is the displacement at the joint  $n$  due to the corrective displacement for plasticity at the joint  $j$ ;  $\theta_j$  is a generalized coordinate proportional to the angle of the plastic kink at the joint  $n = j$ ; and  $\Psi_{jn}$  is the deflection curve at the points  $n$  of a fictional elastic beam if a hinge were introduced at the point  $x = x_j$  and the two portions of the structure on either side of the point  $j$  were rotated by a certain angle. This angle is selected so that  $\delta^2 \Psi_{nn}$  is equal to minus unity (of length), in which case the plastic kink angle at the joint  $j$  is equal to  $\theta_j/h$ . The displacement is shown in Fig. 5 for the case of the simply supported beam. The deflection curve consists of straight lines with a kink at the point  $n = j$  where the plasticity occurred. If plasticity occurs at several points, the corrected displacement at any joint  $n$  due to the plasticity at the several joints  $j$  is ob-

tained by summation

$$y_n^c = \sum_j \theta_j \psi_{jn} \dots \dots \dots (30)$$

The expression for the true deflection at any point  $n$  is given by

$$y_n = y_{nel} + y_n^c = y_{nel} + \sum_j \theta_j \psi_{jn} \dots \dots \dots (31)$$

in which  $y_{nel}$  is the elastic deflection at the joint  $n$ , and the corresponding equation for the moment  $M_n$  becomes

$$M_n = -\frac{EI}{h^2} \delta^2 y_{nel} = -\frac{EI}{h^2} \delta^2 \left[ y_n - \sum_j \theta_j \psi_{jn} \right] \dots (32)$$

Writing Eq. 32 as

$$M_n = -\frac{EI}{h^2} \delta^2 y_n + \frac{EI}{h^2} \sum_j \theta_j \delta^2 \psi_{jn} \dots \dots \dots (33)$$

and noting from Fig. 5 that

$$\left. \begin{aligned} \delta^2 \psi_{jn} &= 0, j \neq n \\ &= -1, j = n \end{aligned} \right\} \dots \dots \dots (34)$$

it is seen that the corrective moment applied at the hinge to produce the plastic angle generalized coordinate  $\theta_j$  at the joint  $n = j$  produces a moment at the

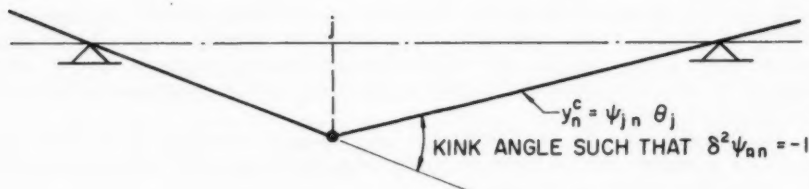


FIG. 5.—PLASTIC KINK

point  $j$  only and at no other point on the beam. This allows Eq. 33 to be written without the summation

$$M_n = -\frac{EI}{h^2} \delta^2 y_n + \frac{EI}{h^2} \theta_n \delta^2 \psi_{nn} \dots \dots (35a)$$

and

$$M_n = - \frac{EI}{h^2} \delta^2 y_n - \frac{EI}{h^2} \theta_n \dots\dots\dots (35b)$$

(By definition  $\delta^2 \psi_{nn} = -1$ , in order that the kink angle  $\theta_n$  be positive.)

The plastic angle generalized coordinate at the joint  $n$ ,  $\theta_n(t)$  may be written in terms of the previous plastic angle coordinate at the time step  $-k$ , plus the change in the plastic angle coordinate in the interval  $t - k$  to  $t$

$$\theta_n(t) = \theta_n(t-k) + \Delta \theta_n(t-k) \dots\dots\dots (36)$$

Using Eq. 36, Eq. 35b is written as

$$M_n(t) = M_n^e(t) - \frac{EI}{h^2} \Delta \theta_n(t-k) \dots\dots\dots (37)$$

in which

$$M_n^e(t) = - \frac{EI}{h^2} \delta^2 y_n(t) - \frac{EI}{h^2} \theta_n(t-k) \dots\dots (38)$$

Once the deflections  $y_n(t)$  have been found from Eqs. 25, Eq. 38 may be used to compute the moment  $M_n^e(t)$ , and the condition that  $M_n(t) < M_c$  is then used to evaluate the change in the plastic angle coordinate,  $\Delta \theta_n(t-k)$ . The moments  $M_n(t)$  are then evaluated by means of Eq. 37 and are used in Eqs. 25 for the determination of the deflection  $y_n(t+k)$ .

It remains now to discuss the procedure for finding  $\Delta \theta_n(t-k)$ . The increment of plastic angle may be positive, thus indicating an increase in the plastic deformation of the beam at the joint  $n$  in the time interval  $t - k$  to  $t$ , or zero, thus indicating no further plasticity in this time interval and a return of the joint  $n$  to the elastic range. It should be noted that when a point of the beam re-enters an elastic stage, it maintains a permanent plastic kink with an angle proportional to  $\theta_n = \theta_n(t-k)$ . Moreover, any or all points on the structure may enter and leave the plastic stage at any time with no fundamental difficulty in applying the equations.

To find  $\Delta \theta_n(t-k)$ , let the plastic angle  $\theta_n$  be known up to the time step  $t - k$  and consider the increment of plastic angle in the interval  $t - k$  to  $t$ . The following procedure can be used:

1. Compute the deflections  $y_n(t)$  from the equations of motion of the mass points, Eqs. 25.
2. Using the values of  $y_n(t)$ , compute the moments  $\bar{M}_n(t)$  from Eqs. 23, considering the beam to be elastic.
3. Evaluate

$$M_n^e(t) = \bar{M}_n(t) - \frac{EI}{h^2} \theta_n(t-k) \dots\dots\dots (39)$$



The moment  $M_n^e(t)$  is a combination of the moment at the joint  $n$  in our physical model if the structure were to undergo the deflections  $y_n(t)$  plus the effect of all previous plastic deformations up to the time step  $t - k$ .

4. Compare  $M_n^e(t)$  with the capacity moment of the beam,  $M_c(t)$ . If  $M_n^e(t) \leq M_c$ , then the beam has reentered the elastic stage at the point  $n$  and there is no further plastic flow at this joint in the interval  $t - k$  to  $t$ . If  $M_n^e(t) > M_c$ , an additional plastic flow occurs and the change in the plastic angle coordinate is given by

$$\begin{aligned} \frac{M_n^e(t)}{M_c} &\leq 1 & \Delta \theta_n(t - k) &= 0 \\ \frac{M_n^e(t)}{M_c} &> 1 & \Delta \theta_n(t - k) &= \left[ \frac{M_n^e(t) - M_c}{EI} \right] h^2 \dots (40) \end{aligned}$$

The plastic angle coordinate  $\theta_n(t)$  is then computed

$$\theta_n(t) = \theta_n(t - k) + \Delta \theta_n(t - k) \dots \dots \dots (41)$$

The moments  $M_n(t)$  which are to be used in Eqs. 25 to obtain the deflections of the beam in the next time step  $y_n(t + k)$ , become

$$M_n(t) = \begin{cases} M_n^e(t) & \text{if } \frac{M_n^e(t)}{M_c} \leq 1 \\ M_c & \text{if } \frac{M_n^e(t)}{M_c} > 1 \end{cases} \dots \dots (42)$$

#### MODE APPROACHES IN THE DYNAMIC ANALYSIS OF ELASTIC-PLASTIC STRUCTURES

*General Methods.*—A general method of analysis of elastic-plastic structures in which plastic flow may develop at various points in the structure, was presented<sup>7</sup> by Bleich and Mario G. Salvadori, F. ASCE. This method uses a normal mode of vibration approach; one expansion is used during the elastic stage and when the first plastic hinge appears, a new set of modes is used. Whenever a new plastic hinge appears, or a significant change in the location of a hinge occurs, different modes must be used. This is also true when a section reelasticizes or replastifies. The method is effective in relatively simple cases, particularly for symmetrical loadings in which only a single significant stationary plastic hinge occurs.

The method is impractical in more complicated problems where many significant plastic hinges occur, since the determination of the modes and the changes required to go from one set to another require considerable computational work. Moreover, convergence problems with the series of modes for determining the flexural moment make it extremely difficult to apply the method to structures which are loaded in such a manner that they reelasticize and re-

<sup>7</sup> "Impulse Motion of Elasto-Plastic Beams," by H. H. Bleich and M. G. Salvadori, *Transactions, ASCE*, Vol. 120, 1955, p. 499.

plasticize a number of times. A general mode approach which avoids some of these difficulties is available.<sup>5</sup>

For simple structures in which the location of a single significant plastic hinge can be postulated, the mode method has been used extensively in a further simplified version to be subsequently presented.

*Simplified Mode Analysis - One Mode Elastic Stage Followed by a Rigid Plastic One Hinge Stage.*—For relatively simple structures under appropriately simple time-dependent loadings (such as the simply supported beam loaded by a pressure which decays exponentially in time), a simple approximation to the general-mode method previously given has been widely used, in which only a single elastic mode is followed by a rigid-plastic one-hinge motion. This approximation, which might be called a "one degree of freedom" method, is easily derived from the general-mode method. The fundamental elastic mode of the beam is used during the elastic stage. At the instant that the maximum moment at the center of the beam reaches  $M_C$ , the fundamental mode of a simply sup-

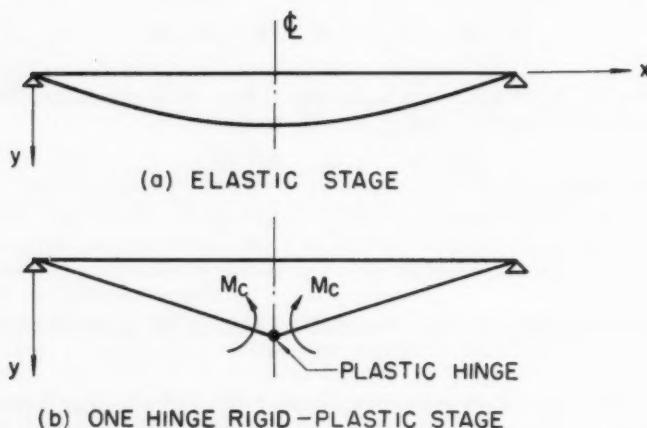


FIG. 6.—SIMPLIFIED MODE ANALYSIS (III-b)

ported beam with a yield hinge at the center is used. This plastic mode corresponds to a rigid body rotational motion (zero frequency) and hence to the rigid-plastic one hinge stage (Fig. 6).

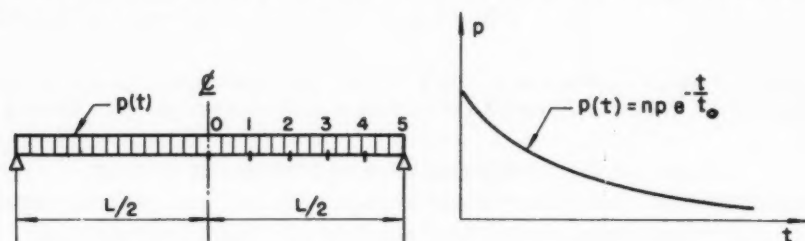
The conditions on velocity and displacement at the end of the elastic stage serve as initial conditions for the start of the rigid-plastic stage. Due to the fact that the motion of the simple beam is approximated in both the elastic and plastic stages by a single fundamental mode, the conservation of momentum requirement necessitates a jump in the velocity of magnitude  $4/\pi$  when determining the initial velocity for the plastic stage.

Computed results obtained by applying this simplified theory to the analysis of the simply supported beam will be shown in the subsequent section of this paper.

*Rigid Plastic Analysis.*—The dynamic analysis of elastic-plastic systems under loadings which produce fairly large plastic deformations may, under certain circumstances, be made in a sufficiently accurate and quite simple manner

by assuming the system to be composed of an ideal rigid-plastic material. The solution thus obtained neglects the elastic part of the displacement and the response predicted by this type of solution is accurate only if the plastic deformations are large compared to the elastic deformations. E. H. Lee and P. and S. Symonds, F. ASCE have presented<sup>8</sup> a general rigid plastic beam solution for initial velocity loadings, while a simplified one-hinge rigid-plastic analysis

TABLE 1.—EXPONENTIALLY DECAYING PRESSURE—FINITE DIFFERENCE METHOD



$p_0$  Static capacity load

$\Delta$  Static elastic deflection due to  $p_0$

$T$  Fundamental Period of beam

Effect of exponentially decaying pressure  $\left[ t_0 = \frac{T}{2} \right]$

n	Total Plastic Angle $\bar{\theta} \times 10^4$ in Radians					Ratio $\bar{\theta}_1/\bar{\theta}_0$	Maximum Deflection
	$\bar{\theta}_0$	$\bar{\theta}_1$	$\bar{\theta}_2$	$\bar{\theta}_3$	$\bar{\theta}_4$		
0.50	0	0	0	0	0	—	0.67 $\Delta$
0.75	3.5	0	0	0	0	0	1.01 $\Delta$
1.00	67	0.32	0	0	0	0.0048	1.56 $\Delta$
1.25	162	3.26	0	0	0	0.020	2.43 $\Delta$
1.50	319	0.98	0	0	0	0.0031	3.83 $\Delta$
1.75	515	10.01	0	0	0	0.0195	5.73 $\Delta$
2.00	747	35.5	7.6	0	0	0.048	8.30 $\Delta$
3.00	2560	92.3	26.3	0	0	0.034	25.9 $\Delta$
4.00	5860	127	4.7	0.24	0	0.022	57 $\Delta \approx L/6$
5.00	10200	370	5.2	12	0	0.037	100 $\Delta \approx L/4$

which also includes the effect of shear yielding was presented<sup>9</sup> by Salvadori and Paul Weidlinger, F. ASCE. The formulas for the rigid-plastic one-hinge analysis of the simply supported beam under consideration are given in detail by Salvadori and Weidlinger.<sup>9</sup> Comparative results of the analysis and the an-

<sup>8</sup> "Large Plastic Deformations of Beams Under Transverse Impact," by E. H. Lee and P. S. Symonds, Journal of Applied Mechanics, Transactions, ASME, Vol. 74, 1952, p. 308.

<sup>9</sup> "On the Dynamic Strength of Rigid-Plastic Beams Under Blast Loads," by M. G. Salvadori and P. Weidlinger, Proceedings, ASCE, Vol. 83, EM 4, October, 1957.

alysis considered in the two preceding sections of this paper are given in the following.

# NUMERICAL EXAMPLES AND COMPARISON OF RESULTS

*Finite Difference Method.*—The finite difference method is applied to the simply supported beam under the loading given in Eq. 1:

$$p(t) = n p_0 e^{-t/t_0} \dots\dots\dots (1)$$

in which the decay constant is  $t_0 = T/2$ ,  $T$  being the fundamental period of the elastic beam. Numerical results for various values of  $n$  are given in Table 1.

TABLE 2.—STEP PRESSURE  $np_0$ —FINITE DIFFERENCE METHOD

n	Total Plastic Angle $\bar{\theta}_i \times 10^4$ in radians					Ratio $\frac{\bar{\theta}_1}{\bar{\theta}_0}$	Maximum Deflection
	$\bar{\theta}_0$	$\bar{\theta}_1$	$\bar{\theta}_2$	$\bar{\theta}_3$	$\bar{\theta}_4$		
0.50	3.34	0	0	0	0	0	1.02Δ
0.75	146	0.40	0	0	0	.0027	2.28Δ
1.00	—	—	—	—	—	—	∞

TABLE 3.—COMPARISON OF MAXIMUM DEFLECTION EXPONENTIALLY  
DECAYING PRESSURE;  $p(t) = np_0 e^{-\frac{t}{t_0}}$

Load Factor $n =$	0.75	2	3	5	Type of Computer
Finite Difference Method	1.01Δ	8.3Δ	25.8	100Δ	Electronic
Simplified Analysis (One Mode Elastic State Followed by a Rigid-Plastic One Hinge Stage)	1Δ	6.8Δ	22.5Δ	90Δ	Desk
Rigid-Plastic Analysis (One-Hinge)	0	3.9Δ	19.7Δ	90Δ	

The total plastic angle  $\theta_i$  is given at various points on the beam,  $i = 0, 1, 2, 3$ , and 4. The maximum total midspan deflection due to the dynamic load  $p(t)$  is given in terms of the maximum static elastic midspan deflection  $\Delta$ , due to the capacity pressure  $p_0$ . It is of interest to note that for all values of  $n$ , the largest plastic angle is produced at midspan; this angle is significantly larger than the plastic angle at the other points on the beam.

Table 2 shows similar results for a constant step pressure loading of magnitude  $np_0$  for the values  $n = 0.50, 0.75$ , and 1.00. For values of  $n$  greater than 1.00, the deflection of the beam at midspan increases indefinitely with time.

*Comparison of Results.*—For the exponentially decaying loading, the results obtained from the finite difference analysis are compared in Table 3 with those obtained from the following simplified analyses:

1. A simplified elastic-plastic analysis consisting of a single mode elastic stage followed by a one hinge (at midspan) rigid plastic stage, that is the first elastic-plastic mode. (The simplified mode analysis presented in the preceding section.)

2. A single hinge (at midspan) rigid plastic analysis. (The rigid plastic analysis of the preceding section).

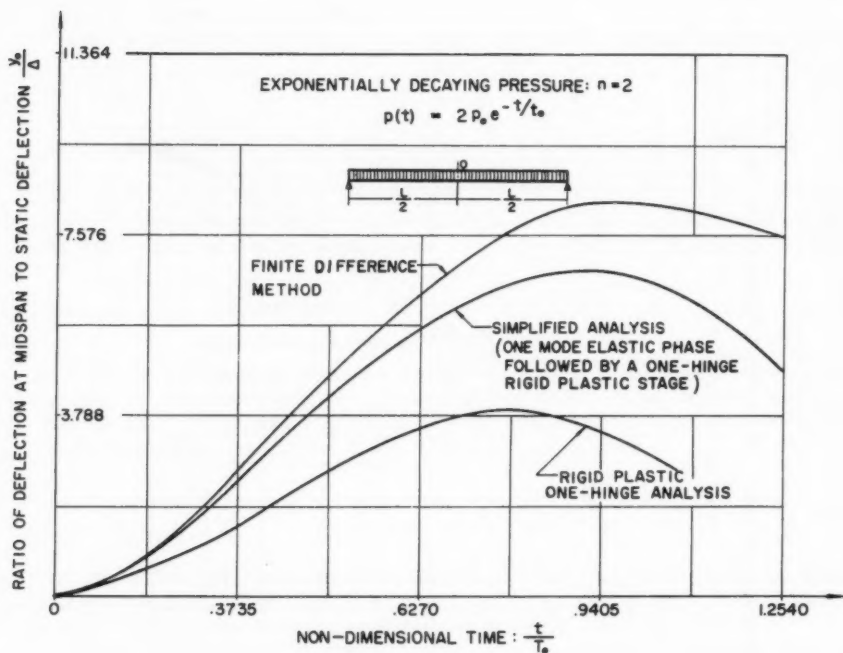


FIG. 7.—TYPICAL DISPLACEMENT-TIME CURVE

Typical deflection-time curves for the three cases are shown in Fig. 7 for the case of the amplification factor  $n = 2$ . Fig. 8 shows a curve of  $y_0 \text{ Max}/\Delta$  versus  $n$ ; this curve is obtained from the finite difference analysis results. Points for  $n = 0.75, 2.00, 3.00$ , and  $5.00$ , computed by the approximate analysis (1) and (2), are also shown on Fig. 8. The comparative results are shown in Table 3.

*General Conclusions.*—The numerical results that the authors have obtained from the finite difference method (Tables 1 and 2) have shown that a time-dependent loading, uniform in space over the beam, produces a single well defined point of large yielding at midspan. At this point, a major portion of the plastic

energy is absorbed, and consequently, additional yield hinges which may develop at other points on the structure at a later time, do not contribute substantially to the final deformation of the beam. This implies that a single plastic hinge can be assumed to form at midspan and a simplified one-hinge analysis will predict the maximum deflection with sufficient precision for many practical purposes. In the particular cases that have been examined, the simplified analyses result in deflections which are smaller than those obtained by the more elaborate and accurate finite difference analysis, which includes the effects of higher modes. It is not certain however that the simplified analysis will always show smaller deflections.

For more complex structures and loading situations, the simplified methods may give quite bad results. The authors have found that even for the relatively

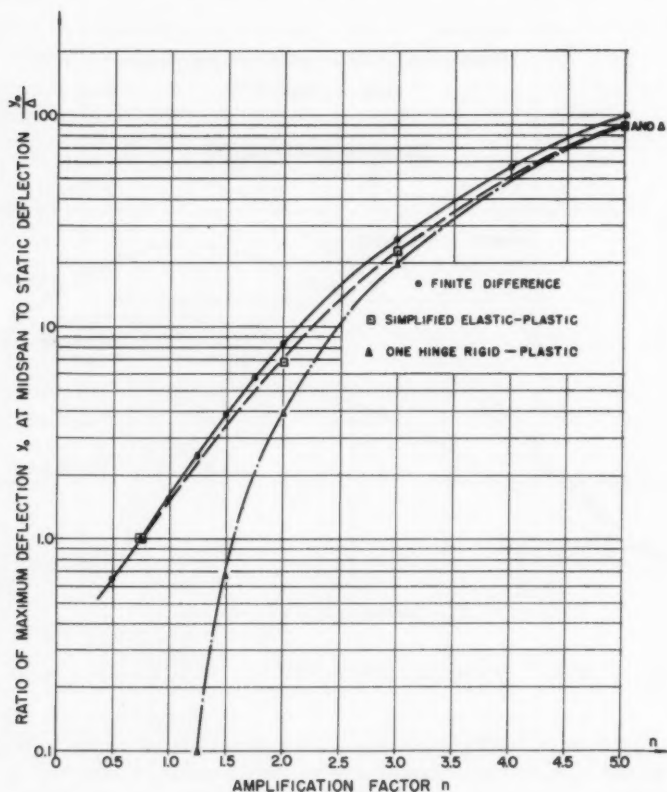


FIG. 8.—DEFLECTION RATIO  $\frac{y_0}{\Delta}$  VERSUS AMPLIFICATION "n"

simple case of a beam with cantilevers, the simplified methods may give results with significant errors. Generally, when a more complex distribution in space of the load is present, or where the strength of the structure is not constant along its centerline, higher modes of the structure may produce significant contributions to the deflection. In such cases, the elastic-plastic mode analysis becomes impracticable and the more powerful finite difference method must be

used. This method has been applied successfully by the authors to problems of the more complex type previously described.

## APPENDIX.—STABILITY OF THE NUMERICAL INTEGRATION

The stability of the numerical integration in time of the equations of motion, Eqs. 21, 22a and 22b, is considered with a view towards determining the maximum value of the time step  $k$  for which the solution will not diverge with an increasing number of time steps.

Eq. 21 is conveniently written in terms of the displacements alone (Eqs. 15).

$$\left[ \frac{m_n + m_{n+1}}{2} \right] \ddot{y}_n + \frac{EI}{h^4} \delta^4 y_n = \frac{q_n + q_{n+1}}{2}; \quad n = 0, 1, 2, 3, 4 \dots \quad (15)$$

The solution of these equations of motion of the beam in Fig. 2 is equivalent to a modal analysis of the lumped mass beam having five symmetrical modes of vibration. Eq. 15 can be transformed into a set of five equations of the form

$$\ddot{Y}_n + \omega_n^2 Y_n = \frac{Q_n}{M_n}; \quad n = 0, 1, 2, 3, 4 \dots \dots \dots (43)$$

in which  $\omega_n$  is the frequency of vibration of the  $n$ th mode of the lumped mass system,  $M_n$  is a constant, and  $Q_n$  is a linear combination of the loads  $q_n(t)$ . The stability criterion for the solution of this system of equations,<sup>10</sup> using the finite difference substitution of Eq. (23) for  $\ddot{Y}_n$ , requires

$$k_{\max} < \frac{T_n}{\pi} = \frac{2}{\omega_n} \dots \dots \dots (44)$$

For the present problem, the shortest period,  $T_4$ , of the beam with the lumped masses controls. This period is approximately equal to the period of the fifth symmetrical mode of vibration of the beam with distributed mass.

A stable solution does not imply accuracy, which is also dependent on the accumulation of round-off errors in the various stages of the analysis. A considerably smaller value of  $k$  than that given by Eq. 44,  $k_{\max} < \frac{T_4}{\pi}$ , should be used in the numerical computations.

## APPENDIX II.—NOTATION

E = modulus of elasticity of beam material

<sup>10</sup> "Numerical Methods in Engineering," by M. G. Salvadori and M. L. Baron, Prentice Hall, 2nd Ed., 1955, pp. 121-132, Problem 3.99.



$I$	=	moment of inertia of beam cross section
$M$	=	moment
$m$	=	mass per unit length of span
$np_0$	=	initial value of dynamic load at time $t = 0$
$p$	=	static capacity load which will produce yielding in the structure
$T$	=	fundamental period of elastic beam
$t_0$	=	decay constant
$y$	=	deflection, positive downward
$y_n^c$	=	displacement at joint $n$ due to the corrective displacement for plasticity at the joint $j$
$\Delta$	=	static elastic deflection
$\theta_j$	=	a generalized coordinate proportional to the angle of the plastic kink at the joint $n = j$
$\psi_{jn}$	=	deflection curve at the points $n$ of a fictional elastic beam if a hinge were introduced at the point $x = x_j$ and the two portions of the structure on either side of the point were rotated by a certain angle
$\omega_n$	=	frequency of vibration of the $n^{\text{th}}$ mode of the lumped mass system



---

Journal of the  
ENGINEERING MECHANICS DIVISION  
Proceedings of the American Society of Civil Engineers

---

VISCOELASTIC PLATE ON A VISCOELASTIC FOUNDATION

By Karl S. Pister,<sup>1</sup> M. ASCE

---

SYNOPSIS

Axisymmetric bending of a viscoelastic plate of finite thickness supported by a viscoelastic foundation of infinite extent is examined. Assuming frictionless interface conditions, a formal solution of the problem is obtained by the use of iterated integral transforms. An example involving the method of computation is presented.

---

INTRODUCTION

The analysis of plates on a deformable foundation rests on assumptions concerning the behavior of the plate-foundation system. These assumptions involve: (1) System of equations by which the plate behavior is defined, (2) description of the foundation, that is, whether a solid continuum or a set of independent or partially interconnected individual elements, and (3) conditions to be met at the plate-foundation interface (full continuity of displacement, frictionless or an intermediate condition). In view of these factors many theories of behavior have appeared. Among these may be cited the papers of Hertz for a thin plate on a Winkler foundation, D. L. Holl for a thin plate on an elastic half-space, Szabo for a thick plate on an elastic half-space, and P. M. Naghdi and J. C. Rowley for a thick plate on a Winkler foundation. A short bibliography of such works has been presented by S. Timoshenko and S. Woinowsky-Krieger.<sup>2</sup> Avoiding a detailed review of previous work in this

---

Note.—Discussion open until July 1, 1961. To extend the closing date one month, a written request must be filed with the Executive Secretary, ASCE. This paper is part of the copyrighted Journal of the Engineering Mechanics Division, Proceedings of the American Society of Civil Engineers, Vol. 87, No. EM 1, February, 1961.

<sup>1</sup> Assoc. Prof. of Civ. Engrg., Univ. of California, Berkeley, Calif.

<sup>2</sup> "Theory of Plates and Shells," by S. Timoshenko and S. Woinowsky-Krieger, McGraw-Hill Book Co., Inc., New York, 2nd Ed., 1959, p. 281.

area, it may be noted that the thin plate theory (Poisson-Kirchhoff) is inadequate for treating problems involving localized surface loads. The thick plate theory within the framework of three-dimensional elastic theory involves cumbersome mathematics, and the Winkler foundation does not permit examination of stress conditions in the foundation itself.

This paper treats the problem of axisymmetric bending of a thick plate of infinite extent resting on a semi-infinite solid. In order to retain the analytical advantages of a two-dimensional plate theory, the theory of E. Reissner, which includes the effects of transverse normal and shearing stresses, is adopted. The Boussinesq solution for surface loading of a half-space along with the assumption of a frictionless interface completes the description of the plate-foundation system. In order to account for the possibility of viscoelastic material properties in the plate and foundation, the well-known correspondence principle relating linear elastic and viscoelastic boundary value problems is utilized.

*Notation.*—The letter symbols adopted for use in this paper are defined where they first appear, in the illustrations or in the text, and are arranged alphabetically, for convenience of reference, in the Appendix.

### EQUATIONS FOR THE PLATE

The equations describing Reissner's theory of bending of plates on an elastic foundation of the Winkler type have been extensively presented elsewhere.<sup>3,4,5</sup> Here, it will be sufficient to restate the necessary equations in a

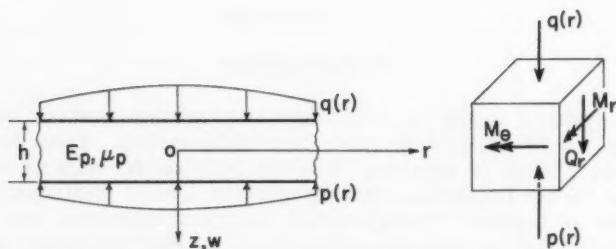


FIG. 1.—AXISYMMETRICALLY LOADED PLATE AND PLATE ELEMENT

form suitable for application to the problem of axisymmetric bending of a plate resting on an elastic half-space. Using notation defined by Timoshenko

<sup>3</sup> "On the Bending of Axially Symmetric Plates on Elastic Foundations," by P. M. Naghdi and J. C. Rowley, Proceedings, First Midwestern Conf. on Solid Mechanics, Univ. of Illinois, 1953, pp. 119-123.

<sup>4</sup> "Thick Rectangular Plates on an Elastic Foundation," by D. Frederick, *Transactions*, ASCE, Vol. 122, 1957, pp. 1069-1087.

<sup>5</sup> "On Some Problems in Bending of Thick Circular Plates on an Elastic Foundation," by D. Frederick, *Transactions*, ASME, Vol. 78, 1956, pp. 195-200.

and Woinowsky-Krieger<sup>2</sup> and shown in Fig. 1, the plate middle surface deflection satisfies the equation

$$D \nabla^4 w + \beta h^2 \nabla^2 (q - p) - (q - p) = 0 \dots \dots \dots (1)$$

in which

$$\nabla^2 = \frac{\partial^2}{\partial r^2} + \frac{1}{r} \frac{\partial}{\partial r} \dots \dots \dots (2a)$$

and

$$\beta = \frac{2 - \mu_p}{10(1 - \mu_p)} \dots \dots \dots (2b)$$

In these equations  $w$  represents the vertical displacement of the plate's middle surface;  $q$  is the transverse surface pressure on the plate;  $p$  is the pressure at plate-foundation interface;  $h$  denotes the plate thickness; and  $\mu$  represents Poisson's ratio. Anticipation of the time dependence of the deflection for viscoelastic problems accounts for the retention of partial derivatives in the axisymmetric Laplacian operator.

The stress-couples are given by

$$M_r = -D \left( w_{,rr} + \frac{\mu_p}{r} w_{,r} \right) + \frac{h^2}{5} Q_{r,r} - \frac{\mu_p h^2}{10(1 - \mu_p)} (q - p) \dots \dots (3)$$

and

$$M_\theta = -D \left( \frac{1}{r} w_{,r} + \mu_p w_{,rr} \right) + \frac{h^2}{5r} Q_r - \frac{\mu_p h^2}{10(1 - \mu_p)} (q - p) \dots \dots (4)$$

and the transverse shear stress resultant by

$$Q_r = -\frac{1}{r} \int_0^r [q(\rho) - p(\rho)] \rho \, d\rho \dots \dots \dots (5)$$

Flexural stresses  $\sigma_r$ ,  $\sigma_\theta$ , transverse shearing stress  $\tau_{rz}$ , and transverse normal stress  $\sigma_z$ , are obtained from  $M_r$ ,  $M_\theta$ ,  $Q_r$ ,  $q$  and  $p$  in the usual manner for the Reissner theory.

Boundary conditions associated with Eq. 1 have been examined previously.<sup>3,4,5</sup> In the present problem for a plate of infinite extent, the middle surface deflection and appropriate combinations of its derivatives must vanish at infinity.

#### EQUATIONS FOR THE ELASTIC HALF-SPACE

To complete the formulation of the plate bending problem, an expression for the surface displacement of an elastic half-space subjected to an axisymmetric normal pressure is required. For the present purposes the solution of the problem is most conveniently expressed in the form given by Tereza-wa.<sup>6</sup> Referring to Fig. 2 the surface deflection is

$$w(r) = \frac{1}{k} \int_0^\infty \bar{p}(\alpha) J_0(\alpha r) \alpha \, d\alpha \dots \dots \dots (6)$$

<sup>6</sup> "Fourier Transforms," by I. N. Sneddon, McGraw-Hill Book Co., Inc., New York, 1951, p. 470, (a) pp. 60-62 (b) p. 528.

in which

$$k = \frac{E_f}{2(1 - \mu_f^2)} \dots\dots\dots (7)$$

and

$$\bar{p}(\alpha) = \int_0^\infty p(r) \, r \, J_0(\alpha \, r) \, dr \dots\dots\dots (8)$$

is the Hankel transform of zero order of the surface pressure  $p(r)$ . The stresses and displacements in the interior of the half-space are expressible in a similar form. Because attention is focused, herein, on plate behavior,

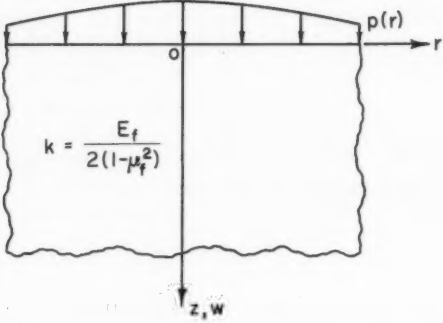


FIG. 2.—AXISYMMETRICALLY LOADED HALF-SPACE

the reader is referred to the work of I. N. Sneddon<sup>6</sup> for further details concerning the computation of stresses and displacements in the half-space, once the surface pressure is determined.

ELASTIC PLATE ON ELASTIC FOUNDATION

From the previously stated equations, it is possible to obtain axisymmetric solutions of an elastic plate-foundation system. A frictionless interface condition is assumed, and the plate middle-surface displacement is set equal to the surface displacement of the foundation. Operating on Eq. 1 with the Hankel transform

$$D \, \alpha^4 \bar{w}(\alpha) - \beta \, h^2 \, \alpha^2 [\bar{q}(\alpha) - \bar{p}(\alpha)] - [\bar{q}(\alpha) - \bar{p}(\alpha)] = 0 \dots\dots\dots (9)$$

in which  $D$  refers to the plate thickness and

$$\bar{w}(\alpha) = \int_0^\infty w(r) \, r \, J_0(\alpha \, r) \, dr \dots\dots\dots (10)$$

is the Hankel transform of the plate deflection  $w(r)$ . (In this paper "Hankel transform" is to be understood as Hankel transform of zero order.) The terms  $\bar{q}(\alpha)$ ,  $\bar{p}(\alpha)$  are obtained in the same fashion. To obtain Eq. 9 we have assumed the following properties of the solution:  $rw$ ,  $rw_{,r}$ ,  $r \nabla^2 w$ , and  $(r \nabla^2 w)_{,r}$  tend to zero as  $r$  approaches zero or infinity.<sup>6a</sup> A comma followed by a subscript indicates partial differentiation with respect to the subscript.

Rearranging Eq. 9 leads to

$$\bar{p}(\alpha) = \frac{\bar{q}(\alpha) [1 + \beta h^2 \alpha^2] - D \alpha^4 \bar{w}(\alpha)}{1 + \beta h^2 \alpha^2} \dots \dots \dots (11)$$

Substituting Eq. 11 into Eq. 6 gives

$$w(r) = \frac{1}{k} \int_0^\infty \left\{ \frac{\bar{q}(\alpha) [1 + \beta h^2 \alpha^2] - D \alpha^4 \bar{w}(\alpha)}{1 + \beta h^2 \alpha^2} \right\} J_0(\alpha r) d\alpha \dots (12)$$

The Hankel inversion integral (inverse of Eq. 10) gives another expression for  $w(r)$

$$w(r) = \int_0^\infty \left\{ \alpha \bar{w}(\alpha) \right\} J_0(\alpha r) d\alpha \dots \dots \dots (13)$$

Inasmuch as Eqs. 12 and 13 are equivalent for all values of  $r$ , the bracketed expressions must be equal. Accordingly,

$$\bar{w}(\alpha) = \frac{\bar{q}(\alpha) [1 + \beta h^2 \alpha^2]}{\alpha k [1 + \beta h^2 \alpha^2 + \frac{D}{k} \alpha^3]} \dots \dots \dots (14)$$

Inversion of Eq. 14 yields

$$w(r) = \frac{1}{k} \int_0^\infty \frac{\bar{q}(\alpha) [1 + \beta h^2 \alpha^2] J_0(\alpha r) d\alpha}{1 + \beta h^2 \alpha^2 + \frac{D}{k} \alpha^3} \dots \dots (15)$$

In this equation  $\bar{q}(\alpha)$ , the Hankel transform of the applied load on the plate is obtained from

$$\bar{q}(\alpha) = \int_0^\infty q(r) r J_0(\alpha r) dr \dots \dots \dots (16)$$

At this stage it is convenient to introduce the following notation to non-dimensionalize the system parameters:

$$l_0^3 = \frac{D}{k} \dots \dots \dots (17a)$$

and

$$\lambda = \alpha l_0 \dots \dots \dots (17b)$$

Eq. 15 then assumes the form

$$w\left(\frac{r}{l_0}\right) = \frac{l_0^2}{D} \int_0^\infty \frac{\bar{q}\left(\frac{\lambda}{l_0}\right) \left[1 + \beta \frac{h^2 \lambda^2}{l_0^2}\right] J_0\left(\frac{\lambda r}{l_0}\right) d\lambda}{1 + \frac{\beta h^2 \lambda^2}{l_0^2} + \lambda^3} \dots (18)$$

For prescribed plate loading  $q(r)$ , value of Poisson's ratio for the plate (from which  $\beta$  is computed), and thickness parameter  $h/l_0$ , the formal solution for the deflection of the plate is complete. The Hankel transform of the interface pressure can be found by substituting Eq. 14 into Eq. 11. The result is

$$\bar{p}(\alpha) = \frac{\bar{q}(\alpha) \left[ 1 + \beta h^2 \alpha^2 \right]}{1 + \beta h^2 \alpha^2 + \frac{D}{k} \alpha^3} \dots\dots\dots (19)$$

Using Eqs. 17 and the Hankel inversion theorem,

$$p\left(\frac{r}{l_0}\right) = \frac{1}{l_0^2} \int_0^\infty \frac{\bar{q}\left(\frac{\lambda}{l_0}\right) \left[ 1 + \beta \frac{h^2 \lambda^2}{l_0^2} \right] \lambda J_0\left(\frac{\lambda r}{l_0}\right) d\lambda}{1 + \beta \frac{h^2 \lambda^2}{l_0^2} + \lambda^3} \dots\dots (20)$$

Returning now to Eq. 5, a solution for the shear resultant  $Q_r$  can be obtained by substituting Eq. 20 into Eq. 5 and interchanging the order of integration. After some manipulation

$$Q_r\left(\frac{r}{l_0}\right) = -\frac{1}{r} \int_0^r q(\rho) \rho d\rho + \frac{1}{l_0} \int_0^\infty \frac{\bar{q}\left(\frac{\lambda}{l_0}\right) \left[ 1 + \beta \frac{h^2 \lambda^2}{l_0^2} \right] J_1 \frac{\lambda r}{l_0} d\lambda}{1 + \beta \frac{h^2 \lambda^2}{l_0^2} + \lambda^3} \dots\dots (21)$$

To evaluate the bending moments from Eqs. 3 and 4,  $Q_{r,r}$  is needed. Differentiating Eq. 21 and simplifying gives

$$\begin{aligned} Q_{r,r} = & \frac{1}{r^2} \int_0^r q(\rho) \rho d\rho - q(r) \\ & + \frac{1}{l_0^2} \int_0^\infty \frac{q\left(\frac{\lambda}{l_0}\right) \left[ 1 + \beta \frac{h^2 \lambda^2}{l_0^2} \right] \left[ J_0\left(\frac{\lambda r}{l_0}\right) - \frac{l_0}{\lambda r} J_1\left(\frac{\lambda r}{l_0}\right) \right] \lambda d\lambda}{1 + \beta \frac{h^2 \lambda^2}{l_0^2} + \lambda^3} \dots\dots (22) \end{aligned}$$

Appropriate differentiation of Eq. 18 and substitution into Eq. 3 gives the radial bending moment:

$$\begin{aligned} M_r\left(\frac{r}{l_0}\right) = & l_0^2 \int_0^\infty \frac{\bar{q}\left(\frac{\lambda}{l_0}\right) \left[ 1 + \beta \frac{h^2 \lambda^2}{l_0^2} \right]}{1 + \beta \frac{h^2 \lambda^2}{l_0^2} + \lambda^3} \left\{ \frac{\lambda^2}{l_0^2} J_0\left(\frac{\lambda r}{l_0}\right) - \frac{(1 - \mu_p) \lambda}{l_0 r} J_1\left(\frac{\lambda r}{l_0}\right) \right\} d\lambda \\ & + \frac{h^2}{5} Q_{r,r} - \frac{\mu_p h^2}{10(1 - \mu_p)} (q - p) \dots\dots\dots (23) \end{aligned}$$

All terms appearing in this expression have now been determined. A similar expression can be written for  $M_\theta$ . Since the twisting moment  $M_{r\theta}$  and shear resultant  $Q_\theta$  vanish, this completes the formal solution for the elastic plate on elastic foundation.

It may be noted in passing that when the parameter  $h/l_0 \rightarrow 0$  in Eq. 23, the solution for the Poisson-Kirchhoff plate on elastic foundation is recovered. This form of solution has been previously given by Holl<sup>7</sup> and Woinowsky-Krieger.<sup>8</sup>

### VISCOELASTIC PLATE ON VISCOELASTIC FOUNDATION

In the instance that the plate, foundation or both are assumed to exhibit linear viscoelastic behavior, the preceding analysis is readily extended. Direct application of the correspondence principle relating elastic and viscoelastic boundary value problems leads immediately to the formal solution of the problem.

Assuming an operator-type stress-strain law for plate and foundation,<sup>9</sup> and following the correspondence principle, we replace the elastic coefficients appearing in all of the previous equations by the Laplace transforms of the viscoelastic operators. At the same time the surface load, now a function of time, as well as all other dependent variables are replaced by their Laplace transforms with respect to time.

Denoting the Laplace transform of  $w(r, t)$  by  $\bar{w}(r, s)$ , we recall

$$\bar{w}(r, s) = \int_0^\infty w(r, t) e^{-st} dt \dots \dots \dots (24)$$

under suitable restrictions on the function  $w(r, t)$ . Denote the Laplace transforms of the plate and foundation time-dependent stiffness operators by  $\bar{D}(s)$  and  $\bar{k}(s)$ , respectively, and the transform of the plate parameter  $\beta$  by  $\bar{\beta}(s)$ . Then the correspondence principle leads from Eq. 15 to the following expression for the Laplace transform of the plate deflection:

$$\bar{w}(r, s) = \int_0^\infty \frac{\bar{q}(\alpha, s) \left[ 1 + \bar{\beta}(s) h^2 \alpha^2 \right] J_0(\alpha r) d\alpha}{\bar{k}(s) \left[ 1 + \bar{\beta}(s) h^2 \alpha^2 + \frac{\bar{D}(s)}{\bar{k}(s)} \alpha^3 \right]} \dots \dots \dots (25)$$

In a similar manner Eq. 19 and the Hankel inversion theorem gives the Laplace transform of the foundation interface pressure:

$$\bar{p}(r, s) = \int_0^\infty \frac{\bar{q}(\alpha, s) \left[ 1 + \bar{\beta}(s) h^2 \alpha^2 \right] \alpha J_0(\alpha r) d\alpha}{1 + \bar{\beta}(s) h^2 \alpha^2 + \frac{\bar{D}(s)}{\bar{k}(s)} \alpha^3} \dots \dots (26)$$

<sup>7</sup> "Thin Plates on Elastic Foundations," by D. L. Holl, Proceedings, Fifth Internatl. Congress of Applied Mechanics, Cambridge, Mass., 1938, pp. 71-74.

<sup>8</sup> "Biegung dünner rechteckiger Platten durch Kreislasten," by S. Woinowsky-Krieger, Ing. Archiv., Vol. 3, 1932, p. 250.

<sup>9</sup> "Rheology, Theory and Applications," by F. R. Eirich, Vol. 1, Academic Press, New York, 1956, p. 400.



The term  $\bar{q}(\alpha, s)$  is the iterated Hankel-Laplace transform of the surface pressure on the plate. Similar expressions can be written for the shear resultant and bending moments, replacing Eqs. 21, 22, and 23. In actually performing the inverse transformations to recover the time and space dependent variables, it is expedient to compute the inverse Laplace transform before performing the Hankel inversion. Inasmuch as the Laplace transforms of the viscoelastic operators  $\bar{D}(s)$ ,  $\bar{K}(s)$ ,  $\bar{\beta}(s)$  are expressed as polynomials, the Laplace inversion involves, in general, inversion of the ratio of rational functions. On the other hand, performing the Hankel inversion first, if at all possible in closed form, invariably leads to a difficult integration in the complex plane. This feature of the solution of axisymmetric problems in viscoelasticity by transform methods has been noted by Naghdi and W. C. Orthwein.<sup>10</sup> In the following section an example will clarify the details of the procedure previously outlined.

### INFINITE VISCOELASTIC PLATE UNIFORMLY LOADED OVER A CIRCULAR AREA

As an example of the method of solution, the problem of an infinite plate uniformly loaded over a circular area will be treated. Maxwell-type viscoelastic properties will be assumed for plate and foundation. Furthermore, in the interest of simplicity, the plate and foundation will be taken as incompressible,  $\mu_p = \mu_f = 1/2$ . Accordingly,

$$\bar{D}(s) = \frac{D s}{\tau_p^{-1} + s}, \quad D = \frac{E_p h^3}{12(1 - \mu_p^2)} \dots \dots \dots (27a)$$

$$\bar{K}(s) = \frac{k s}{\tau_f^{-1} + s}, \quad k = \frac{E_f}{2(1 - \mu_f^2)} \dots \dots \dots (27b)$$

and

$$\bar{\beta}(s) = \beta = \frac{3}{10} \dots \dots \dots (27c)$$

The terms  $\tau_p$ ,  $\tau_f$  are relaxation times for the plate and foundation, respectively. The surface pressure is given by

$$q(r, t) = \begin{cases} q H(t), & 0 \leq r \leq a \\ 0, & a < r \end{cases} \dots \dots \dots (28)$$

in which  $H(t)$  is the unit step function. The iterated Hankel-Laplace transform of  $q(r, t)$  for this case is<sup>8b</sup>

$$\bar{q}\left(\frac{\lambda}{l_0}, s\right) = \frac{q a l_0}{\lambda s} J_1\left(\frac{\lambda a}{l_0}\right) \dots \dots \dots (29)$$

Substituting Eqs. 27 and 29 into Eqs. 25 and 26 and recalling the definitions of  $l_0$  and  $\lambda$  leads to expressions for which the Laplace inversion is readily performed.

<sup>10</sup> "Response of Shallow Viscoelastic Spherical Shells to Time-Dependent Axisymmetric Loads," by P. M. Naghdi and W. C. Orthwein, Quarterly of Applied Mathematics, Vol. 18, Providence, R. I., July, 1960, pp. 107-121.



Omitting the details of the computation, the final results are

$$w\left(\frac{r}{l_0}, \frac{t}{\tau_p}\right) = \frac{q l_0^4}{D} \cdot \frac{a}{l_0} \int_0^\infty \frac{\left[1 + \beta \frac{h^2 \lambda^2}{l_0^2}\right] J_1\left(\frac{\lambda a}{l_0}\right) J_0\left(\frac{\lambda r}{l_0}\right) \langle 1 \rangle d\lambda}{\lambda \left[1 + \beta \frac{h^2 \lambda^2}{l_0^2} + \lambda^3\right]} \dots (30)$$

in which

$$\langle 1 \rangle \equiv e^{-\frac{t}{\tau_p} \frac{F_2}{F_1}} + \left(1 - e^{-\frac{t}{\tau_p} \frac{F_2}{F_1}}\right) \frac{F_1}{F_2} \left[1 + \frac{\tau_p}{\tau_f} \left(1 - \frac{F_1}{F_2}\right)\right] + \frac{F_1}{F_2} \frac{\tau_p}{\tau_f} \frac{t}{\tau_p} \dots (31)$$

and

$$F_1 \equiv 1 + \beta \frac{h^2 \lambda^2}{l_0^2} + \lambda^3, \quad F_2 \equiv 1 + \beta \frac{h^2 \lambda^2}{l_0^2} + \frac{\tau_p}{\tau_f} \lambda^3 \dots (32)$$

Similarly,

$$p\left(\frac{r}{l_0}, \frac{t}{\tau_p}\right) = \frac{qa}{l_0} \int_0^\infty \frac{\left[1 + \beta \frac{h^2 \lambda^2}{l_0^2}\right] J_1\left(\frac{\lambda a}{l_0}\right) J_0\left(\frac{\lambda r}{l_0}\right) \langle 2 \rangle d\lambda}{1 + \beta \frac{h^2 \lambda^2}{l_0^2} + \lambda^3} \dots (33)$$

in which

$$\langle 2 \rangle \equiv e^{-\frac{t}{\tau_p} \frac{F_2}{F_1}} + \frac{F_1}{F_2} \left(1 - e^{-\frac{t}{\tau_p} \frac{F_2}{F_1}}\right) \dots (34)$$

In the same manner, expressions for the transverse shear resultant and bending moments can be obtained from Eqs. 22 and 23.

Inasmuch as closed form representations of the integrals appearing in the formal solution of the problem are not available, evaluation of the integrals has been carried out on a computer using FORTRAN programming for a number of cases of interest.

### NUMERICAL EXAMPLE

The evaluation of maximum deflection and maximum interface pressure was carried out for the preceding example by numerical integration, using Simpson's Rule, of Eqs. 30 and 33, with  $r = 0$ . The geometric parameters in the problem were taken to be  $\frac{h}{l_0} = \frac{a}{l_0} = 1$ . Computations were performed for  $\frac{t}{\tau_p} = 0, 5, 10, 20$  for values of  $\tau_p/\tau_f = 0, 0.10, 1.0, 10.0$ . The results of these computations are shown in Figs. 3 and 4. Referring first to Fig. 3, it is interesting to note that for the case  $\tau_p/\tau_f = 0$ , corresponding to a viscoelastic plate on elastic foundation, the maximum deflection is quickly attained. As the ratio  $\tau_p/\tau_f$  increases to 1.0, the response becomes largely linearly viscoelastic. In Fig. 4 it may be noted that for the case  $\frac{\tau_p}{\tau_f} = 1$ , the pressure corre-

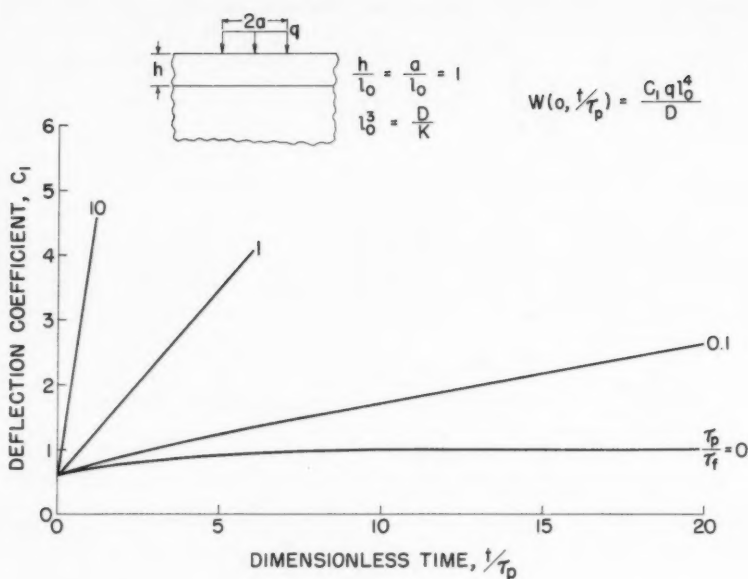


FIG. 3.—CENTER DEFLECTION VS. TIME FOR VISCOELASTIC PLATE ON VISCOELASTIC FOUNDATION

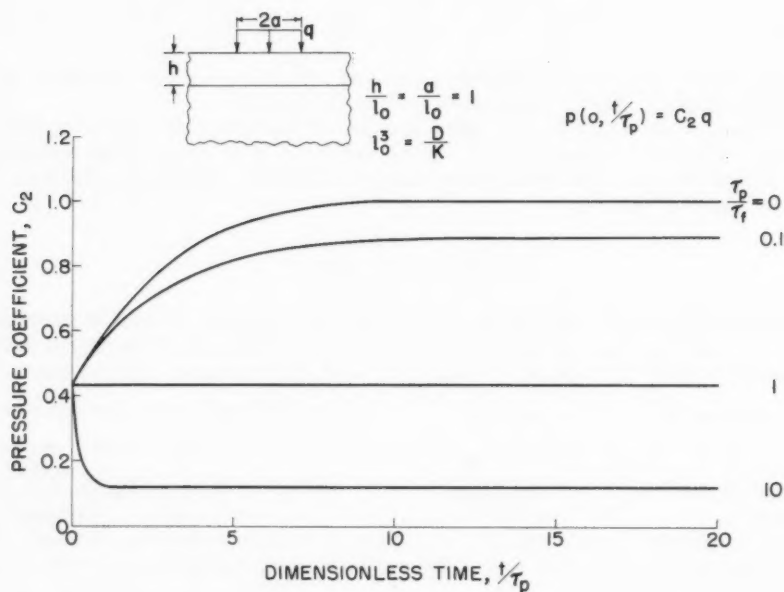


FIG. 4.—MAXIMUM INTERFACE PRESSURE VS. TIME FOR VISCOELASTIC PLATE ON VISCOELASTIC FOUNDATION

sponding to an elastic plate on elastic foundation is attained and maintained as the plate and foundation relax. Returning to the case of a viscoelastic plate on elastic foundation ( $\tau_p/\tau_f = 0$ ), a limit evaluation of Eqs. 30 and 33 gives

$$\left. \begin{aligned} w\left(0, \frac{t}{\tau_p}\right) &\rightarrow \frac{qa}{k} = \frac{2qa}{E_f} \frac{1 - \nu_f^2}{2} \text{ as } t \rightarrow \infty \\ p\left(0, \frac{t}{\tau_p}\right) &\rightarrow q \text{ as } t \rightarrow \infty \end{aligned} \right\} \dots\dots\dots (35)$$

Thus, in the limit the plate is completely relaxed and the system behaves as if the load were applied directly to the foundation.

Another limiting case appears if  $\tau_p/\tau_f = \infty$ , corresponding to an elastic plate on a viscoelastic foundation. The related problem of a thin plate ( $\beta = 0$ ) on a Winkler foundation ( $k = p/w$ ) has been studied by B. C. Hoskin and E. H. Lee.<sup>11</sup>

### SUMMARY

A method of solution of axisymmetric bending problems for plates on a deformable foundation has been presented. The plate theory incorporates the effect of transverse shear deformation, and the possibility of viscoelastic material properties in both plate and foundation is included. Using integral transform methods the deflection, interface pressure, and plate bending moments are expressible in terms of integrals containing geometric, viscoelastic, and dimensionless time parameters. This form of solution, in contrast to direct solution of the differential equations governing the system, is particularly suited to numerical computation. For selected values of geometric variables, a parameter study for viscoelastic and time variables is readily carried out. It should be pointed out that the integrals arising in computation of the bending moments in the plate are slowly convergent and asymptotic expansions of the Bessel functions occurring in the integrands is required.

Finally it may be noted that a Maxwell-type viscoelastic model is unsuited for describing the long-time behavior of a physical system and is used here only for convenience of illustration.

### ACKNOWLEDGMENTS

The author is indebted to R. A. Westmann, A.M. ASCE for assistance in checking the equations and in preparation of the manuscript and to I. Mitroff

<sup>11</sup> "Analysis of Flexible Surfaces over Subgrades with Viscoelastic Material Behavior," by B. C. Hoskin and E. H. Lee, Proceedings, ASCE, Vol. 85, No. EM 4, October, 1959, pp. 11-30.

for programming the numerical computations. This work was supported in part by a grant from the California Research Corporation, Richmond, Calif.

---

#### APPENDIX.—NOTATION

---

The following symbols, adopted for use in the paper, conform essentially with "American Standard Letter Symbols for Structural Analysis" (ASA Z110.8-1949) prepared by a committee of the American Standards Association with Society representation, and approval by the Association in 1949:

$D$	= plate stiffness
$E$	= modulus of elasticity
$h$	= plate thickness
$J_n$ ; $n = 0, 1$	= Bessel function of first kind of order $n$
$l_0$	= characteristic length of plate-foundation system
$M_r, M_\theta$	= radial and tangential bending moments
$p$	= pressure at plate-foundation interface
$Q_r$	= radial transverse shear stress resultant
$q$	= transverse surface pressure on the plate
$s$	= Laplace transform parameter
$w$	= vertical displacement of plate middle surface
$\alpha$	= Hankel transform parameter
$\mu$	= Poisson's ratio
$\tau$	= relaxation time

---

Journal of the  
ENGINEERING MECHANICS DIVISION  
Proceedings of the American Society of Civil Engineers

---

MOIRÉ FRINGES AS A MEANS OF ANALYSING STRAINS

By C. A. Sciammarella<sup>1</sup> and A. J. Durelli<sup>2</sup>

---

SYNOPSIS

The objective of this paper is to show the application of moiré fringes in the determination of strains in two-dimensional models. The moiré pattern is interpreted as a function of displacements only from which strains in the Lagrangian and Eulerian descriptions are determined. This presentation is not limited to small deformations, and sets of formulas appropriate for every case are given here.

---

INTRODUCTION

In recent years, moiré fringes have found increasing application in the field of stress analysis. Two are the main fields of application, deflections of plates and strains in two dimensional problems. In this paper attention is focused from moiré data on the latter.

In order to obtain strains, two different approaches have been followed, one that can be called "geometrical" and the other which consists in relating the fringes to the displacement field. The purpose of this paper is to present this last approach in the most general form.

The "geometrical" interpretation seems to have been originated in a paper published in Dutch in 1945 by D. Tollenard,<sup>3</sup> and was applied for the first time

---

Note.—Discussion open until July 1, 1961. To extend the closing date one month, a written request must be filed with the Executive Secretary, ASCE. This paper is part of the copyrighted Journal of the Engineering Mechanics Division, Proceedings of the American Society of Civil Engineers, Vol. 87, No. EM 1, February, 1961.

<sup>1</sup> Assoc. Research Engr., Illinois Inst. of Technology, Chicago, Ill.

<sup>2</sup> Prof. Civ. Engrg., Illinois Inst. of Technology, Chicago, Ill.

<sup>3</sup> "Moiré—Interferentieverschijnselen bij rasterdruk," by D. Tollenaar, Amsterdam Instituut voor Grafische Techniek, 1945.

to the subject of the strain determination in 1952 by J. K. Kaczer and F. Kroupa<sup>4</sup> of the Physics Institute of the Charles University in Prague.

The basic idea behind the "geometrical approach" is the following. Moire fringes are formed by two interfering line screens. One is printed in the model and is subjected to deformations produced by the applied loads. The second screen applied on top of the first is used as reference or master. The moire pattern formation can be studied as the result of the intersections of the two above mentioned systems of lines. Knowing the distance between the master grid lines and measuring the distance between fringes, it is possible by geometric analysis of the intersections of the two systems of lines to compute the distance between the model grid lines at a point, and the corresponding change in direction. With these two data, normal and shear strains can be computed. The "geometrical" approach gives values of the strains that are the average values in a region limited by two fringes, because the applied formulas are valid for a homogeneous field.

Similar approaches are presented in other papers.<sup>5,6,7</sup> R. Bromley<sup>8</sup> obtains results similar to those previously referred to by using tensor notation. A different point of view in the analysis of the moire patterns was presented in 1948 by R. Weller and W. Shepphard.<sup>9</sup> These authors described the application of the moire fringes as a means of measuring displacements. In 1954, M. Dantu,<sup>10</sup> following the same lines, introduced the interpretation of the moire patterns in terms of the components of the displacements. Dantu's presentation is limited to the field of small strains and deformations. A broader point of view is presented herein, together with the corresponding set of formulas to be used in different cases.

#### FUNDAMENTAL PROPERTY OF THE MOIRE FRINGES

Two line screens are used in the strain analysis, the "model grid" and the "master grid." The distance between the grid lines is called pitch and is represented by  $p$ . By interference of the two screens a pattern of fringes is produced. The distance between fringes is called "fringe spacing" and has been assigned the symbol  $\delta$ . Any line perpendicular to the master grid lines will be called principal section and a line parallel to the master grid lines, a secondary section. Model and master grids are assumed to be in the same plane.

Let us consider the interference of two line screens parallel to each other but of different pitch. It can be assumed that one is obtained from the other by uniform contraction or elongation. This mechanism of fringe formation is shown

<sup>4</sup> "The Determination of Strains by Mechanical Interference," by J. Kaczer and F. Kroupa, Czechoslovak Journal of Physics, Vol. 1, 1952, p. 80.

<sup>5</sup> "Untersuchungen zur Theorie der Doppelraster als Mittel zur Meszanzeige," by R. Lehman and A. Wiemer, Feingeratetechnik Heft, 1953, pp. 5-199.

<sup>6</sup> "The Measurement of Plane Strains by a Photoscreen Method," by J. D. C. Crips, Proceedings, SESA, Vol. 15, No. 1, 1957.

<sup>7</sup> "Use of Moire Effect to Measure Plastic Strains," by A. Vinckier and R. Dechaene, Transactions, ASME, No. 59-Met. 7.

<sup>8</sup> "Two-Dimensional Strain Measurement by Moire," by R. Bromley, Proceedings, Physical Soc., Vol. 69, Part 3 B, 1956.

<sup>9</sup> "Displacement Measurement by Mechanical Interferometry," by R. Weller and B. M. Shepard, Proceedings, SESA, Vol. 6, No. 1, 1948.

<sup>10</sup> "Recherches Diverses d'Extensometrie et de Determination des Contraintes," by M. Dantu, Conference faite au GAMAC, le 22 fevrier, 1954.

in Fig. 1. A dark fringe will appear at the points where an opaque strip falls over a transparent strip. When two opaque strips coincide, there is a maximum of light intensity and one has a light fringe. If it is assumed that the model grid is the one with the largest pitch, a point  $P$  in the undeformed state has undergone a displacement equal to the pitch  $p$  of the master grid and is now at  $P'$ . Then the center line of the first light fringe indicates a displacement in the direction of the principal section equal to  $p$ ; if the center of the light fringe is considered to the right of the first one, the displacement is equal to  $2p$ , and for the  $n$ th fringe, the displacement is  $np$ . It can be concluded that the moire pattern gives the relative displacement in the direction of the principal section referred to the final or deformed shape of the body. The pattern indicates that point  $P'$  in the deformed state of the model has undergone a displacement  $p$ .

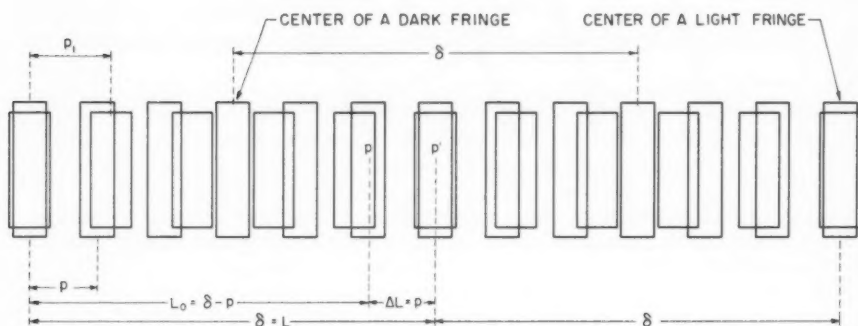


FIG. 1.—FORMATION OF MOIRE FRINGES IN A TENSILE SPECIMEN

In the mechanics of continua, the description of the displacements with the final coordinates of the points as independent variables is called Eulerian description. The so-called nominal reduction-area strain

$$\epsilon^E = \frac{L - L_0}{L} \quad \dots \dots \dots (1)$$

in which  $L_0$  is the initial length of the specimen and  $L$ , the final length, is consistent with the Eulerian description. Applying this definition to the pattern of Fig. 1

$$\epsilon^E = \frac{p}{\delta} \quad \dots \dots \dots (2)$$

Consistent with the Lagrangian description is the so-called engineering or conventional strain

$$\epsilon^L = \frac{L - L_0}{L_0} \quad \dots \dots \dots (3)$$

In terms of the moire data the engineering strain is

$$\epsilon^L = \frac{p}{\delta - p} \quad \dots \dots \dots (4)$$

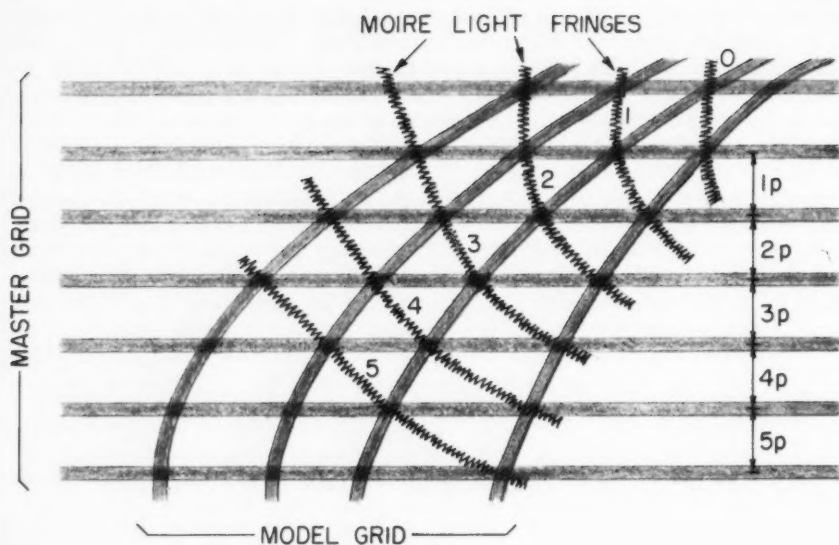


FIG. 2.—MOIRE FRINGES ARE THE LOCI OF THE POINTS PRESENTING THE SAME RELATIVE DISPLACEMENT IN THE DIRECTION NORMAL TO THE MASTER GRID

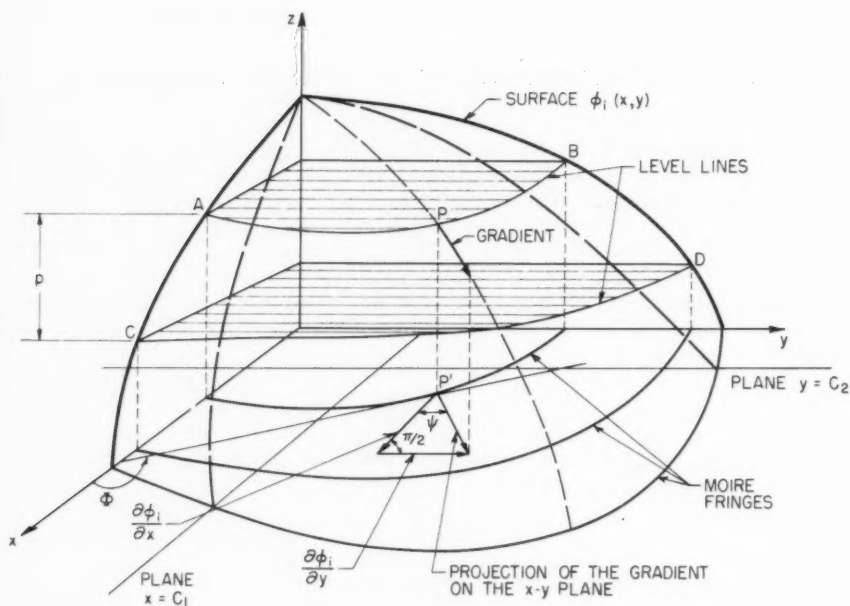


FIG. 3.—SURFACE OF THE COMPONENTS OF DISPLACEMENTS  $\phi_1(x, y)$



It can be easily shown that

$$\epsilon L = \frac{\epsilon E}{1 - \epsilon E} \dots\dots\dots (5)$$

As shown in Fig. 2, the Moire fringes are the loci of the points presenting the same relative displacement in the direction normal to the master grid. Call zero the first fringe to the right in Fig. 2, one the second fringe, two the third fringe, and so on. Assuming that the points of fringe zero do not experience any displacement, the fringe one is produced by the displacement  $p$  of the points of the model grid in the direction of the principal section, fringe two is produced by the displacement  $2p$ , and the  $n$ th fringe by the displacement  $np$ . Then the moire fringes are the loci of points with a relative displacement in the direction of the principal section which is equal to an integer number times the pitch of the master grid. These displacements are given with respect to the deformed or final shape of the model. Each fringe is characterized by a parameter. This parameter is arbitrary since we are considering relative displacements. This parameter is called "order of the fringes" and is assigned the letter  $n$ .

In the following, a cartesian system of axes  $x$  and  $y$  is used as a reference system. The component of the displacement parallel to the  $x$ -axis is given the symbol  $u$  and the component of the displacement parallel to the  $y$ -axis is assigned the symbol  $v$ .

The component of displacement of a point in a two-dimensional continuous medium parallel to a reference direction is given by a function of two variables  $\phi_i(x, y)$ . Here  $i$  can take the values 1 or 2, 1 if the reference direction is the  $x$ -axis, 2 if the reference direction is the  $y$ -axis. The prior mentioned function has the following geometric interpretation. The function  $z = \phi_i(x, y)$  in cartesian coordinates represents a surface (Fig. 3). This surface can be represented by the projection of its contour lines on the  $x$ - $y$  plane. These lines are intersection of the surface with planes of equation  $z = np$ . The resulting lines are given by

$$\phi_i(x, y) = k \dots\dots\dots (6)$$

in which  $k$  is a constant. This is also the property of the moire fringes.

To determine strains from displacements, it is necessary to compute the derivatives of the displacements. The rate of change of the surface of displacements  $\phi_i(x, y)$  at a point is given by the gradient shown in Fig. 3. Because this gradient is also a function of  $x, y$ , it can be represented by its projection in the  $x$ - $y$  plane.

The partial derivatives of  $\phi_i(x, y)$  are given by

$$\frac{\partial \phi_i}{\partial x} = \text{grad } \phi_i(x, y) \cos \psi \dots\dots\dots (7a)$$

and

$$\frac{\partial \phi_i}{\partial y} = \text{grad } \phi_i(x, y) \sin \psi \dots\dots\dots (7b)$$

in which  $\psi$  is the angle between the  $x$ -axis and  $\text{grad } \phi_i$ . The tangent of  $\psi$  is given by (Fig. 3)

$$\tan \psi = \frac{\frac{\partial \phi_i}{\partial y}}{\frac{\partial \phi_i}{\partial x}} \dots\dots\dots (8)$$

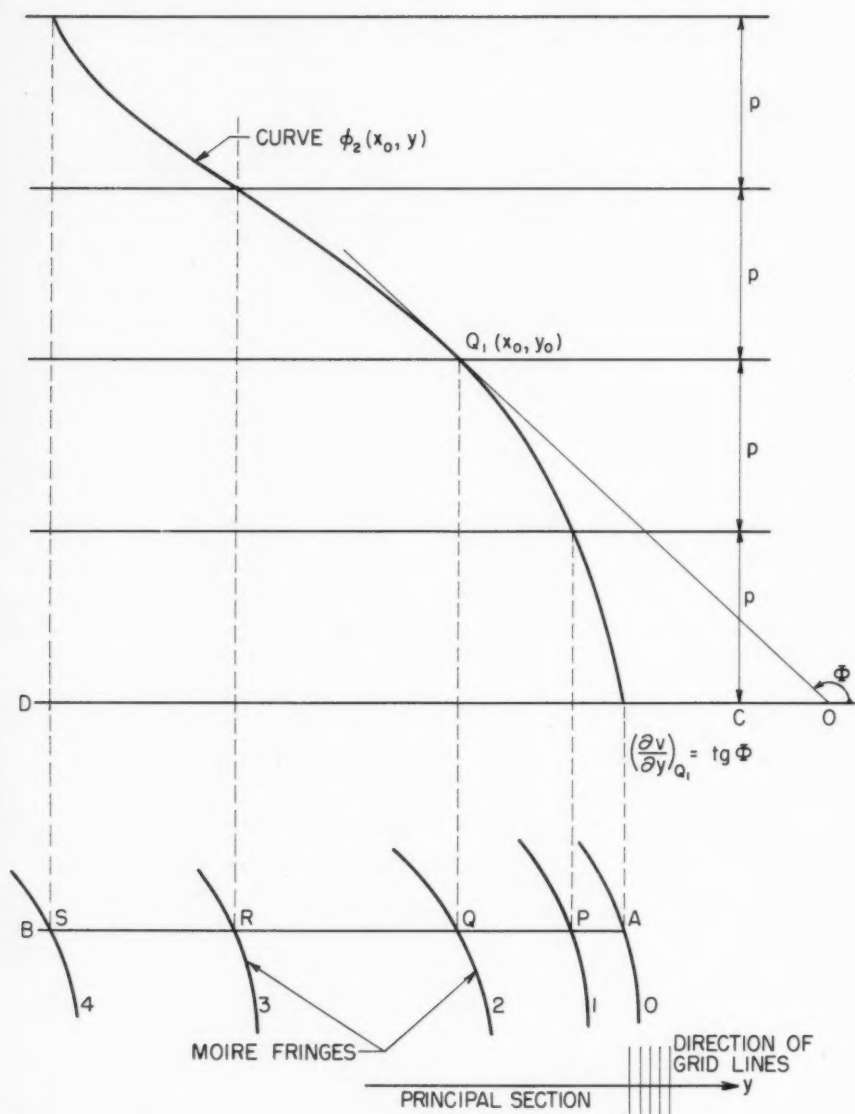


FIG. 4.—CONSTRUCTION OF THE INTERSECTION CURVE OF THE SURFACE  $\phi_2(x, y)$  WITH THE PLANE  $x = x_0$

To compute the partial derivatives of  $\phi_i(x, y)$ , the curves of intersection of the surface with planes of equations  $x = C_1$  and  $y = C_2$  can be drawn, in which  $C_1$  and  $C_2$  are constants. The procedure used to obtain a partial derivative is illustrated in Fig. 4. The horizontal position of each point of intersection of the moire fringes with the line AB (trace of the intersecting plane) is first projected on to the base line CD. The orders are read from the moire fringes and distances equal to  $np$  are scaled up from the base line. A line drawn through the points, thus plotted, defines the cross-section. The slope of this curve at a point gives the derivative  $\partial\phi_2/\partial y$ .

If the preceding data are plotted directly from the moire pattern, the results obtained correspond to the Eulerian description. There are two possible solutions to the Lagrangian description. Assume that the patterns corresponding to two orthogonal directions have been determined. A point  $P_0$  of initial coordinates  $x_0$  and  $y_0$  moves, after deformation, to point  $P_1$  with coordinates  $x_1$  and  $y_1$ . If the components of the displacements experienced by the point  $P_0$  are  $u$  and  $v$

$$x_0 = x_1 - u \quad \dots\dots\dots (9)$$

and

$$y_0 = y_1 - v \quad \dots\dots\dots (10)$$

By using the preceding relationships, it is possible to obtain the necessary data to replot the moire patterns referred to the initial configuration.

Another possibility is the following. The derivative of  $u$  with respect to  $x_0$  can be expressed as a function of the derivative of  $u$  with respect to  $x_1$

$$\frac{\partial u}{\partial x_0} = \frac{\frac{\partial u}{\partial x_1}}{\frac{\partial x_0}{\partial x_1}} \quad \dots\dots\dots (11)$$

From Eq. 9

$$\frac{\partial x_0}{\partial x_1} = 1 - \frac{\partial u}{\partial x_1} \quad \dots\dots\dots (12)$$

and then

$$\frac{\partial u}{\partial x_0} = \frac{\frac{\partial u}{\partial x_1}}{1 - \frac{\partial u}{\partial x_1}} \quad \dots\dots\dots (13)$$

Likewise, it is possible to prove that

$$\frac{\partial u}{\partial y_0} = \frac{\frac{\partial u}{\partial y_1}}{1 - \frac{\partial v}{\partial y_1}} \quad \dots\dots\dots (14)$$

Using the preceding equations, it is possible to go from one type of description to the other.

### STRAIN ANALYSIS

In the case of large strains, the deformations at a point is characterized in the Lagrangian description by the following quantities and components of the strain tensor.<sup>11</sup>

$$e_{xx}^L = \frac{\partial u_0}{\partial x_0} + \frac{1}{2} \left[ \left( \frac{\partial u_0}{\partial x_0} \right)^2 + \left( \frac{\partial v_0}{\partial x_0} \right)^2 \right] \dots\dots\dots (15a)$$

$$e_{yy}^L = \frac{\partial v_0}{\partial y_0} + \frac{1}{2} \left[ \left( \frac{\partial v_0}{\partial y_0} \right)^2 + \left( \frac{\partial u_0}{\partial y_0} \right)^2 \right] \dots\dots\dots (15b)$$

and

$$e_{xy}^L = \frac{\partial u_0}{\partial y_0} + \frac{\partial v_0}{\partial x_0} + \frac{\partial u_0}{\partial x_0} \frac{\partial u_0}{\partial y_0} + \frac{\partial v_0}{\partial y_0} \frac{\partial v_0}{\partial x_0} \dots\dots\dots (15c)$$

In Eqs. 15, the subscript zero is used to indicate that the initial coordinates of the points are the independent variables.

In the Eulerian description, using the subscript 1 to denote that the final coordinates are the independent variables,

$$e_{xx}^E = \frac{\partial u_1}{\partial x_1} - \frac{1}{2} \left[ \left( \frac{\partial u_1}{\partial x_1} \right)^2 + \left( \frac{\partial v_1}{\partial x_1} \right)^2 \right] \dots\dots\dots (16a)$$

$$e_{yy}^E = \frac{\partial v_1}{\partial y_1} - \frac{1}{2} \left[ \left( \frac{\partial v_1}{\partial y_1} \right)^2 + \left( \frac{\partial u_1}{\partial y_1} \right)^2 \right] \dots\dots\dots (16b)$$

and

$$e_{xy}^E = \frac{\partial u_1}{\partial y_1} + \frac{\partial v_1}{\partial x_1} - \left[ \frac{\partial u_1}{\partial x_1} \frac{\partial u_1}{\partial y_1} + \frac{\partial v_1}{\partial x_1} \frac{\partial v_1}{\partial y_1} \right] \dots\dots\dots (16c)$$

From the moire patterns in two orthogonal directions, it is possible to compute the derivatives appearing in Eqs. 15 and 16 by using the procedures outlined previously under the heading "Fundamental Property of the Moire Fringes."

The components of the strain tensor given by Eqs. 15 or 16 can be given a physical significance which is important when the classical theory of elasticity linearizations are made. In the following reference is made only to the Lagrangian description used in the theory of elasticity.

Applying the definition of strain given in Eq. 3 to the elements of line  $M_1N_1$  and  $M_1P_1$  (Fig. 5) which before deformation are equal to  $M_0N_0 = dx_0 = 1$  and  $M_0P_0 = dy_0 = 1$ ,

$$\epsilon_{xx}^L = \sqrt{1 + 2 e_{xx}^L} - 1 \dots\dots\dots (17a)$$

and

$$\epsilon_{yy}^L = \sqrt{1 + 2 e_{yy}^L} - 1 \dots\dots\dots (17b)$$

<sup>11</sup> "Tensor Analysis," by I. S. Sokolnikoff, John Wiley and Sons Inc., New York, 1951.

From Fig. 5, it is also possible to obtain the sine of the change in angle of the initially perpendicular directions  $M_0N_0$  and  $M_0P_0$

$$\sin \gamma^L = \frac{e_{xy}^L}{(1 + \epsilon_{xx}^L)(1 + \epsilon_{yy}^L)} \dots \dots \dots (18)$$

Eqs. 17 can be applied to compute the normal and shearing strains from the data obtained from the moire patterns corresponding to two orthogonal directions  $x$  and  $y$ .

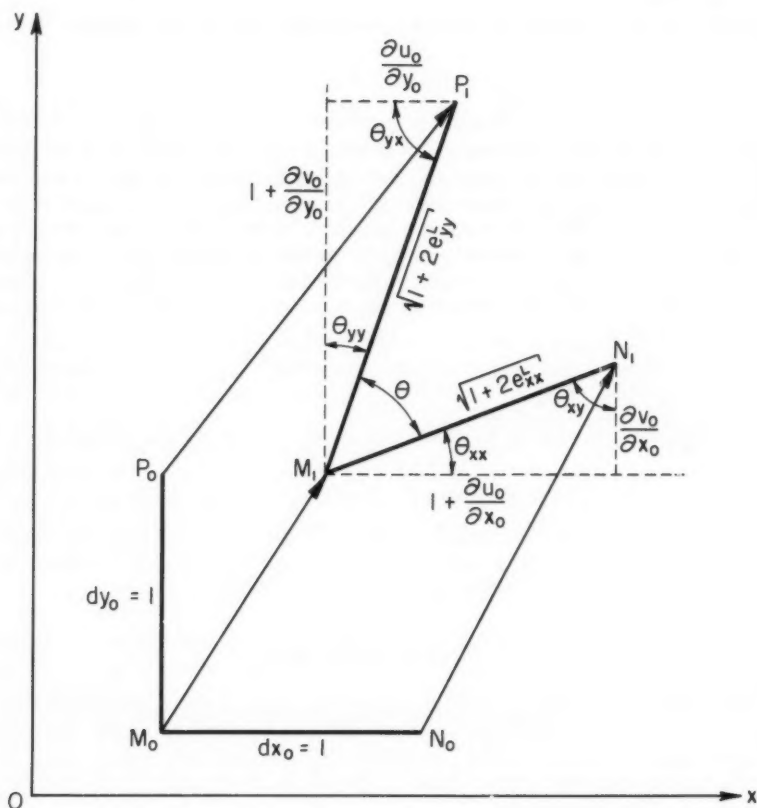


FIG. 5.—DEFORMATION IN THE NEIGHBORHOOD OF A POINT (LAGRANGIAN DESCRIPTION)

Eqs. 17 and 18 can be simplified by expanding the square root in series.

$$\epsilon_{xx}^L = \frac{\partial u_0}{\partial x_0} + \frac{1}{2} \left( \frac{\partial v_0}{\partial x_0} \right)^2 - \frac{1}{8} \left( \frac{\partial u_0}{\partial x_0} \right)^4 - \frac{1}{8} \left( \frac{\partial v_0}{\partial x_0} \right)^4 + \dots \dots \dots (19)$$

If  $\partial u_0/\partial x_0$  is so small that the fourth power can be neglected with respect to unity, and  $\partial v_0/\partial x_0$  is so small that the second power can be neglected with respect to unity, then,

$$\epsilon_{xx}^L = \frac{\partial u_0}{\partial x_0} \dots\dots\dots (20)$$

From Fig. 5, it is possible to see that the preceding simplification is geometrically equivalent to replacing the strain of the line element  $M_1N_1$  by the strain of its projection on the x-axis. From Fig. 5 it is also possible to conclude that if there is no rotation of the line element, that is if  $\partial v_0/\partial x_0 = 0$ , Eq. 20 is rigorous.

By expanding in series Eq. 18 and neglecting terms higher than the first order

$$\gamma_{xy}^L = \frac{\partial u_0}{\partial y_0} + \frac{\partial v_0}{\partial x_0} \dots\dots\dots (21)$$

Eqs. 20 and 21 are the equations used in the classical theory of elasticity.

Sometimes  $\partial u_0/\partial x_0$  is small and can be neglected in the series expansion of Eqs. 17a and b, and the shear strains are also small, but the rigid body rotations are large. This is found for example, in the case of the bending of a very slender bar. The classical theory of elasticity can be applied to the prior mentioned cases, but Eqs. 20 and 21 must be corrected for the effect of rotation. For moderately large rotations, the second term in the series expansion Eq. 19 can be kept.

$$\epsilon_{xy}^L = \frac{\partial u_0}{\partial x_0} + \frac{1}{2} \left( \frac{\partial v_0}{\partial x_0} \right)^2 \dots\dots\dots (22)$$

With the same degree of approximation, Eq. 18 can be simplified to

$$\gamma_{xy}^L = e_{xy}^L \dots\dots\dots (23)$$

Regarding the range of application of Eqs. 20 and 21 or 22 and 23, from the moire data, it is possible in each particular case to conclude whether or not the non-linear terms should be retained.

#### SIGN CONVENTION

This section is devoted to the fundamental rules of sign determination.

By convention, the derivatives in the direction of the principal section are positive when the strain of the projected line element is tensile. To find the sign of the derivatives from a moire pattern, it is necessary to observe the whole field of displacements.

Assuming that the principal section is in the direction of the x-axis, the displacement of a point at a distance L from the origin of coordinates will be

$$L' - L = \int_0^L \frac{\partial u_0}{\partial x_0} dx_0 \dots\dots\dots (24)$$

If  $\partial u_0/\partial x_0$  does not change sign at an intermediate point, the sign of the displacement and the sign of the derivative are the same. From the continuity of

the displacements and their derivatives, it follows that, to change sign, the derivative must go through zero. Since, at every point the gradient is perpendicular to the contour line through that point (Fig. 3) and taking into consideration Eq. 8, the tangent of the moire fringes is given by

$$\tan \Phi = - \frac{\frac{\partial \phi_i}{\partial x_0}}{\frac{\partial \phi_i}{\partial y_0}} \dots \dots \dots (25)$$

According to Eq. 25, when  $\partial u_0 / \partial x_0 = 0$ ,

$$\tan \Phi = - \frac{0}{\frac{\partial u_0}{\partial y_0}} = 0 \dots \dots \dots (26)$$

Therefore, the moire fringes have a tangent parallel to the x-axis. If the principal section is in the direction of the y-axis, and  $\partial v_0 / \partial y_0 = 0$ ,

$$\tan \Phi = - \frac{\frac{\partial v_0}{\partial x_0}}{\frac{\partial v_0}{\partial y_0}} = -\infty \dots \dots \dots (27)$$

and the moire fringes have a tangent parallel to the y-axis.

Due to the continuity of the displacements, all points corresponding to changes of sign are located on lines which are boundaries between regions of different sign. By locating these lines, the relative signs of the derivatives can be established. To know the absolute signs, it is necessary to know the absolute displacement of a point of the model. From Eq. 25, the sign of the derivatives in the direction of the secondary sections is known, if the sign of the derivatives in the direction of the principal section is known.

### MOHR'S CIRCLE CONSTRUCTION

In the preceding, the method of computing the derivatives of the displacements by using sections parallel to the coordinate axes was developed. Another possibility is to use the gradient and to apply Eqs. 7a and b. This method can be used in connection with the construction of Mohr's circle at a point.

In order to find the gradient at a point, a section of the displacement surface in the direction of the gradient can be used. If less precision is required, the direction of the gradient can be assumed to be that of the common normal to two neighboring fringes. If  $\delta_n$  is the distance between fringes measured along the common normal, and  $p$  is the grid pitch,

$$\text{modulus grad } \Phi_1 = \frac{p}{\delta_n} \dots \dots \dots (28)$$

The angle  $\psi$  can be measured directly with the protractor. No reference is made to the type of description used because the following derivations are independent of this type of description.





In the following, the gradient at a point will be indicated by the symbol  $\phi_{n1}$  or  $\phi_{n2}$  according to the case. The derivatives in the direction of the coordinate axes will be indicated by

$$\frac{\partial u}{\partial x} = \epsilon_{xx} \dots \dots \dots (29a)$$

$$\frac{\partial v}{\partial y} = \epsilon_{yy} \dots \dots \dots (29b)$$

and

$$\frac{\partial u}{\partial y} + \frac{\partial v}{\partial x} = \gamma_{xy} \dots \dots \dots (29c)$$

These symbols represent, in general, the derivatives of the displacements in the direction of the principal sections and the sum of the derivatives in the direction of the secondary sections. They represent the components of the strain tensor only when the strains are small.

The construction of Mohr's circle is shown in Fig. 6. The x-axis is assumed to be in the direction of the algebraically greatest derivative. With this convention, the angle between  $\phi_{n1}$  and the  $\epsilon$ -axis is the same as the angle between  $\phi_{n1}$  and the x-axis.

Going from the physical plane to the  $\epsilon$ - $\gamma$  plane, the y-axis must be rotated clockwise  $\pi/2$ . The  $\phi_{n2}$  vector rotates rigidly attached to the y-axis.

In the  $\epsilon$ - $\gamma$  plane, Fig. 6b, a pole Q is taken and, from this pole, the vector QN parallel to  $\phi_{n1}$  is drawn. From Q, the vector QM which is perpendicular to  $\phi_{n2}$  is also drawn. The direction of QM is obtained from  $\phi_{n2}$  by a clockwise rotation of  $\pi/2$ .

If the points M and N are joined, the vector MN is obtained, whose projections MP and NP are equal to

$$MP = \phi_{n1} \cos \psi_1 - \phi_{n2} \sin \psi_2 \dots \dots \dots (30)$$

but

$$\phi_{n1} \cos \psi_1 = \epsilon_{xx} \dots \dots \dots (31a)$$

and

$$\phi_{n2} \sin \psi_2 = \epsilon_{yy} \dots \dots \dots (31b)$$

then

$$MP = \epsilon_{xx} - \epsilon_{yy} \dots \dots \dots (32)$$

The projection NP is equal to

$$NP = \phi_{n1} \sin \psi_1 + \phi_{n2} \cos \psi_2 = \gamma_{xy} \dots \dots \dots (33)$$

Point C, which is located at MP/2, is the center of Mohr's circle. The radius of the circle is obtained by joining point C with point L. The origin of coordinates is the projection of the pole Q on the line MC.

### EXAMPLE

As an example of the application of the moire method, the study of a disk under diametral loading was performed. The solution of this problem using the geometric approach was presented elsewhere.<sup>12</sup> A 1/2 in. thick sheet of

<sup>12</sup> "Geometry of Moire Fringes in Strain Analysis," by S. Morse, A. J. Durelli, and C. A. Sciammarella, Proceedings, ASCE, Vol. 86, No. EM 4, August, 1960.

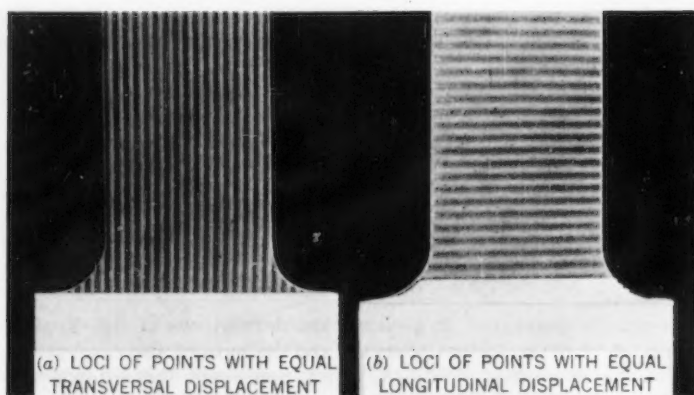
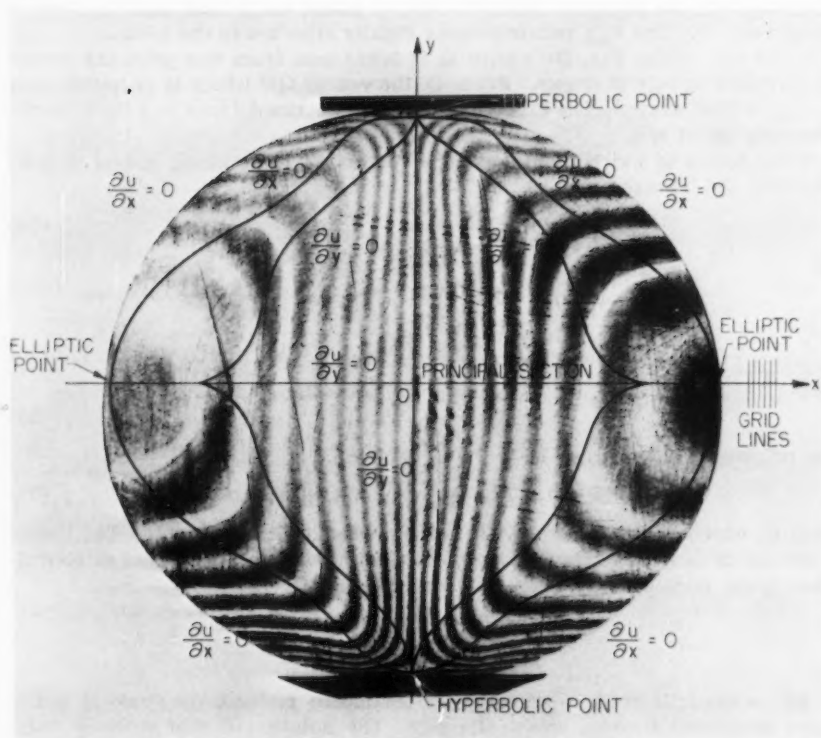


FIG. 7.—MOIRÉ PATTERNS ON A TENSILE SPECIMEN

FIG. 8.—DISK UNDER DIAMETRICAL COMPRESSION  
(HORIZONTAL DISPLACEMENTS  $u$ )

a urethane rubber (Hysol 8705) was cast. A 300-lines per in. grid was photo-printed on the rubber using a photoengraver's albumenoid base coating. After printing, a 4-in. disk and two tensile specimens were machined from the sheet.

Two tensile tests were performed to find the elastic constants of the material. Fig. 7 shows the corresponding patterns at one stage of loading. In Fig. 7(a), fringes are the loci of points with equal transversal displacement, and

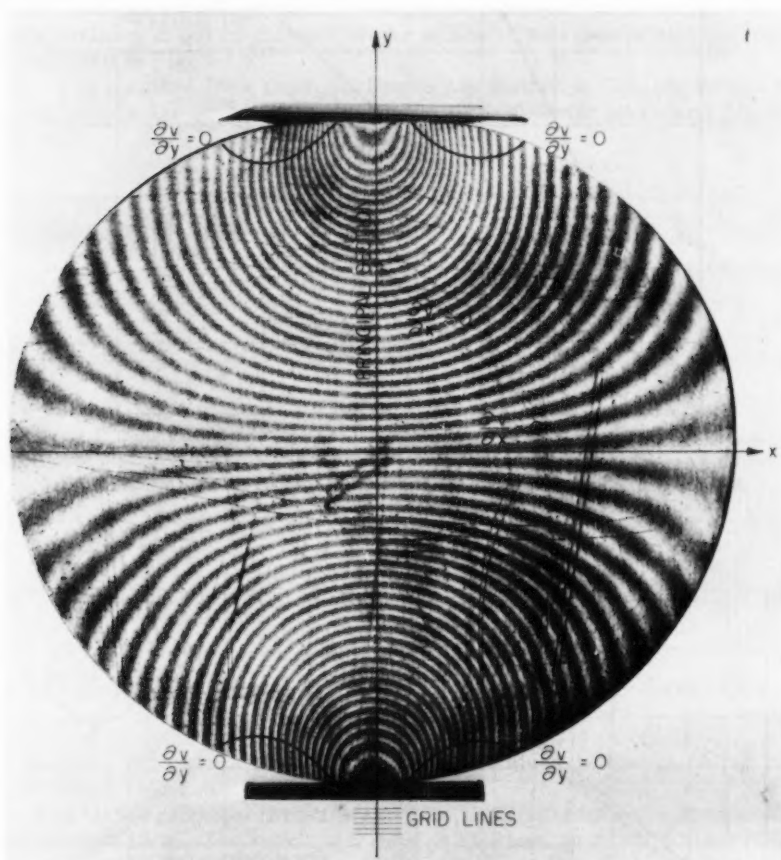


FIG. 9.—DISK UNDER DIAMETRICAL COMPRESSION  
(VERTICAL DISPLACEMENTS  $v$ )

in Fig. 7(b) fringes are the loci of points with equal longitudinal displacement. The patterns were obtained by the double exposure method, the unloaded and loaded conditions being successively exposed on the same film.

The disk was loaded between flat plates, with the grid lines in the direction of the load, Fig. 8, and with the lines perpendicular to the loading direction, Fig. 9. In Fig. 8 Moiré fringes give horizontal displacements  $u$ , and in Fig. 9 give vertical displacements  $v$ .

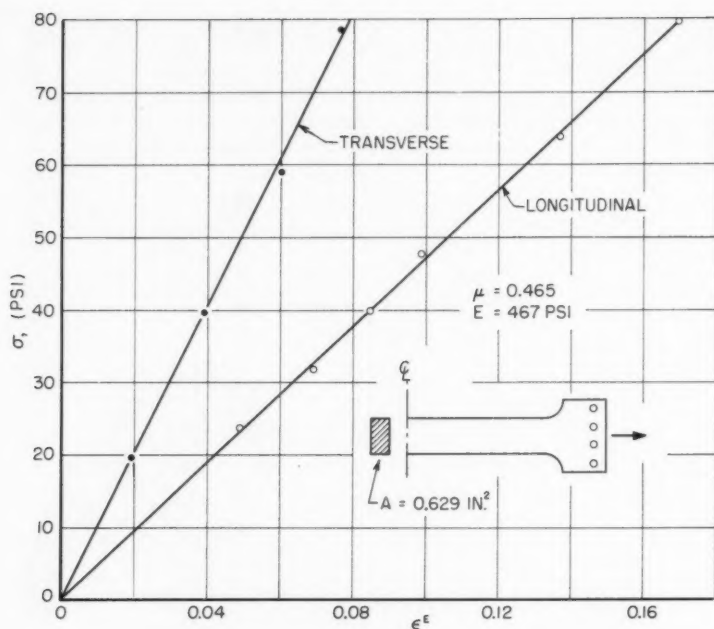


FIG. 10.—STRESS-STRAIN AND POISSON'S RATIO DETERMINATIONS ON A TENSILE SPECIMEN

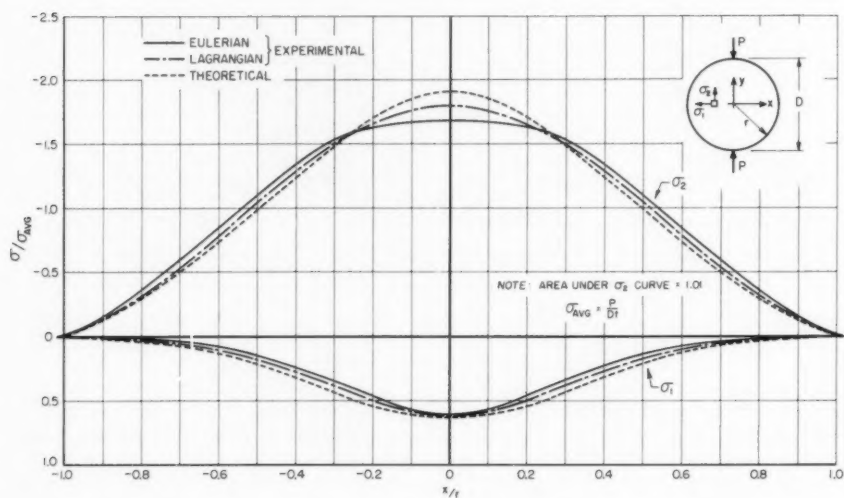


FIG. 11.—PRINCIPAL STRESSES ON THE HORIZONTAL AXIS OF A DISK UNDER DIAMETRICAL COMPRESSION

The loci of points at which the derivatives in the direction of the principal and the secondary sections are equal to zero, are indicated in Figs. 8 and 9. On the horizontal diameter (Fig. 8), the displacements are positive and, therefore, all of the central region enclosed by the line  $\partial u / \partial x = 0$  has positive derivatives. In Fig. 9 the displacements in the vertical diameter are negative and, therefore, the derivatives in the direction of the principal section are negative throughout the model except for small regions near the boundaries where the sign changes. The lines of zero derivative intersect the principal and secondary sections at points called singular points. Two types of singular points are indicated in Fig. 8.

The data obtained from the tensile tests are plotted in Fig. 10. In this figure, the results are expressed as functions of the Eulerian strain and the nom-

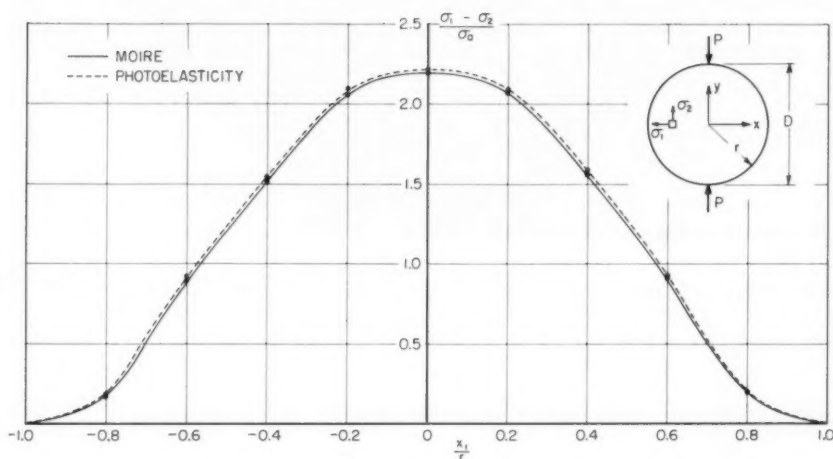


FIG. 12.—DIFFERENCE OF THE PRINCIPAL STRESSES IN THE HORIZONTAL AXIS

inal stress. The stress-strain relationship obtained is the so-called true stress-strain relationship.

In Fig. 11, the principal stresses along the horizontal diameter are shown in dimensionless form. The ratio  $x/r$  is used as abscissa, in which  $r$  is the radius of the disk. The ratio of the stresses to the average stress  $\sigma_{avg} = P/Dt$  is used as ordinates. The diameter of the disk and its thickness is denoted by  $D$ . The experimental results are given in the Eulerian and Lagrangian descriptions. The Eulerian description was obtained directly from the moire patterns, and the elastic constants of Fig. 10 were employed to compute the stresses from the strains. The value of  $\sigma_{avg}$  was computed according to the initial dimensions of the disk.

The strains in the Lagrangian description were obtained from the strains in the Eulerian description by using Eq. 13, and the coordinates of the points were computed by applying Eq. 10. In order to obtain the stresses from the strains, values of the tangent elastic modulus of the stress-strain relationship, nominal stress versus engineering strain, were computed. In Fig. 11,

the abscissae are referred to the undeformed shape of the disk. Also shown in the same figure are the results of the theory of elasticity. In Fig. 12, the difference of the principal stresses on the horizontal diameter, obtained by photoelasticity, is compared with the moire results.

The maximum difference between the theoretical and the moire values of  $\sigma_2$  on the horizontal axis is of the order of 4% of the maximum stress in the disk. The same figure applies for  $\sigma_1$ . The difference of  $\sigma_1 - \sigma_2$ , computed by the moire method and photoelasticity is 1.5% of the maximum value.

For a point with coordinates

$$x = 0.2 r$$

$$y = 0.5 r$$

a rectangular three-gage,  $45^\circ$  strain rosette analysis was also performed. For this purpose, the moire pattern with a model grid at  $45^\circ$  with the line of loading was determined (Fig. 13). The engineering strains at the point are

$$\epsilon_{xx} = 0.0241$$

$$\epsilon_{45} = -0.1785$$

$$\epsilon_{yy} = -0.0430$$

The rosette computation gives the values

$$\epsilon_1 = 0.0281$$

$$\epsilon_2 = -0.0463$$

$$\alpha = 9^\circ 30'$$

The value of  $\epsilon_1 - \epsilon_2$  computed by photoelasticity is

$$\epsilon_1 - \epsilon_2 = 0.073$$

and from moire

$$\epsilon_1 - \epsilon_2 = 0.074$$

For the same point, the construction of Mohr's circle is shown in Fig. 14. From Mohr's circle

$$\epsilon_1 = 0.0282$$

$$\epsilon_2 = -0.0462$$

$$\alpha = 10^\circ$$

The rigid body rotation of the point can be computed from the moire data

$$\frac{\partial u}{\partial y} = 0.0262 \sin 5^\circ = 0.00228$$

$$\frac{\partial v}{\partial x} = 0.0509 \sin 28^\circ = 0.0239$$

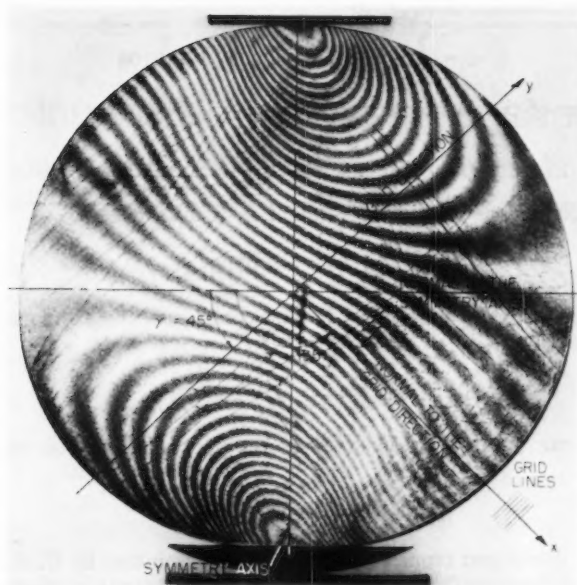


FIG. 13.—MOIRÉ PATTERN OF A DISK UNDER DIAMETRICAL LOAD OBTAINED WITH A MODEL GRID AT AN ANGLE OF  $45^\circ$  WITH THE LOAD DIRECTION

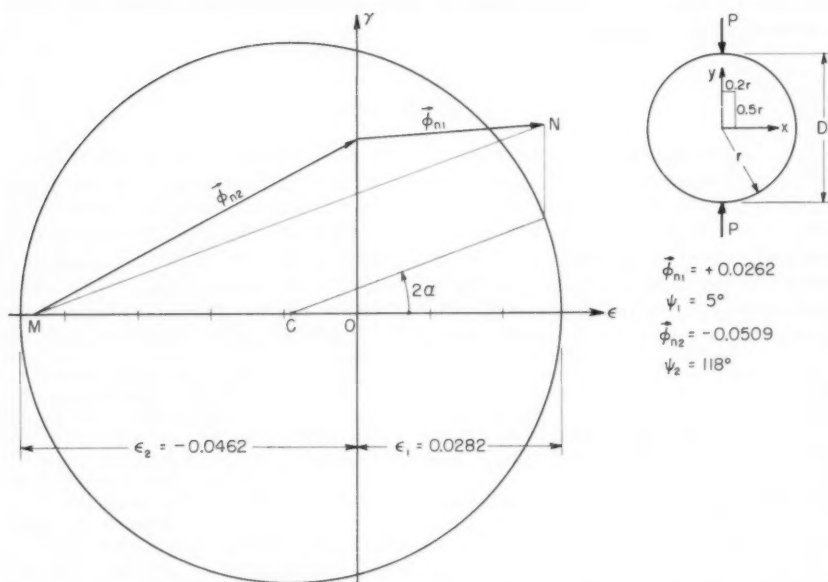


FIG. 14.—MOHR'S CIRCLE CONSTRUCTION IN THE POINT  $x = 0, 2r, y = 0, 5r$

The rigid body rotation is equal to

$$\omega = \frac{1}{2} [0.0239 - 0.00228] = 0.0108$$

In the direction of the principal derivatives

$$\gamma_{xy} = \frac{1}{2} \left[ \frac{\partial u}{\partial y} - \frac{\partial v}{\partial x} \right] = 0$$

Taking into account the preceding value of  $\omega$ , it follows that

$$\frac{\partial u}{\partial y} = - \frac{\partial v}{\partial x} = \omega = 0.0108$$

According to Eq. 22, the correction for the rotation of the element of length is equal

$$\frac{1}{2} \left( \frac{\partial u}{\partial y} \right)^2 = \frac{1}{2} \left( \frac{\partial v}{\partial x} \right)^2 = 0.00058$$

This quantity can be neglected in view of the precision used in this example.

#### ACKNOWLEDGMENTS

This paper developed from a doctoral thesis submitted by C. Sciammarella to the Civil Engineering Department of the Illinois Institute of Technology. The work reported herein was sponsored by the National Science Foundation whose support is gratefully acknowledged. The writers wish to thank the Armour Research Foundation for the use of laboratory facilities and for reproducing the manuscript. Sincere thanks are due to E. I. Fiesenheiser, F. ASCE, Chairman of the Civil Engineering Department of the Illinois Institute of Technology for his support and cooperation.



---

Journal of the  
ENGINEERING MECHANICS DIVISION  
Proceedings of the American Society of Civil Engineers

---

MINIMUM-WEIGHT DESIGN OF BEAMS FOR DEFLECTION

By Ralph L. Barnett,<sup>1</sup> A. M. ASCE

---

SYNOPSIS

Design procedures for minimum weight, statically determinate beams are developed using a deflection criterion. Optimum flange width and web thickness variations are described for I-beams designed with respect to bending and shear deflection. The role of material properties for these beams is discussed from the point of view of stiffness and strength.

---

INTRODUCTION

This paper is concerned with the minimum weight-stiffness design of statically determinate bending members with specified depth variations. In 1936, H. Roxbee Cox treated a similar problem for torsional stiffness.<sup>2</sup> He concluded that maximum stiffness for a given weight is attained when the stress level is constant. In April, 1958, B. Saelman demonstrated that this condition generally does not result in maximum stiffness for the torsion problem.<sup>3</sup> Several months prior to the Saelman article, a design procedure for optimum stiffness-weight bending members was developed<sup>4</sup> for Rock Island Arsenal, which procedure

---

Note.—Discussion open until July 1, 1961. To extend the closing date one month, a written request must be filed with the Executive Secretary, ASCE. This paper is part of the copyrighted Journal of the Engineering Mechanics Division, Proceedings of the American Society of Civil Engineers, Vol. 87, No. EM 2, February, 1961.

<sup>1</sup> Assoc. Research Engr., Armour Research Foundation of Illinois Inst. of Tech. Tech. Center, Chicago, Ill.

<sup>2</sup> "Stiffness of Thin Shells," by H. Roxbee Cox, *Aircraft Engineering*, September, 1936, pp. 245-246.

<sup>3</sup> "A Note on the Optimum Distribution of Material in a Beam for Stiffness," by B. Saelman, *Journal of Aeronautical Sciences*, April, 1958, p. 268.

<sup>4</sup> "Lightweight Structures and Prestressed Launcher Components, Rock Island Arsenal, Ordnance Project No. TU2-70, Phase I Report," by Ralph L. Barnett, January, 1958.

also demonstrated that a constant stress level is not generally a sufficient condition for maximum stiffness. This paper represents an extension of the latter work.

Basically, the problem treated herein is that of adjusting one or two dimensions of a beam cross section in such a way that the deflection at a given station assumes a specified value and the total beam weight is minimized.

The body of this paper consists of three sections. In the first of these, beam sections are treated for cases where only the bending deflection is considered and only one dimension of the beam section is varied (one-parameter beam). For this problem, three distinct situations arise depending on the nature of the loading and the specified deflection. In one instance, no solution exists; in another, a zero-weight beam can be approached which satisfies the specified deflection; and in the last, the optimum beam dimensions are obtained by solving the simplest isoperimetric problem of variational calculus. In the latter case, two examples of I-beams are examined. Very simple relationships are obtained among their important parameters—weight, deflection, depth, span length, and material properties. For beams with large span-to-depth ratios, these relationships closely approximate the corresponding, but more cumbersome, relationships obtained in the third section of this paper, which deals with beam sections designed for bending and shear deflection in which two dimensions of the beam section are varied (two-parameter beam). For certain types of single-parameter beam sections, the results developed in the first section can be modified slightly to take account of both bending and shear deflection. Example 3 in the third section utilizes such a modification for a rectangular cross section.

In the second section of the body of the paper, constant-strength beams are compared to the optimum deflection designs developed in the first section. Conditions on the loading are established for which the two types of beams are identical.

The third section considers three types of two-parameter beam sections designed for bending and shear stiffness: (1) an I-beam with an optimum flange width and an optimum web thickness variation, (2) an I-beam with an optimum flange width variation and an optimum constant thickness web, and (3) an optimum prismatic I-beam. The discussions of the first two cases follow closely that given for the one-parameter beam sections; however, the details are somewhat more involved. In the third case, ordinary calculus is used to establish the optimum flange width and web thickness for prismatic beams. The three types of deflection designs are then compared for a particular case.

For each case studied in the various sections, the method of design and pertinent formulas are indicated. A number of examples have been worked out to demonstrate the design techniques and to indicate some of the properties of minimum-weight deflection designs.

*Notation.*—The letter symbols adopted for use in this paper are defined where they first appear, in the illustrations or in the text, and are arranged alphabetically, for convenience of reference, in the Appendix.

#### BENDING DEFLECTIONS OF SYMMETRICAL BEAMS (SINGLE-PARAMETER BEAM SECTIONS)

In this section, we shall determine that distribution of material along a beam which both minimizes its weight and keeps the bending deflection at any station

at a specified value. Consider a statically determinate, symmetrical beam subjected to an arbitrary static loading in the plane of symmetry. It will be assumed that the bending deflection at a station  $x = \xi$  is given by the virtual-work expression

$$\Delta(\xi) = \int_S \frac{M m}{E I(x)} dx \dots\dots\dots (1)$$

in which  $x$  is the coordinate along the beam,  $M$  denotes the external bending moment,  $m$  is the moment due to a vertical unit load acting at station  $x = \xi$ ,  $E$  represents the modulus of elasticity, and  $I(x)$  is a variable principal moment of inertia in the plane of bending.<sup>5</sup> The integration extends over the entire span  $S$ . It is further assumed that the external moment  $M$  is independent of the beam displacements and the beam geometry.

Three situations can be distinguished with regard to the product  $M m$ : (1) the sign of  $M m$  is not the same as the sign of the specified deflection  $\Delta(\xi)$  anywhere in the span; (2)  $M m$  assumes both positive and negative values in the values in the span; or (3) the sign of  $M m$  does not differ from the sign of  $\Delta(\xi)$  anywhere in the span. We shall consider each of these cases separately.

Case 1.— $M m/\Delta(\xi) \leq 0$

No physical distribution of material exists that will provide the specified deflection  $\Delta(\xi)$ . The satisfaction of Eq. 1 can only be achieved with a nonpositive moment-of-inertia distribution.

Case 2.— $M m > 0$  and  $M m < 0$  in  $S$

For this case, any specified finite deflection can be obtained with a member of arbitrarily small weight. The integral in Eq. 1 can be written as

$$\Delta(\xi) = \int_{\text{positive}} \frac{M m}{E I'(x)} dx - \int_{\text{negative}} \frac{|M m|}{E I''(x)} dx \dots\dots\dots (2)$$

in which the first and second integrals extend over the portions of the span where the product  $M m$  is positive and negative respectively. An  $I'(x)$  and an  $I''(x)$  are sought which will produce a specified value of  $\Delta(\xi)$ . If  $I'(x)$  and  $I''(x)$  are taken as constant in their respective spans, it is readily seen that as  $I''$  is taken smaller and smaller the magnitude of  $I'$  required to keep the right side of Eq. 2 at a specified positive value also becomes smaller and smaller. By reversing the roles of  $I'$  and  $I''$ , the same argument holds when a specified negative value is sought. Clearly, any value of  $\Delta(\xi)$  can be obtained with moments of inertia  $I'$  and  $I''$  of vanishing magnitude. Vanishing moments of inertia imply vanishing areas and, hence, an arbitrarily light bending member. It should be noted that as the beam weight approaches zero the deflections at stations other than  $x = \xi$  increase indefinitely. This case will be discussed further in subsequent sections.

Case 3.— $M m/\Delta(\xi) \geq 0$

The product  $M m$  and the specified deflection  $\Delta(\xi)$  will be considered, without loss in generality, as non-negative quantities. In this case, it will be assumed that the area and the moment of inertia of a beam section depend on one

<sup>5</sup> "Formulas for Stress and Strain," by R. J. Roark, McGraw-Hill Book Co., New York, 3rd Ed., 1954, p. 143.

open parameter  $t(x)$ , which must be determined. The beam weight,  $W$ , to be minimized is given by

$$W = \int_S \rho A [t(x)] dx \quad \dots\dots\dots (3)$$

subject to Eq. 1,

$$\Delta(\xi) = \int_S \frac{M m}{E I [t(x)]} dx = \text{specified positive constant} \quad \dots\dots (4)$$

in which  $A$  is the beam area and  $\rho$  denotes the weight density. This formulation is the simplest isoperimetric problem of variational calculus.<sup>6</sup> The stationary character of the integral in Eq. 3 is equivalent to the existence of a constant multiplier  $\lambda$  such that  $\Delta(\xi) = \text{constant}$  and

$$\frac{\partial}{\partial t} \left[ \rho A(t) + \lambda \frac{M m}{E I(t)} \right] = 0 \quad \dots\dots\dots (5)$$

are satisfied. Consider the following form of the moment of inertia and area:

$$I[x, t(x)] = a + b t(x) \quad \dots\dots\dots (6)$$

and

$$A[x, t(x)] = c + e t(x) \quad \dots\dots\dots (7)$$

where

$$a = a(x) \geq 0 \quad \dots\dots\dots (8a)$$

$$b = b(x) > 0 \quad \dots\dots\dots (8b)$$

$$c = c(x) \geq 0 \quad \dots\dots\dots (8c)$$

and

$$e = e(x) > 0 \quad \dots\dots\dots (8d)$$

are specified piecewise continuous functions. By substituting Eqs. 6 and 7 into 5, one obtains an algebraic expression that can be solved explicitly for  $t(x)$  in terms of the parameter  $\lambda$ ; thus,

$$t(x) = \sqrt{\frac{\lambda M m}{E \rho b e}} - \frac{a}{b} \quad \dots\dots\dots (9)$$

To cause this function to satisfy Eq. 4,  $\lambda$  is determined from the equation obtained by substituting Eqs. 6 and 9 into 4; hence

$$\lambda^{1/2} = \frac{1}{\Delta(\xi)} \int_S \left( \frac{M m \rho e}{E b} \right)^{1/2} dx \quad \dots\dots\dots (10)$$

<sup>6</sup> "Methods of Mathematical Physics," by R. Courant and D. Hilbert, Vol. I, Interscience Publishers, Inc., 1953, p. 216.

If Eq. 10 is substituted into Eq. 9, the extremal function  $t^0(x)$  becomes

$$t^0(x) = \frac{1}{E \Delta(\xi)} \sqrt{\frac{M m}{b e}} \int_S \left( \frac{M m e}{b} \right)^{1/2} dx - \frac{a}{b} \dots \dots \dots (11)$$

Notice that  $t^0(x)$  becomes a complex function when the product  $M m$  assumes both positive and negative values in the span; hence, an extremal does not exist for this case. When  $M m \geq 0$ , the extremal does exist; however, it must be shown that it minimizes the beam weight since the stationary character of the weight integral is not a sufficient condition for the occurrence of an extremum. From the definitions of terms in Eq. 10, it can be seen that

$$I^0 \equiv a + b t^0(x) \geq 0 \dots \dots \dots (12)$$

It will be shown that  $W(t) \geq W(t^0)$ , for any  $t(x)$  that renders

$$I = a + b t(x) \geq 0 \dots \dots \dots (13)$$

and satisfies the subsidiary condition  $\Delta(\xi) = \text{positive constant}$ .

Define the quantity

$$F \equiv W(t) - W(t^0) \dots \dots \dots (14)$$

By definition, then,

$$F \equiv \int_S \rho [c + e t(x)] dx - \int_S \rho [c + e t^0(x)] dx \dots \dots \dots (15)$$

Substitute for  $t^0(x)$  and clear terms:

$$F = \frac{\rho}{E \Delta(\xi)} \left\{ E \Delta(\xi) \int_S \frac{e}{b} [a + b t(x)] dx - \left[ \int_S \left( \frac{M m e}{b} \right)^{1/2} dx \right]^2 \right\} \dots (16)$$

Substitute from Eqs. 4 and 6 for  $\Delta(\xi)$  and  $I$ , respectively. Then, Eq. 16 becomes

$$F = \frac{\rho}{E \Delta(\xi)} \left\{ \int_S \frac{M m}{(a + b t)} dx \int_S \frac{e}{b} (a + b t) dx - \left[ \int_S \sqrt{\frac{M m}{(a + b t)}} \sqrt{\frac{e}{b} (a + b t)} dx \right]^2 \right\} \dots \dots \dots (17)$$

Since the quantities  $[M m / (a + b t)]^{1/2}$  and  $[(e/b)(a + b t)]^{1/2}$  are real, positive, and piecewise continuous, the quantity in braces is non-negative by

Schwarz' Inequality.<sup>7</sup> Since  $\rho/[E \Delta(\xi)] > 0$ ,  $F = 0$ . This proves that  $t^0(x)$  provides the absolute minimum weight.

A relationship between the beam weight  $W$  and the deflection  $\Delta(\xi)$  can be obtained by substituting Eqs. 7 and 11 into 3:

$$\Delta(\xi) = \frac{1}{(E/\rho)} \left[ \int_S \left( \frac{M m e}{b} \right)^{1/2} dx \right]^2 \frac{1}{W - \int_S \rho \left( c - \frac{a e}{b} \right) dx} \dots (18)$$

Then,  $t^0(x)$  can be expressed in terms of weight by using Eq. 18:

$$t^0(x) = \frac{W - \int_S \rho \left( c - \frac{a e}{b} \right) dx}{\rho \int_S \left( \frac{M m e}{b} \right)^{1/2} dx} \sqrt{\frac{M m}{b e}} - \frac{a}{b} \dots (19)$$

Because of the reciprocity of the isoperimetric problem, the function  $t^0(x)$  given by Eq. 19 will minimize the deflection integral when the weight is specified.<sup>8</sup> That is, the problem of minimizing the deflection with a given mass is the same as the problem of minimizing the weight for a specified deflection.

Another easily handled form of the moment of inertia and area is given by

$$I(x) = w t^k(x) \dots (20)$$

and

$$A(x) = z t^n(x) \dots (21)$$

in which

$$w = w(x) > 0 \dots (22a)$$

$$z = z(x) > 0 \dots (22b)$$

are specified piecewise continuous functions,  $n > 0$ , and  $k > 0$ . For these forms, the extremal function and the weight-deflection relationship are given by Eqs. 23 and 24, respectively. Their development parallels the previous case precisely, but when demonstrating that the  $t^0(x)$  given by Eq. 23 provides absolute minimum weight, one should use Holder's Inequality<sup>9</sup> for integrals rather than Schwarz' Inequality:

$$t^0(x) = \left( \frac{M m}{w z} \right)^{\frac{1}{n+k}} \left[ \frac{1}{E \Delta(\xi)} \int_S (M m)^{\frac{n}{n+k}} \left( \frac{z^k}{w^n} \right)^{\frac{1}{n+k}} dx \right]^{1/k} \dots (23)$$

<sup>7</sup> "Foundations of Potential Theory," by O. D. Kellogg, Dover Publications, 1953, pp. 107-108.

<sup>8</sup> "Methods of Mathematical Physics," by R. Courant and D. Hilbert, Vol. I, Interscience Publishers, Inc., 1953, p. 258.

<sup>9</sup> "Theory of Functions of a Real Variable," by E. W. Hobson, Vol. I, Dover Publications, Inc., 1957, p. 643.

and

$$W \Delta^{n/k}(\xi) = \frac{1}{(E^{n/k}/\rho)} \left[ \int_S (M m)^{\frac{n}{n+k}} \left( \frac{z^k}{w n} \right)^{\frac{1}{n+k}} dx \right]^{\frac{n+k}{k}} \dots \dots \dots (24)$$

Note that the weight given by Eq. 24 is inversely proportional to the term  $E^{n/k}/\rho$ , which provides a measure of material efficiency.

When expressions more complicated than those considered here are used for the area and moment of inertia, Eq. 5 cannot generally be solved explicitly for the extremal. Furthermore, a direct numerical solution of this equation is not possible since it will contain the unknown constant  $\lambda$ . If  $\lambda$  were known, it could easily be determined numerically for every value of  $x$ . This suggests the following trial-and-error procedure: Assume a value of  $\lambda$  in Eq. 5 and construct numerically a function  $t(x)$ . With this function, evaluate numerically the integral in the subsidiary condition, Eq. 4. If the value of the integral is equal to the specified constant, the function  $t(x)$  is an extremal function; if not, repeat the procedure with another assumed  $\lambda$ . Since Eq. 5 usually has several roots for each value of  $x$  and  $\lambda$ , several functions  $t(x)$  may be found for each  $\lambda$ .

Two examples will be treated to demonstrate the design procedure based on the derived relationships.

*Example 1: Ideal I-Section.*—Consider the design of an ideal I-section, that is, two extremely thin parallel plates separated by a distance  $d$ . The area of each plate or flange at any station  $x$  is  $t(x)/2$ ; therefore,

$$A(x) = t(x) \dots \dots \dots (25)$$

The moment of inertia at any station is

$$I(x) = \frac{t(x) d^2(x)}{4} \dots \dots \dots (26)$$

The optimum flange-area distribution for this type of section is found from Eq. 11, where  $a = c = 0$ ,  $b = d^2(x)/4$ , and  $e = 1$ ; thus,

$$A^0(x) = t^0(x) = \frac{4}{E \Delta(\xi)} \sqrt{\frac{M m}{d^2}} \int_S \left( \frac{M m}{d^2} \right)^{1/2} dx \dots \dots \dots (27)$$

Eq. 18 specializes into an extremely simple relationship between the weight, deflection, and material properties of an optimum designed ideal I-section; thus

$$W \Delta(\xi) (E/\rho) = 4 \left[ \int_S \frac{\sqrt{M m}}{d} dx \right]^2 = \text{constant} \dots \dots \dots (28)$$

It can be seen from Eq. 28 that the weight is inversely proportional to the deflection and the specific stiffness,  $E/\rho$ . Eq. 28 indicates that the weights of optimum beams designed with steel, aluminum, magnesium, and titanium would all be equivalent since the specific stiffness is almost the same ( $E/\rho = 10^8$  in.) for most structural materials. This fact provides one of the motivations for



considering ceramic materials, which generally demonstrate specific stiffnesses many times greater than ordinary structural materials (boron carbide:  $E/\rho = 7.22 \times 10^8$  in.). The optimum flange area given by Eq. 27 is inversely proportional to the modulus of elasticity; consequently, all other things being equal, the lighter structural materials lead to bulkier flanges, which are advantageous from the point of view of stability.

*Example 2: Conventional I-Section or Box-Section.*—Consider the minimum weight-deflection design of a simply supported I-beam subjected to a downward-acting load system. The cross-sectional geometry at any station is described in Fig. 1. The flange thickness  $r$  and the web thickness  $s$  are specified positive functions of  $x$ , the depth variation  $d(x)$  is specified such that  $d(x) > 2r$ , and the flange width  $t(x)$  is treated as the open parameter. The moment of inertia and the area of this section are given by Eqs. 6 and 7, respectively, where

$$a \equiv s g > 0 \quad \dots\dots\dots (29a)$$

$$b \equiv \frac{d^3 - (d - 2r)^3}{12} > 0 \quad \dots\dots\dots (29b)$$

$$c \equiv s h > 0 \quad \dots\dots\dots (29c)$$

$$e \equiv 2r > 0 \quad \dots\dots\dots (29d)$$

$$g \equiv \frac{(d - 2r)^3}{12} \quad \dots\dots\dots (29e)$$

and

$$h \equiv d - 2r \quad \dots\dots\dots (29f)$$

For a downward-acting load system on a simply supported beam, the external moment diagram is continuous, convex with respect to the moment diagram baseline, and zero at the ends. Consequently, the product  $M m$  can always be taken as non-negative when a downward deflection is specified. The optimum flange width variation  $t^0(x)$ , then, is given by Eq. 11.

As the ends of the beam are approached, the product  $M m$  decreases continuously to zero. For this reason, Eq. 11 indicates that  $t^0(x)$  is negative in some finite region at the beam ends. The stations where the flange width goes from positive to negative (cross-over points) can easily be located by finding the roots of the equation  $t^0(x) = 0$ .

The solution to a real problem demands, of course, that  $t(x) \geq 0$ ; consequently, Eq. 11 represents a mathematical rather than a real solution to the problem. If one formulates the original problem in a slightly different fashion, an optimum flange width variation  $t^*(x)$  may be found subject to the additional condition that  $t(x) \geq 0$ .

For the beam section under consideration, define the moment of inertia and area distributions as follows:

$$I = a; A = c \quad 0 \leq x \leq \xi \quad \dots\dots\dots (30a)$$

$$I = a + b t(x); A = c + e t(x) \quad \xi \leq x \leq \eta \quad \dots\dots\dots (30b)$$

$$I = a; A = c \quad \eta \leq x \leq L \quad \dots\dots\dots (30c)$$



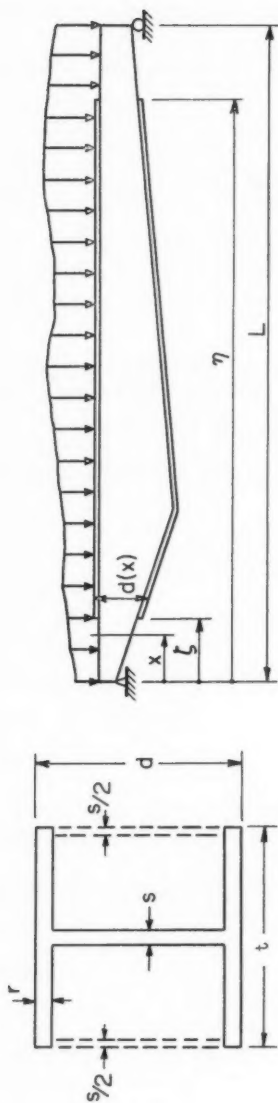
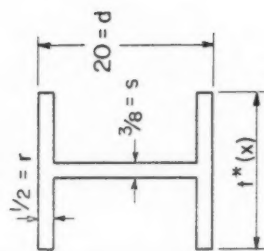
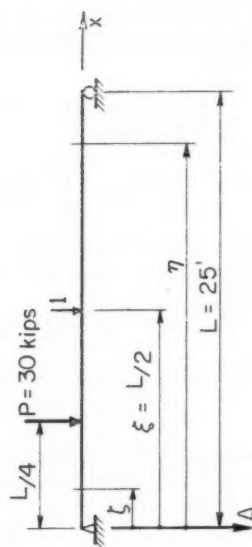


FIG. 1. - I-SECTION OR BOX-SECTION

FIG. 2. - TYPICAL BEAM SHOWING THE LOCATION OF THE CROSS-OVER POINTS



(b) Cross Section



(a) Elevation

FIG. 3. - MINIMUM-WEIGHT DESIGN OF A CONSTANT-DEPTH I-BEAM

Fig. 2 illustrates such a beam. The objective is to find an extremum  $t^*(x)$  for  $\xi \leq x \leq \eta$  such that  $\xi$  and  $\eta$  locate its cross-over points. The expressions for the weight and deflection of this beam are given by

$$X \equiv W - \int_0^{\xi} \rho c \, dx - \int_{\eta}^L \rho c \, dx = \int_{\xi}^{\eta} \rho [c + e t(x)] \, dx \quad \dots (31)$$

and

$$Y \equiv \Delta(\xi) - \int_0^{\xi} \frac{M m}{E a} \, dx - \int_{\eta}^L \frac{M m}{E a} \, dx$$

$$= \int_{\xi}^{\eta} \frac{M m}{E [a + b t(x)]} \, dx = \text{constant} \quad \dots (32)$$

The minimization of  $W$  subject to the condition that  $\Delta(\xi) = \text{constant}$  is equivalent to minimizing  $X$  with  $Y = \text{constant}$ . This latter problem was solved at the beginning of this subsection; hence, the results given by Eqs. 11, 18, and 19 apply here if  $W$  is replaced by  $X$ ,  $\Delta(\xi)$  is replaced by  $Y$ , and the integration over the span is contracted to the interval  $\xi \leq x \leq \eta$ . The extremal function  $t^*(x)$  then becomes

$$t^*(x) = \frac{\sqrt{\frac{M m}{b e}}}{E \Delta(\xi) - \int_0^{\xi} \frac{M m}{a} \, dx - \int_{\eta}^L \frac{M m}{a} \, dx} \int_{\xi}^{\eta} \left( \frac{M m e}{b} \right)^{1/2} \, dx - \frac{a}{b} \dots (33)$$

for  $\xi \leq x \leq \eta$ . At the cross-over points, the flange width is zero; consequently,  $\xi$  and  $\eta$  may be determined from the conditions:

$$t^*(\xi) = 0 \quad \dots (34a)$$

and

$$t^*(\eta) = 0 \quad \dots (34b)$$

**Numerical Example.**—For a beam with the geometry and loading shown in Fig. 3, the following quantities may be computed:

$$M = \frac{3 P}{4} x \quad 0 \leq x \leq L/4 \quad \dots (35a)$$

$$M = \frac{P}{4} (L - x) \quad L/4 \leq x \leq L \quad \dots (35b)$$

$$m = \frac{x}{2} \quad 0 \leq x \leq L/2 \quad \dots (35c)$$

$$m = \frac{1}{2} (L - x) \quad L/2 \leq x \leq L \quad \dots (35d)$$

$$a = \frac{s(d - 2r)^3}{12} = \frac{0.375}{12} [20 - 2(1/2)]^3 = 214.34 \text{ in.}^4 \quad \dots (35e)$$

and

b, c, and e are constants.

For these quantities and Eq. 33, conditions 34 become

$$t^*(\xi) = 0 = \frac{\frac{P\sqrt{3}}{8b} \xi \left[ \frac{L^2}{48} (6 + \pi + 3\sqrt{3}) - \frac{\sqrt{3}}{2} \xi^2 - \frac{(L - \eta)^2}{2} \right]}{E \Delta(\xi) - \frac{P\xi^3}{8a} - \frac{P(L - \eta)^3}{24a}} - \frac{a}{b} \dots (36)$$

and

$$t^*(\eta) = 0 = \frac{\frac{P}{8b} (L - \eta) \left[ \frac{L^2}{48} (6 + \pi + 3\sqrt{3}) - \frac{\sqrt{3}}{2} \xi^2 - \frac{(L - \eta)^2}{2} \right]}{E \Delta(\xi) - \frac{P\xi^3}{8a} - \frac{P(L - \eta)^3}{24a}} - \frac{a}{b} \dots (37)$$

The ratio of Eqs. 36 and 37 yields

$$L - \eta = \sqrt{3} \xi \dots (38)$$

When this relationship is substituted into Eq. 30, that equation reduces to

$$\xi^3 - \xi \frac{L^2(6\sqrt{3} + \pi\sqrt{3} + 9)}{24(1 + \sqrt{3})} + \frac{16 E a \Delta(\xi)}{(1 + \sqrt{3}) P} = 0 \dots (39)$$

When this cubic is solved for  $P = 30$  kips,  $L = 300$  in.,  $E = 30 \times 10^6$  psi,  $a = 214.34$  in.<sup>4</sup>, and  $\Delta(150) = 1/2$  in.,

$$\xi = 18.60 \text{ in.}$$

From Eq. 38, then

$$\eta = 267.78 \text{ in.}$$

The cross-over points  $\xi$  and  $\eta$  obtained from the equation  $t^0(x) = 0$ , where  $t^0(x)$  is given by Eq. 11 are

$$\xi^0 = \frac{384}{6\sqrt{3} + \pi\sqrt{3} + 9} \frac{E a \Delta(\xi)}{L^2 P} = 18.41 \text{ in.}$$

and

$$\eta^0 = L - \sqrt{3} \xi^0 = 268.11 \text{ in.}$$

They closely approximate  $\xi$  and  $\eta$ .

#### CONSTANT-STRENGTH BEAMS

The attention given to the stiffness and strength of constant-strength beams in the literature and the insight that such beams provide about the properties of minimum-deflection beams, furnish the motivation for the ensuing discussion.

For a constant-strength beam with a doubly symmetric cross section and loaded in a plane of symmetry, the moment-of-inertia distribution is given by the expression,<sup>10</sup>

$$I^0(x) = \frac{|M(x)| q(x)}{\sigma_0} \dots \dots \dots (40)$$

where  $\sigma_0$  is a constant specified positive stress and  $q(x)$  is the distance from the neutral axis to the outermost fibers ( $q = d/2 > 0$ ). By substituting Eq. 40 into the deflection equation, Eq. 1, the stress  $\sigma_0$  can be related to the deflection  $\Delta(\xi)$ :

$$\sigma_0 = \frac{E \Delta(\xi)}{\int_S \frac{M}{|M|} \frac{m}{q} dx} \dots \dots \dots (41)$$

And, by using Eq. 41, the moment of inertia can be related to the deflection; thus,

$$I^0(x) = \frac{|M| d}{E \Delta(\xi)} \int_S \frac{M}{|M|} \frac{m}{d} dx \dots \dots \dots (42)$$

For beam sections that are defined by one open parameter  $t(x)$ , the parameter can be calculated from the relationship

$$I[x, t(x)] = I^0(x) \dots \dots \dots (43)$$

The resulting  $t(x)$  may then be used to establish the area  $A[x, t(x)]$  and, hence, the weight. For the ideal I-section, the moment of inertia given by Eq. 26 is set equal to  $I^0(x)$ . The open parameter then becomes

$$t(x) = \frac{4}{d^2} I^0 = \frac{4|M|}{E \Delta(\xi) d} \int_S \frac{M}{|M|} \frac{m}{d} dx \dots \dots \dots (44)$$

and the weight of the constant strength beam  $W_c$ , Eq. 25, becomes

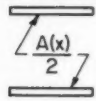
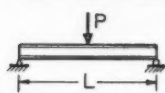
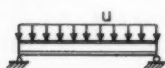



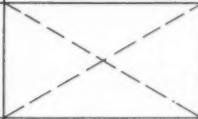
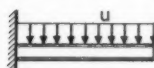
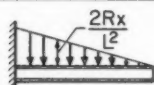
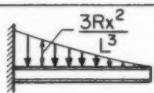
$$W_c = \int_S \rho t(x) dx = \frac{4 \rho}{E \Delta(\xi)} \int_S \frac{|M|}{d} dx \int_S \frac{M}{|M|} \frac{m}{d} dx \dots \dots \dots (45)$$

To clarify comparison of the weights of the optimum deflection beam and the constant strength beam, the weight of the optimum deflection beam,  $W_d$ , given by Eq. 28 may be rewritten as

$$W_d = \frac{4 \rho}{E \Delta(\xi)} \left[ \int_S \sqrt{\frac{M m}{|M| d}} \sqrt{\frac{|M|}{d}} dx \right]^2 \dots \dots \dots (46)$$

<sup>10</sup> "Strength of Materials," by S. Timoshenko, Vol. I, D. Van Nostrand Co., Inc., 3rd Ed., 1955, p. 210.

TABLE 1.—WEIGHT OF BEAM FLANGES DESIGNED FOR DEFLECTION

IDEAL I-SECTION  $I = \frac{Ad^2}{4}$ ; $q = \frac{d}{2}$	PRISMATIC BEAM $W_p = \frac{4\rho L}{E\Delta} \int_s \frac{Mm}{d^2} dx$	CONSTANT STRENGTH BEAM $W_c = \frac{4\rho}{E\Delta} \int_s \frac{M}{d} dx \int_s \frac{m}{d} dx$	MINIMUM DEFLECTION BEAM $W_d = \frac{4\rho}{E\Delta} \left[ \int_s \frac{\sqrt{Mm}}{d} dx \right]^2$
	$\frac{P\rho L^4}{E\Delta d^2}$ (0.08333) $\Delta \cdots$ CNTRL DEFL	$\frac{P\rho L^4}{E\Delta d^2}$ (0.06250) $W_c = 0.7500 W_p$	$\frac{P\rho L^4}{E\Delta d^2}$ (0.06250) $W_d = 0.7500 W_p$
	$\frac{u\rho L^5}{E\Delta d^2}$ (0.05208) $\Delta \cdots$ CNTRL DEFL	$\frac{u\rho L^5}{E\Delta d^2}$ (0.04167) $W_c = 0.8001 W_p$	$\frac{u\rho L^5}{E\Delta d^2}$ (0.04135) $W_d = 0.7940 W_p$
	$\frac{R\rho L^4}{E\Delta d^2}$ (0.06667) $\Delta \cdots$ CNTRL DEFL	$\frac{R\rho L^4}{E\Delta d^2}$ (0.05208) $W_c = 0.7812 W_p$	$\frac{R\rho L^4}{E\Delta d^2}$ (0.05191) $W_d = 0.7786 W_p$
	$\frac{T\rho L^3}{E\Delta d^2}$ (0.5000) $\Delta \cdots$ CNTRL DEFL	$\frac{T\rho L^3}{E\Delta d^2}$ (0.5000) $W_c = W_p$	$\frac{T\rho L^3}{E\Delta d^2}$ (0.4444) $W_d = 0.8889 W_p$
		$\frac{4P\rho}{E\Delta} \left[ \frac{L}{2b} - \frac{a}{b^2} \log \left( 1 + \frac{bL}{2a} \right) \right]^2$ , $b \neq 0$ $\Delta \cdots$ CENTRAL DEFLECTION	
	$\frac{u\rho L^5}{E\Delta d^2}$ (0.5000) $\Delta \cdots$ TIP DEFL	$\frac{u\rho L^5}{E\Delta d^2}$ (0.3333) $W_c = 0.6667 W_p$	$\frac{u\rho L^5}{E\Delta d^2}$ (0.3200) $W_d = 0.6400 W_p$
	$\frac{R\rho L^4}{E\Delta d^2}$ (0.2666) $\Delta \cdots$ TIP DEFL	$\frac{R\rho L^4}{E\Delta d^2}$ (0.1667) $W_c = 0.6250 W_p$	$\frac{R\rho L^4}{E\Delta d^2}$ (0.1481) $W_d = 0.5556 W_p$
	$\frac{R\rho L^4}{E\Delta d^2}$ (0.1667) $\Delta \cdots$ TIP DEFL	$\frac{R\rho L^4}{E\Delta d^2}$ (0.1000) $W_c = 0.6000 W_p$	$\frac{R\rho L^4}{E\Delta d^2}$ (0.08163) $W_d = 0.4898 W_p$

It is readily apparent from the Schwarz' Inequality that

$$W_d \left( \frac{E \Delta(\xi)}{4 \rho} \right) = \left[ \int_S \sqrt{\frac{M m}{|M| d}} \sqrt{\frac{|M|}{d}} dx \right]^2 \leq \int_S \frac{|M|}{d} dx \int_S \frac{M m}{|M| d} dx$$

$$= \left( \frac{E \Delta(\xi)}{4 \rho} \right) W_c \dots \dots \dots (47)$$

the equality sign holding if and only if the integrands  $|M|/d$  and  $M m/(|M|d)$  are proportional. Thus, the equality holds only when  $M/m = \text{constant}$ .

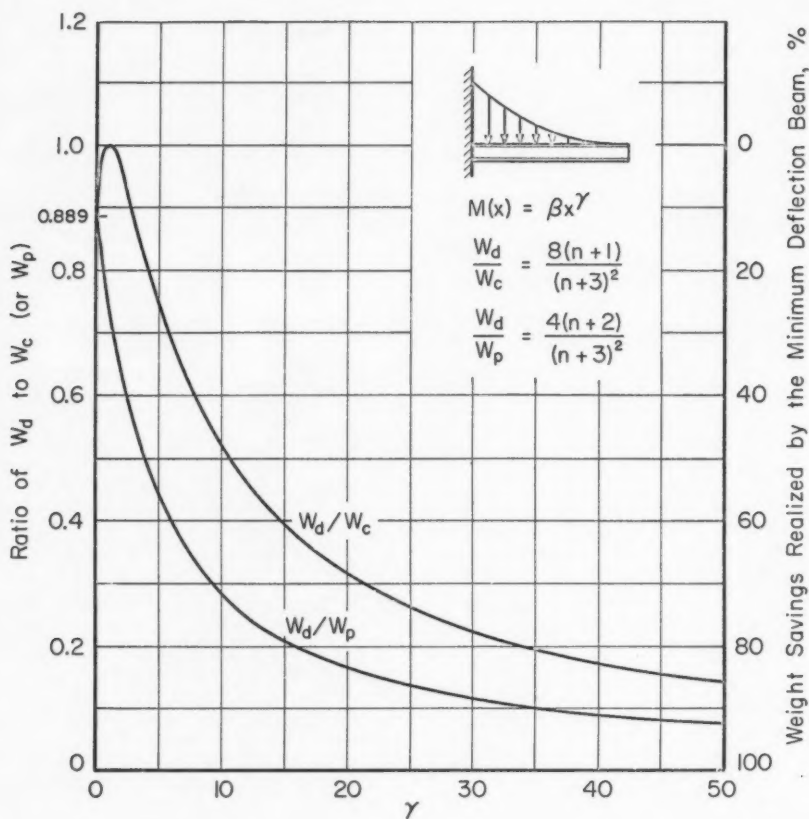


FIG. 4.—COMPARISONS AMONG PRISMATIC, CONSTANT STRENGTH, AND MINIMUM DEFLECTION CANTILEVER BEAMS DESIGNED FOR A SPECIFIED TIP DEFLECTION

In Table 1, the weights of prismatic, constant strength, and minimum deflection beams are compared with respect to different loadings and end conditions. For the more common loadings on simply supported beams, it can be

observed that the weights of the constant-strength beams very closely approximate those of the minimum-deflection beams. In these cases, one would expect the properties of the minimum-deflection beam to be somewhat similar to those of the constant-strength beam; that is, the stress level should be nearly constant, and the deflection curve of a uniform-depth member should be nearly circular with the maximum deflection occurring at the center. The cantilevers in Table 1 show considerable disparity, however, between the weights of the constant strength and minimum deflection beams. As is illustrated in Fig. 4, the differences become more pronounced with increasing order of loading.

### BENDING AND SHEAR DEFLECTIONS OF SYMMETRICAL BEAMS (TWO-PARAMETER BEAM SECTIONS)

In the previous material, only the bending deflection was considered. Here, account is taken of both bending and shear deflections and three cases are treated: (1) an I-beam with an optimum flange width and an optimum web thickness variation, (2) an I-beam with an optimum flange width variation and an optimum constant thickness web, and (3) an optimum prismatic beam.

The shear deflections of a beam may be approximated by the virtual-work expression

$$\delta(\xi) = \int_S \frac{\alpha V v}{G A(x)} dx \dots\dots\dots (48)$$

in which  $V$  is the external shear,  $v$  denotes the shear due to a vertical unit load acting at station  $x = \xi$ ,  $G$  is the modulus of rigidity, and  $\alpha$  represents a dimensionless factor which depends on the form of the cross section. For rectangular sections,  $\alpha = 6/5$ ; for I-sections or box-sections,  $\alpha$  is given by<sup>11</sup>

$$\alpha = f + j \frac{t}{s} \frac{A}{I} \dots\dots\dots (49)$$

in which

$$j \equiv \frac{0.6 r}{d} (d - r)(d - 2r) > 0 \dots\dots\dots (50)$$

$$f \equiv \frac{d^2}{10} - j > 0 \dots\dots\dots (51)$$

and  $s$ ,  $t$ ,  $r$ , and  $d$  are the dimensions shown in Fig. 1.

*Case 1: Optimum Flange Width and Web Thickness Distributions.*—The moment of inertia and the area of the I-beam section shown in Fig. 1 are, respectively,

$$I(x) = b t(x) + g s(x) \dots\dots\dots (52)$$

and

$$A(x) = e t(x) + h s(x) \dots\dots\dots (53)$$

<sup>11</sup> "Deflections of Beams with Special Reference to Shear Deformation," by J. A. Newlin and G. W. Trayer, Nat. Adv. Comm. Aero., Report 180, 1924.

With the use of Eqs. 52 and 53 and the form factor given by Eq. 49, the beam weight and the beam deflection become

$$W = \int_S \rho A \, dx = \int_S \rho (e t + h s) \, dx \dots\dots\dots (54)$$

and

$$\Delta(\xi) = \int_S \left( \frac{M m}{E I} + \frac{\alpha V v}{G A} \right) dx = \int_S \frac{\frac{M m}{E} + \frac{V v}{G} \left( f + j \frac{t}{s} \right)}{b t + g s} dx \dots\dots\dots (55)$$

Two functions,  $t^0$  and  $s^0$ , are sought that will minimize the weight  $W$  while satisfying the specified deflection requirement  $\Delta(\xi) = \text{positive constant}$ . It should be noted that the unit load must be applied in the same direction as the specified deflection. If the dimensions  $t$  and  $s$  are required to be non-negative, Eq. 55 reveals five distinct possibilities with regard to the products  $M m$  and  $V v$ . Each case from this exhaustive set of possibilities will be discussed separately.

Case 1-a.—  $V v > 0$  and  $V v < 0$  in  $S$

Instead of dealing with the two open parameters  $t$  and  $s$ , we shall consider the equivalent, but more convenient, parameters  $s$  and  $t/s$  in which  $s > 0$  and  $0 \leq \frac{t}{s} < \infty$ .

Eq. 55 may be written as

$$\Delta(\xi) = \int_S \frac{\frac{M m}{E} + \frac{V v}{G} \left( f + j \frac{t}{s} \right)}{s \left( g + b \frac{t}{s} \right)} dx = \text{positive constant} \dots\dots\dots (56)$$

Regardless of the value of  $M m/E$ , the ratio  $t/s$  may be set equal to a constant of sufficient magnitude to cause the numerator of the integrand of Eq. 56 to change signs in  $S$ . With the dimension  $s$  still at our disposal, we have a situation similar to that discussed in Case 2 under the heading "Bending Deflections of Symmetrical Beams." Consequently, any deflection can be obtained with a beam of vanishing lateral dimensions.

Case 1-b.—  $V v \leq 0$  throughout  $S$ ;  $M m > -V v f E/G$  somewhere in  $S$ .

Clearly, in any portion of the span, the ratio  $t/s$  can be set sufficiently large to ensure that the numerator of the integrand of Eq. 56 is negative. If  $M m > -V v f E/G$  anywhere in the span, the numerator can be made positive by setting  $t/s = 0$ . Since the numerator can be made positive in some portion of the span and negative in other portions, the circumstances are equivalent to that of Case 1-a. Thus, a member of vanishing weight may be obtained which will provide any specified deflection.

Case 1-c.—  $V v \leq 0$  and  $M m \leq -V v f E/G$  throughout  $S$ .

If the conditions defining this case are fulfilled, the numerator of the integrand of Eq. 56 will be nonpositive throughout the span regardless of the value assumed by the ratio  $t/s$ . For this condition, the integral in Eq. 56 can yield a positive value for the specified deflection only if negative values of  $t$  and  $s$  are admitted. Since this violates the original hypothesis, no solution exists for this case.



Case 1-d.— $V v \geq 0$  throughout  $S$ ;  $M m < -V v f E/G$  somewhere in  $S$ .

In this case, the ratio  $t/s$  can be set sufficiently great to ensure that the numerator of the integrand of Eq. 56 is positive in any portion of the span. Furthermore, if  $t/s$  is set equal to zero, this numerator will be negative somewhere in the span. Again the circumstances of Case 1-a prevail and a beam of vanishing weight that can achieve any specified positive deflection can be approached.

Case 1-e.— $V v \geq 0$  and  $M m \geq -V v f E/G$  throughout  $S$ .

The conditions defining this case insure that the numerator of the integrand of Eq. 56 is non-negative. In this case, it is possible to find two non-negative functions  $t(x)$  and  $s(x)$  such that Eq. 56 will be satisfied. We seek those functions which, in addition, will minimize the weight integral, Eq. 54. This problem is an isoperimetric problem in two arguments. The two extremal functions  $t^0(x)$  and  $s^0(x)$  must be determined to satisfy the following reduced forms of the Euler equations for a suitable value of the parameter  $\lambda$ . This parameter is determined from the condition  $\Delta(\xi) = \text{positive constant}$ :

$$\frac{\partial}{\partial t} \left\{ \rho(e t + h s) + \lambda \left[ \frac{\frac{M m}{E} + \frac{V v}{G} \left( f + j \frac{t}{s} \right)}{b t + g s} \right] \right\} = 0 \dots\dots\dots (57)$$

and

$$\frac{\partial}{\partial s} \left\{ \rho(e t + h s) + \lambda \left[ \frac{\frac{M m}{E} + \frac{V v}{G} \left( f + j \frac{t}{s} \right)}{b t + g s} \right] \right\} = 0 \dots\dots\dots (58)$$

Performing the operations indicated in Eqs. 57 and 58 and solving the resulting simultaneous equations, one obtains

$$\frac{t}{s} = -\frac{g}{b} + \sqrt{\frac{h b - g e}{b e j} \left( \frac{M m G}{V v E} + f - \frac{g j}{b} \right)} \dots\dots\dots (59)$$

and

$$s = \lambda^{1/2} \sqrt{\frac{V v j}{G \rho (h b - g e)}} \dots\dots\dots (60)$$

The parameter  $\lambda$  is determined by substituting Eqs. 59 and 60 into 55; hence,

$$\lambda^{1/2} = \frac{\rho^{1/2}}{\Delta(\xi)} \int_S \left[ \sqrt{\frac{M m e}{E b} + \frac{V v e}{G} \left( \frac{f b - j g}{b^2} \right)} + \sqrt{\frac{V v j}{G} \left( \frac{h b - g e}{b^2} \right)} \right] dx \dots\dots (61)$$

The expressions for the optimum flange width and web thickness variations become

$$s^0(x) = \frac{1}{\Delta(\xi)} \sqrt{\frac{V v j}{G (h b - g e)}} \int_S \left[ \sqrt{\frac{M m e}{E b} + \frac{V v e}{G} \left( \frac{f b - j g}{b^2} \right)} + \sqrt{\frac{V v j}{G} \left( \frac{h b - g e}{b^2} \right)} \right] dx \dots\dots\dots (62)$$

and

$$t^0(x) = \frac{1}{\Delta(\xi)} \left\{ \left[ \sqrt{\frac{M m}{E b e} + \frac{V v}{G e} \left( \frac{f b - j g}{b^2} \right)} \right] - \frac{g}{b} \sqrt{\frac{V v j}{G (h b - g e)}} \right\} \int_S \left[ \sqrt{\frac{M m e}{E b} + \frac{V v e}{G} \left( \frac{f b - j g}{b^2} \right)} + \sqrt{\frac{V v j}{G} \left( \frac{h b - g e}{b^2} \right)} \right] dx \dots \dots \dots (63)$$

With the use of Eqs. 62 and 63, the optimum beam weight becomes

$$W^0 = \frac{1}{\Delta(\xi)} \left\{ \int_S \left[ \sqrt{\frac{M m e}{(E/\rho) b} + \frac{V v e}{(G/\rho)} \left( \frac{f b - j g}{b^2} \right)} + \sqrt{\frac{V v j}{(G/\rho)} \left( \frac{h b - g e}{b^2} \right)} \right] dx \right\}^2 \dots (64)$$

Since  $E/G = 2.5$  for most structural materials, the weight  $W^0$  is inversely proportional to specific stiffness,  $E/\rho$ .

Noting that the quantities  $(h b - g e)$  and  $(f b - j g)$  are positive when the depth  $d$  is greater than  $2 r$ , one can readily show that the extremals cannot be real and non-negative when any of the conditions given for Cases 1-a to 1-d are fulfilled. Examination of Eq. 62 indicates that the web thickness  $s^0$  is always non-negative. On the other hand, Eq. 63 indicates that the flange width  $t^0$  is non-negative only when

$$M m \geq \frac{V v E}{G} \left( \frac{g h j}{h b - g e} - f \right) \dots \dots \dots (65)$$

It is possible, as was demonstrated in Example 2, to define the beam geometry in those regions where  $t^0$  would become negative. In Example 2, the flange width was allowed to decrease to zero; here, a slightly greater weight savings can be realized by permitting the flange width to decrease no smaller than the web thickness (a rectangular section is more efficient than a degenerate I-section). Thus, in those regions where  $t^0$  would normally be less than  $s^0$ , the sections will be taken as rectangles of width  $s(x)$  and depth  $d(x)$ . The design procedure will be illustrated in the following example.

**Example 3: Simply Supported I-Section or Box-Section.**—For a simply supported beam subjected to a downward-acting load system,  $t^0$  may become less than  $s^0$  in the regions adjacent to the supports. In a manner similar to that shown in Fig. 2, three regions of such a beam are identified: region 1,  $0 \leq x \leq \xi$ ; region 2,  $\xi \leq x \leq \eta$ ; and region 3,  $\eta \leq x \leq L$ . The total beam weight and deflection are distributed among these regions. The weight and deflection contribution of each region will be denoted by  $W_i$  and  $\Delta_i$  respectively, where the subscript identifies the region. The total beam weight is

$$W = W_1 + W_2 + W_3 \dots \dots \dots (66)$$

where

$$W_1 = \int_0^{\xi} \rho \, ds \, dx \quad 0 \leq x \leq \xi \quad [\text{note: } t(x) = s(x)] \dots (67a)$$

$$W_2 = \int_{\xi}^{\eta} \rho [e t + h s] \, dx \quad \xi \leq x \leq \eta$$

and

$$W_3 = \int_{\eta}^L \rho \, ds \, dx \quad \eta \leq x \leq L \quad [\text{note: } t(x) = s(x)] \dots (67c)$$

The total deflection becomes

$$\Delta(\xi) = \Delta_1(\xi) + \Delta_2(\xi) + \Delta_3(\xi) = \text{constant} \dots (68)$$

where

$$\Delta_1 = \int_0^{\xi} \left[ \frac{\frac{M m}{E} + \frac{V v}{G} (f + j)}{b + g} \right] \frac{dx}{s} \quad 0 \leq x \leq \xi \dots (69a)$$

$$\Delta_2 = \int_{\xi}^{\eta} \left[ \frac{\frac{M m}{E} + \frac{V v}{G} \left( f + j \frac{t}{s} \right)}{b t + g s} \right] dx \quad \xi \leq x \leq \eta \dots (69b)$$

and

$$\Delta_3 = \int_{\eta}^L \left[ \frac{\frac{M m}{E} + \frac{V v}{G} (f + j)}{b + g} \right] \frac{dx}{s} \quad \eta \leq x \leq L \dots (69c)$$

Assuming that  $\xi$  and  $\eta$  are known and that the values of  $\Delta_i$  equal known constants  $C_i$ , the weight  $W$  can be minimized by minimizing each of the values of  $W_i$  subject to the conditions  $\Delta_i = C_i$ . The extremals  $S_{1,3}^*$  for the regions 1 and 3 are obtained from Eq. 23, when the following replacements are made:  $t^0(x)$  by

$$s^0(x); w \text{ by } \frac{M m}{E} \left/ \left[ \frac{\frac{M m}{E} + \frac{V v}{G} (f + j)}{b + g} \right] \right.; z \text{ by } d; \Delta(\xi) \text{ by } \Delta_{1,3}; \text{ and } S \text{ by}$$

$0 \leq x \leq \xi$  for region 1,  $S$  by  $\eta \leq x \leq L$  for region 3, and  $k$  and  $n$  by unity. For

region 2, the extremal functions  $S_2^*$  and  $t_2^*$  are obtained from Eqs. 62 and 63, respectively, where  $S$  is replaced by  $\xi \leq x \leq \eta$ . Hence,

$$s_1^*(x, \Delta_1, \xi) = \frac{1}{\Delta_1} \sqrt{\frac{1}{d} \left[ \frac{M m}{E} + \frac{V v}{G} (f+j) \right] \frac{1}{b+g}} \int_0^\xi \sqrt{\frac{1}{d} \left[ \frac{M m}{E} + \frac{V v}{G} (f+j) \right] \frac{1}{b+g}} dx; \quad 0 \leq x \leq \xi \quad \dots \quad (70)$$

$$t_1^*(x, \Delta_1, \xi) = s_1^*(x, \Delta_1, \xi); \quad 0 \leq x \leq \xi \quad \dots \quad (71)$$

$$s_2^*(x, \Delta_2, \xi, \eta) = \frac{1}{\Delta_2} \sqrt{\frac{V v j}{G b^2 J}} \int_\xi^\eta \left[ \sqrt{\frac{M m e}{E b} + \frac{V v e K}{G}} + \sqrt{\frac{V v j J}{G}} \right] dx; \quad \xi \leq x \leq \eta \quad \dots \quad (72)$$

$$t_2^*(x, \Delta_2, \xi, \eta) = \frac{1}{\Delta_2} \left[ \sqrt{\frac{M m}{E b e} + \frac{V v K}{G e}} - \frac{g}{b^2} \sqrt{\frac{V v j}{G J}} \right] \int_\xi^\eta \left[ \sqrt{\frac{M m e}{E b} + \frac{V v e K}{G}} + \sqrt{\frac{V v j J}{G}} \right] dx; \quad \xi \leq x \leq \eta \quad \dots \quad (73)$$

$$s_3^*(x, \Delta_3, \eta) = \frac{1}{\Delta_3} \sqrt{\frac{1}{d} \left[ \frac{M m}{E} + \frac{V v}{G} (f+j) \right] \frac{1}{b+g}} \int_\eta^L \sqrt{\frac{1}{d} \left[ \frac{M m}{E} + \frac{V v}{G} (f+j) \right] \frac{1}{b+g}} dx; \quad \eta \leq x \leq L \quad \dots \quad (74)$$

$$t_3^*(x, \Delta_3, \eta) = s_3^*(x, \Delta_3, \eta); \quad \eta \leq x \leq L \quad \dots \quad (75)$$

in which

$$J \equiv \frac{h b - g e}{b^2} \quad \dots \quad (76)$$

and

$$K \equiv \frac{f b - j g}{b^2} \quad \dots \quad (77)$$

Eq. 70 through 75 completely describe the beam geometry when the quantities  $\Delta_1$ ,  $\Delta_2$ ,  $\Delta_3$ ,  $\xi$ , and  $\eta$  are specified. The values of these quantities are determined from the expressions for the total deflection (Eq. 68), the continuity of the web thickness at stations  $\xi$  and  $\eta$ , and the equality of the flange and web widths at stations  $\xi$  and  $\eta$ . Hence,

$$\Delta_3 = \Delta - \Delta_1 - \Delta_2 \quad \dots \quad (78)$$

$$s_1^*(x, \Delta_1, \xi) \Big|_{x=\xi} = s_2^*(x, \Delta_2, \xi, \eta) \Big|_{x=\xi} \quad \dots \quad (79)$$

$$s_3^*(x, \Delta_1, \eta) \Big|_{x=\eta} = s_2^*(x, \Delta_2, \xi, \eta) \Big|_{x=\eta} \quad \dots \quad (80)$$

$$t_2^*(x, \Delta_2, \xi, \eta) \Big|_{x=\xi} = s_2^*(x, \Delta_2, \xi, \eta) \Big|_{x=\xi} \quad \dots \quad (81)$$

and

$$t_2^*(x, \Delta_2, \xi, \eta) \Big|_{x=\eta} = s_2^*(x, \Delta_2, \xi, \eta) \Big|_{x=\eta} \dots\dots\dots (82)$$

The following numerical example for the conditions shown in Fig. 5 will illustrate the foregoing design technique.

*Numerical Example.*—From symmetry,  $\Delta_1 = \Delta_3$  and  $\xi = L - \eta$ . With the use of Eq. 78,  $\Delta_1 = \frac{1}{2} (\Delta - \Delta_2)$ . Substituting for  $M$ ,  $m$ ,  $V$ , and  $v$  in Eqs. 70 through 75, one obtains

Between  $0 \leq x \leq \xi$ :

$$s_1^* = \frac{PN}{4(\Delta - \Delta_2)} \sqrt{\frac{x^2}{E} + \frac{f+g}{G}} \dots\dots\dots (83)$$

and

$$t_1^* = s_1^* \dots\dots\dots (84)$$

in which

$$N \equiv \frac{1}{b+g} \left\{ \xi \sqrt{\frac{\xi^2}{E} + \frac{f+j}{G}} + \frac{f+j}{G} \sqrt{E} \log \left[ \sqrt{\frac{G\xi^2}{E(f+j)}} + \sqrt{\frac{G\xi^2}{E(f+j)} + 1} \right] \right\} \dots (85)$$

Between  $\xi \leq x \leq L/2$ :

$$s_2^* = \frac{PH}{4\Delta_2 b} \sqrt{\frac{j}{GJ}} \dots\dots\dots (86)$$

and

$$t_2^* = \frac{PH}{4\Delta_2} \left[ \sqrt{\frac{x^2}{Ebe} + \frac{K}{Ge}} - \frac{g}{b^2} \sqrt{\frac{j}{GJ}} \right] \dots\dots\dots (87)$$

in which

$$H \equiv \sqrt{\frac{jJ}{G}} (L - 2\xi) + \frac{L}{2} \sqrt{\frac{L^2 e}{4Eb} + \frac{eK}{G}} - \xi \sqrt{\frac{\xi^2 e}{Eb} + \frac{eK}{G}} \\ + \frac{K\sqrt{Eb e}}{G} \log \left( \frac{\frac{L}{2} + \sqrt{\frac{L^2}{4} + \frac{EbK}{G}}}{\xi + \sqrt{\xi^2 + \frac{EbK}{G}}} \right) \dots\dots\dots (88)$$

When one substitutes Eqs. 86 and 87 into 81 and clears terms,  $\xi$  becomes

$$\xi = \sqrt{\frac{E}{G} \left[ \frac{(b+g)^2 e j}{b^3 J} - bK \right]} \dots\dots\dots (89)$$

With this value of  $\xi$ ,  $\Delta_2$  is found from Eq. 79 to be

$$\Delta_2 = \frac{\Delta}{1 + \frac{Nb}{H} \sqrt{\frac{J}{j} \left( \frac{\xi^2 G}{E} + f + j \right)}} \dots\dots\dots (90)$$

For the geometry and loading shown in Fig. 5, the beam defined by Eqs. 83 through 90 is plotted in Fig. 6, with  $E = 30 \times 10^6$  psi,  $G = 12 \times 10^6$  psi, and  $\Delta = \frac{1}{2}$  in. The weight of region 2 of this beam can be computed from Eq. 64 when S

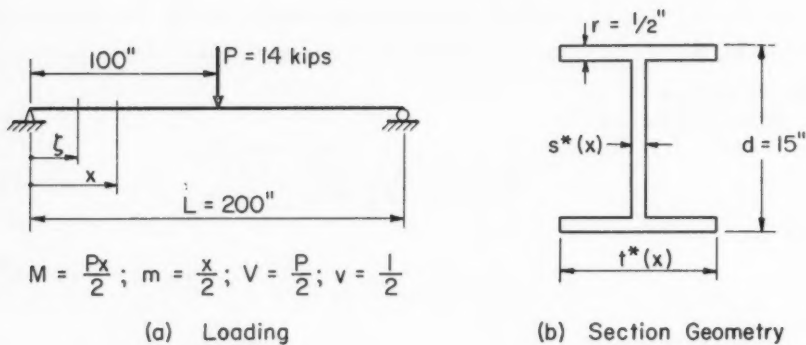


FIG. 5.—MINIMUM-WEIGHT DESIGN OF A CONSTANT-DEPTH I-BEAM FOR SHEAR AND BENDING DEFLECTION

is replaced by  $\xi \leq x \leq \eta$ . With the use of the replacements made in the computation of  $s_{1,3}^*$ , Eq. 24 gives the weights of regions 1 and 3. The pertinent data for this beam are:

$$E = 30 \times 10^6 \text{ psi}$$

$$G = 12 \times 10^6 \text{ psi}$$

$$\rho = 0.283 \text{ lb per cu in.,}$$

$$s_1^* = \sqrt{3.527 (10)^{-5} x^2 + 1.984 (10)^{-3}} \text{ in.}$$

$$t_1^* = s_1^*,$$

$$s_2^* = 0.05459 \text{ in.}$$

$$t_2^* = \sqrt{2.833 (10)^{-3} x^2 + 5.557 (10)^{-3}} - 0.2374 \text{ in.}$$

$$W_{1,3} = 1.0807 \text{ lb}$$

$$W_2 = 178.543 \text{ lb}$$

$$W = 179.624 \text{ lb}$$

$$\Delta_{1,3} = 0.002995 \text{ in.}$$

$$\Delta_2 = 0.4940 \text{ in.}$$

$$\Delta = 0.5000 \text{ in.}$$

$$\xi = 5.3031 \text{ in.}$$

$$d = 15.000 \text{ in.}$$

$$r = 0.5000 \text{ in.}$$

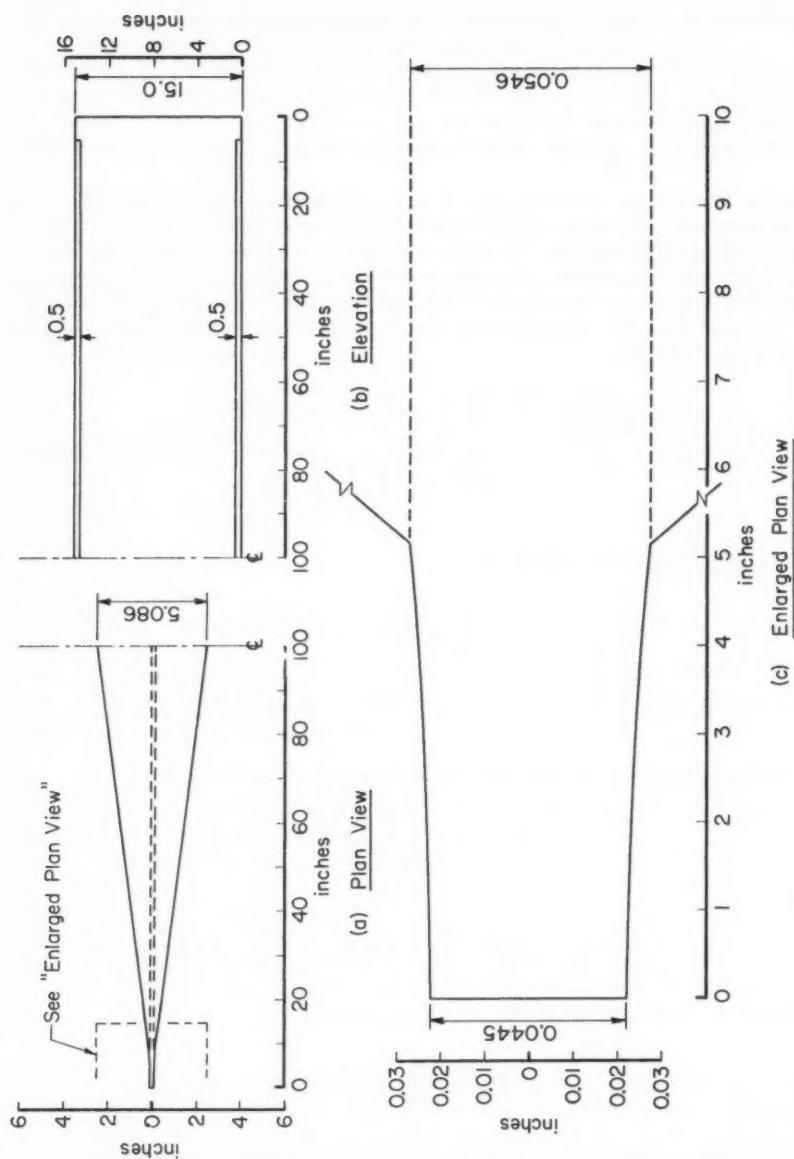


FIG. 6.—OPTIMUM STIFFNESS-WEIGHT DESIGN OF A SIMPLY SUPPORTED I-BEAM

*Case 2: Optimum Flange-Width Variation and Optimum-Constant Thickness Web.*—The difficulties inherent in the manufacture of a variable-thickness web plate lead naturally to an investigation of constant thickness webs. Once again for the I-section of Fig. 1, the moment of inertia and area are

$$I(x) = b t(x) + g s \dots\dots\dots (91)$$

and

$$A(x) = e t(x) + h s \dots\dots\dots (92)$$

in which  $s$  is taken as constant and  $b$ ,  $g$ ,  $e$ , and  $h$  are defined in Eq. 29. With these stipulations, the beam weight and deflection are given by Eqs. 54 and 55, respectively. In this section, we shall consider only those cases where an extremal function  $t^0(x)$  exists. Proceeding formally, the condition for minimizing the weight  $W$  when  $\Delta(\xi)$  is a specified positive constant is given by Eq. 57 alone. When one performs the operations in Eq. 57, solves for  $t$ , and eliminates  $\lambda$  by Eq. 55,  $t^0(x)$  becomes

$$t^0(x) = \frac{\sqrt{\frac{M m}{E b e} + \frac{V v K}{G e}} \int_S \sqrt{\frac{M m e}{E b} + \frac{V v e K}{G}} dx}{\Delta(\xi) - \frac{1}{s} \int_S \frac{V v j}{G b} dx} - \frac{g s}{b} \dots\dots (93)$$

The corresponding beam weight is

$$W^0 = s \rho \left[ \int_S b J dx + \frac{\left( \int_S \sqrt{\frac{M m e}{E b} + \frac{V v e K}{G}} dx \right)^2}{s \Delta(\xi) - \int_S \frac{V v j}{G b} dx} \right] \dots\dots\dots (94)$$

It is clear from Eq. 93 that the extremal function exists if

$$s \Delta(\xi) = \int_S \frac{V v j}{G b} dx \dots\dots\dots (95)$$

and if

$$\left( \frac{M m}{E b} + \frac{V v K}{G} \right) \geq 0 \dots\dots\dots (96)$$

throughout  $S$ . Note that  $t^0(x)$  is always negative if

$$s \Delta(\xi) < \int_S \frac{V v j}{G b} dx \dots\dots\dots (97)$$

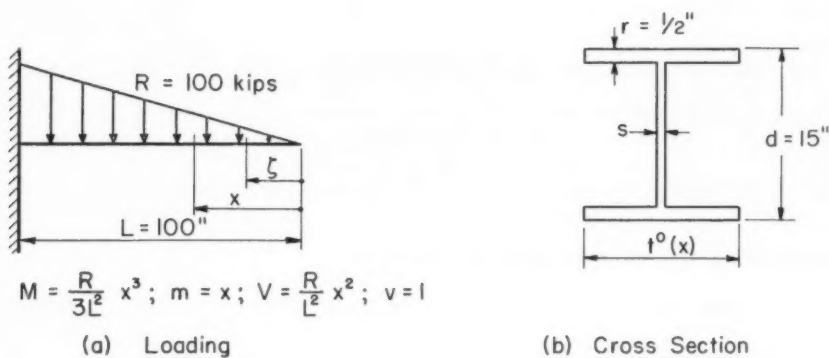
Physically this means that the web is so flexible in shear that the total deflection can never be restricted to  $\Delta(\xi)$ . Even when

$$s \Delta(\xi) < \int_S \frac{V v j}{G b} dx \dots\dots\dots (98)$$



it is possible for  $t^0(x)$  to become negative in some regions of a beam. As in the previous cases discussed, these regions may be isolated and their flange widths suitably defined. In the following example, the design procedure is demonstrated for a cantilever I-beam under a triangular loading. The flange width  $t$  is restricted to be greater or equal to the constant web thickness  $s$ .

**Example 4: Cantilever I-Section.**—For the loading shown in Fig. 7, the products  $M$  and  $V$  increase from zero at the tip to a maximum value at the support. Under these circumstances, Eq. 93 indicates that  $t^0(x)$  is negative in some interval at the tip, say  $0 \leq x \leq \xi$ . In this interval, the beam section is



$$M = \frac{R}{3L^2} x^3; \quad m = x; \quad V = \frac{R}{L^2} x^2; \quad v = 1$$

(a) Loading

(b) Cross Section

FIG. 7.—CANTILEVER I-SECTION UNDER A TRIANGULAR LOADING

taken as rectangular, the width as  $s$ , and the depth as  $d$ . The weight and deflection of this beam are given by

$$X \equiv W - \int_0^{\xi} \rho s d \, dx = \int_{\xi}^L \rho (h s + e t) \, dx \quad \dots \dots \dots (98)$$

and

$$Y \equiv \Delta(\xi) - \int_0^{\xi} \frac{\frac{M m}{E} + \frac{V v}{G} (f + j)}{(b + g) s} \, dx = \int_{\xi}^L \frac{\frac{M m}{E} + \frac{V v}{G} f + j \frac{t}{s}}{g s + b t} \, dx \quad \dots \dots (99)$$

As in Example 2, the minimization of  $W$  subject to the condition  $\Delta(\xi) = \text{constant}$  is equivalent to the minimization of  $X$  subject to the condition  $Y = \text{constant}$ . The extremal for the latter case,  $t^*(x)$ , is given by Eq. 93 when  $\Delta(\xi)$  is replaced by  $Y$  and the interval  $S$  is contracted to  $0 \leq x \leq \xi$ . The weight of the re-

sulting beam can be found from Eq. 98 when  $W^0$  is replaced by  $X$ ,  $\Delta(\xi)$  is replaced by  $Y$ , and  $S$  is replaced by the interval  $0 \leq x \leq \xi$ . Thus,

$$t^*(x, \xi) = \frac{\sqrt{\frac{M m}{E b e} + \frac{V v K}{G e}} \int_{\xi}^L \sqrt{\frac{M m e}{E b} + \frac{V v e K}{G}} dx}{\Delta(\xi) - \frac{1}{s} \left[ \int_0^{\xi} \frac{\frac{M m}{E} + \frac{V v}{G} (f+j)}{b+g} dx + \int_{\xi}^L \frac{V v j}{G b} dx \right]} - \frac{g s}{b}; \quad \xi \leq x \leq L \quad \dots (100)$$

$$W^* = s \rho \left[ \int_0^{\xi} d dx + \int_{\xi}^L b J dx + \frac{\left( \int_{\xi}^L \sqrt{\frac{M m e}{E b} + \frac{V v e K}{G}} dx \right)^2}{s \Delta(\xi) - \int_0^{\xi} \frac{\frac{M m}{E} + \frac{V v}{G} (f+j)}{b+g} dx + \int_{\xi}^L \frac{V v j}{G b} dx} \right] \dots (101)$$

Summarizing, the optimum beam is defined as

$$t(x) = s \quad 0 \leq x \leq \xi \quad \dots (102a)$$

and

$$t(x) = t^*(x, \xi) \quad \xi \leq x \leq L \quad \dots (102b)$$

Consequently,

$$t^*(x, \xi) \Big|_{x=\xi} = s \quad \dots (103)$$

from which  $\xi$  can be determined. For a given  $s$ , Eq. 103 must, in general, be solved numerically for  $\xi$ .

The optimum  $s$  may be found by a straightforward, although cumbersome, procedure. Because Eq. 103 can be solved explicitly for  $s$ , this quantity is substituted into Eq. 101 yielding an equation for  $W^*$  as a function of the independent variable  $\xi$ . The quantity  $W^*$  is then minimized by differentiating it with respect to  $\xi$ , setting the result equal to zero, and solving that equation for the optimum  $\xi$  (in general, this must be done numerically). Substituting this  $\xi$  into Eq. 103 immediately yields the optimum  $s$ .

In the following numerical example, the relationship between  $W^*$  and  $s$  is presented for the cantilever beam shown in Fig. 7. It was derived by guessing a value of  $\xi$ ; substituting it into Eq. 103 and solving explicitly for  $s$ ; computing  $W^*$  using the resulting  $s$  and the original; and repeating the procedure with another  $\xi$ .

**Numerical Example.**—Using the loading and geometry shown in Fig. 7, a tip deflection of  $1/2$ , and the same values of  $E$ ,  $G$ , and  $\rho$  used in Example 3, Eq.

103 is specialized and solved for  $s$ ; thus,

$$s = \frac{R}{L^2(b+g)\Delta(\xi)} \left[ b^2 E \xi \left( \frac{\xi^2}{3Eb} + \frac{K}{G} \right)^{1/2} \left( \frac{L^2}{3Eb} + \frac{K}{G} \right)^{3/2} - \frac{2}{45E} \xi^5 - \frac{bK}{3G} \xi^3 - \frac{Eb^2K^2}{G^2} \xi + \frac{jL^3(b+g)}{3Gb} \right] \dots \dots \dots (104a)$$

from which

$$s = 7.1111(10)^{-10} \left[ 255014 \xi \sqrt{2.1130 \xi^2 + 12.432} - 0.14815 \xi^5 - 2.1791 \xi^3 - 12.821 \xi + 6032093 \right] \dots \dots \dots (104b)$$

where  $s$  and  $\xi$  are expressed in inches. For the same conditions,  $W^*$  is specialized, giving,

$$W^* = s \rho \quad \xi (d - bJ) + bJL$$

$$\left\{ + \frac{Ee(b+g)}{\xi} \left[ \left( \frac{L^2}{3Eb} + \frac{K}{G} \right)^{3/2} - \left( \frac{\xi^2}{3Eb} + \frac{K}{G} \right)^{1/2} \right] \right\} \dots \dots (105a)$$

from which

$$W^* = 0.28300 s \left\{ 5.3487 \xi + 965.13 + \frac{8.4375}{\xi} \left[ \frac{307431}{\sqrt{2.1130 \xi^2 + 12.432}} - (0.21130 \xi^2 + 1.2432) \right] \right\} \dots \dots (105b)$$

where  $W^*$  is expressed in pounds and  $s$  and  $\xi$  in inches. By using Eqs. 104 and 105, values of  $s$  and  $W^*$  were computed for different values of  $\xi$ . The resulting relationships between  $W^*$  and  $\xi$  and between  $W^*$  and  $s$  are shown in Fig. 8. It is apparent from this figure that the weight  $W^*$  increases very rapidly as  $s$  is decreased from its optimum value or extreme point. On the other hand, for values of  $s$  greater than the optimum value, the curves are very flat. This insensitivity is very useful in the sense that the web thickness can be increased for strength purposes with little increase in the weight over  $W_{\min}^*$ .

The minimum-weight beam with the optimum constant-thickness web can be found from Fig. 8. It is characterized by  $W_{\min}^* = 227.205$  lb,  $s_{\min} = 0.1800$  in.,

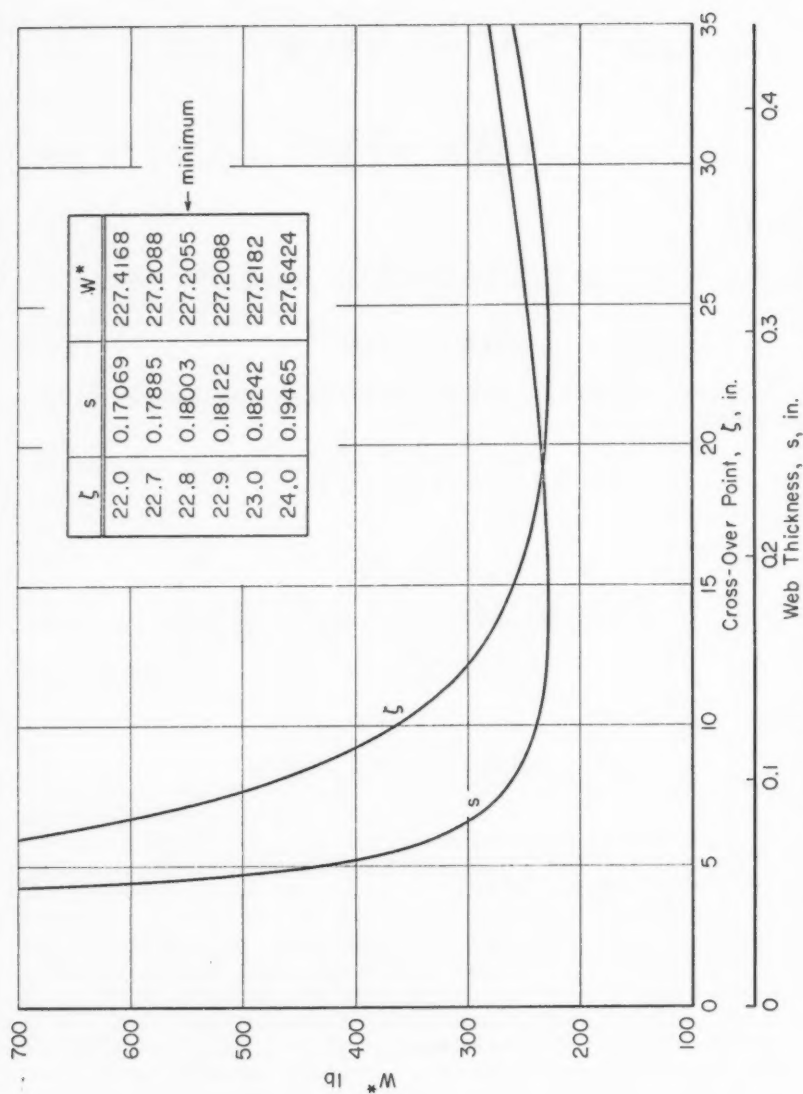


FIG. 8.—WEIGHT-WEB THICKNESS RELATIONSHIP FOR A CANTILEVER I-BEAM UNDER A TRIANGULAR LOAD

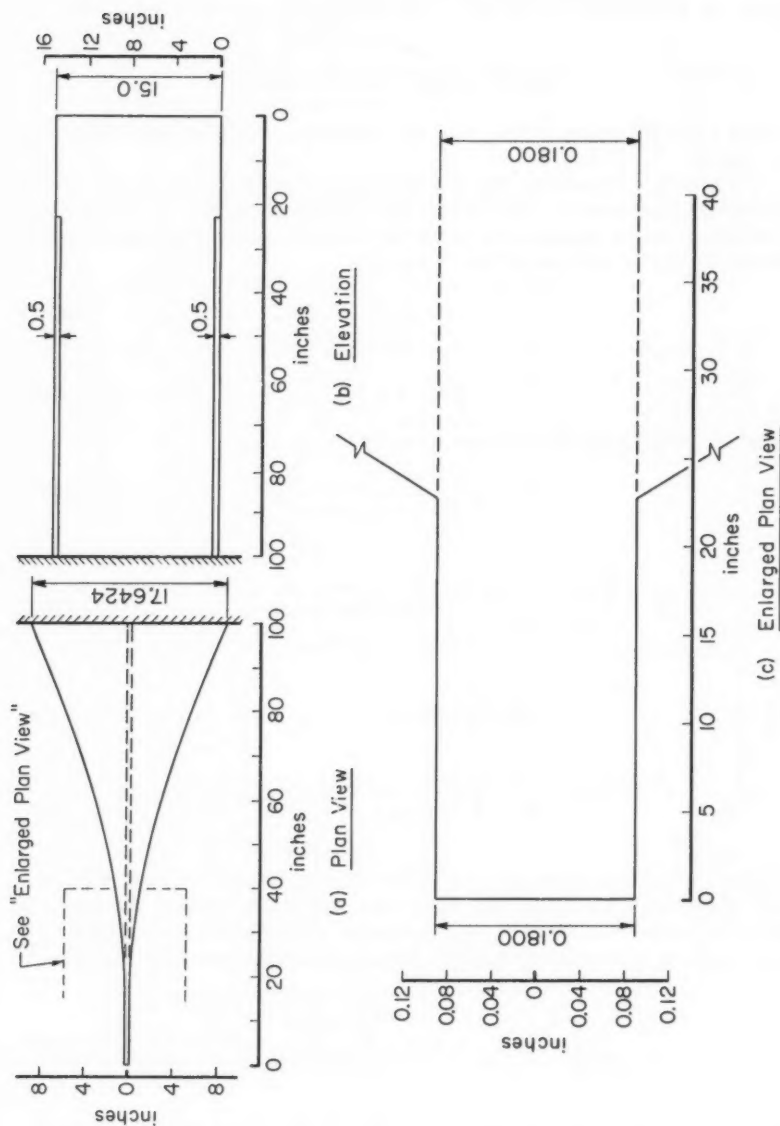


FIG. 9.—MINIMUM-WEIGHT CANTILEVER I-BEAM WITH AN OPTIMUM CONSTANT-THICKNESS WEB

and  $\xi_{\min} = 22.8$  in. When the values of  $s_{\min}$  and  $\xi_{\min}$  are substituted into Eq. 100, the flange width of this beam becomes

$$t(x) = t_{\min}^* = x \sqrt{(3.3929 x^2 + 19.962)} 10^{-6} - 0.78290 \quad 22.8 \leq x \leq 100$$

and

$$t(x) = 0.1800 \leq 0 \leq x \leq 22.8,$$

where  $x$  and  $t$  are in inches. The plan and elevation views of this beam are shown in Fig. 9.

*Case 3: Optimum Prismatic Beam.*—The cross-sectional geometry of the prismatic beam considered in this subsection is defined in Fig. 1, where  $r$  and  $d$  are specified constant dimensions and  $s$  and  $t$  are open constant parameters. The moment of inertia and area of this beam are

$$I = b t + g s \quad \dots\dots\dots (106a)$$

and

$$A = e t + h s \quad \dots\dots\dots (106b)$$

The weight and deflection expressions become

$$W = A L \rho = \rho L(e t + h s) \quad \dots\dots\dots (107)$$

and

$$\Delta(\xi) = \frac{\frac{D}{E} + \frac{B}{G} \left( f + j \frac{t}{s} \right)}{b t + g s} = \text{specified constant} \quad \dots\dots\dots (108)$$

in which

$$D \equiv \int_S M m \, dx \quad \dots\dots\dots (109)$$

and

$$B \equiv \int_S V v \, dx \quad \dots\dots\dots (110)$$

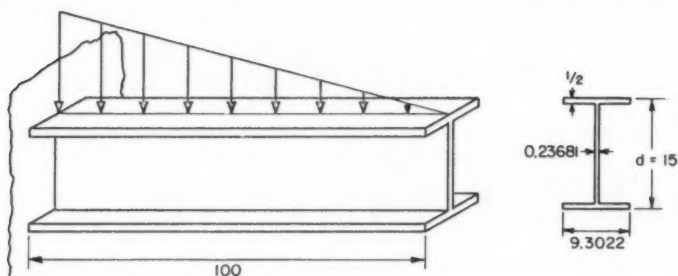
Our objective is to find values of  $s$  and  $t$  that will minimize the weight  $W$  subject to the subsidiary condition that  $\Delta(\xi)$  be a specified positive constant. If one applies Lagrange's method of undetermined multipliers, the optimum dimensions  $s^0$  and  $t^0$  must satisfy Eq. 108 and the following two relationships:<sup>12</sup>

$$\frac{\partial}{\partial s} \left[ \rho L(e t + h s) + \lambda \frac{\frac{D}{E} + \frac{B}{G} \left( f + j \frac{t}{s} \right)}{b t + g s} \right] = 0 \quad \dots\dots (111)$$

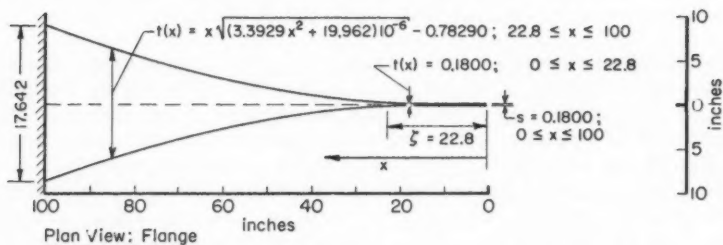
and

$$\frac{\partial}{\partial t} \left[ \rho L(e t + h s) + \lambda \frac{\frac{D}{E} + \frac{B}{G} \left( f + j \frac{t}{s} \right)}{b t + g s} \right] = 0 \quad \dots\dots (112)$$

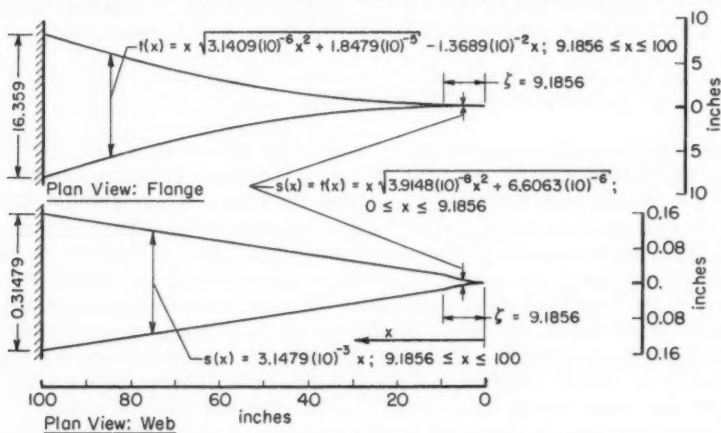
<sup>12</sup> "Differential and Integral Calculus," by R. Courant, Vol. II, Interscience Publishers, Inc., 1952, p. 190.



(a) Optimum Prismatic Beam; Weight---357.08 lb



(b) Optimum Flange and Optimum Constant Thickness Web; Weight---227.21 lb



(c) Optimum Flange and Optimum Web; Weight---212.29 lb

FIG. 10.—MINIMUM WEIGHT CANTILEVER DESIGN (TIP DEFLECTION - 1/2 IN., DEPTH - 15 IN., FLANGE THICKNESS - 1/2 IN., LOAD - 100 kips, SPAN - 100 IN.)

After performing the operations in Eqs. 111 and 112 and eliminating Lagrange's multiplier  $\lambda$  with Eq. 108, the optimum dimensions  $s^0$  and  $t^0$  and the associated beam weight  $W^0$  become

$$s^0 = \frac{1}{b \Delta(\xi)} \left[ \frac{Bj}{G} + \sqrt{\frac{Bje}{GJ} \left( \frac{D}{Eb} + \frac{BK}{G} \right)} \right] \dots\dots (113)$$

$$t^0 = \frac{1}{\Delta(\xi)} \left[ \sqrt{\frac{D}{Ebe} + \frac{BK}{Ge}} - \frac{g}{b^2} \sqrt{\frac{Bj}{GJ}} \right] \left[ \sqrt{\frac{De}{Eb} + \frac{BeK}{G}} + \sqrt{\frac{BjJ}{G}} \right] \dots\dots (114)$$

and

$$W^0 = \frac{\rho L}{\Delta(\xi)} \left[ \sqrt{\frac{De}{Eb} + \frac{BeK}{G}} + \sqrt{\frac{BjJ}{G}} \right]^2 \dots\dots\dots (115)$$

When these results are applied to the beam treated in the numerical example of Example 3,  $s^0 = 0.06157$  in.,  $t^0 = 3.20676$  in., and  $W^0 = 229,880$  lb. Recalling that the beam of Example 3 weighed 179,624 lb, we find that the optimum tapered flange and web produces a 28% weight savings over the optimum prismatic beam. In Fig. 10, the weights and geometries of the cantilever beam considered in Example 4 are compared for the cases: (a) optimum prismatic, (b) optimum flange and optimum constant thickness web, and (c) optimum flange and optimum web. Case (c) represents a 40.6% weight savings compared to Case (a). Based on bending deflection along, this savings is predicted from Fig. 4 as 44.4% ( $\gamma = 3$ ). Case (b) provides a 36.4% weight savings compared to Case (a), only 4.2% less than the optimum flange-optimum web combination.

## CONCLUSIONS

The investigations herein have dealt principally with I-beams of specified depths and flange thicknesses. For the elementary deflection theory considered here, one would find that the optimum flange thickness is vanishingly small and that the optimum depth is infinitely large. Changes in the flange thickness have very little effect on the beam weight as long as the  $(d/r)$ -ratio is reasonably large; however, the weight is strongly influenced by the depth. Eq. 28 indicates that the weight of a constant-depth I-beam is inversely proportional to the square of the depth. It should be pointed out that single-parameter beam sections exist that can be proportioned by using the techniques developed without specifying the depth. For example, the optimum radius variation  $t^0(x)$  of a solid circular beam can be found from Eq. 23 when  $w = \pi/4$  and  $z = \pi$ .

Frequently, the optimum web thickness based on a deflection design is so small that web buckling is experienced. Since the specific stiffnesses of most common metals are the same, the relationships given herein indicate that the use of a lower density metal will give a thicker, and consequently more stable, design without an increase in weight. But, the flange width very often becomes intolerably large for such a material substitution. In these situations, it may be possible to use a bimetallic beam, with a high-density flange material and a low density web material.



In general, if an element of a beam is replaced by an equal-depth element of a different material, the bending stiffness will remain unchanged if the width  $t_n$  of the new element is given by <sup>13</sup>

$$t_n = t_o \frac{E_o}{E_n} = t_o \frac{E_o/\rho_o}{E_n/\rho_n} \frac{\rho_o}{\rho_n} \dots\dots\dots (116)$$

where the subscript  $n$  refers to the new element and the subscript  $o$  refers to the original element. When the specific stiffnesses are equal,

$$\rho_n t_n = \rho_o t_o \dots\dots\dots (117)$$

which indicates that the weight is unchanged for a bimetallic member of equivalent stiffness. The same argument holds for the shear stiffness since the  $(E/G)$ -ratios of most common metals are the same.

Several investigators have studied the design of constant strength beams wherein the weight of the beam itself was considered part of the loading. In this paper, the weight of the beam is neglected; consequently, the results are exact only when the live-load deflection is specified. However, the deflections due to the beam weight are usually very small compared to the live-load deflections and can be minimized or eliminated by cambering or prestressing techniques.

As indicated in Example 2, the results described for I-beams apply without modification to box beams. It is often advantageous, from the point of view of lateral buckling, torsional stiffness, and shear lag, to use such multiple-web bending members.

#### ACKNOWLEDGMENTS

The writer would like to acknowledge the assistance of Miss Anne Humphreys, Technical Assistant, Armour Research Foundation, who carried out all of the numerical calculations.

#### APPENDIX.—NOTATION

- A = beam area;  
 a = specified function; in the I-beam, the moment of inertia of the web; Eq. 29;  
 B = area under the  $V$   $v$  diagram; defined by Eq. 110;  
 b = specified function; defined for the I-beam by Eq. 29;  
 c = specified function; in the I-beam, the web area; Eq. 29; also subscript denoting constant strength;

<sup>13</sup> "Strength of Materials," by S. Timoshenko, Vol. I, D. Van Nostrand Co., Inc., 3rd Ed., 1955, p. 217.

- D = area under the  $M$   $m$  diagram; defined by Eq. 109;
- d = total depth at any section of an I-beam; also subscript denoting deflection design;
- E = modulus of elasticity;
- e = specified function; in the I-beam, twice the flange thickness; Eq. 29;
- F = defined by Eq. 15;
- f = defined by Eq. 51;
- G = modulus of rigidity;
- g = defined by Eq. 29;
- H = defined by Eq. 88;
- h = web height of an I-beam; defined by Eq. 29;
- I = principal moment of inertia;
- J = defined by Eq. 76;
- j = defined by Eq. 50;
- K = defined by Eq. 77;
- k = constant; used as a power in Eq. 20;
- L = span length;
- M = bending moment;
- m = virtual bending moment;
- N = defined by Eq. 85;
- n = constant; used as a power in Eq. 21; also subscript denoting new element; Eq. 116;
- o = superscript denoting association with an extremal function; also subscript denoting original element;
- P = concentrated lateral load;
- p = subscript denoting prismatic beam;
- q = distance from neutral axis to outermost fiber;
- R = total beam load;
- r = flange thickness of an I-beam;
- S = span;
- s = web thickness of an I-beam or box-beam; specified function or open parameter;
- T = terminal moment;
- t = flange width of an I-beam; open parameter;
- u = uniform load;
- V = external shear;

- $v$  = virtual shear;
- $W$  = Beam weight;
- $w$  = specified function; used in Eq. 20;
- $X$  = defined where used; see Eq. 31 or Eq. 98;
- $x$  = coordinate along a beam;
- $Y$  = defined where used; see Eq. 32 or Eq. 99;
- $z$  = specified function; used in Eq. 21;
- $*$  = superscript denoting association with a modified extremal function;
- $'$  = defined where used;
- $''$  = defined where used;
- $\alpha$  = shape factor; defined by Eq. 49;
- $\beta$  = constant;
- $\xi$  = station along beam where deflection is specified;
- $\eta$  = cross-over point; used to designate regions of a beam;
- $\zeta$  = cross-over point; used to designate regions of a beam;
- $\Delta$  = specified deflection; either bending deflection or total deflection;
- $\delta$  = shear deflection;
- $\sigma_0$  = specified positive stress level;
- $\lambda$  = constant multiplier or Lagrange's multiplier;
- $\rho$  = weight density (weight/unit volume); and
- $\gamma$  = constant; degree of the bending moment in Fig. 4.

THE UNIVERSITY OF CHICAGO

---

Journal of the  
ENGINEERING MECHANICS DIVISION  
Proceedings of the American Society of Civil Engineers

---

STRESS ANALYSIS OF TRANSLATIONAL SHELLS

By Kristoffer Apeland<sup>1</sup>

---

SYNOPSIS

A method of solution of the problem of bending of thin shallow translational shells is presented. A generalized Levy-type solution including hyperbolic and elliptic paraboloids and cylindrical shells is obtained. Design tables and numerical examples are included.

---

INTRODUCTION

This paper is concerned with the problem of structural analysis of thin shallow shells in the form of a translational surface. In recent years, such shapes as the hyperbolic and elliptic paraboloids have been frequently used in the field of thin-shell construction, and much attention has been devoted to the study of the structural behavior of such shells.

The problem of bending of this class of shell surfaces can be studied within the scope of Marguerre's general theory for shallow shells.<sup>2</sup> In this paper the Marguerre equations of the small deflection theory are specialized to shells in the form of a parabolic translational surface, resulting in a system of two fourth order partial differential equations with constant coefficients. The Marguerre formulation in terms of stresses and displacements projected on the

---

Note.—Discussion open until July 1, 1961. To extend the closing date one month, a written request must be filed with the Executive Secretary, ASCE. This paper is part of the copyrighted Journal of the Engineering Mechanics Division, Proceedings of the American Society of Civil Engineers, Vol. 87, No. EM 1, February, 1961.

<sup>1</sup> Struct. Engr., Oslo, Norway, Presently (1960) visiting research engineer at Univ. of California, Berkeley, Calif.

<sup>2</sup> "Zur Theorie der gekrümmten Platte grosser Formänderung," by K. Marguerre, Proc. Fifth Internatl. Congress on Appl. Mech., 1938, pp. 93-101.

coordinate planes leads to inconvenient expressions for the in-plane displacements. W. Flügge and D. A. Conrad<sup>3</sup> arrived at more suitable expressions by formulating the problem in terms of normal and tangential components. Two different systems of three simultaneous differential equations for the displacement components  $u$ ,  $v$ , and  $w$  resulting from the two formulations will be given, from which it will be apparent that the Flugge-Conrad equations are most convenient in application, and further developments in this paper will be based on these equations. A suitably defined stress-displacement function is introduced, from which all the remaining unknowns of the problem of bending can be obtained by differentiation. It is shown that the stress-displacement function has to satisfy an eighth order partial differential equation. This equation is integrated using the Levy-type solution, applicable to a class of boundary value problems. By inclusion of a shape parameter, the solution is valid for hyperbolic and elliptic paraboloids and cylindrical surfaces.

The solutions obtained are developed explicitly, essentially by deriving characteristic coefficients for the statical quantities in the shell in the manner of I. Holand,<sup>4</sup> by which the computational work in application is greatly reduced. The form of the solution is such that it lends itself to tabulation as in Rüdiger-Urban,<sup>5</sup> where influence coefficients are presented. The solutions are well suited for comparative shell shape studies. Tables of the roots of the characteristic equation are included. The method is illustrated with examples of uniformly loaded shells with various values of the shell parameters.

It should be noted that the theory used is a shallow shell theory, which is based on the assumptions that the squares of the first order derivatives of the surface functions,  $(z_x)^2$ ,  $(z_y)^2$ , and  $(z_x)^*(z_y)$ , are negligible in comparison with unity. This limitation on the application of the shallow shell theory has been examined by E. Reissner,<sup>6</sup> who states as a general rule that shallow shell theory will be more than sufficiently accurate as long as  $(z_x)$ ,  $(z_y) \leq 1/8$ , and often accurate enough for practical purposes as long as  $(z_x)$ ,  $(z_y) \leq 1/2$ .

*Notation.*—The letter symbols adopted for use in this paper are defined where they first appear, in the illustrations or in the text, and are arranged alphabetically, for convenience of reference, in the Appendix.

## STATEMENT OF THE PROBLEM

*Geometry of the Shell: Differential Equations.*—Consider in the following a class of thin shallow translational shells, rectangular in plan, the middle surface of which is defined in cartesian coordinates by

$$z(x,y) = (1/2)k_2(\gamma x^2 - y^2) \dots \dots \dots (1)$$

in which  $\gamma = k_1/k_2$  is a shape or curvature parameter of the surface. Depending on the sign of  $\gamma$ , Eq. 1 represents a hyperbolic paraboloid ( $\gamma > 0$ ), a parabolic cylinder ( $\gamma = 0$ ), or an elliptic paraboloid ( $\gamma < 0$ ).

<sup>3</sup> "On the Calculation of Shallow Shells," by W. Flügge and D. A. Conrad, Stanford Univ., Div. of Engrg. Mech., Tech. Report No. 101, 1956.

<sup>4</sup> "Design of Circular Cylindrical Shells," by I. Holand, Oslo Univ. Press, Oslo, 1957.

<sup>5</sup> "Kreiszyllinderschalen," by Rüdiger-Urban, G. Teubner Verlagsgesellschaft, Leipzig, 1955.

<sup>6</sup> "On Some Aspects of the Theory of Thin Elastic Shells," by E. Reissner, Journal, Boston Soc. of Civ. Engrs., 1955, pp. 100-133.

For small deflections and a distributed transverse load  $q_z(x, y)$ , the Marguerre equations reduce to the system

$$\left. \begin{aligned} \nabla^4 F - E h [2z_{,xy} w_{,xy} - z_{,xx} w_{,yy} - z_{,yy} w_{,xx}] &= 0 \\ D \nabla^4 w - z_{,xx} F_{,yy} - z_{,yy} F_{,xx} + 2z_{,xy} F_{,xy} &= q_z \end{aligned} \right\} \dots (2)$$

in which  $w$  is the displacement component in the  $z$ -direction and  $F$  is an Airy stress function defined by

$$\left. \begin{aligned} F_{,yy} &= N_{xx} \\ F_{,xx} &= N_{yy} \\ -F_{,xy} &= N_{xy} \end{aligned} \right\} \dots (3)$$

Substitution of the surface Eq. 1 into Eqs. 2 yields

$$\left. \begin{aligned} \nabla^4 F - k_2 E h (w_{,xx} - \gamma w_{,yy}) &= 0 \\ D \nabla^4 w + k_2 (F_{,xx} - \gamma F_{,yy}) &= q_z \end{aligned} \right\} \dots (4)$$

By introduction of a stress-displacement function  $\phi(x, y)$  defined by

$$w = \nabla^4 \phi \dots (5a)$$

and

$$F = E h k_2 (\phi_{,xx} - \gamma \phi_{,yy}) = E h k_2 \nabla_\gamma^2 \phi \dots (5b)$$

in which

$$\nabla_\gamma^2 = \frac{\partial^2}{\partial x^2} - \gamma \frac{\partial^2}{\partial y^2} \dots (5c)$$

the system of Eqs. 4 reduces to the single equation

$$\nabla^8 \phi + \alpha \nabla_\gamma^2 \nabla_\gamma^2 \phi = \frac{q_z}{D} \dots (6a)$$

in which

$$\alpha = \frac{E h k_2^2}{D} = 12(1 - \nu^2) \left( \frac{k_2}{h} \right)^2 \dots (6b)$$

All the unknown stresses and displacements in the shell are given in terms of the stress-displacement function  $\phi(x, y)$  by the following relations:

$$N_{xx} = F_{,yy} = E h k_2 \nabla_\gamma^2 (\phi_{,yy}) \dots (7a)$$

$$N_{yy} = F_{,xx} = E h k_2 \nabla_\gamma^2 (\phi_{,xx}) \dots (7b)$$

$$N_{xy} = -F_{,xy} = -E h k_2 \nabla_\gamma^2 (\phi_{,xy}) \dots (7c)$$

$$M_{xx} = -D(w_{,xx} + \nu w_{,yy}) = -D \nabla^4 (\phi_{,xx} + \nu \phi_{,yy}) \dots (7d)$$

$$M_{yy} = -D(w_{,yy} + \nu w_{,xx}) = -D \nabla^4 (\phi_{,yy} + \nu \phi_{,xx}) \dots (7e)$$

$$M_{xy} = -D(1 - \nu)w_{,xy} = -D(1 - \nu) \nabla^4 (\phi_{,xy}) \dots (7f)$$

$$Q_x = -D(\nabla^2 w)_{,x} = -D \nabla^6(\phi, x) \dots \dots \dots (7g)$$

$$Q_y = -D(\nabla^2 w)_{,y} = -D \nabla^6(\phi, y) \dots \dots \dots (7h)$$

$$R_x = Q_x + M_{xy,y} = -D[\nabla^6(\phi, x) + (1-\nu) \nabla^4(\phi, xyy)] \dots \dots \dots (7i)$$

$$R_y = Q_y + M_{xy,x} = -D[\nabla^6(\phi, y) + (1-\nu) \nabla^4(\phi, xxy)] \dots \dots \dots (7j)$$

$$V_x = Q_x + z_{,x} N_{xx} + z_{,y} N_{xy} = -D[\nabla^6(\phi, x) - \gamma \alpha x \nabla \gamma^2(\phi, yy) - \alpha y \nabla \gamma^2(\phi, xy)] \dots \dots \dots (7k)$$

$$\bar{V}_x = V_x + M_{xy,y} = V_x - D(1-\nu) \nabla^4(\phi, xyy) \dots \dots \dots (7l)$$

$$V_y = Q_y + z_{,x} N_{xy} + z_{,y} N_{yy} = -D[\nabla^6(\phi, y) + \gamma \alpha x \nabla \gamma^2(\phi, xy) + \alpha y \nabla \gamma^2(\phi, xx)] \dots \dots \dots (7m)$$

and

$$V_y = V_y + M_{xy,x} = V_y - D(1-\nu) \nabla^4(\phi, xxy) \dots \dots \dots (7n)$$

where the notation of Reissner<sup>6</sup> is employed; in which  $\nu$  refers to Poisson's ratio;  $M_{xx}, M_{yy}$  are flexural moments;  $N_{xx}, N_{yy}$  refer to stress resultants tangential to the shell surface; and  $N_{xy}$  is the shear stress resultant tangential to the shell surface. It should be noted that to the degree of approximation involved in the use of the shallow shell theory the difference between tangential stress resultants and stress resultants in the xy-plane is negligible. Stress resultants in the z-direction, however, must incorporate both the transverse shear stress resultants and the components in the z-direction of the tangential stress resultants. In Eqs. 7 the transverse shear stress resultants and the transverse effective edge stress resultants are denoted  $Q_x, Q_y$  and  $R_x, R_y$  respectively, whereas the corresponding stress resultants in the z-direction are denoted  $V_x, V_y$  and  $\bar{V}_x, \bar{V}_y$ .

The displacement components  $u$  and  $v$  are determined from the following system of displacement equations which has been derived from the system of equations given by Flügge-Conrad;<sup>3</sup> that is

$$\left. \begin{aligned} u_{,xx} + (1/2)(1-\nu)u_{,yy} + (1/2)(1+\nu)v_{,xy} - ((z_{,xx} + \nu z_{,yy})w)_{,x} - (1-\nu)(z_{,xy}w)_{,y} &= 0 \\ v_{,yy} + (1/2)(1-\nu)v_{,xx} + (1/2)(1+\nu)u_{,xy} - ((z_{,yy} + \nu z_{,xx})w)_{,y} - (1-\nu)(z_{,xy}w)_{,x} &= 0 \end{aligned} \right\} \dots (8)$$

$$\text{and}$$

$$\frac{(z_{,xx} + \nu z_{,yy})u_{,x} + (z_{,yy} + \nu z_{,xx})v_{,y} + (1-\nu)z_{,xy}(u_{,y} + v_{,x}) - (z_{,xx}^2 + 2\nu z_{,xx}z_{,yy} + z_{,yy}^2 + 2(1-\nu)z_{,xy}^2)w - (h^2/12) \nabla^4 w = q_z(1-\nu^2)}{Eh}$$

which is equivalent to the system given in Eqs. 2. Introduction of the surface function given in Eq. 1 and elimination of  $u$  and  $v$  results in a single equation in  $w$  which, by introduction of Eqs. 5 yields Eq. 6a. The elimination yields the following relations between  $u, v$  and  $w$  for  $q_z = 0$

$$\nabla^4 u = k_2((1+\gamma)(\nabla^2 w)_{,x} - (1+\nu)(\nabla \gamma^2 w)_{,x}) \dots \dots \dots (9a)$$



and

$$\nabla^4 v = k_2 \left( -(1+\gamma)(\nabla^2 w)_{,y} - (1+\nu)(\nabla^2 w)_{,y} \right) \dots \dots \dots (9b)$$

which by introduction of the stress-displacement function, Eqs. 5 yield

$$u = k_2 \left( (1+\gamma)(\nabla^2 \phi)_{,x} - (1+\nu)(\nabla^2 \phi)_{,x} \right) \dots \dots \dots (10a)$$

and

$$v = k_2 \left( (1+\gamma)(\nabla^2 \phi)_{,y} - (1+\nu)(\nabla^2 \phi)_{,y} \right) \dots \dots \dots (10b)$$

The displacement equations resulting from the Marguerre formulation in terms of projected displacements U, V and W corresponding to the system of Eqs. 8 appear in the form

$$U_{,xx} + (1/2)(1-\nu)U_{,yy} + (1/2)(1+\nu)V_{,xy} + (z_{,x}W_{,x} + \nu z_{,y}W_{,y})_{,x} \\ + (1/2)(1-\nu)(z_{,y}W_{,x} + z_{,x}W_{,y})_{,y} = 0 \dots \dots \dots (11a)$$

$$V_{,yy} + (1/2)(1-\nu)V_{,xx} + (1/2)(1+\nu)U_{,xy} + (z_{,y}W_{,y} + \nu z_{,x}W_{,z})_{,y} \\ + (1/2)(1-\nu)(z_{,y}W_{,x} + z_{,x}W_{,y})_{,x} = 0 \dots \dots \dots (11b)$$

and

$$(z_{,xx} + \nu z_{,yy})U_{,x} + (z_{,yy} + \nu z_{,xx})V_{,y} + (1-\nu)z_{,xy}(U_{,y} + V_{,x}) \\ + z_{,xx}(z_{,x}W_{,x} + \nu z_{,y}W_{,y}) + z_{,yy}(\nu z_{,x}W_{,x} + z_{,y}W_{,y}) \\ + (1-\nu)z_{,xy}(z_{,y}W_{,x} + z_{,x}W_{,y}) - (h^2/12)\nabla^4 W = q_z(1-\nu^2) \\ \hline E h \dots \dots \dots (11c)$$

in which capital letters have been used to distinguish the projected displacements from the normal and tangential components.

Elimination of U and V from the system of Eqs. 11 again yields the differential Eq. 6a. The resulting displacement components U and V, however, are given by the relations

$$U = k_2 \left( (1+\gamma)(\nabla^2 \phi)_{,x} - (1+\nu)(\nabla^2 \phi)_{,x} - \gamma x \nabla^4 \phi \right) \dots (12a)$$

and

$$V = k_2 \left( -(1+\gamma)(\nabla^2 \phi)_{,y} - (1+\nu)(\nabla^2 \phi)_{,y} + y \nabla^4 \phi \right) \dots \dots (12b)$$

which results in the following relations between the two sets of displacements:

$$U = u - z_{,x}W \dots \dots \dots (13a)$$

and

$$V = v - z_{,y}W \dots \dots \dots (13b)$$

which may be easily verified by geometric consideration. In the solution of boundary value problems Eqs. 10 will be used.

Thus, the problem of bending of thin shallow translational shells with distributed surface load of intensity  $q_z$  is reduced to the solution of the partial differential Eq. 6a subject to appropriate boundary conditions on the edges.

*Boundary Conditions.*—On each edge of the shell there are four independent boundary conditions, two of which are stated in terms of the in-plane stresses and displacements and two are stated in terms of the flexural quantities of the shell.

In the following it is assumed that the two opposite edges  $x = \pm a/2$  have moment-free support, and that the edge stiffening members are rigid in the direction of their axes and have negligible bending resistance in planes tangent to the shell, that is

$$w = 0, M_{xx} = 0, N_{xx} = 0, \epsilon_y = \frac{1}{Eh} (N_{yy} - \nu N_{xx}) = 0 \dots (14a)$$

which, in terms of the stress-displacement function  $\phi$ , yields

$$\nabla^4 \phi = -D \nabla^4 (\phi_{,yy} + \nu \phi_{,xx}) = \nabla^2 (\phi_{,yy}) = \nabla^2 (\phi_{,xx}) = 0 \dots (14b)$$

In the following an edge having the edge conditions given in Eqs. 14(a) will be denoted a simply supported edge.

A solution of the differential equation is sought in such a form that arbitrary boundary conditions can be satisfied along the remaining edges  $y = \pm b/2$ .

#### SOLUTION OF THE DIFFERENTIAL EQUATION

Since the differential equation (Eq. 6a) is linear, solutions may be obtained by superposition of a particular integral and the solution of the corresponding homogeneous equation. The form of the equation is such that separable single series solutions of the Levy-type can be obtained.

*Solution of the Homogeneous Equation.*—In view of the specified edge conditions (Eqs. 14a) a solution of Eq. 6a for  $q_z = 0$  may be assumed in the form

$$\phi = \sum_{n=1}^{\infty} \phi_n(y) \cos \lambda x = \sum_{n=1}^{\infty} C_n e^{\rho \lambda y} \cos \lambda x \dots (15)$$

in which  $\lambda x$  and  $\lambda y$  are nondimensional variables. When added to an appropriate particular integral, the solution of Eq. 15 is sufficiently general to satisfy arbitrary boundary conditions along the two edges  $y = \pm b/2$ .

Introduction of Eq. 15 into Eq. 16 yields, for each term of the series,

$$[(-\lambda^2 + \lambda^2 \rho^2)^4 + \alpha(-\lambda^2 - \gamma \lambda^2 \rho^2)^2] C_n e^{\rho \lambda y} \cos \lambda x = 0 \dots (16)$$

We now set

$$\rho = \sqrt{m+1} \dots (17)$$

and introduce the shell parameter  $\epsilon$  defined by

$$\epsilon = \frac{2\lambda}{4\sqrt{4\alpha}} = \frac{n\pi}{a\sqrt{3(1-\nu^2)\left(\frac{k_2}{h}\right)^2}} \dots (18)$$

Substitution of Eqs. 17 and 18 into Eq. 16 gives the equation

$$m^4 + \frac{4}{\epsilon^4} (\gamma m + 1 + \gamma)^2 = 0 \dots (19)$$

which has the solutions

$$\left. \begin{aligned} \frac{m_1}{m_2} &= \frac{1}{\sqrt{2} \epsilon^2} \left[ \sqrt{\gamma^4 + 4 \epsilon^4 (1+\gamma)^2 - \gamma^2} - i \left[ -\sqrt{2} \gamma + \sqrt{\gamma^4 + 4 \epsilon^4 (1+\gamma)^2 + \gamma^2} \right] \right] \\ \frac{m_3}{m_4} &= \frac{1}{\sqrt{2} \epsilon^2} \left[ \sqrt{\gamma^4 + 4 \epsilon^4 (1+\gamma)^2 - \gamma^2} + i \left[ \sqrt{2} \gamma + \sqrt{\gamma^4 + 4 \epsilon^4 (1+\gamma)^2 + \gamma^2} \right] \right] \end{aligned} \right\} \quad (20)$$

Substitution of Eqs. 20 into the Eq. 17 gives the roots of the characteristic equation, Eq. 16, on the form

$$\left. \begin{aligned} \rho_{1-4} &= \pm (\mathcal{X}_1 \pm i \mu_1) \\ \rho_{5-8} &= \pm (\mathcal{X}_2 \pm i \mu_2) \end{aligned} \right\} \dots\dots\dots (21)$$

in which the quantities  $\mathcal{X}_1$ ,  $\mu_1$ ,  $\mathcal{X}_2$  and  $\mu_2$  are the following functions of the shell parameters  $\epsilon$  and  $\gamma$ :

$$\left. \begin{aligned} \mathcal{X}_1 &= \frac{1}{\sqrt{8} \epsilon^2} \left\{ \left[ \sqrt{2} \epsilon^2 + \sqrt{\gamma^4 + 4 \epsilon^4 (1+\gamma)^2 - \gamma^2} \right]^2 + \left[ \sqrt{2} \gamma + \sqrt{\gamma^4 + 4 \epsilon^4 (1+\gamma)^2 + \gamma^2} \right]^2 \right\}^{1/2} + \\ &\quad + \left[ \sqrt{2} \epsilon^2 + \sqrt{\gamma^4 + 4 \epsilon^4 (1+\gamma)^2 - \gamma^2} \right] \left\{ \right\}^{1/2} \\ \mathcal{X}_2 &= \frac{1}{\sqrt{8} \epsilon^2} \left\{ \left[ \sqrt{2} \epsilon^2 - \sqrt{\gamma^4 + 4 \epsilon^4 (1+\gamma)^2 - \gamma^2} \right]^2 + \left[ -\sqrt{2} \gamma + \sqrt{\gamma^4 + 4 \epsilon^4 (1+\gamma)^2 + \gamma^2} \right]^2 \right\}^{1/2} + \\ &\quad + \left[ \sqrt{2} \epsilon^2 - \sqrt{\gamma^4 + 4 \epsilon^4 (1+\gamma)^2 - \gamma^2} \right] \left\{ \right\}^{1/2} \end{aligned} \right\} \dots\dots\dots (22)$$

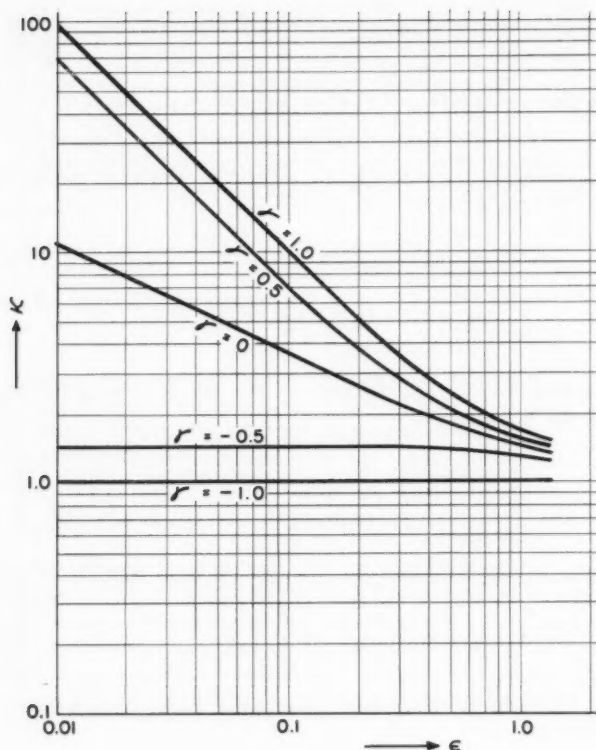
from which the solution of the homogeneous equation is obtained by substitution into Eq. 15, that is

$$\begin{aligned} \phi(x, y) = \sum_n \left[ C_1 e^{\rho_1 \lambda y} + C_2 e^{\rho_2 \lambda y} + C_3 e^{\rho_3 \lambda y} + C_4 e^{\rho_4 \lambda y} \right. \\ \left. + C_5 e^{\rho_5 \lambda y} + C_6 e^{\rho_6 \lambda y} + C_7 e^{\rho_7 \lambda y} + C_8 e^{\rho_8 \lambda y} \right] \cos \lambda x \dots\dots\dots (23) \end{aligned}$$

Although the quantities of Eqs. 22 are rather involved arithmetic expressions, their form is such that a numerical tabulation may easily be made by means of an automatic digital computer. The use of numerical tables in design will be discussed subsequently.

To illustrate the use of Eqs. 21 for comparative shell shape studies, the real parts  $\mathcal{X}_1$  and  $\mathcal{X}_2$  of the roots are plotted in Fig. 1 and Fig. 2 for various values of the shell parameters  $\epsilon$  and  $\gamma$ . Because of the exponential form of the solution Eq. 15,  $\mathcal{X}_1$  and  $\mathcal{X}_2$  characterize the dampening of the edge disturbances from the edges  $y = \text{constant}$ . Note the small values of  $\mathcal{X}_2$  for positive values of  $\gamma$  in Fig. 2, which indicates slow dampening of the edge disturbances for hyperbolic paraboloid shells.

*Particular Integrals of Eq. 6a: Surface Load.*—Appropriate particular integrals can be obtained by expanding the load function in trigonometric series.

FIG. 1.—REAL ROOT  $\kappa_1$  OF THE CHARACTERISTIC EQUATION

**Variable Surface Load  $q_z$ : Navier-Type Solution.**—For various shapes of the load function a particular integral can be obtained in double Fourier series form

$$q_z = \sum_m \sum_n q_{mn} \cos \delta y \cos \lambda x \dots\dots\dots (24a)$$

and

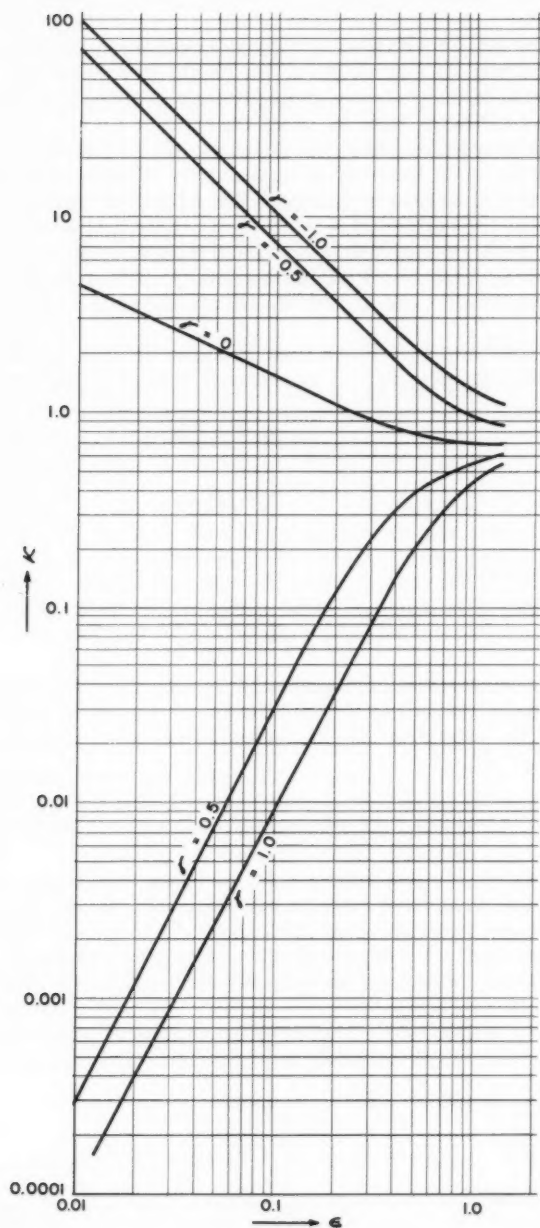
$$\phi(x, y) = \sum_m \sum_n \phi_{mn} \cos \delta y \cos \lambda x \dots\dots\dots (24b)$$

in which  $m$  and  $n$  are integers and  $\delta$  and  $\lambda$  are defined by

$$\delta = \frac{m\pi}{b}, \lambda = \frac{n\pi}{a} \dots\dots\dots (25)$$

The coefficients  $q_{mn}$  are determined from the form of the load function. Substitution of the expansions, Eqs. 24 into Eq. 6a yields the coefficients  $\phi_{mn}$

$$\phi_{mn} = [(\lambda^2 + \delta^2)^4 + \alpha(\lambda^2 - \gamma\delta^2)^2]^{-1} \frac{q_{mn}}{D} \dots\dots\dots (26)$$

FIG. 2.—REAL ROOT  $\kappa_2$  OF THE CHARACTERISTIC EQUATION

from which the stresses and displacements are obtained by introduction into Eqs. 7.

The solution of Eq. 24 satisfies identical boundary conditions for simply supported edges along all four edges of the shell. It follows that Eqs. 24 are a complete solution of the boundary value problem given by the differential Eq. 6a, the boundary conditions, Eqs. 12, along the edges  $x = \pm a/2$  and corresponding simple support conditions along the edges  $y = \pm b/2$ . Solutions of this problem have been given by K. Hruban,<sup>7</sup> S. A. Ambartsumyan<sup>8</sup> and Flugge and Conrad.<sup>9</sup> By inspection it is seen from Eq. 26 that for  $\gamma > 0$ , that is for hyperbolic paraboloidal shells, the factor  $(\lambda^2 - \gamma \delta^2)$  may vanish for particular span-curvature ratios. If such a relationship exists and the load function is symmetric, the complete solution for simply supported shells reduces to the Navier plate solution, which shows that the hyperbolic paraboloid is an improper shell for such conditions.

**Uniform Surface Load  $q_z$ .**—For a load function which is constant in the  $y$ -direction, a particular integral can be obtained in single Fourier series form

$$q_z = \sum_n q_n \cos \lambda x \dots\dots\dots (27a)$$

and

$$\phi(x, y) = \sum_n \phi_n \cos \lambda x \dots\dots\dots (27b)$$

resulting in the solution

$$\phi_n = \frac{1}{\lambda^8 + \alpha \lambda^4} \frac{q_n}{D} \dots\dots\dots (28)$$

from which the stresses and displacements are obtained by introduction into Eqs. 7. The complete solution of the differential Eq. 6a is then obtained by superposition of the solution of Eq. 23 and one of the particular integrals, Eqs. 24 or 27.

## SOLUTIONS OF THE BOUNDARY VALUE PROBLEMS

For the application of the solution of Eq. 23 in the solution of actual boundary value problems, it is convenient to substitute Eq. 23 back into Eqs. 7 and express the statical quantities in the shell in terms of the solution. In analogy with the methods used in the design of circular cylindrical shells, characteristic coefficients will be derived and a systematic solution procedure will be developed.

**Characteristic Coefficients.**—In view of the symmetry of the roots, Eqs. 21, Eq. 23 can be written in the following form for each term of the series:

$$\begin{aligned} \phi_n(x, y) = & \left[ C_1 e^{\rho_1 \lambda y} + C_2 e^{\rho_2 \lambda y} + C_3 e^{\bar{\rho}_1 \lambda y} + C_4 e^{\bar{\rho}_2 \lambda y} \right. \\ & \left. + C_5 e^{\bar{\rho}_1 \lambda y} + C_6 e^{\bar{\rho}_2 \lambda y} + C_7 e^{-\bar{\rho}_1 \lambda y} + C_8 e^{-\bar{\rho}_2 \lambda y} \right] \cos \lambda x \dots\dots (29) \end{aligned}$$

<sup>7</sup> "Biegetheorie der Translationsflächen und ihre Anwendung im Hallenbau," by K. Hruban, Acta Technica 1953, Tomus VII, Fasciculi 3-4.

<sup>8</sup> "On the Calculation of Shallow Shells," by S. A. Ambartsumyan, Prikl. Mat. i Mekh., Vol. XI, 1947. (NACA, TM 1425)

<sup>9</sup> "On the Calculation of Shallow Shells," by W. Flugge and D. A. Conrad, Journal of Applied Mechanics, December, 1959.

where the eight roots from the Eqs. 21 are represented by two principal roots defined by

$$\left. \begin{aligned} \rho_1 &= -(\mathcal{X}_1 + i\mu_1) \\ \rho_2 &= -(\mathcal{X}_2 + i\mu_2) \end{aligned} \right\} \dots\dots\dots (30)$$

and where  $C_1$ - $C_8$  are the eight complex constants of integration. By definition the stress-displacement function is a real function, from which the following relations between the constants of integration results:

$$C_5 = \bar{C}_1, C_6 = \bar{C}_2, C_7 = \bar{C}_3, C_8 = \bar{C}_4 \dots\dots\dots (31)$$

Introducing new constants, the solution given in Eq. 29 may be written in the form

$$\phi_n(x, y) = \text{Re} \left\{ C_1 e^{\rho_1 \lambda y} + C_2 e^{\rho_2 \lambda y} + C_3 e^{-\rho_1 \lambda y} + C_4 e^{-\rho_2 \lambda y} \right\} \cos \lambda x \dots (32)$$

in which the notation  $\text{Re} \{f\}$  is used to denote the real part of  $f$ .

By inspection, it is seen from Eqs. 7 that most of the stresses and displacements in the shell can be written in the form

$$H = [H] \text{Re} \left\{ C_1 \hat{H}_1 e^{\rho_1 \lambda y} + C_2 \hat{H}_2 e^{\rho_2 \lambda y} + C_3 \hat{H}_1 e^{-\rho_1 \lambda y} + C_4 \hat{H}_2 e^{-\rho_2 \lambda y} \right\} \dots (33)$$

in which  $[H]$  is a multiplier containing functions of the independent variable;  $x$ , and  $\hat{H}_1$ , and  $\hat{H}_2$  are polynomials in the two principal roots, Eqs. 30, which, by suitable choice of the multiplier  $[H]$  and change in the constants of integration, can be made quantities of the order of magnitude 1. Using cylindrical shell theory notation these polynomials will be denoted characteristic coefficients.

The characteristic coefficients  $\hat{H}_1$  and  $\hat{H}_2$  and the corresponding multipliers  $[H]$  are listed in Table 1. In order to simplify the expressions, the coefficients  $\hat{H}_1$  are divided by  $(1 - \rho_1^2)^2$  and the coefficients  $\hat{H}_2$  are divided by  $(1 - \rho_2^2)^2$  and all the multipliers are reduced by a constant factor  $(1/2)Ehk_2\epsilon^2$ , all of which represent changes in the arbitrary constants of integration only. Reduced values are introduced for the roots of the characteristic equation, that is

$$\left. \begin{aligned} \mathcal{X}_1 &= \frac{1}{\sqrt{\epsilon}} \hat{\mathcal{X}}_1 \\ \mu_1 &= \frac{1}{\sqrt{\epsilon}} \hat{\mu}_1 \\ \mathcal{X}_2 &= \frac{1}{\sqrt{\epsilon}} \hat{\mathcal{X}}_2 \\ \mu_2 &= \frac{1}{\sqrt{\epsilon}} \hat{\mu}_2 \end{aligned} \right\} \dots\dots\dots (34)$$

The characteristic coefficients for the displacement components  $u$  and  $v$  are given in complex fractional form because it is simpler to carry the expansions through after numerical values have been introduced.

*Solution Procedure for Particular Boundary Value Problems.*—The solution method for a boundary value problem given by the differential Eq. 6a, the bound-



ary conditions of Eq. 14a, and arbitrary boundary conditions along the edges  $y = \text{constant}$ , will in general proceed as follows:

1. The actual edge conditions are stated along the edges  $y = \text{constant}$ .
2. The principal roots of the characteristic equation are computed from Eqs. 22 for the actual parameter values and the characteristic coefficients are determined from the formulas in Table 1.

TABLE 1.—CHARACTERISTIC COEFFICIENTS

H	$[H]$	$\hat{H}_1$	$\hat{H}_2$
$N_{xx}$	$\frac{1}{E} \cos \lambda x$	$2\hat{\mu}_1^2 - 1(\hat{\mu}_1^2 + \hat{\mu}_1^2)$	$-2\hat{\mu}_2^2 + 1(\hat{\mu}_2^2 + \hat{\mu}_2^2)$
$N_{yy}$	$\cos \lambda x$	-1	+1
$M_{yx}$	$\frac{1}{\sqrt{E}} \sin \lambda x$	$-\hat{\mu}_1 + i\hat{\mu}_1$	$\hat{\mu}_2 - i\hat{\mu}_2$
$M_{xx}$	$\frac{E k_2}{2\lambda} \cos \lambda x$	$E - 1(\hat{\mu}_1^2 + \hat{\mu}_1^2) - 1(2\hat{\mu}_1^2 \hat{\mu}_1)$	$E - 1(\hat{\mu}_2^2 + \hat{\mu}_2^2) - 1(2\hat{\mu}_2^2 \hat{\mu}_2)$
$M_{yy}$	$\frac{E k_2}{2\lambda} \cos \lambda x$	$1E - (\hat{\mu}_1^2 + \hat{\mu}_1^2) - 1(2\hat{\mu}_1^2 \hat{\mu}_1)$	$1E - (\hat{\mu}_2^2 + \hat{\mu}_2^2) - 1(2\hat{\mu}_2^2 \hat{\mu}_2)$
$M_{yx}$	$\frac{\sqrt{E} k_2 (1-i)}{2\lambda^2} \sin \lambda x$	$-\hat{\mu}_1 - i\hat{\mu}_1$	$-\hat{\mu}_2 - i\hat{\mu}_2$
$Q_x$	$\frac{E k_2}{2\lambda} \sin \lambda x$	$(\hat{\mu}_1^2 + \hat{\mu}_1^2) - E + i(2\hat{\mu}_1^2 \hat{\mu}_1)$	$(\hat{\mu}_2^2 + \hat{\mu}_2^2) - E + i(2\hat{\mu}_2^2 \hat{\mu}_2)$
$R_x$	$\frac{E k_2}{2\lambda} \sin \lambda x$	$(2-i)(\hat{\mu}_1^2 + \hat{\mu}_1^2) - E + i(2(2-i)\hat{\mu}_1^2 \hat{\mu}_1)$	$(2-i)(\hat{\mu}_2^2 + \hat{\mu}_2^2) - E + i(2(2-i)\hat{\mu}_2^2 \hat{\mu}_2)$
$Q_y$	$\frac{\sqrt{E} k_2}{2\lambda} \cos \lambda x$	$\hat{\mu}_1(E - \hat{\mu}_1^2 + \hat{\mu}_1^2) - 1(\hat{\mu}_1(E - 3\hat{\mu}_1^2 + \hat{\mu}_1^2))$	$\hat{\mu}_2(E - \hat{\mu}_2^2 + \hat{\mu}_2^2) - 1(\hat{\mu}_2(E - 3\hat{\mu}_2^2 + \hat{\mu}_2^2))$
$R_y$	$\frac{\sqrt{E} k_2}{2\lambda} \cos \lambda x$	$\hat{\mu}_1(E - 3\hat{\mu}_1^2 + \hat{\mu}_1^2) - 1(\hat{\mu}_1(E - 3\hat{\mu}_1^2 + \hat{\mu}_1^2))$	$\hat{\mu}_2(E - 3\hat{\mu}_2^2 + \hat{\mu}_2^2) - 1(\hat{\mu}_2(E - 3\hat{\mu}_2^2 + \hat{\mu}_2^2))$
$w$	$\frac{2}{E h k_2 E} \cos \lambda x$	1	1
$w_x$	$\frac{2\lambda}{E h k_2 E} \sin \lambda x$	-1	-1
$w_y$	$\frac{2\lambda}{E h k_2 E} \cos \lambda x$	$-\hat{\mu}_1 - i\hat{\mu}_1$	$-\hat{\mu}_2 - i\hat{\mu}_2$
$u$	$\frac{1}{E h \lambda} \sin \lambda x$	$\frac{2(1+i)}{E(\hat{\mu}_1^2 + \hat{\mu}_1^2 - 12\hat{\mu}_1^2 \hat{\mu}_1)} + i(1+i)$	$\frac{2(1+i)}{E(\hat{\mu}_2^2 + \hat{\mu}_2^2 - 12\hat{\mu}_2^2 \hat{\mu}_2)} + i(1+i)$
$v$	$\frac{1}{E h \lambda \sqrt{E}} \cos \lambda x$	$\frac{-2(1+i)\hat{\mu}_1^2 \hat{\mu}_1}{E(\hat{\mu}_1^2 + \hat{\mu}_1^2 - 12\hat{\mu}_1^2 \hat{\mu}_1)} + (1+i)(\hat{\mu}_1 - i\hat{\mu}_1)$	$\frac{-2(1+i)\hat{\mu}_2^2 \hat{\mu}_2}{E(\hat{\mu}_2^2 + \hat{\mu}_2^2 - 12\hat{\mu}_2^2 \hat{\mu}_2)} + (1+i)(\hat{\mu}_2 - i\hat{\mu}_2)$

3. Particular integrals are determined from Eqs. 24 or 27 using the relations given in Eqs. 7.

4. The edge values of the homogeneous and the particular solutions are substituted into the edge conditions and the constants of integration are determined.

5. Finally the stresses and the displacements in the shell are found by superposition of the homogeneous and the particular solutions evaluated for the computed values of the constants of integration.



In dealing with edge disturbances from two opposite edges, it often proves convenient to consider each edge separately. Thus, for the edge  $y = -b/2$  the solution given in Eq. 32 reduces to

$$\phi_n(x, y) = \text{Re} \left\{ C_1 e^{\rho_1 \lambda y} + C_2 e^{\rho_2 \lambda y} \right\} \cos \lambda x \dots \dots \dots (35)$$

and the edge value of the typical shell quantity has the form

$$H_{(-b/2)} = [H] \text{Re} \left\{ C_1 \hat{H}_1 e^{-\rho_1 \lambda b/2} + C_2 \hat{H}_2 e^{-\rho_2 \lambda b/2} \right\} \dots \dots \dots (36)$$

Changing the independent variable to

$$\frac{y'}{2} = \frac{y + b}{2} \dots \dots \dots (37)$$

the typical shell quantity is expressed in the same form as before

$$H = [H] \text{Re} \left\{ C_1^1 \hat{H}_1 e^{\rho_1 \lambda y'} + C_2^1 \hat{H}_2 e^{\rho_2 \lambda y'} \right\} \dots \dots \dots (38)$$

and the edge value at  $y' = 0$  simplifies to

$$H_{(y'=0)} = [H] \text{Re} \left\{ C_1^1 \hat{H}_1 + C_2^1 \hat{H}_2 \right\} \dots \dots \dots (39)$$

By introduction of the real and imaginary parts of the constants

$$\left. \begin{aligned} C_1^1 &= A_1 + i B_1 \\ C_2^1 &= A_2 + i B_2 \end{aligned} \right\} \dots \dots \dots (40)$$

the edge values are expressed in terms of the characteristic coefficients and the real constants  $A_1$ ,  $B_1$ ,  $A_2$  and  $B_2$  which in turn must be determined from the edge conditions at  $y = -b/2$ , ( $y' = 0$ ).

The value of the unknown statical quantity at an arbitrary point in the shell is finally found by substituting the constants of integration back into Eq. 38. By expansion of the complex exponential functions, Eq. 38 is transformed to the expression

$$H = [H] [a_1 f_1 + a_2 f_2 + a_3 f_3 + a_4 f_4] \dots \dots \dots (41)$$

in which

$$f_1 = e^{-\mathcal{K}_1 \lambda y'} \cos (\mu_1 \lambda y') \dots \dots \dots (42a)$$

$$f_2 = e^{-\mathcal{K}_1 \lambda y'} \sin (\mu_1 \lambda y') \dots \dots \dots (42b)$$

$$f_3 = e^{-\mathcal{K}_2 \lambda y'} \cos (\mu_2 \lambda y') \dots \dots \dots (42c)$$

$$f_4 = e^{-\mathcal{K}_2 \lambda y'} \sin (\mu_2 \lambda y') \dots \dots \dots (42d)$$

and

and

$$a_1 = A_1 \text{Re} \left\{ \hat{H}_1 \right\} - B_1 \text{I} \left\{ \hat{H}_1 \right\} \dots \dots \dots (43a)$$

$$a_2 = A_1 \text{I} \left\{ \hat{H}_1 \right\} + B_1 \text{Re} \left\{ \hat{H}_1 \right\} \dots \dots \dots (43b)$$

$$a_3 = A_2 \text{Re} \left\{ \hat{H}_2 \right\} - B_2 \text{I} \left\{ \hat{H}_2 \right\} \dots \dots \dots (43c)$$

TABLE 2.—ROOTS OF CHARACTERISTIC EQUATION FOR  $\gamma = 1.00$ 

$\varepsilon$	$\alpha_1$	$\mu_1$	$\alpha_2$	$\mu_2$
0.01	100.007326	99.992676	0.000080	0.964418
0.02	50.014954	49.985059	0.000393	0.994738
0.03	33.335840	33.310870	0.000901	0.999004
0.04	25.030040	24.970060	0.001596	0.999496
0.05	20.037592	19.962604	0.002499	0.999788
0.06	16.711833	16.621838	0.003598	0.999946
0.07	14.338478	14.233486	0.004899	0.999924
0.08	12.560394	12.440406	0.006398	0.999924
0.09	11.179171	11.044191	0.008098	0.999869
0.10	10.075765	9.925797	0.009996	0.999844
0.11	9.174423	9.009474	0.012094	0.999779
0.12	8.424642	8.244722	0.014389	0.999688
0.13	7.791463	7.596581	0.016883	0.999569
0.14	7.249912	7.040082	0.019574	0.999424
0.15	6.781677	6.556917	0.022460	0.999242
0.16	6.373024	6.133355	0.025542	0.999019
0.17	6.013451	5.758899	0.028816	0.998753
0.18	5.694790	5.425385	0.032282	0.998435
0.19	5.410592	5.126370	0.035937	0.998060
0.20	5.155698	4.856701	0.039779	0.997623
0.21	4.925930	4.612208	0.043804	0.997117
0.22	4.717072	4.389480	0.048010	0.996536
0.23	4.528698	4.185700	0.052393	0.995874
0.24	4.356054	3.998523	0.056948	0.995123
0.25	4.197964	3.825978	0.061671	0.994279
0.26	4.052750	3.666402	0.066556	0.993333
0.27	3.918987	3.518375	0.071598	0.992281
0.28	3.795449	3.380683	0.076790	0.991116
0.29	3.681079	3.252279	0.082126	0.989832
0.30	3.574961	3.132257	0.087598	0.988424
0.31	3.476293	3.019827	0.093199	0.986886
0.32	3.384376	2.914299	0.098921	0.985214
0.33	3.298592	2.815066	0.104756	0.983404
0.34	3.218395	2.721593	0.110693	0.981452
0.35	3.143300	2.633405	0.116725	0.979355
0.36	3.072876	2.550081	0.122842	0.977110
0.37	3.006736	2.471124	0.129034	0.974715
0.38	2.944534	2.396554	0.135292	0.972170
0.39	2.885959	2.325711	0.141606	0.969473
0.40	2.830728	2.258440	0.147967	0.966624
0.41	2.778587	2.194493	0.154364	0.963625
0.42	2.729305	2.133646	0.160790	0.960476
0.43	2.682672	2.075693	0.167234	0.957180
0.44	2.638496	2.020448	0.173687	0.953739
0.45	2.596602	1.967739	0.180142	0.950156
0.46	2.556303	1.917325	0.186693	0.946435
0.47	2.517486	1.869178	0.193343	0.942571
0.48	2.480038	1.823325	0.199993	0.938569
0.49	2.443956	1.779728	0.206643	0.934435
0.50	2.409233	1.738333	0.213193	0.930176
0.51	2.375866	1.699000	0.219643	0.925799
0.52	2.343843	1.661588	0.225993	0.921312
0.53	2.313154	1.626066	0.232243	0.916725
0.54	2.283797	1.592393	0.238393	0.912048
0.55	2.255772	1.560528	0.244443	0.907291
0.56	2.229077	1.530433	0.250393	0.902454
0.57	2.203712	1.502078	0.256243	0.897547
0.58	2.179677	1.475433	0.261993	0.892580
0.59	2.156972	1.450478	0.267643	0.887563
0.60	2.135597	1.427193	0.273193	0.882506
0.61	2.115552	1.405558	0.278643	0.877409
0.62	2.096847	1.385573	0.283993	0.872282
0.63	2.079482	1.367238	0.289243	0.867125
0.64	2.063457	1.350453	0.294393	0.861948
0.65	2.048772	1.335218	0.299443	0.856751
0.66	2.035427	1.321433	0.304393	0.851534
0.67	2.023422	1.309098	0.309243	0.846307
0.68	2.012757	1.298113	0.313993	0.841070
0.69	2.003432	1.288478	0.318643	0.835823
0.70	1.995457	1.280093	0.323193	0.830576
0.71	1.988832	1.272858	0.327643	0.825329
0.72	1.983557	1.266673	0.331993	0.820082
0.73	1.979632	1.261438	0.336243	0.814835
0.74	1.976957	1.257153	0.340393	0.809588
0.75	1.975432	1.253818	0.344443	0.804341

TABLE 2.-CONTINUED

$\epsilon$	$\mathcal{H}_1$	$\mu_1$	$\mathcal{H}_2$	$\mu_2$
0.78	1.880598	1.025828	0.363618	0.785203
0.81	1.847464	0.981725	0.376585	0.768866
0.84	1.816884	0.941194	0.389011	0.752694
0.87	1.788559	0.903834	0.400933	0.736734
0.90	1.762239	0.869296	0.412366	0.721022
0.93	1.737708	0.837283	0.423404	0.705590
0.96	1.714781	0.807533	0.434019	0.690461
0.99	1.693299	0.779821	0.444259	0.675654
1.02	1.673124	0.753947	0.454152	0.661182
1.05	1.654135	0.729737	0.463721	0.647057
1.08	1.636226	0.707039	0.472969	0.633284
1.11	1.619304	0.685717	0.481975	0.619868
1.14	1.603286	0.665650	0.490697	0.606810
1.17	1.588100	0.646733	0.499170	0.594111
1.20	1.573679	0.628869	0.507408	0.581767
1.23	1.559966	0.611974	0.515424	0.569776
1.26	1.546908	0.595972	0.523229	0.558133
1.29	1.534459	0.580793	0.530833	0.546833
1.32	1.522574	0.566376	0.538244	0.535869
1.35	1.511216	0.552666	0.545471	0.525235

and

$$a_4 = A_2 I \{\hat{H}_2\} + B_2 \operatorname{Re} \{\hat{H}_2\} \dots \dots \dots (43d)$$

In treating the two opposite edges separately, the effects from the two edge disturbances must be superimposed on each other. In superimposing such effects the contributions must be added for quantities which are defined as even quantities in the  $y$ -direction, and the contributions must be subtracted from each other for the odd quantities.

#### DESIGN TABLES AND NUMERICAL EXAMPLES

The form of the solution obtained is such that it lends itself to tabulation as presented by Rudiger-Urban.<sup>5</sup> They listed influence coefficients for circular cylindrical shells.

In view of Eq. 39 a tabulation of the constants of integration for a unit line load system on the edge is easily performed if the characteristic coefficients are tabulated for various values of the shell parameters. It proves to be convenient to choose the following unit line load system on the edge

$$\left. \begin{array}{cccc} \hat{N}_{yy} = 1 & \hat{N}_{yy} = 0 & \hat{N}_{yy} = 0 & \hat{N}_{yy} = 0 \\ \hat{R}_y = 0 & \hat{R}_y = 1 & \hat{R}_y = 0 & \hat{R}_y = 0 \\ \hat{N}_{yx} = 0 & \hat{N}_{yx} = 0 & \hat{N}_{yx} = 1 & \hat{N}_{yx} = 0 \\ \hat{M}_{yy} = 0 & \hat{M}_{yy} = 0 & \hat{M}_{yy} = 0 & \hat{M}_{yy} = 1 \end{array} \right\} \dots \dots \dots (44)$$

TABLE 3.—ROOTS OF CHARACTERISTIC EQUATION FOR  $\gamma = 0.50$ 

$\varepsilon$	$\mathcal{L}_1$	$\mu_1$	$\mathcal{L}_2$	$\mu_2$
0.01	70.724679	70.696686	0.000278	1.399567
0.02	35.383645	35.327106	0.001268	1.413463
0.03	23.612773	23.527927	0.002861	1.414110
0.04	17.734529	17.621399	0.005090	1.414158
0.05	14.213411	14.072009	0.007952	1.414096
0.06	11.870936	11.701275	0.011449	1.414009
0.07	10.202047	10.004153	0.015579	1.413836
0.08	8.954228	8.728139	0.020336	1.413579
0.09	7.987195	7.732970	0.025717	1.413199
0.10	7.216783	6.934503	0.031712	1.412670
0.11	6.589432	6.279208	0.038312	1.411961
0.12	6.069434	5.731412	0.045502	1.411033
0.13	5.632065	5.266433	0.053263	1.409853
0.14	5.259660	4.866650	0.061573	1.408379
0.15	4.939255	4.519153	0.070405	1.406576
0.16	4.661121	4.214268	0.079722	1.404404
0.17	4.417806	3.944603	0.089489	1.401829
0.18	4.203503	3.704413	0.099664	1.398818
0.19	4.013617	3.489167	0.110197	1.395342
0.20	3.844460	3.295237	0.121038	1.391379
0.21	3.693036	3.119689	0.132131	1.386909
0.22	3.556883	2.960114	0.143422	1.381923
0.23	3.433956	2.814519	0.154852	1.376414
0.24	3.322547	2.681239	0.166366	1.370386
0.25	3.221212	2.558863	0.177909	1.363847
0.26	3.128725	2.446194	0.189428	1.356812
0.27	3.044038	2.342202	0.200876	1.349300
0.28	2.966253	2.245997	0.212208	1.341337
0.29	2.894591	2.156803	0.223385	1.332952
0.30	2.828383	2.073944	0.234373	1.324174
0.31	2.767042	1.996820	0.245143	1.315038
0.32	2.710060	1.924906	0.255671	1.305577
0.33	2.656992	1.857732	0.265939	1.295826
0.34	2.607448	1.794881	0.275932	1.285818
0.35	2.561085	1.735980	0.285640	1.275587
0.36	2.517671	1.680695	0.295056	1.265164
0.37	2.476731	1.628726	0.304176	1.254580
0.38	2.438238	1.579803	0.313001	1.243863
0.39	2.401913	1.533683	0.321532	1.233039
0.40	2.367571	1.490146	0.329773	1.222133
0.41	2.335047	1.448993	0.337729	1.211166
0.42	2.304192	1.410043	0.345406	1.200161
0.43	2.274875	1.373133	0.352813	1.189135
0.44	2.246978	1.338114	0.359957	1.178104
0.45	2.220392	1.304850	0.366848	1.167085
0.46	2.194756	1.273146	0.373494	1.156080
0.47	2.170000	1.242846	0.379907	1.145094
0.48	2.147596	1.214406	0.386094	1.134220
0.49	2.126365	1.187589	0.392077	1.123462
0.50	2.106264	1.162162	0.397868	1.112818
0.51	2.087283	1.138106	0.403397	1.102289
0.52	2.069428	1.115389	0.408707	1.091874
0.53	2.052600	1.093971	0.413847	1.081574
0.54	2.036800	1.073811	0.418777	1.071389
0.55	2.022028	1.054871	0.423557	1.061319
0.56	2.008284	1.037111	0.428147	1.051364
0.57	1.995568	1.020491	0.432607	1.041524
0.58	1.983880	1.004971	0.436907	1.031799
0.59	1.973220	0.990511	0.441017	1.022189
0.60	1.963588	0.977071	0.444917	1.012694
0.61	1.954984	0.964621	0.448687	1.003314
0.62	1.947408	0.953141	0.452307	0.994039
0.63	1.940860	0.942601	0.455767	0.984869
0.64	1.935340	0.932981	0.459047	0.975804
0.65	1.930848	0.924261	0.462147	0.966844
0.66	1.927384	0.916421	0.465067	0.958079
0.67	1.924948	0.909441	0.467797	0.949509
0.68	1.923540	0.903301	0.470347	0.941134
0.69	1.923160	0.897901	0.472717	0.932954
0.70	1.923808	0.893241	0.474907	0.925069
0.71	1.925474	0.889321	0.476917	0.917479
0.72	1.928148	0.886041	0.478747	0.910184

TABLE 3.—CONTINUED

$\epsilon$	$\mathcal{K}_1$	$\mu_1$	$\mathcal{K}_2$	$\mu_2$
0.75	1.756319	0.753555	0.497201	0.874081
0.78	1.729254	0.723711	0.505585	0.849811
0.81	1.704112	0.696250	0.513551	0.826419
0.84	1.680688	0.670894	0.521158	0.803876
0.87	1.658805	0.647407	0.528456	0.782154
0.90	1.638314	0.625587	0.535486	0.761222
0.93	1.619081	0.605259	0.542285	0.741051
0.96	1.600991	0.586272	0.548882	0.721614
0.99	1.583942	0.568496	0.555302	0.702884
1.02	1.567847	0.551816	0.561564	0.684833
1.05	1.552624	0.536132	0.567687	0.667438
1.08	1.538204	0.521355	0.573684	0.650672
1.11	1.524524	0.507407	0.579565	0.634514
1.14	1.511527	0.494219	0.585341	0.618940
1.17	1.499163	0.481729	0.591018	0.603929
1.20	1.487386	0.469881	0.596602	0.589459
1.23	1.476154	0.458627	0.602097	0.575511
1.26	1.465431	0.447922	0.607506	0.562064
1.29	1.455181	0.437726	0.612833	0.549101
1.32	1.445374	0.428001	0.618078	0.536602
1.35	1.435982	0.418717	0.623243	0.524549

where the symbol  $\wedge$  denotes that the stress resultant is reduced by its multiplier.

In an actual set of boundary conditions the internal quantities

$$\hat{N}_{yy} = 1, \hat{R}_y = 1, \hat{N}_{yx} = 1, \hat{M}_{yy} = 1 \dots \dots \dots (45)$$

will represent redundant forces which have to be determined in such a manner that the shell and the edge member form a compatible structure.

*Tables for Parabolic Cylindrical Shells.*—For  $\gamma = 0$  the solution given in Eq. 21 becomes identical to the solution of the Donnell theory equation for circular cylindrical shells as given by Rüdiger-Urban,<sup>5</sup> provided  $k_2$  is replaced by the inverse of the radius of the circular shell. It follows that the extensive tables given by Rudiger-Urban can be directly adopted in the design of shallow parabolic cylindrical shells. In applying these tables the tangential and transverse stress resultants and the flexural moments are directly replaced by the corresponding quantities of the circular shell. The displacement component  $w$  in the  $z$ -direction is replaced by the radial displacement  $v_{zz}$ , and the first order derivatives of  $w$  with respect to  $x$  and  $y$  are replaced by the corresponding slopes for the circular shell. Also note that the quantities  $\mathcal{K}_1$ ,  $\mu_1$ ,  $\mathcal{K}_2$  and  $\mu_2$  are all reduced by  $1/\sqrt{\epsilon}$  by Rüdiger-Urban.<sup>5</sup>

*Tables for Hyperbolic and Elliptic Paraboloidal Shells.*—Design tables of the type given by Rudiger-Urban<sup>5</sup> can be developed for any form of hyperbolic and elliptic paraboloidal shells by assigning various values to the shape parameter  $\gamma$  between  $+1$  and  $-1$ . A general program for such table computation by means of an automatic digital computer is in progress. An assembly of such tables for a suitable choice of parameter values will be the subject of a separate publication.

TABLE 4.—ROOTS OF CHARACTERISTIC EQUATION FOR  $\gamma = 0$ 

$\varepsilon$	$\mathcal{L}_1$	$\mu_1$	$\mathcal{L}_2$	$\mu_2$
0.01	11.025657	4.534877	4.567057	10.947968
0.02	7.823723	3.195410	3.240921	7.713856
0.03	6.410387	2.599947	2.655692	6.275829
0.04	5.570879	2.243811	2.308186	5.415508
0.05	5.000000	2.000000	2.071983	4.826294
0.06	4.580082	1.819473	1.898339	4.389802
0.07	4.254869	1.678749	1.763951	4.049350
0.08	3.993643	1.564987	1.656093	3.773943
0.09	3.778023	1.470493	1.567150	3.545006
0.10	3.596253	1.390336	1.492251	3.350644
0.11	3.440416	1.321193	1.428116	3.182833
0.12	3.304962	1.260730	1.372446	3.035942
0.13	3.185870	1.207254	1.323575	2.905883
0.14	3.080146	1.159500	1.280261	2.789610
0.15	2.985507	1.116505	1.241559	2.684797
0.16	2.900181	1.077519	1.206734	2.589635
0.17	2.822766	1.041948	1.175206	2.502691
0.18	2.752140	1.009316	1.146508	2.422816
0.19	2.687388	0.979233	1.120263	2.349073
0.20	2.627760	0.951380	1.096158	2.280693
0.21	2.572633	0.925492	1.073936	2.217035
0.22	2.521483	0.901345	1.053379	2.157559
0.23	2.473869	0.878750	1.034304	2.101812
0.24	2.429414	0.857546	1.016556	2.049403
0.25	2.387794	0.837593	1.000000	2.000000
0.26	2.348732	0.818772	0.984520	1.953314
0.27	2.311984	0.800979	0.970017	1.909093
0.28	2.277340	0.784123	0.956401	1.867119
0.29	2.244613	0.768123	0.943597	1.827198
0.30	2.213640	0.752908	0.931536	1.789160
0.31	2.184276	0.738415	0.920158	1.752854
0.32	2.156393	0.724590	0.909410	1.718146
0.33	2.129875	0.711361	0.899244	1.684916
0.34	2.104618	0.698743	0.889618	1.653057
0.35	2.080532	0.686638	0.880492	1.622470
0.36	2.057532	0.675027	0.871832	1.593069
0.37	2.035543	0.663878	0.863607	1.564775
0.38	2.014497	0.653160	0.855789	1.537516
0.39	1.994331	0.642848	0.848352	1.511226
0.40	1.974989	0.632915	0.841272	1.485846
0.41	1.956419	0.623339	0.834527	1.461321
0.42	1.938574	0.614099	0.828099	1.437602
0.43	1.921411	0.605176	0.821968	1.414642
0.44	1.904889	0.596551	0.816119	1.392400
0.45	1.888971	0.588210	0.810536	1.370836
0.48	1.844522	0.564735	0.795246	1.309867
0.51	1.804435	0.543324	0.781902	1.253856
0.54	1.768079	0.523690	0.770737	1.202131
0.57	1.734941	0.505604	0.760039	1.154143
0.60	1.704601	0.488873	0.751129	1.109442
0.63	1.676708	0.473339	0.743360	1.067654
0.66	1.650972	0.458866	0.736608	1.028466
0.69	1.627146	0.445343	0.730767	0.991613
0.72	1.605021	0.432670	0.725747	0.956869
0.75	1.584417	0.420765	0.721469	0.924041



TABLE 4.—CONTINUED

$\mathcal{E}$	$\mathcal{H}_1$	$\mu_1$	$\mathcal{H}_2$	$\mu_2$
0.78	1.565179	0.409554	0.717865	0.892962
0.81	1.547175	0.398975	0.714873	0.863488
0.84	1.530286	0.388972	0.712440	0.835492
0.87	1.514412	0.379496	0.710518	0.808864
0.90	1.499461	0.370503	0.709063	0.783506
0.93	1.485356	0.361957	0.708036	0.759332
0.96	1.472025	0.353821	0.707401	0.736263
0.99	1.459405	0.346066	0.707125	0.714231
1.02	1.447441	0.338664	0.707176	0.693174
1.05	1.436083	0.331590	0.707527	0.673035
1.08	1.425284	0.324822	0.708152	0.653762
1.11	1.415005	0.318338	0.709025	0.635309
1.14	1.405209	0.312122	0.710125	0.617633
1.17	1.395862	0.306155	0.711429	0.600693
1.20	1.386935	0.300423	0.712918	0.584453
1.23	1.378398	0.294911	0.714572	0.568878
1.26	1.370227	0.289606	0.716375	0.553935
1.29	1.362399	0.284496	0.718310	0.539596
1.32	1.354893	0.279570	0.720362	0.525830
1.35	1.347689	0.274819	0.722516	0.512612

Tables 2, 3, 4, 5, and 6 give the roots of the characteristic equation for two hyperbolic paraboloids, cylindrical shells, and two elliptic paraboloids, that is for  $\gamma = +1, +1/2, 0, -1/2$  and  $-1$ , respectively.

For the case of a rotational paraboloid, that is for  $\gamma = -1$ , the differential Eq. 6a reduces to the well-known form

$$\nabla^4 (\nabla^4 + \alpha) \phi = \frac{q_z}{D} \dots \dots \dots (46)$$

and the solution degenerates to a sum of the solutions for the free plate and for the plate on elastic foundation. The procedure previously outlined does not apply directly to this case, in which the biharmonic operator vanishes. The multiple roots of the biharmonic equation are represented by the first principal root, (Eqs. 24) where  $\mu_1$  becomes identically equal to zero. Table 6 is included for illustrative reasons. The roots  $\mathcal{H}_2$  and  $\mu_2$  represent solutions for the rectangular plate on elastic foundation.

*Numerical Examples.*—The solutions obtained are particularly useful for comparative studies of shell shapes. To investigate the effects of change in shape, four different shells have been analyzed, two hyperbolic paraboloids, one cylindrical shell, and one elliptic paraboloid, which had the following values of the shape parameter  $\gamma$ :  $+1, +1/2, 0$  and  $-1/2$ , respectively. The pa-

TABLE 5.—ROOTS OF CHARACTERISTIC EQUATION FOR  $\gamma = -0.50$ 

$\varepsilon$	$\mathcal{H}_1$	$\mu_1$	$\mathcal{H}_2$	$\mu_2$
0.01	1.401803	0.000113	70.710802	70.710555
0.02	1.412357	0.000113	35.355379	35.355305
0.03	1.413862	0.000302	23.570246	23.570225
0.04	1.414035	0.000556	17.677699	17.677685
0.05	1.414138	0.000880	14.142184	14.142176
0.06	1.414193	0.001270	11.785191	11.785188
0.07	1.414183	0.001729	10.101649	10.101645
0.08	1.414181	0.002260	8.839018	8.839013
0.09	1.414166	0.002860	7.857004	7.856995
0.10	1.414145	0.003533	7.071429	7.071414
0.11	1.414116	0.004273	6.428725	6.428702
0.12	1.414076	0.005085	5.893184	5.893149
0.13	1.414024	0.005966	5.440085	5.440032
0.14	1.413959	0.006917	5.051769	5.051693
0.15	1.413879	0.007933	4.715289	4.715162
0.16	1.413780	0.009023	4.420934	4.420787
0.17	1.413663	0.010178	4.161281	4.161081
0.18	1.413522	0.011400	3.930554	3.930289
0.19	1.413357	0.012688	3.724197	3.723850
0.20	1.413164	0.014040	3.538563	3.538115
0.21	1.412941	0.015456	3.370701	3.370132
0.22	1.412684	0.016933	3.218199	3.217483
0.23	1.412392	0.018471	3.079063	3.078171
0.24	1.412061	0.020066	2.951633	2.950534
0.25	1.411689	0.021718	2.834513	2.833171
0.26	1.411272	0.023423	2.726525	2.724900
0.27	1.410809	0.025178	2.626664	2.624711
0.28	1.410296	0.026983	2.534069	2.531741
0.29	1.409731	0.028832	2.447999	2.445242
0.30	1.409112	0.030723	2.367810	2.364568
0.31	1.408437	0.032652	2.292945	2.289154
0.32	1.407704	0.034616	2.222912	2.218506
0.33	1.406910	0.036611	2.157281	2.152189
0.34	1.406055	0.038633	2.095674	2.089820
0.35	1.405137	0.040678	2.037753	2.031057
0.36	1.404156	0.042741	1.983219	1.975597
0.37	1.403110	0.044819	1.931805	1.923169
0.38	1.402000	0.046907	1.883272	1.873531
0.39	1.400826	0.049001	1.837405	1.826484
0.40	1.399587	0.051096	1.794010	1.781771
0.41	1.398285	0.053190	1.752912	1.739274
0.42	1.396920	0.055277	1.713953	1.698813
0.43	1.395494	0.057353	1.676987	1.660240
0.44	1.394007	0.059416	1.641883	1.623424
0.45	1.392462	0.061461	1.608520	1.588241
0.46	1.387495	0.067456	1.517823	1.491435
0.47	1.382080	0.073182	1.439321	1.405858
0.48	1.376286	0.078578	1.371018	1.329541
0.49	1.370186	0.083602	1.311314	1.260938
0.50	1.363854	0.088230	1.258917	1.198826
0.51	1.357357	0.092451	1.212768	1.142224
0.52	1.350758	0.096269	1.171995	1.090344
0.53	1.344111	0.099693	1.135872	1.042545
0.54	1.337461	0.102741	1.103793	0.998302



TABLE 5.—CONTINUED

$\epsilon$	$\mathcal{K}_1$	$\mu_1$	$\mathcal{K}_2$	$\mu_2$
0.75	1.330849	0.105435	1.075247	0.957182
0.78	1.324305	0.107798	1.049800	0.918827
0.81	1.317853	0.109854	1.027086	0.882936
0.84	1.311515	0.111629	1.006789	0.849255
0.87	1.305303	0.113146	0.988638	0.817569
0.90	1.299230	0.114429	0.972399	0.787695
0.93	1.293303	0.115499	0.957867	0.759475
0.96	1.287527	0.116375	0.944866	0.732772
0.99	1.281904	0.117078	0.933240	0.707465
1.02	1.276436	0.117623	0.922850	0.683452
1.05	1.271123	0.118027	0.913575	0.660638
1.08	1.265962	0.118304	0.905307	0.638941
1.11	1.260953	0.118466	0.897949	0.618289
1.14	1.256092	0.118526	0.891415	0.598614
1.17	1.251375	0.118494	0.885628	0.579858
1.20	1.246799	0.118380	0.880517	0.561965
1.23	1.242361	0.118193	0.876019	0.544885
1.26	1.238056	0.117940	0.872077	0.528573
1.29	1.233879	0.117628	0.868640	0.512988
1.32	1.229827	0.117264	0.865660	0.498088
1.35	1.225896	0.116853	0.863095	0.483839

parameter  $\epsilon$  was chosen  $\epsilon = 0.30$  for all shells. All shells were square in plan ( $a = b$ ), and all shells had free edges without edge beams along the two edges  $y = \pm b/2$ , giving the boundary conditions

$$N_{yy} = R_y = N_{yx} = M_{yy} = 0 \dots\dots\dots (47)$$

All shells had uniform load of intensity  $q_z = -p_0$ .

For this load distribution a particular integral is found from Eqs. 27 and 28, which by substitution into Eqs. 7 gives

$$\left. \begin{aligned} N_{yy} &= \sum_n \frac{1}{(1 + \epsilon^4/4)} (q_z/k_2) \cos \lambda x = \sum_n [N_{yy}] q' \\ M_{yy} &= \sum_n \frac{1}{(1 + \epsilon^4/4)} (q_z/k_2) \left( \frac{2\nu}{\epsilon} \right) \left( \frac{1}{2} \epsilon k_2 / \lambda^2 \cos \lambda x \right) \\ &= \sum_n [M_{yy}] \left( \frac{2\nu}{\epsilon} \right) q' \\ N_{xx} &= N_{xp} = R_{yp} = 0 \end{aligned} \right\} \dots\dots (48)$$

Poisson's ratio was chosen as  $\nu = 0.25$ .

The edge values of the quantities  $N_{yy}$ ,  $R_y$ ,  $N_{yx}$ , and  $M_{yy}$  were determined from Eq. 39 and were corrected for effects from the opposite edge by means of Eq. 41. The characteristic coefficients were obtained from Table 1 using

TABLE 6.—ROOTS OF CHARACTERISTIC EQUATION FOR  $\gamma = -1.00$ 

$\varepsilon$	$\sigma_1$	$\mu_1$	$\sigma_2$	$\mu_2$
0.01	1.000000	0.0000	100.002501	99.997500
0.02	1.000000	0.0000	50.005001	49.995000
0.03	1.000000	0.0000	33.340834	33.325835
0.04	1.000000	0.0000	25.010002	24.990002
0.05	1.000000	0.0000	20.012504	19.987504
0.06	1.000000	0.0000	16.681674	16.651674
0.07	1.000000	0.0000	14.303225	14.268225
0.08	1.000000	0.0000	12.520016	12.480016
0.09	1.000000	0.0000	11.193694	11.088694
0.10	1.000000	0.0000	10.025031	9.975031
0.11	1.000000	0.0000	9.118451	9.063451
0.12	1.000000	0.0000	8.363387	8.303388
0.13	1.000000	0.0000	7.724876	7.659877
0.14	1.000000	0.0000	7.177943	7.107943
0.15	1.000000	0.0000	6.704272	6.629273
0.16	1.000000	0.0000	6.290127	6.210129
0.17	1.000000	0.0000	5.925005	5.840008
0.18	1.000000	0.0000	5.600736	5.510739
0.19	1.000000	0.0000	5.310870	5.215874
0.20	1.000000	0.0000	5.050248	4.950253
0.21	1.000000	0.0000	4.814691	4.709697
0.22	1.000000	0.0000	4.600783	4.490791
0.23	1.000000	0.0000	4.405701	4.290711
0.24	1.000000	0.0000	4.227092	4.107105
0.25	1.000000	0.0000	4.062981	3.937996
0.26	1.000000	0.0000	3.911694	3.781712
0.27	1.000000	0.0000	3.771807	3.636830
0.28	1.000000	0.0000	3.642101	3.502128
0.29	1.000000	0.0000	3.521522	3.376554
0.30	1.000000	0.0000	3.409158	3.259196
0.31	1.000000	0.0000	3.304215	3.149259
0.32	1.000000	0.0000	3.205997	3.046049
0.33	1.000000	0.0000	3.113895	2.948956
0.34	1.000000	0.0000	3.027368	2.857439
0.35	1.000000	0.0000	2.945940	2.771022
0.36	1.000000	0.0000	2.869187	2.689281
0.37	1.000000	0.0000	2.796729	2.611838
0.38	1.000000	0.0000	2.728229	2.538353
0.39	1.000000	0.0000	2.663383	2.468523
0.40	1.000000	0.0000	2.601916	2.402076
0.41	1.000000	0.0000	2.543583	2.338764
0.42	1.000000	0.0000	2.488160	2.278364
0.43	1.000000	0.0000	2.435445	2.220674
0.44	1.000000	0.0000	2.385253	2.165510
0.45	1.000000	0.0000	2.337417	2.112705
0.48	1.000000	0.0000	2.206577	1.966973
0.51	1.000000	0.0000	2.092141	1.837676
0.54	1.000000	0.0000	1.991385	1.722096
0.57	1.000000	0.0000	1.902162	1.618091
0.60	1.000000	0.0000	1.822751	1.523949
0.63	1.000000	0.0000	1.751759	1.438284
0.66	1.000000	0.0000	1.688047	1.359965
0.69	1.000000	0.0000	1.630672	1.288057
0.72	1.000000	0.0000	1.578848	1.221785

TABLE 6.—CONTINUED

$\epsilon$	$\mathcal{K}_1$	$\mu_1$	$\mathcal{K}_2$	$\mu_2$
0.75	1.000000	0.0000	1.531911	1.160497
0.78	1.000000	0.0000	1.489303	1.103641
0.81	1.000000	0.0000	1.450543	1.050750
0.84	1.000000	0.0000	1.415220	1.001423
0.87	1.000000	0.0000	1.382977	0.955315
0.90	1.000000	0.0000	1.353505	0.912127
0.93	1.000000	0.0000	1.326531	0.871599
0.96	1.000000	0.0000	1.301817	0.833504
0.99	1.000000	0.0000	1.279152	0.797641
1.02	1.000000	0.0000	1.258349	0.763834
1.05	1.000000	0.0000	1.239239	0.731925
1.08	1.000000	0.0000	1.221674	0.701774
1.11	1.000000	0.0000	1.205518	0.673256
1.14	1.000000	0.0000	1.190651	0.646258
1.17	1.000000	0.0000	1.176962	0.620677
1.20	1.000000	0.0000	1.164353	0.596421
1.23	1.000000	0.0000	1.152733	0.573405
1.26	1.000000	0.0000	1.142019	0.551551
1.29	1.000000	0.0000	1.132138	0.530788
1.32	1.000000	0.0000	1.123020	0.511052
1.35	1.000000	0.0000	1.114603	0.492280

the tabulated values of  $\mathcal{K}_1$ ,  $\mu_1$ ,  $\mathcal{K}_2$ , and  $\mu_2$  from Tables 2, 3, 4, and 5. The constants of integration were obtained from the boundary conditions of Eq. 47 by introduction of the particular integral of Eqs. 48 and the edge values from the homogeneous solution.

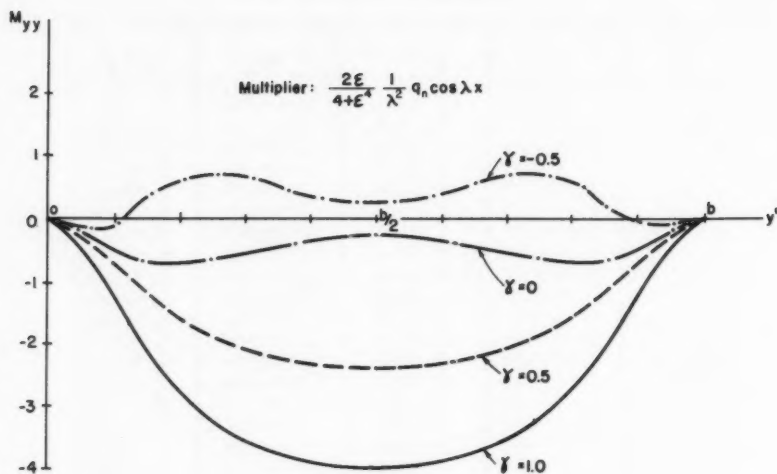
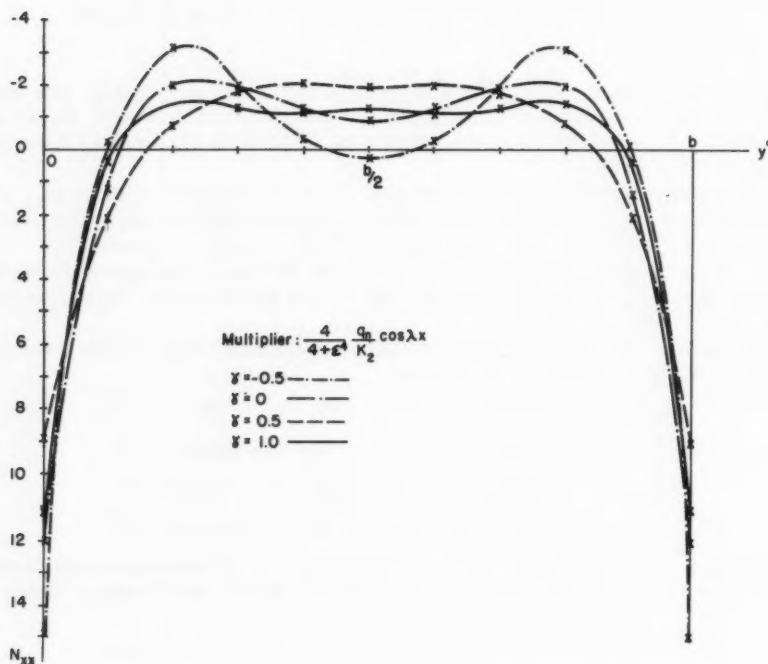
For illustration the transverse distribution of the flexural moment  $M_{yy}$  and the longitudinal normal stress  $N_{xx}$  resulting from the first term of the series expansion of the load function are shown in Figs. 3 and 4, respectively.

The numerical computations involved will be shown for the hyperbolic paraboloidal shell with  $\gamma = 0.50$ . Only the first term of the series expansion will be included, that is  $n = 1$ .

The roots of the characteristic equation are obtained from Table 3 for the chosen value  $\epsilon = 0.30$  for  $n = 1$ , that is

$$\begin{array}{ll}
 \mathcal{K}_1 = 2.828383 & ; \quad \mathcal{K}_1 = 1.54917 \\
 \mu_1 = 2.073944 & ; \quad \hat{\mu}_1 = 1.13595 \\
 \mathcal{K}_2 = 0.234373 & ; \quad \mathcal{K}_2 = 0.128372 \\
 \mu_2 = 1.324174 & ; \quad \hat{\mu}_2 = 0.725278
 \end{array}$$

The characteristic coefficients are then computed by means of the formulas listed in Table 1 and are given for a number of stress resultants in Table 7.

FIG. 3.—TRANSVERSE MOMENTS,  $M_{yy}$ FIG. 4.—LONGITUDINAL NORMAL STRESS  $N_{xx}$

The distribution functions  $f_1$ -- $f_4$  are determined from Eqs. 42 and are given in Table 8.

It can be observed from Table 8 that  $f_3$  and  $f_4$  dampen slowly, which means that effects from the edge disturbance at the opposite edge must be considered. The edge values at  $y = 0$  resulting from the edge disturbance at  $y = b$  are found from Eq. 41 yielding

$$\left. \begin{aligned} \hat{N}_{yy2} &= -0.4081 A_2 + 0.2505 B_2 \\ \hat{R}_{y2} &= -0.3636 A_2 + 0.07266 B_2 \\ \hat{N}_{yx2} &= 0.1293 A_2 + 0.3281 B_2 \\ \hat{M}_{yy2} &= -0.07044 A_2 - 0.2852 B_2 \end{aligned} \right\} \dots \dots \dots (49)$$

Since the boundary conditions of Eqs. 47 are symmetric, the total edge values at  $y = 0$  are obtained by adding Eqs. 49 to the values obtained from Table

TABLE 7.—CHARACTERISTIC COEFFICIENTS FOR  $\gamma = 0.50$ ,  $\epsilon = 0.30$

H	[H]	$H_1$	$H_2$
$N_{yy}$	$\cos \lambda x$	$-i$	$i$
$R_y$	$\frac{\sqrt{\epsilon k_2}}{2\lambda} \cos \lambda x$	$-3.09245 + i6.11641$	$-0.26786 - i0.72644$
$N_{yx}$	$\frac{1}{\sqrt{\epsilon}} \sin \lambda x$	$-1.13595 + i1.54917$	$.725278 - i .128372$
$M_{yy}$	$\frac{\epsilon k_2}{2\lambda^2} \cos \lambda x$	$-1.034552 - i3.519544$	$0.584552 - i0.186210$
$N_{xx}$	$\frac{1}{\epsilon} \cos \lambda x$	$3.51954 - i1.10955$	$- .186210 - i .509552$

7. Introduction of these values and the particular integrals of Eqs. 48 into the boundary conditions of Eqs. 47 yields

$$\left. \begin{aligned} B_1 - .408110 A_2 - .749500 B_2 &= q' \\ -3.09245 A_1 - 6.11641 B_1 - .63142 A_2 + .79910 B_2 &= 0 \\ -1.13595 A_1 - 1.54917 B_1 + .854578 A_2 + .456472 B_2 &= 0 \\ -1.034552 A_1 + 3.519544 B_1 + .514114 A_2 - 0.098992 B_2 &= 1.6667 q' \end{aligned} \right\} \dots (50)$$

in which

$$q' = \frac{1}{4+\epsilon} \frac{q_n}{k_2} \quad q_n = \frac{4}{n\pi} \quad q_z = \frac{4}{\pi} q_z \dots \dots \dots (51)$$

the solution of which gives

$$\left. \begin{aligned} A_1 &= -0.72395 q' \\ B_1 &= 0.23088 q' \\ A_2 &= 0.00621 q' \\ B_2 &= -1.02956 q' \end{aligned} \right\} \dots \dots \dots (52)$$

The stresses and displacements are then obtained by substitution of the constants of integration into Eq. 41. The stress resultant  $N_{xx}$  and the flexural moment  $M_{yy}$  appear in the form

$$\left. \begin{aligned} N_{xx} &= [N_{xx}] (-7.630 f_1 + 4.996 f_2 - 1.755 f_3 + .628 f_4) q' \epsilon \\ M_{yy} &= [M_{yy}] (1.563 f_1 + 2.311 f_2 - 0.188 f_3 + 0.604 f_4) q' \end{aligned} \right\} \dots \dots (53)$$

The distribution in the y-direction is most conveniently computed in tabular form as shown in Tables 9 and 10.

TABLE 8.—DISTRIBUTION FUNCTIONS  $f_1$ – $f_4$ .  $\gamma = 0.50$ ;  $\epsilon = 0.30$ ;  $a = b$

y/a	$\mathcal{K}_1 \lambda y$	$\mu_1 \lambda y$	$\mathcal{K}_2 \lambda y$	$\mu_2 \lambda y$	$f_1$	$f_2$	$f_3$	$f_4$
0	0	0	0	0	1.000	0	1.000	0
0.1	0.888	0.651	.0737	.416	.328	.249	.850	.375
0.2	1.776	1.302	.1474	.832	.045	.163	.581	.635
0.3	2.664	1.953	.2211	1.248	-.026	.065	.254	.760
0.4	3.552	2.604	.2948	1.664	-.024	.014	-.069	.741
0.5			.3685	2.080			-.332	.608
0.6			.4422	2.496			-.513	.387
0.7			.5159	2.912			-.581	.136
0.8			.5896	3.328			-.544	-.103
0.9			.6633	3.744			-.425	-.292
1.0			.7370	4.160			-.251	-.408

Analogous computations must be made for  $n = 3, 5$ —. Note that the shell parameter  $\epsilon$  is a function of  $n$ . For uniform load the series converges rapidly and a good approximation is obtained by the first term only.

### CONCLUSIONS

Levy-type solutions of the problem of bending of thin shallow translational shells are obtained. The solutions are expressed in terms of two parameters, one shape parameter  $\gamma = k_1/k_2$  or  $\gamma = (b/a)^2 (c_1/c_2)$  in which  $c_1$  and  $c_2$  are the rises over the spans  $a$  and  $b$  respectively, and one shell parameter

$$\epsilon = \frac{n \pi}{4 \sqrt{192(1-\nu^2)}} \left( \frac{b}{a} \right) \sqrt{\frac{h}{c_2}} \dots \dots \dots (18)$$

The solutions are developed explicitly and a systematic procedure for the application in solving actual boundary value problems is developed. A number of tables of the roots of the characteristic equation are included, and the use of tables in application is described. Graphs showing stress distributions in a

TABLE 9.— $N_{xx}$  MULTIPLIER:  $\frac{4}{4+\epsilon^4} \frac{q_n}{k_2} \cos \lambda x$

y/a	$a_1 f_1$	$a_2 f_2$	$a_3 f_3$	$a_4 f_4$	$N_{xx}$ y=0	$N_{xx}$ y=b	$N_{xx}$ total
0	-7.630	0	-1.755	0	-9.385	.185	-9.200
0.1	-2.505	1.340	-1.489	.236	-2.418	.568	-1.850
0.2	-.343	.878	-1.019	.399	-.085	.890	.805
0.3	.198	.352	-.446	.479	.583	1.104	1.687
0.4	.184	.076	.122	.466	.848	1.148	1.996
0.5			.582	.382	.964	.964	1.928
0.6			.906	.242	1.148	.848	1.996
0.7			1.019	.085	1.104	.583	1.687
0.8			.955	-.065	.890	-.085	.805
0.9			.748	-.180	.568	-2.418	-1.850
1.0			.439	-.254	.185	-9.385	-9.200

TABLE 10.— $M_{yy}$  MULTIPLIER:  $\frac{2\epsilon}{4+\epsilon^4} \frac{1}{\lambda^2} q_n \cos \lambda x$

y/a	$a_1 f_1$	$a_2 f_2$	$a_3 f_3$	$a_4 f_4$	$M_{yy}$ y=0	$M_{yy}$ y=b	$M_{yy}$ part.	$M_{yy}$ total
0	1.563	0	-.188	0	1.375	.292	-1.667	0
0.1	.512	.576	-.159	-.226	.703	.257	-1.667	-.707
0.2	.071	.375	-.110	-.373	-.037	.164	-1.667	-1.540
0.3	-.041	.150	-.048	-.458	-.397	.027	-1.667	-2.037
0.4	-.038	.032	.013	-.446	-.439	-.135	-1.667	-2.241
0.5			.062	-.368	-.306	-.306	-1.667	-2.279
0.6			.097	-.232	-.135	-.439	-1.667	-2.241
0.7			.110	-.083	.027	-.397	-1.667	-2.037
0.8			.102	.062	.164	-.037	-1.667	-1.540
0.9			.080	.177	.257	.703	-1.667	-.707
1.0			.045	.247	.292	1.375	-1.667	0

number of shells that have been analyzed by the method are included. It is shown that the dampening of edge disturbances is slower in hyperbolic paraboloidal shells than in cylindrical shells and elliptic paraboloidal shells, which in general indicates that edge disturbances produce relatively more significant bending effects in the hyperbolic paraboloidal shells.

*Note.*—After the final copy of the present paper was submitted to ASCE for publication, it came to the writer's attention that the work presented is parallel, in part, to developments made by A. L. Bouma.<sup>10</sup>

### ACKNOWLEDGMENTS

The present study is part of a research program under an appointment supported by the International Cooperation Administration under the Visiting Research Scientists Program administered by the National Academy of Sciences of the United States of America.

The author wishes to express his appreciation of the guidance received from E. P. Popov and S. J. Medwadowski of the University of California at Berkeley.

### APPENDIX.—NOTATION

#### *Dimensions, Coordinates.*

- $x, y, z$  - rectangular cartesian coordinates  
 $z(x, y)$  - surface function of shell  
 $a, b$  - span lengths of shell  
 $c_1, c_2$  - rises of shell  
 $h$  - thickness of shell

$$\lambda x = \frac{n\pi x}{a} \quad \delta y = \frac{m\pi y}{b}$$

- nondimensional coordinates

#### *Stress Resultants, Displacements.*

- $N_{xx}, N_{yy}$  - stress resultants tangential to shell surface  
 $N_{xy}$  - shear stress resultant tangential to shell surface  
 $Q_x, Q_y$  - transverse shear resultants  
 $R_x, R_y$  - effective transverse edge stress resultants  
 $V_x, V_y$  - stress resultants in the  $z$ -direction  
 $\bar{V}_x, \bar{V}_y$  - effective edge stress resultants in the  $z$ -direction  
 $M_{xx}, M_{yy}$  - flexural moments  
 $M_{yx}$  - twisting moment  
 $u, v, w$  - displacement components tangential and normal to shell  
 $U, V, W$  - displacement components in the  $x, y, z$ -directions

<sup>10</sup> "Some Applications of the Bending Theory Regarding Doubly Curved Shells," by A. L. Bouma, *Proceedings, Symposium on the Theory of Thin Elastic Shells*, I. U. T. A. M., North Holland Publishing Co., Amsterdam, Netherlands, 1960.



F	- Airy stress function
$\phi$	- stress-displacement function
H	- arbitrary statical quantity
[H]	- multiplier of H
$\hat{H}$	- reduced value of H

*Constants, Parameters, etc.*

A, B	- real constants of integration
C	- complex constants of integration
$D = \frac{Eh^3}{12(1-\nu^2)}$	- flexural rigidity
E	- modulus of elasticity
$\hat{H}_1, \hat{H}_2$	- characteristic coefficients
$k_1, k_2, \gamma = k_1/k_2$	- shape parameters
$\alpha = \frac{Ehk_2}{D} = 12(1-\nu^2)\left(\frac{k_2}{h}\right)^2$	- shell parameter
$\epsilon = \frac{n\pi}{a \sqrt[4]{3(1-\nu^2)\left(\frac{k_2}{h}\right)^2}}$	- shell parameter
$\nu$	- Poisson's ratio
$\mathcal{L}, \mu$	- real and imaginary parts of the roots of a characteristic equation
$\rho$	- root of a characteristic equation

*Mathematical Symbols.*

Comma in subscript denotes differentiation

$$\nabla^2 f = f_{,xx} + f_{,yy}$$

$$\nabla_\gamma^2 f = f_{,xx} - \gamma f_{,yy}$$

$$\nabla^4 f = \nabla^2 \nabla^2 f$$

$$\nabla^6 f = \nabla^2 \nabla^4 f$$

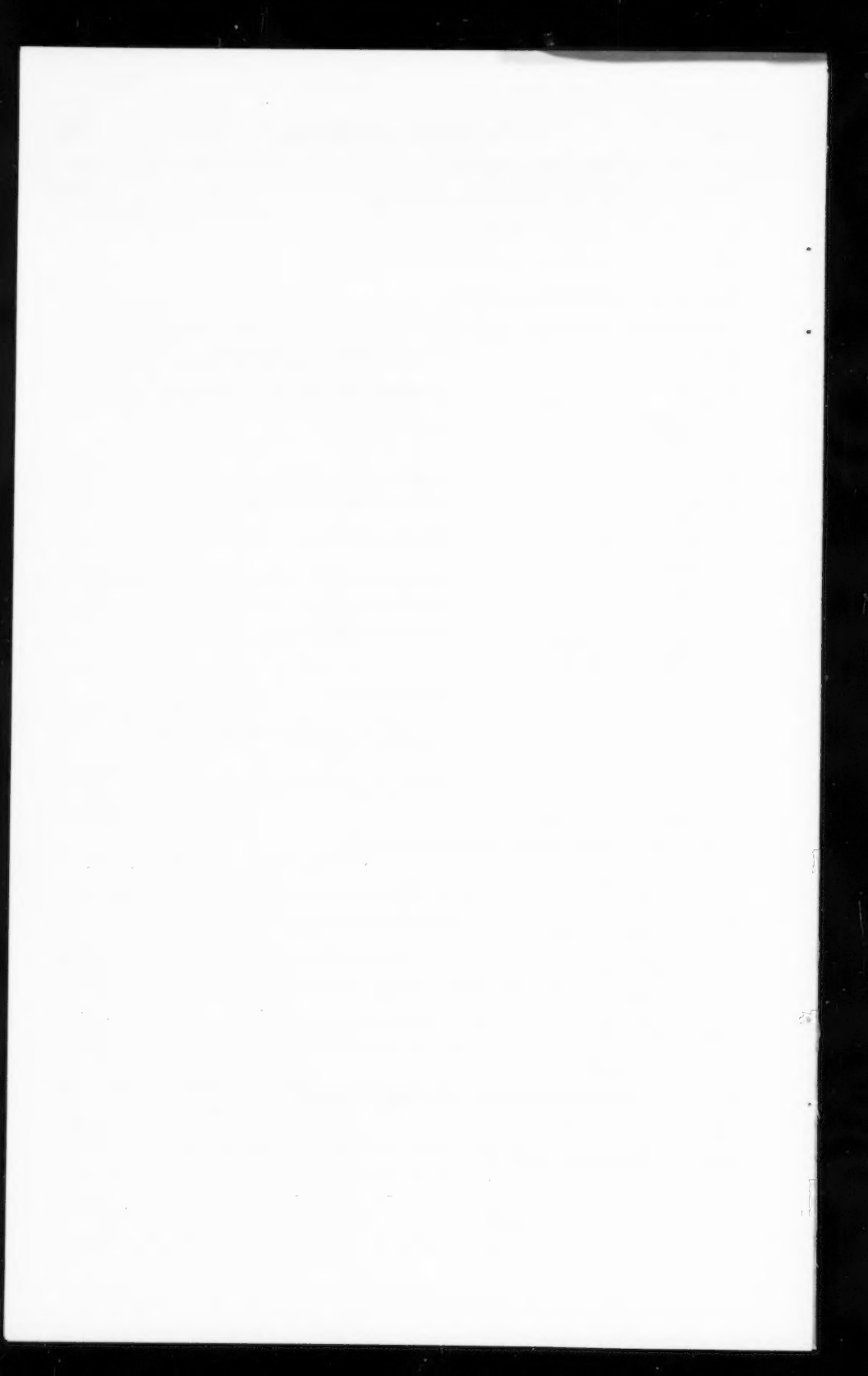
$$\nabla^8 f = \nabla^4 \nabla^4 f$$

i - imaginary unit

$\bar{z}$  - number conjugate to the complex number z

$\text{Re}\{z\}$  - real part of z

$\text{I}\{z\}$  - imaginary part of z



---

Journal of the  
ENGINEERING MECHANICS DIVISION  
Proceedings of the American Society of Civil Engineers

---

WIND-INDUCED VIBRATIONS IN ANTENNA MEMBERS

By William Weaver, Jr.,<sup>1</sup> M. ASCE

---

SYNOPSIS

This paper reports the results of wind-tunnel tests of wind-induced vibrations in the circular aluminum tubular members of large radar antenna space frames. A curve for the RMS von Kármán lift coefficient is established, and a semi-empirical means for evaluating the effect of self-amplification of vibrations is presented. A system of aerodynamic spoilers is also investigated and recommended for applicable cases.

---

INTRODUCTION

*Origin and Background of the Problem.*—A steady wind flow acting on a cylindrical structural member induces lateral vibrations in the member due to the formation of vortices on alternating sides of the member. These vortices are formed and shed from opposite sides of the member at a regular frequency, depending on the velocity of the wind and as a result alternating lateral forces are exerted on the member by the fluid motion. When the frequency of vortex shedding (and hence, the frequency of the alternating forces) is approximately equal to the frequency of one of the normal modes of vibration of the member, a condition of resonance results. If the structural damping and the stiffness of the member are small and the wind remains steady, large amplitudes of vibration will be developed.

These vibrations possess the ability of self-amplification, and for this reason may be considered to be self-exciting for a limited range of wind velocities at

---

Note.—Discussion open until July 1, 1961. To extend the closing date one month, a written request must be filed with the Executive Secretary, ASCE. This paper is part of the copyrighted Journal of the Engineering Mechanics Division, Proceedings of the American Society of Civil Engineers, Vol. 87, No. EM 1, February, 1961.

<sup>1</sup> Asst. Prof. of Civ. Engr., Stanford Univ., Stanford, Calif.

and around the resonant (or "critical") wind velocity. This self-amplification has an upper limit of vibrational stability, however, so that the vibrations produced by the wind are not catastrophic in nature. Oscillation persists for a certain range of wind speed above the critical velocity and reaches a maximum amplitude near the top of the range.

There are several methods by which vibrations of this type can be suppressed:

1. By increasing the flexural stiffness of the member so that its critical velocity is above the range of moderate winds;
2. By reducing the effective length of the member through the introduction of intermediate struts;
3. By use of damping devices to restrict the amplitude of vibration; or
4. By attaching "spoilers" to the member that serve to disrupt the flow near the surface and to interfere with the regular formation of vortices, thereby destroying the cause of the vibrations.

In the past, the first three methods of suppressing wind-induced vibrations have been used repeatedly. The solution to this problem by the method of applying spoilers to the surface of the member has not, in general, been attempted in civil engineering structures because of a lack of information concerning their design and their effectiveness.

This investigation originated with the problem of wind-induced vibrations in individual members of large radar antenna space frames. Several failures have been attributed to the action of von Kármán vortex forces. The failures occurred in slender tubular members subjected to moderate winds, and they were observed to be fatigue-type failures in weld-heated areas at points of maximum flexural stress.

*Notation.*—The letter symbols adopted for use in this paper are defined where they first appear, in the illustrations or in the text, and are arranged alphabetically, for convenience of reference, in Appendix I.

*Object.*—One of the objectives in the current investigation is to obtain an experimental curve for the variation of the von Kármán coefficient,  $C_K$ , with Reynolds number,  $R$ . The range of  $R$  of interest in this experiment is approximately from  $10^4$  to  $10^6$ . A continuous curve for  $C_K$  in the region of interest is a basic necessity for the establishment of design criteria for wind-induced vibrations.

A second objective is to study the self-amplification aspect that characterizes wind-induced vibrations of this type. With sufficient experimental data, involving variations in all of the parameters affecting the response, a semi-empirical solution to the problem can be applied.

Strouhal numbers,  $S$ , are evaluated in this investigation for the purpose of comparing with well-established values previously published in engineering and scientific literature.

Another purpose for these experiments is to test and optimize a system of spoilers attached to the surfaces of a variety of member sizes. The function of these spoilers is to interfere with the periodic circulation and formation of vortices around the periphery of a circular cylinder. The measure of their effectiveness,  $S_e$ , is the ratio of the von Kármán coefficient for the cylinder with spoilers,  $C_{KS}$ , to the von Kármán coefficients for the bare member,  $C_{KB}$ :

$$S_e = C_{KS}/C_{KB} \dots \dots \dots (1)$$

*Scope.*—This investigation is limited to a study of tubular aluminum members in the form of circular cylinders. The types of test members considered are as follows:

1. Stationary rigid-body cylinders;
2. Spring-supported rigid-body cylinders;
3. End-supported flexural members - fixed;
4. End-supported flexural members - partially fixed;
5. End-supported flexural members - pinned; and
6. Cantilever flexural members.

The cylinder and member diameters range from  $1\frac{1}{2}$  in. to 10 in.

The spoiler configuration selected for these experiments consists of small-diameter tubing attached to the surface of the member and wound in a helical pattern over all or part of the length of the member. This particular configuration was chosen because of the ease with which windings can be installed on a cylindrical member and because of the fact that a helical pattern of spoilers is not sensitive to the direction of the wind. The variable parameters for optimization of spoilers of this kind were the following:

- a. Number of windings;
- b. Size of windings;
- c. Pitch of windings; and
- d. Portion of length over which windings are applied.

The appropriate range of  $R$  was obtained by means of subjecting standard-diameter test members and cylinders to the full range of wind speeds in a wind tunnel having a velocity range of 10 mph to 100 mph.

In tests on vibrating members, stiffnesses and structural damping were varied sufficiently to allow the effects of these parameters on the response to be evaluated.

The test program was divided into three main phases: Phase A consisted of tests on stationary cylinders mounted in the wind tunnel with a sensitive transducer built into the supports in such a manner that direct measurements of the reactions due to the lift forces acting on the cylinders were obtained. Spoiler optimization was carried out on the stationary cylinders and confirmed in the later phases. Phase B dealt with the response of spring-supported cylinders oscillating as rigid bodies in the wind stream. Phase C was a study of the response of flexural members vibrating in bending modes under the influence of a steady wind. Each of these phases contributed information on the lift coefficient, the self-amplification phenomenon, the Strouhal number, and the spoiler optimization.

## RESPONSE CONSIDERATIONS

*Response of an Elastic System to Vortex Forces (Without Self-Amplification).*

*Sinusoidal Variable Forcing Function.*—The commonly used expression for the alternating lateral force due to vortex shedding is (1):<sup>2</sup>

$$F_K = q A_p C_K \sin 2 \pi f_v t \dots\dots\dots (2)$$

<sup>2</sup> Numerals in parentheses, thus (1), refer to corresponding items in Appendix II,—References.

in which  $F_K$  is the von Kármán force,  $q$  denotes the stagnation pressure,  $A_p$  is the projected area,  $f_v$  represents the frequency of shedding vortex pairs, and  $t$  is time. For a given velocity this idealized forcing function varies sinusoidally with time and has an unvarying amplitude and a discrete frequency. The dimensionless response of a single-degree-of-freedom system, having viscous damping, to vortex forces of this nature may be written (1):<sup>2</sup>

$$\frac{y}{d} = \frac{C_1 C_K \Omega^2/k}{\sqrt{(1-\Omega^2)^2 + \left(\frac{\delta}{\pi} \Omega\right)^2}} \dots\dots\dots (3)$$

in which  $y$  is the amplitude of vibration of an elastic system,  $d$  represents the diameter of the cylinder or member,  $C_1$  is a constant for a given system,  $\Omega$  denotes the ratio of frequency of forcing function to natural frequency,  $k$  is the spring constant for an elastic system, and  $\delta$  represents the logarithmic damping decrement, or rate of decay.

Eq. 3 may also be applied to the case of a flexural member vibrating in its fundamental mode, in which case the spring constant,  $k_m$ , may be approximated as the total load acting on the member divided by the maximum deflection of the member when that load is applied statically.

**Random Forcing Function.**—For  $R$  above approximately  $3 \times 10^2$  the amplitude of the lift force is not constant for a given stream velocity but becomes increasingly random as  $R$  increases. At an  $R$ -value above approximately  $3 \times 10^5$  the vortex-shedding frequency also becomes random as the separation point moves rearward on the cylinder. Therefore, for the purposes of computing the response of an elastic system, there are two important types of forcing functions to be considered: (1)  $3 \times 10^2 < R < 3 \times 10^5$ , sinusoidal forcing function with discrete frequency but random amplitude; and (2)  $3 \times 10^5 < R$ , harmonic forcing function with random frequency and random amplitude.

**Response at Subcritical Reynolds Numbers.**—The range of  $R$  below approximately  $3 \times 10^5$  is of primary interest in this investigation because most practical-sized antenna members subjected to moderate wind velocities fall into this category.

In this case the force amplitude is random with a steady mean value of zero. The response of the system depends on the energy input from the vortex forces averaged over a period of time. Now, the energy input per cycle is proportional to the product of the force and this amplitude of vibration. But the amplitude itself varies directly with the applied force, so the energy input per cycle varies as the square of the force:

$$\text{Energy input per cycle} \propto F_K y \propto F_K^2 \dots\dots\dots (4)$$

Therefore, the mean square of the force determines the energy input, and the response must be computed on the basis of the standard deviation from the mean, or the root-mean-square (RMS) of all of the random deviations. We may define the non-dimensional lift coefficient,  $\bar{C}_K$ , as the RMS-value of  $C_K$  and present the forcing function as

$$F_K = q A_p \bar{C}_K \sin 2 \pi f_v t \dots\dots\dots (5)$$

and compute the response from

$$\frac{y}{d} = \frac{C_1 \bar{C}_K \Omega^2/k}{\sqrt{(1-\Omega^2)^2 + \left(\frac{\delta}{\pi} \Omega\right)^2}} \dots\dots\dots (6)$$

**Response at Supercritical Reynolds Numbers.**—Supercritical  $R$ -values are of secondary interest in this investigation but are of primary interest for structures with large diameters, such as steel stacks and missels standing on their launching pads.

In this case the force amplitude has a mean value of zero, and both the amplitude and frequency are random. We must, therefore, deal with power input rather than energy input per cycle, because the power depends on the frequency of the excitation as well as the force amplitude:

$$\text{Power input} \propto F_K y f_v \propto F_K^2 f_v \dots\dots\dots (7)$$

The power input must be evaluated in terms of the whole spectrum of frequencies involved. In order to do this, some characteristic function for the power with respect to frequency must be either assumed or evaluated experimentally. The resulting plot of power versus frequency is termed the power spectrum, and the ordinate associated with a particular frequency is referred to as the "power spectral density" (PSD) for that frequency (2) (3). A frequency of high spectral density will produce a high response at resonance.

For the stochastic process under consideration, if the power spectrum is expressed as a function of  $S$ ,

$$\text{PSD} = \phi(S) \dots\dots\dots (8)$$

and is normalized so that

$$\int_0^{\infty} \phi(S) dS = 1 \dots\dots\dots (9)$$

then the mean square amplitude of the forcing function may be expressed in terms of the mean square lift coefficient and the integral of the power spectral density (2):

$$\bar{F}_K^2 = (q A_p \bar{C}_K)^2 \int_0^{\infty} \phi(S) dS \dots\dots\dots (10)$$

The mean square value of the response may then be computed from

$$\bar{y}^2 = \left( \frac{q A_p \bar{C}_K}{k} \right)^2 \int_0^{\infty} \frac{\phi(S) dS}{(1 - \Omega^2)^2 + \left( \frac{\delta}{\pi} \Omega \right)^2} \dots\dots\dots (11)$$

Under the assumption that there are no phase differences along the length of the cylinder, and not considering the effect of self-amplification, Eq. 11 may be evaluated with respect to the power spectrum in a narrow band width at a frequency corresponding to the natural frequency of the elastic system (4).

The mean square response becomes (approximately)

$$\bar{y}^2 = \frac{(q A_p)^2 \bar{C}_K^2}{k^2 \delta} \frac{\pi^2}{2} S \phi(S) \dots\dots\dots (12)$$

High spectral densities at low  $S$ -values would indicate the probability of dangerously large oscillations at fairly high wind velocities.

*Self-Amplification of Vibrations.*

**Incremental Load Factors.**—When an elastically supported cylinder or a flexural member is vibrating in resonance with periodic vortex forces, the vibration itself causes an increase in the magnitude of the lift. The additional aerodynamic force is probably associated with a periodic shifting of the points of separation on the cylinder, resulting in increased circulation. At the same



time, the vortices created in the wake are larger and stronger than in the case of the stationary cylinder.

D. B. Steinman (5), citing the results of experiments at the David Taylor Model Basin, proposed the hypothesis that if eddies are shed at or near each end of the amplitude range, the normal width of the vortex street is increased by the ratio

$$\frac{h + 2y}{h} = 1 + \frac{2y}{1.3d} \dots\dots\dots (13)$$

in which  $h$  is the width between the centers of two rows of eddies behind a non-oscillating circular cylinder ( $h \approx 1.3d$ ).

For stability, the distances between vortices in each row must also increase in the same ratio. It is assumed that the drag, the circulation, and the lift must all increase proportionally. At the same time, the eddy frequency and  $S$  are decreased by the reciprocal ratio.

There is an upper limit of stream velocity,  $v_p$ , beyond which this self-controlling action cannot occur. At this point the amplitude drops abruptly to a lower value determined by the magnification factor corresponding to the frequency ratio,  $\Omega$ .

The ratio of  $v_p$  to  $v_{cr}$  (the critical wind velocity, in which  $f_v = f_n$  and  $f_n$  is the natural undamped frequency of an elastic system) must be the same as the ratio of dimensional increase in the vortex street:

$$\frac{v_p}{v_{cr}} = \frac{\left(\frac{f_v d}{S}\right)_p}{\left(\frac{f_v d}{S}\right)_{cr}} = \frac{(S)_{cr}}{(S)_p} = 1 + \frac{2y}{1.3d} \dots\dots\dots (14)$$

For the case of zero damping, Steinman deduced an upper limit of velocity for peak amplitude of

$$v_p \approx 1.45 v_{cr} \dots\dots\dots (15)$$

in which  $v$  is velocity and  $v_{cr}$  denotes critical wind velocity, in which  $f_v = f_n$ .

The ratio of the self-amplified lift force per unit length of an oscillating cylinder or flexural member to the lift force per unit length, if there were no amplification, may be defined as the "incremental load factor" (ILF):

$$ILF = 1 + \frac{2y}{1.3d} = 1 + 1.54 \frac{y}{d} \dots\dots\dots (16)$$

For an oscillating cylinder the ILF-value is equal to  $v/v_{cr}$ . For a vibrating flexural member the ILF-value at the point of maximum deflection is also assumed to be equal to  $v/v_{cr}$ .

**Incremental Deflection Factors.**—When a cylinder or flexural member is vibrating under the influence of a wind velocity somewhat greater than the critical velocity, the aerodynamic forces exceed those acting at the critical velocity for two reasons. First, the forces increase in proportion to the velocity pressure head increase  $(v/v_{cr})^2$ . Second, the forces increase due to the self-magnification caused by the increased width of the vortex street. In order to account for both of these factors we may define the "incremental deflection factor" (IDF). The IDF-value is the ratio of the peak amplitude to the hypothetical amplitude at the critical velocity. The latter amplitude must be recognized as hypothetical because resonant vibrations of large amplitude cannot be attained when the  $S$ -value for a stationary cylinder exactly equals the nat-



ural frequency of the body. In this instance, as soon as oscillation begins, the Strouhal frequency decreases and goes out of phase from the natural frequency, and a pulsating response results.

For a cylinder oscillating as a rigid body the ILF-value and the IDF-value are determined by the damping, the spring stiffness, and the lift coefficient. For a vibrating flexural member, however, the ILF-value varies along the length of the member; therefore, the IDF-value is a function of the shape of the dynamic deflection curve and the phase relationships of the forces acting over the total length.

If phase differences along the lengths of flexural members are ignored, the deflections of all vibrating members may be approximated by fourth-degree parabolas. The incremental loading on a member may then be assumed to vary as a fourth-degree parabola, and the incremental deflection factors for various types of members are then found in the following manner:

For a simply supported member vibrating under the influence of the wind velocity that causes peak amplitude

$$y_{mp} = \left[ \frac{5}{384} \frac{w l^4}{E I} + \frac{2 y_{mp}}{1.3 d} w \frac{0.01025 l^4}{E I} \right] \frac{\pi}{\delta} \dots \dots \dots (17)$$

in which  $y_{mp}$  is the amplitude of vibration at point of maximum deflection on a flexural members when  $v = v_p$ , including the effect of self-amplification;  $w$  denotes the effective lateral loading per unit length due to vortex shedding on a stationary cylinder with  $v = v_p$ ,  $l$  is length,  $E$  represents the modulus of elasticity, and  $I$  is the moment of inertia. Solving for  $y_{mp}$ ,

$$y_{mp} = \frac{\frac{5}{384} \frac{w l^4}{E I} \text{ (DLF)}}{1 - \frac{2 w}{1.3 d} \frac{0.01025 l^4}{E I} \frac{\pi}{\delta}} \dots \dots \dots (18)$$

By definition,

$$IDF = \frac{y_{mp}}{\frac{5}{384} \frac{w l^4}{E I} \frac{\pi}{\delta}} = \frac{1}{1 - \frac{2 w}{1.3 d} \frac{0.01025 l^4}{E I} \frac{\pi}{\delta}} \dots \dots \dots (19)$$

But,

$$w = \bar{C}_K \left( \frac{1}{2} \rho_a v_p^2 \right) \frac{d}{144} \left( \frac{44}{30} \right)^2 = 1.779 \times 10^{-5} \bar{C}_K v_p^2 d \dots \dots \dots (20)$$

in which  $w$  is in pounds per inch and  $\rho_a$  is the mass density of air. Also,

$$v_p = v_{cr} \text{ (ILF)}_{\max} \dots \dots \dots (21)$$

and

$$v_{cr} = \frac{f_n d}{3.344} = 96,400 \frac{d r}{l^2} \dots \dots \dots (22)$$

in which  $r$  is the radius of gyration. Substituting Eqs. 20, 21, and 22 into Eq. 18 and writing similar equations for other types of members results in the following (in which  $A$  is the cross-sectional area):

Pinned Members:

$$IDF = \frac{1}{1 - 2.41 \times 10^{-4} \bar{C}_K \frac{d^2}{A} \frac{\pi}{\delta} \text{ (ILF)}^2} \dots \dots \dots (23)$$

## Fixed Members:

$$IDF = \frac{1}{1 - 2.64 \times 10^{-4} \bar{C}_K \frac{d^2}{A} \frac{\pi}{\delta} (ILF)^2} \dots \dots \dots (24)$$

## Cantilever Members:

$$IDF = \frac{1}{1 - 2.46 \times 10^{-4} \bar{C}_K \frac{d^2}{A} \frac{\pi}{\delta} (ILF)^2} \dots \dots \dots (25)$$

## Spring-Supported Cylinders:

$$IDF = \frac{1}{1 - 2.44 \times 10^{-4} \bar{C}_K \frac{d^2}{A} \frac{\pi}{\delta} (ILF)^2} \dots \dots \dots (26)$$

**Aeroelastic Suppression Factors.**—The IDF-values in Eqs. 23 through 26 depend, among other things, on the ILF-values. The ILF-value depends, in turn, on the following three elements: (1) the damping, (2) the stiffness, and (3) the relative magnitude of the wind forces. These parameters may be "lumped" into a dimensionless number that will be called the "aeroelastic suppression factor" (ASF). The ASF-value is a reciprocal measure of the relative ability of vibrating systems to amplify their own vibrations.

For the cylinder,

$$ASF = \delta \frac{k_c}{F_K} d \dots \dots \dots (27)$$

Expressing  $k_c$  and  $F_K$  in terms of  $m$ ,  $S$ , and  $\bar{C}_K$  yields:

$$(ASF)_{cyl} = 6.86 \times 10^8 \frac{m S^2 \delta}{\bar{C}_K d^2} \dots \dots \dots (28)$$

in which  $m$  is the mass per unit length of a spring-supported cylinder or a flexural member. The ASF-value for a flexural member vibrating in its fundamental mode may be expressed in a manner similar to that for a spring-supported cylinder. The stiffness,  $k_m$ , of the flexural member, however, will be defined as the total uniformly distributed static load that produces a maximum deflection of unity. Accounting for the fundamental mode shapes and corresponding member stiffnesses in this manner, the following ASF-values are obtained:

## Fixed Member:

$$ASF = 5.28 \times 10^8 \frac{m S^2 \delta}{\bar{C}_K d^2} \dots \dots \dots (29)$$

## Pinned Member:

$$ASF = 5.44 \times 10^8 \frac{m S^2 \delta}{\bar{C}_K d^2} \dots \dots \dots (30)$$

## Cantilever Member:

$$ASF = 4.42 \times 10^8 \frac{m S^2 \delta}{\bar{C}_K d^2} \dots \dots \dots (31)$$

Values for ILF and ASF may be obtained experimentally, and a plot of ILF versus ASF can be constructed. The resulting curve serves as a useful tool for the evaluation of Eqs. 23 through 26, and hence, the degree of self-amplification.

### EXPERIMENTAL PROCEDURES AND RESULTS

*Experimental Procedures.*—The experiments in this investigation were conducted in the low-speed wind tunnel in the Aeroelastic Laboratory of the Massachusetts Institute of Technology, Cambridge, Mass. This tunnel is of the

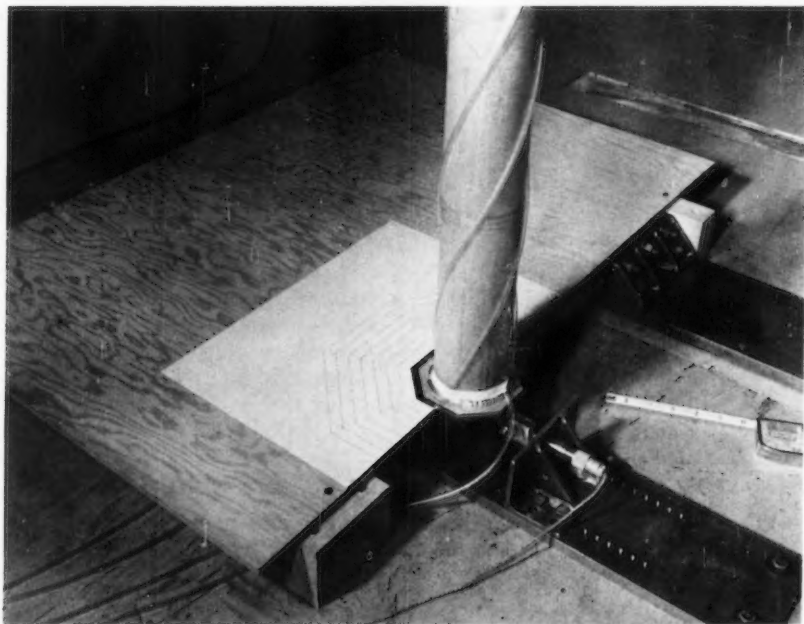
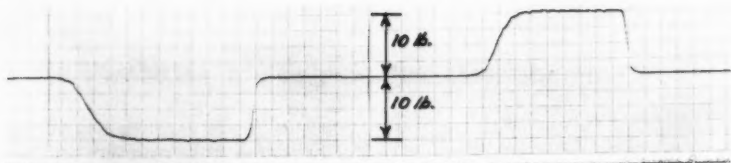


FIG. 1.—PHASE A, BASE LAYOUT (3-IN. DIAMETER CYLINDER)

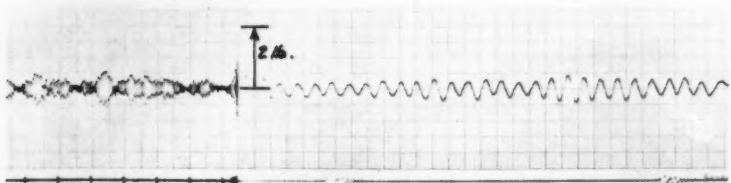
closed-circuit type having a  $5\frac{1}{2}$  ft by  $7\frac{1}{2}$  ft rectangular test section and a velocity range of 10 mph to 100 mph. Screens in front of the transition section served to reduce the scale of turbulence at the test section to approximately 0.5%. Tunnel controls were calibrated and blockage effects of test members were determined using a Prandtl (Göttingen) type pitot tube in conjunction with an alcohol manometer.

A Sanborn oscillograph was used in the experiments whenever feasible. In cases in which the frequencies of the electrical signals exceeded the capacity of the Sanborn, a Heiland oscillograph was used.

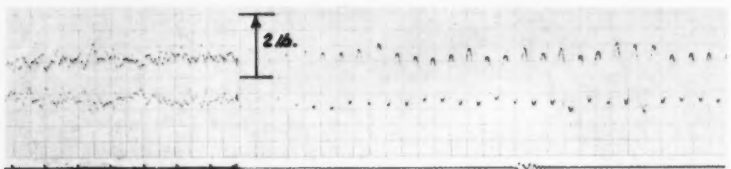
Tests on Stationary Cylinders (Phase A).—Fig. 1 shows the base layout and the force transducer connection for the Phase A tests (with one of the plywood



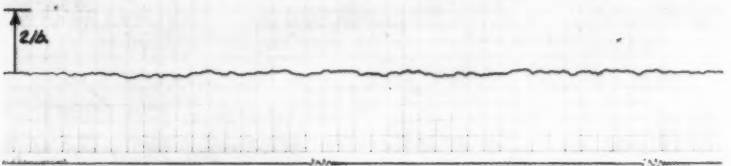
- (a) Transducer Calibration---Sanborn Oscillograph  
10 lb ea. way at x20 attenuation = 20 mm amplitude.



- (b) Example Sanborn Oscillograph Record for Stationary 5" Bare Cylinder (Subcr. NR) Paper speeds 10 and 100 mm per sec.;  
 $v = 30.0$  mph; Atten. x4;  $F_K = 1.3$  lb;  $C_K = 0.303$ ;  $f_v = 20.0$  cps;  
 $S = 0.190$ ;  $R = 1.17 \times 10^5$ .



- (c) Example Sanborn Oscillograph Record for Stationary 5" Cylinder with 8 Windings Paper speeds 10 and 100 mm per sec.;  $v = 30.0$  mph;  
Atten. x4;  $F_K = 2.4$  lb;  $C_K = 0.519$ ;  $f_v = 18.0$ ;  $S = 0.184$ ;  
 $R = 1.26 \times 10^5$ .



- (d) Example Sanborn Oscillograph Record for Stationary 5" Cylinder with Spoilers Paper speed 100 mm per sec.;  $v = 30.0$  mph; Atten. x4;  
 $F_K = 0.15$  lb;  $C_K = 0.035$ ;  $R = 1.17 \times 10^5$ .

FIG. 2

guide plates removed). A "dummy" connection of similar construction was provided at the upper end of the cylinder so that the force reactions at the top and bottom connections would be approximately equal.

The force transducer used is basically a compression force load cell with a 25-lb working range. The load cell was modified for measuring alternating tension and compression forces, however, by precompressing the force-resisting element and attaching a suitable adaptor to the force probe. When this

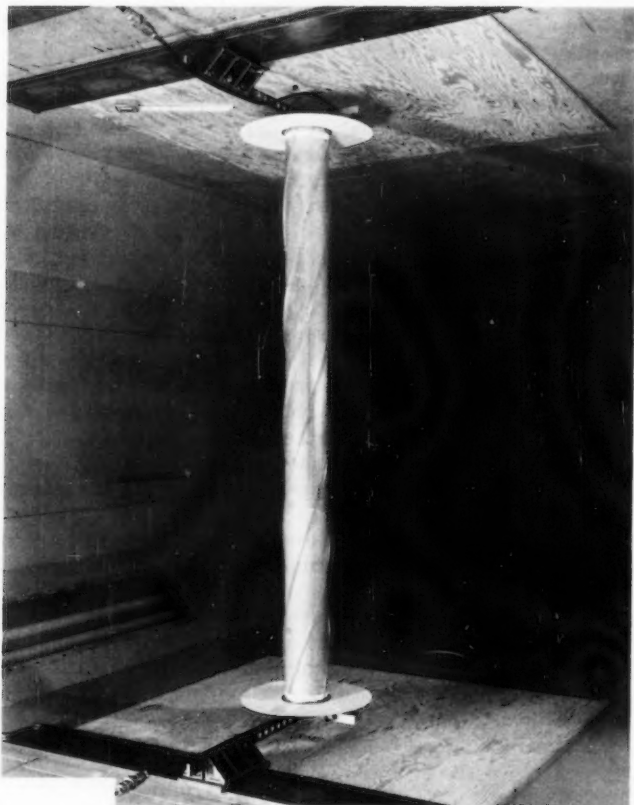


FIG. 3.—PHASE B, (4-IN. DIAMETER SPRING-SUPPORTED CYLINDER)

was done, the range of the instrument was  $\pm 12.5$  lb. The instrument was calibrated with static loads previous to mounting it in the tunnel, and it was again checked after mounting by means of applying static lateral force to the cylinders (Fig. 2(a)).

The bare cylinders were mounted in the tunnel and subjected to steady wind speeds in 5 mph increments. At each velocity an oscillograph record was taken,

an example of which is shown in Fig. 2(b). For certain of the bare cylinders RMS galvanometer voltages were recorded using a voltmeter-analyzer arrangement. This set-up consisted of an AC electronic voltmeter in combination with a DC voltmeter shunted across the recording galvanometer. The former meter was used to determine values of  $\bar{C}_K$ , and the latter meter provided a means of static-load calibration. The voltmeter readings were taken simultaneously with the oscillograph traces.

A series of spoiler designs was also tested on each of the stationary cylinders. An oscillograph record for a cylinder with spoilers is shown in Fig. 2(d).

During the course of spoiler optimization the fact was discovered that configurations of many small-diameter windings had the effect of increasing the lift forces on stationary cylinders instead of suppressing them. Moreover, the lift forces were not only larger in amplitude, but they were more regular in frequency and also more uniform in amplitude than for the case of bare cylinders. Furthermore, this force regularity transcended the critical Reynolds numbers for bare cylinders Fig. 2(c) demonstrates the effect of many small windings applied to a stationary cylinder.

**Tests on Spring-Supported Cylinders (Phase B).**—The same cylinders were used in Phase B that were used in Phase A. The support system was transformed by removing the lateral restraint top and bottom so that the cylinders could oscillate freely on their spring supports. Twin accelerometers were attached at both ends of the test cylinder to complete the Phase B set-up. Variable spring constants for the supports were obtained by using different lengths and thicknesses of the cantilever support strips. These strips were clamped to heavy base plates with rigid connectors and high strength bolts uniformly tensioned with a torque wrench. Fig. 3 shows the 4-in. diameter spring-supported cylinder of Phase B with optimum spoilers attached.

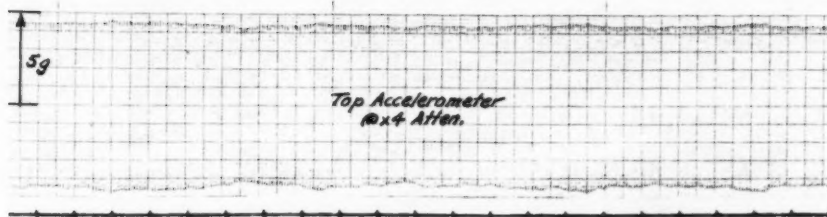
For each test on each bare cylinder accelerometer readings were recorded for a series of wind speeds, and the resonant wind velocity was carefully adjusted in the critical range so that the peak amplitude of vibration was observed in each case. Fig. 4(a) represents an example oscillograph trace for a bare cylinder oscillating at maximum amplitude (note the steadiness of the vibration).

Previously optimized spoiler configurations dramatically reduced the response of the spring-supported cylinders as can be seen by comparing the oscillograph record of Fig. 4(b) with that of Fig. 4(a) (the effect is even greater than a first glance indicates because different gains were used for the two records).

**Tests on Flexural Members (Phase C).**—The types of members tested were the following:

Number	Designation	End Connections	Diameters
3	M1	Fixed	$1\frac{1}{2}$ in. to 3 in.
3	M2	Partly Fixed	$1\frac{1}{2}$ in. to 3 in.
4	M3	Pinned	$1\frac{1}{2}$ in. to 4 in.
6	M6	Cantilever	$1\frac{1}{2}$ in. to 3 in.

Cantilever members with  $l/d = 30$  and  $l/d = 20$  were obtained by cutting off one end of the fixed members after the M1 tests had been completed. In this manner a total of sixteen different members were tested using only ten shop specimens.



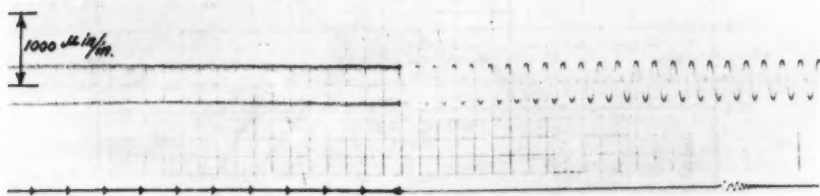
- (a) Example Sanborn Oscillograph Record for 6"  $\phi$  Spring-Supported Bare Cylinder Oscillating at Maximum Amplitude

Paper speed 10 mm per sec.; Atten. x4;  $\delta = 0.022$ ;  $k_c = 533$  lb/in;  
 $f_n = 15.05$  cps;  $v_p = 29.8$  mph; accel. =  $5.00g$ ;  $y/d = 0.036$ .



- (b) Example Sanborn Oscillograph Record for 6"  $\phi$  Spring-Supported Cylinder with Spoilers 4-3/8"  $\phi$  at 12d, Oscillating at Maximum Amplitude

Paper speed 10 mm per sec.; Atten. x1;  $\delta = 0.022$ ;  $k_c = 533$  lb/in;  
 $f_c = 15.05$  cps;  $v = 31.3$  mph; accel. =  $0.07g$ ;  $y/d = 0.0005$ .



- (c) Example Sanborn Oscillograph Record for M<sub>4</sub>bl (Bare) Vibrating at Max. Amplitude

Paper speeds 10 and 100 mm per sec.; Atten. x 20;  
 $\delta = 0.013$ ;  $f_n = 20.0$  cps;  $v_p = 13.21$  mph; strain =  $300 \mu$  in/in;  
 $y/d = 0.134$ .

FIG. 4



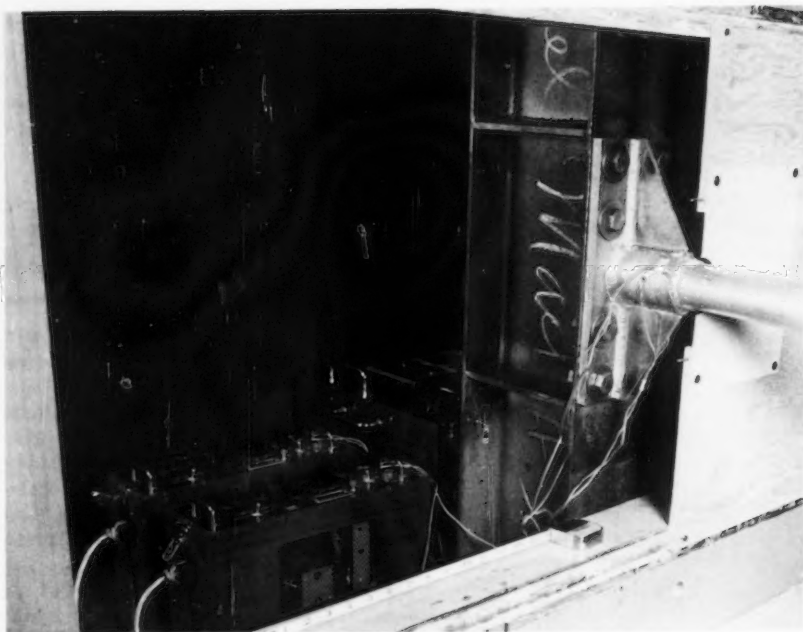


FIG. 5.—PHASE C, END CONNECTION FOR 2-IN. DIAMETER MEMBER

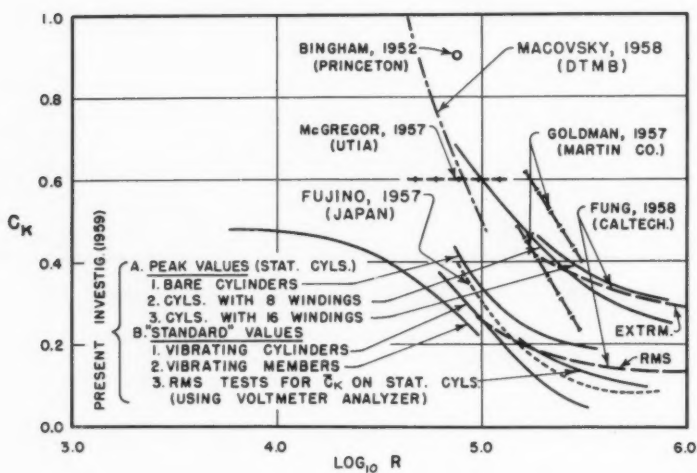


FIG. 6.—COMPARISON OF RESULTS OF PRESENT TESTS WITH PREVIOUSLY REPORTED EXPERIMENTAL VALUES OF  $C_k$



Fig. 5 shows an example end connection for M1b as it was mounted horizontally in the wind tunnel. The bolted connections were tightened uniformly with a torque wrench, and the guide plates (one of which is removed) were cut to clear the members by  $\frac{1}{4}$  in. Bonded strain gages (SR-4) were used in the tests of Phase C to measure vibrational fiber strains.

Bare flexural members were subjected to the range of wind velocities as in the previous tests, and fundamental modes of vibration were readily developed (Fig. 4(c)) at or near the predicted critical wind speeds. In the more flexible members the second and even the third modes of vibration were developed with similar ease. The layouts of strain gages were oriented to the first mode, however, so no quantitative results are reported for these higher modes.

Optimum spoilers were applied to the members over various portions of their lengths. The length increments tested were 100%, 80%, 60%, 40%, and 20% of the lengths of the members.

TABLE 1.—PREVIOUSLY PUBLISHED VALUES FOR  $C_K$ 

Date	Source	Ref.	Experimental (E) or Analytical (A)	$N_R$	$C_K$
1932	Tyler	6	E	-	0.61 -1.05
1935	Reudy	7	A	-	0.93
1935	Schwabe	8	E	735	0.45
1946	Steinman	5	A	-	1.71
1952	Bingham	9	E	$7.6 \times 10^4$	0.90
1956	Phillips	10	-	40 - 160	0.76
1957	Goldman	11	E	(See Fig. 6)	
1957	McGregor	12	E	$4.5 \times 10^4$ $-1.3 \times 10^5$	0.60
1957	Macovsky	3	E	(See Fig. 6)	
1958	Fung	13	E	(See Fig. 6)	
1958	Fujino	14	E	(See Fig. 6)	

#### Test Results.

**Lift Coefficient.**—All of the  $C_K$  and  $\bar{C}_K$  curves determined in this investigation are presented in Fig. 6, together with values of  $C_K$  reported by previous investigators. Table 1 summarizes published values for  $C_K$  and notes whether they are experimental or analytical.

The three curves for standard  $\bar{C}_K$  from each of the three phases merge into each other fairly well except where the curve for vibrating cylinders descends to a low value in the vicinity of  $R \approx 3 \times 10^5$ . Moreover, the  $\bar{C}_K$ -curves show fair correlation with curves by Fung and Fujino for RMS  $C_K$  shown in Fig. 6.

The upper  $C_K$ -curves for cylinders fitted with numerous small-diameter windings delineate the high lift forces observed in these cases. The peak  $C_K$ -curves for eight and sixteen windings correspond closely to the values given by McGregor and Goldman and the curves given by Fung and Macovsky for extreme values of  $C_K$ . It appears, then, that applying a pattern of small windings

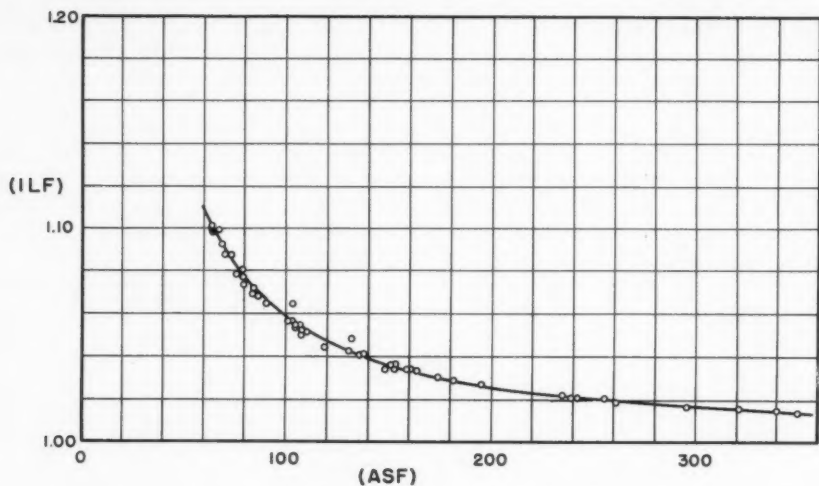


FIG. 7.—ILF FOR OSCILLATING CYLINDERS

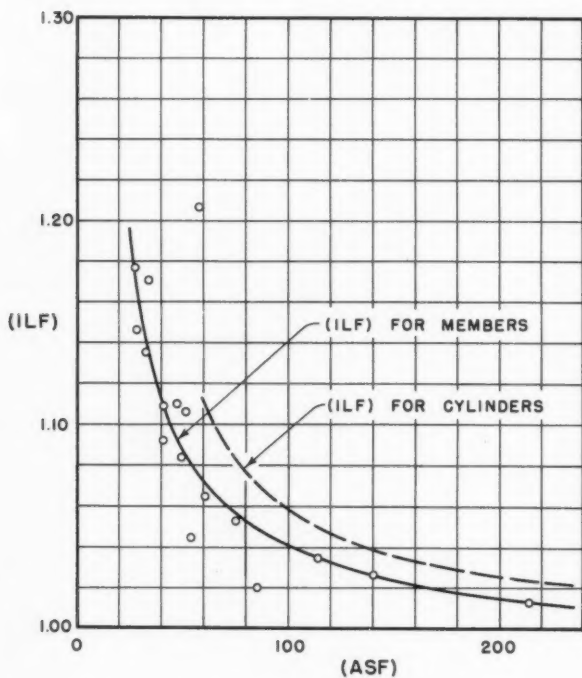


FIG. 8.—ILF FOR VIBRATING MEMBERS

to the surfaces of cylinders in the present investigation has the effect of raising the peak values of  $C_K$  to approximately the same values reported by several experimenters. A possible explanation for this phenomenon is that for some reason, spanwise correlation of vortex shedding is improved by this type of surface roughening. The peak  $C_K$ -curve for bare cylinders probably depends to some extent on the turbulence characteristics of the wind tunnel for its relative location. Neither this curve nor the other peak  $C_K$ -curves have any practical value for the purpose of computing the response of a vibrating member. It is the  $\bar{C}_K$ -curve that assumes great importance in this respect.

**Self-Amplification.**—The ILF-values computed for the cylinders and the members at resonance are plotted against ASF in Figs. 7 and 8. Similar curves for  $v_p/v_{cr}$  are practically identical with the ILF-curves. Thus, the supposition that  $ILF = v_p/v_{cr}$  is verified, and the ASF-value proves itself to be a valid basis for determining the degree of self-amplification. The ILF-data for the vibrating members is more scattered, and the curve is definitely lower than for the cylinder tests. The latter discrepancy is probably due to phase differences along the lengths of the members that do not arise along the lengths of cylinders oscillating as rigid bodies.

**Strouhal Numbers.**—Curves for **5** obtained in this investigation are compared in Fig. 9 with a curve obtained (15) by B. Etkin, et al (shown dashed), that represents a summary of the works of several previous investigators. In general, the curves check fairly well, and the maximum difference in ordinates is approximately 5%.

**Spoiler Optimization.**—Fig. 10 demonstrates, in a general manner, the influence of the number of windings on spoiler effectiveness. Configurations with four windings repeatedly gave maximum suppression of lift forces.

Fig. 11 illustrates the influence of winding diameter on spoiler effectiveness for the 3-in. cylinder. The knee of this type of curve occurs consistently at a spoiler diameter of roughly  $d/12$  to  $3d/32$ . The curves rise toward  $C_{KS}/C_{KB} = 1$  for small-diameter windings and appear to rise only slowly for large size windings.

The relative insensitivity of the phenomenon to spoiler pitch is shown in Fig. 12 for the 6-in. cylinder. A wide effective range exists from a pitch of approximately  $8d$  to about  $16d$ . The most effective pitch appears to be at about  $12d$ .

Thus, optimum spoilers may be assumed to be 4 windings of size  $d/16$  or larger at a pitch of  $12d$ .

Sample response curves for a bare test member and for the member with spoilers over varying portions of its length are presented in Fig. 13. For most of the members tested, vibration amplitudes were suppressed to approximately 10% by optimum spoilers wound over portions as short as 20% of the member lengths. A spoiler length of  $0.40 l_m$  gave the best results in most cases. Spoilers were most effective for relatively stiff (fixed end) members at  $R$ -values in the vicinity of  $10^5$ .

## DISCUSSION OF RESULTS

**Spanwise Correlation.**—The question of spanwise correlation is not considered in this paper. D. M. Macovsky (3) produced visual evidence that the flow picture at subcritical Reynolds numbers is not two-dimensional in its nature. The extent to which oscillation of a cylinder aids spanwise correlation is an open question that warrents further investigation.

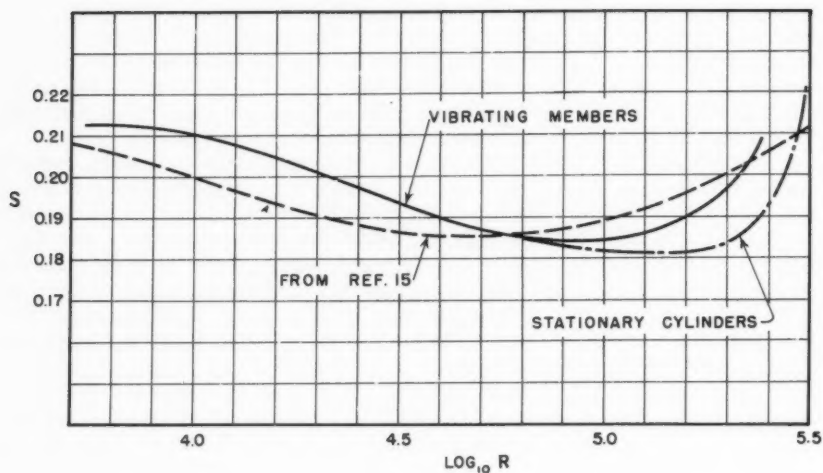
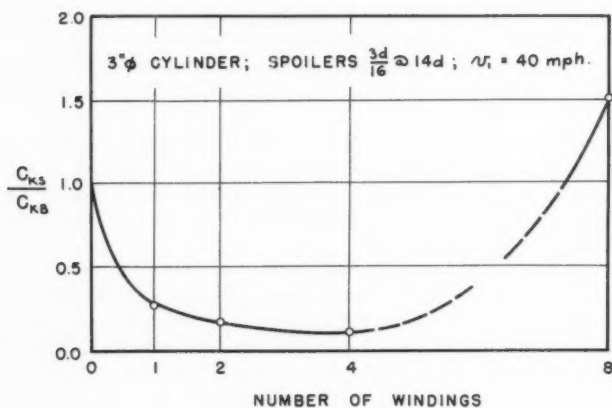
FIG. 9.—COMPARISON OF **S**-CURVES WITH PUBLISHED VALUES

FIG. 10.—INFLUENCE OF NUMBER OF WINDINGS ON SPOILER EFFECTIVENESS

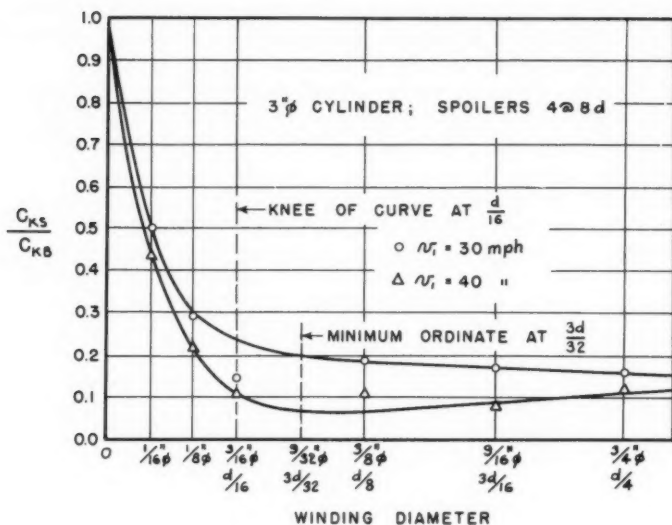


FIG. 11.—INFLUENCE OF WINDING DIAMETER ON SPOILER EFFECTIVENESS

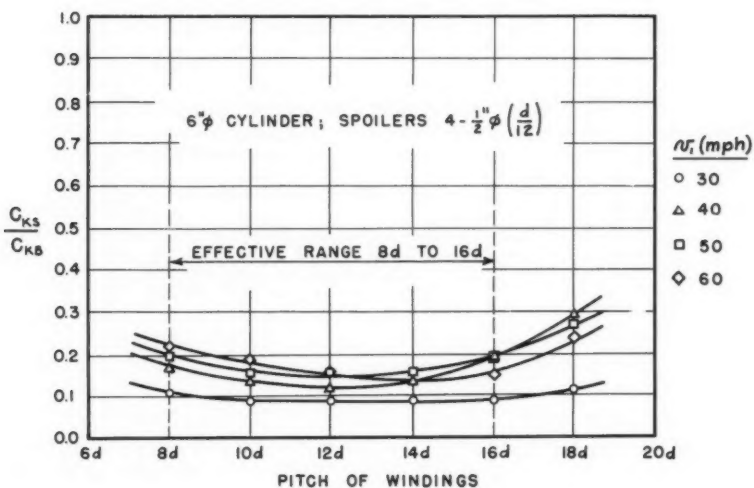


FIG. 12.—INFLUENCE OF PITCH ON SPOILER EFFECTIVENESS

The ability of vortices to conform to the motion of flexural members is demonstrated by the ease with which higher modes of vibration are developed. In these higher modes, vortices must be shed simultaneously from opposite sides of the member along different portions of the span, and yet the flow picture readily adjusts itself to accomplish this complex feat.

*Cautions on the Use of Spoilers.*—Spoilers are not recommended for Reynolds numbers below  $1 \times 10^4$  or above  $4 \times 10^5$ , because it was in this range that spoiler optimization was carried out. Fluid flow has greater ability to over-

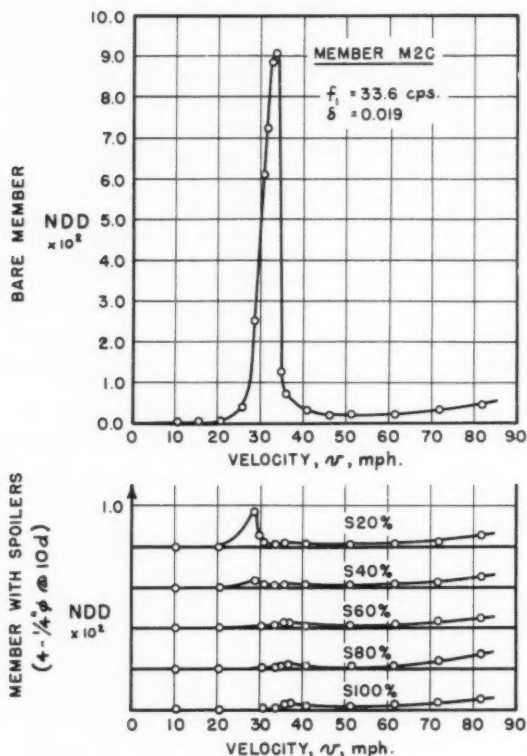


FIG. 13.—RESPONSE OF MEMBER M2C

ride protuberances at the lower  $R$ -values. At high Reynolds numbers the lift forces on bare cylinders are quite erratic without the addition of spoilers, and Phase A tests revealed no differences in the oscillograph records for supercritical  $R$ -values with and without spoilers.

Spoilers are not recommended for members with diameters smaller than 2 in. or for cantilevers with  $l/d$  greater than 20. This statement is based on the fact that test members having small diameters and large nondimensional amplitudes of vibration during bare runs demonstrated an ability to persist in

fairly large amplitudes of oscillation with spoilers attached, whereas, vibrations in other types of members were readily suppressed with spoilers.

### CONCLUSIONS

*Information Obtained from Tests.*—The experiments conducted in this investigation have provided a curve for  $\bar{C}_K$  in the range of Reynolds numbers of interest for antenna members. This curve represents the basic tool with which the problem of wind-induced vibrations may be solved. In the subcritical range of  $R$ -values the concept of the "standard"  $\bar{C}_K$  as a basis for response computations not only accounts for the randomness in the amplitude of  $C_K$ , but it also provides independence from the mode shape of a particular vibration and the various other factors that affect the degree of self-amplification.

In the supercritical range of  $R$ -values the stochastic response concepts outlined herein identify this method of approach to the problem of vibrating stacks, missiles, and so forth, as a valid and promising means of coping with past and present difficulties on the subject.

The curves for ILF versus ASF from Phases B and C, when used in conjunction with the expressions for IDF, permit the computation of the degree of self-amplification for any of the types of members considered in this project. Moreover, the method can be extended to other types of members by writing appropriate expressions for ASF and IDF for the particular mode shapes involved.

Experimental plots of Strouhal numbers check well with previously published information. The accuracy of this agreement (within 5%) is sufficient for engineering purposes. Considering all of the possibilities for experimental error involved in the laboratory tests, this discrepancy is reasonable.

*Effectiveness of Spoilers.*—Spoiler tests show that a configuration of four helical windings is most effective in suppressing lift forces. A spoiler diameter of  $d/16$  to  $d/8$  is necessary for good suppression, and a diameter of  $3d/32$  reduces the lift forces to a minimum. Although the pitch of windings is an important property of the spoilers, the phenomenon is not particularly sensitive to the pitch. The most effective pitch in the wide range of choice ( $8d$  to  $16d$ ) was determined to be  $12d$ .

Considering the results of spoiler optimization, it is interesting to compare the tubular windings with a configuration of spiral fins, or "strakes," tested by C. Scruton and D. Walshe (16). They introduced a design consisting of three helical strakes of height up to  $d/8$  and set at a pitch of  $15d$ . He states that the strakes must be of sufficient height and number and that their helical formation is an essential feature. Scruton and Walshe further stated that their effectiveness increases with size but that they need be no longer than  $1/8d$ . In addition, they report that the result is not sensitive to pitch and that a single strake is not effective because of the opposite-side characteristic of vortices. It is apparent that the tubular windings optimized in the present investigation show characteristics similar to these strakes, with some reservations.

*Further Research.*—There are two experiments of a different nature from this investigation which would be of general use to engineers:

1. A series of tests with cylindrical models may be conducted in a water channel in order to obtain a continuous curve for  $\bar{C}_K$  in the range of Reynolds numbers below  $10^4$ .



2. Studies similar to those by Fung (13) and Fujino (14) should be carried out using large, light-weight spring-supported cylinders in order to obtain information on the random response of important cylindrical structures.

### ACKNOWLEDGMENTS

The research program described in this paper was sponsored by the M.I.T. Lincoln Laboratory in Lexington, Mass.

### APPENDIX I.—NOTATION

The following symbols, adopted for use in the paper and for the guidance of discussers, conform essentially with "American Standards Letter Symbols for Structural Analysis" (ASA Z10.8-1949), prepared by a committee of the American Standards Association, with Society representation, and approved by the Association in 1949:

- A = cross-sectional area, in square inches;
- $A_p$  = projected area, in square feet;
- ASF = aeroelastic suppression factor;
- $C_K$  = von Kármán coefficient, or the maximum value of the fluctuating lift
- $\bar{C}_K$  = standard value of  $C_K$ , or the RMS value of  $C_K$ , or the standard deviation of  $C_K$ ;
- $C_{KB}$  = value of  $C_K$  for a bare cylinder;
- $C_{KS}$  = value of  $C_K$  for a cylinder with spoilers;
- $C_1$  = constant for a given system;
- d = diameter of cylinder or member, in inches;
- E = modulus of elasticity of material, in pounds per square inch;
- $F_K$  = von Kármán force =  $C_K q A_p$ , in pounds;
- $f_n$  = natural undamped frequency of an elastic system, in cycles per second;
- $f_v$  = frequency of shedding vortex pairs, in cycles per second;
- h = width between the centers of two rows of eddies behind a nonoscillating circular cylinder, in inches,  $\approx 1.3 d$ ;
- I = moment of inertia, in inches<sup>4</sup>;
- IDF = incremental deflection factor;
- ILF = incremental load factor;
- k = spring constant of an elastic system, in pounds per inch;



- $k_c$  = spring constant of a spring-supported cylinder with respect to a uniform loading = the total load,  $wl$ , that produces a deflection of unity, in pounds per inch;
- $k_m$  = spring constant of a member with respect to a uniform loading = the total load,  $wl$ , that produces a maximum static deflection of unity, in pounds per inch;
- $l$  = length, in inches;
- $m$  = mass per unit length of a spring-supported cylinder or a flexural member, in pound-seconds<sup>2</sup> per square inch;
- PSD = power spectral density;
- $q$  = stagnation pressure, in pounds per square foot;
- $R$  = Reynolds number =  $780 v d$ , in air at standard temperature and pressure;
- $r$  = radius of gyration, in inches;
- $S$  = Strouhal number =  $(f_v d)/(17.6 v)$ , in air at standard temperature and pressure;
- $S_e$  = spoiler effectiveness;
- $t$  = time, in seconds;
- $v$  = velocity, in miles per hour;
- $v_{cr}$  = critical wind velocity, at which  $f_v = f_n$ , in miles per hour;
- $v_p$  = velocity corresponding to peak amplitude of vibration, in miles per hour;
- $w$  = effective lateral loading per unit length due to vortex shedding on a stationary cylinder with  $v = v_p$ , in pounds per inch;
- $y$  = amplitude of vibration of an elastic system, in inches;
- $y_{mp}$  = amplitude of vibration at point of maximum deflection on a flexural member when  $v = v_p$ , including the effect of self-amplification, in inches;
- $\delta$  = logarithmic damping decrement, or rate of decay;
- $\Omega$  = ratio of frequency of forcing function to natural frequency; and
- $\rho_a$  = mass density of air.

---

## APPENDIX II.—REFERENCES

---

1. "Wind-Induced Vibration of Cylindrical Structures," by J. Penzien, Proceedings, ASCE, Vol. 83, No. EM 1, January, 1957.
2. "An Introduction to the Theory of Aeroelasticity," by Y. C. Fung, John Wiley and Sons, New York, 1955.

3. M. S. Macovsky, David Taylor Model Basin Report No. 1190, July, 1958.
4. "Experimental Investigation of Wind-Induced Vibrations in Antenna Members," by William Weaver, Jr., Presented to the Massachusetts Institute of Technology at Cambridge, Massachusetts in 1959, in partial fulfillment of the requirements for the degree of Doctor of Sc.
5. "Problems of Aerodynamic and Hydrodynamic Stability," by D. B. Steinman, Proceedings, Third Hydraulics Conference, Univ. of Iowa Studies in Engrg., Bulletin No. 31, 1946.
6. "Vortex Formation Behind Obstacles of Various Sections," by E. Tyler, Phil. Magazine, Vol. 11, 1931, p. 848.
7. "Vibrations of Power Lines in a Steady Wind," by R. Reudy, Canadian Journal of Research, October, 1935.
8. Ingenieur-Archiv, M. Schwabe, 6, pp. 34-50, 1935.
9. "The Cylinder and Semi-cylinder in Subsonic Flow," by B. H. Bingham, D. K. Weimer, and W. Griffith, Tech. Report 11-13, Princeton Univ. Dept. of Physics, July, 1952.
10. "The Intensity of Aeolian Tones," by O. M. Phillips, Journal of Fluid Mechanics, Vol. 1, 1956, pp. 607-624.
11. "The Generation and Suppression of von Kármán Vortex Forces," by R. Goldman, Engineering Report No. 8984, Martin Co., Baltimore, Md., 1957.
12. "An Experimental Investigation of the Oscillating Pressures on a Circular Cylinder in a Fluid Stream," by D. M. McGregor, Tech. Note No. 14, Inst. of Aerophysics, Univ. of Toronto, June, 1957.
13. "Fluctuating Lift and Drag Acting on a Cylinder in a Flow at Supercritical Reynolds Number," by Y. C. Fung, Shock and Vibration Bulletin, No. 26, Part II, U. S. Naval Research Lab., Washington, D. C., 1958.
14. Fujino, et al., Proceedings, Seventh Japan National Congress for Applied Mechanics, 1957.
15. "Acoustic Radiation from a Stationary Cylinder in a Fluid Stream (Aolian Tones)," by B. Etkin, G. K. Korbacher, and R. T. Keefe, Inst. of Aerophysics, Univ. of Toronto, Report No. 39, May, 1956.
16. "A Means for Avoiding Wind-Excited Oscillations of Structures with Circular or Nearly Circular Cross-Section," by C. Scruton and D. E. J. Walshe, N.P.L. Aero. 335, October, 1957.
17. "Über den Mechanismus des Flusigkeits und Luftwiderstandes," by Th. von Kármán and H. Rubach, Phys. Zeits., Bd. 13, Heft 2, January 15, 1912 (Translated by Jack Lotsof, Cornell Aeronautical Lab., Ithaca, N. Y., October, 1947).
18. "Frequency of Eddies Generated by Motion of a Cylinder Through Fluid," by E. F. Relf and L. F. G. Simmons, British A. R. C., R. and M. 917, 1924.
19. "On the Development of Turbulent Wakes from Vortex Streets," by A. Roshko, N.A.C.A. Technical Notes 2913, 1953.
20. "Low Speed Drag of Cylinders of Various Shapes," by N. K. Delaney and N. E. Sorensen, N.A.C.A., T.N.3038, November, 1953.

21. "Vibration Problems in Engineering," by S. Timoshenko, D. Van Nostrand Co., New York, Third Edition, 1955.
22. "The Response of Mechanical Systems to Random Excitation," by W. T. Thompson and M. V. Barton, Journal of Applied Mechanics, 24, pp. 248-251, 1957.



---

Journal of the  
ENGINEERING MECHANICS DIVISION  
Proceedings of the American Society of Civil Engineers

---

DISCUSSION

---

Note.—This paper is a part of the copyrighted Journal of the Engineering Mechanics Division, Proceedings of the American Society of Civil Engineers, Vol. 87, No. EM 1, February, 1961.



THE NEUTRAL AXIS IN PLASTIC BENDING OF BEAMS<sup>a</sup>

---

Closure by Aris Phillips

---

ARIS PHILLIPS,<sup>1</sup> F. ASCE.—The author wishes to thank Messrs. Abramson and Sprague for their interest in his paper.

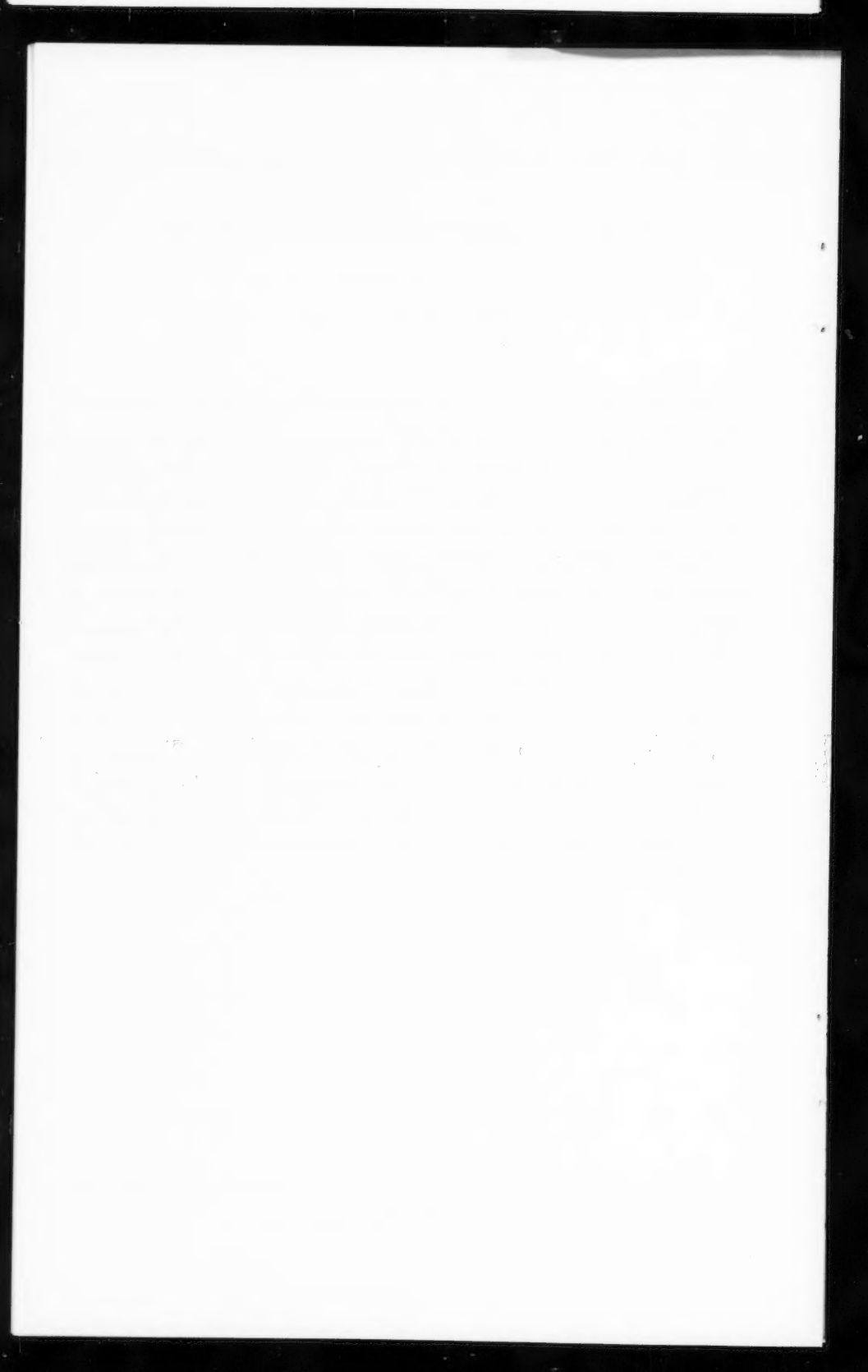
Concerning Mr. Sprague's comments, the author believes that the applicability of the method presented in his paper to a beam of a given material depends on whether the stress-strain law of this material can be approximated with sufficient accuracy by the stress-strain law that forms the basis of the method. The method has not been devised with a specific material in mind. It has been devised with a specific stress-strain diagram in mind, namely the stress-strain diagram of a perfectly plastic material. It follows that whether or not the method is applicable to plain concrete beams depends on whether the perfectly plastic stress-strain diagram can be considered as a sufficiently good approximation of the stress-strain diagram of plain concrete.

Mr. Abramson's comments on the rotation of the neutral axis for unsymmetrical bending of beams are of much interest because they show that, even when the plane of bending remains constant, the neutral axis in unsymmetrical bending will not only translate but also rotate. This rotation occurs even in the case of a first approximation theory in which the deflections of the beam are assumed to have no influence on the stress distribution. In general, the rotation of the neutral axis should be more pronounced when the influence of the deflections on the stress distribution is taken into account. The author believes that additional study of this problem, in extension of the analysis and experiments presented by Mr. Abramson in the papers mentioned by him, will be of considerable interest.

---

<sup>a</sup> October 1959, by Aris Phillips (Proc. Paper 2198).

<sup>1</sup> Prof., Dept. of Civ. Engrg., Yale Univ., New Haven, Conn.





EXPERIMENTAL STUDIES OF BEAMS ON ELASTIC FOUNDATIONS<sup>a</sup>

Discussion by M. T. Davisson

M. T. DAVISSON,<sup>8</sup> A. M. ASCE.—At least one other mechanical analog method of analyzing a beam on an elastic foundation is available in the literature and is mentioned here for the sake of completeness. A. A. Wells<sup>9</sup> used a piano wire as the flexural member for his model studies. Although not as versatile as the model presented by the author, it has the advantage of simplicity.

A review of the author's comments concerning the solution of Eq. 1 and its application to a laterally loaded pile appears to be in order. By extending the work of M. Hetenyi,<sup>10</sup> the writer<sup>11</sup> has presented a derivation of the governing differential equation for a pile subjected to lateral, moment, and axial (W) loads. Eqs. 14 is the governing equation with the subscript x denoting that I, W, and Es may be functions of x. The writer used the same assumptions as the author in deriving the equations.

$$\left. \begin{aligned} \left( \frac{d^2 M}{dx^2} + \frac{d(Wx)}{dx} \right) \frac{dy}{dx} + E s_x y &= 0 \\ M &= E I_x \frac{d^2 y}{dx^2} \end{aligned} \right\} \dots\dots\dots (14)$$

Eqs. 14 is nonlinear if  $E s_x$  is also made a function of  $y$  ( $E s_{xy}$ ). By solving the linear equation for several variations of  $E s_x$ , it is possible to converge on a single variation that will represent  $E s_{xy}$  (secant modulus) for a given set of conditions. This is the same procedure used by the author. The axial load term has been included for the obvious reason that a pile usually supports such a load as its primary function. In many cases the axial load may be ignored. However, where the soil near the ground surface is weak or a free length of pile exists, serious errors in the flexural calculations may arise if the axial load is ignored. The axial load has the effect of magnifying moments, deflections, and so forth.

The advantages and disadvantages of the several methods of solving the boundary value problems represented by Eqs. 14 are of interest. Series solu-

<sup>a</sup> June 1960, by Robert L. Thomas (Proc. Paper 2505).

<sup>8</sup> Asst. Prof., Dept. of Civ. Engrg., Univ. of Illinois, Urbana, Ill.

<sup>9</sup> "Beams on Elastic Foundations," by A. A. Wells, Proceedings, Inst. of Mech. Engrs., Vol. 163, 1950, pp. 307-310.

<sup>10</sup> "Beams on Elastic Foundations," by M. Hetenyi, University of Michigan Press, Ann Arbor, Michigan, 1946.

<sup>11</sup> "The Behavior of Flexible Verticle Piles Subjected to Moment, Shear, and Axial Load," by M. T. Davisson, Thesis presented to the Univ. of Illinois, at Urbana, Ill. in 1960, in partial fulfillment of the requirements for the degree of Doctor of Philosophy.

tions are very easily obtained where idealizations of  $I_x$ ,  $W_x$ , and  $E s_x$  are introduced but are cumbersome and difficult to program for a digital computer. Finite difference solutions have been obtained, both by hand and digital computer procedures, where the axial load is ignored or assumed zero. When  $I$  is a function of  $x$ , the finite difference equations become quite cumbersome; the situation is made worse by the addition of axial load terms. Analogs, such as the mechanical methods of Wells and the author, can be quite useful. However, when an axial load is added, the writer envisions additional mechanical errors caused by restraints at the points of load application. Boundary conditions other than free ends may also introduce mechanical difficulties. The writer has found that an electronic differential analyzer (analog computer) is readily adoptable to solving Eqs. 14. In an analog computer, the equation is electrically reproduced and the accuracy of the solutions is more than satisfactory. Versatility in the variations of  $I$ ,  $W$ , and  $E s$  with  $x$  is an important advantage of the analog computer.

In summary, the writer would like to again emphasize the importance of considering the axial load in beam-columns on elastic foundations. Furthermore, in contrast to the authors conclusions, the writer believes the analog computer is a simple and versatile means of solving Eqs. 14.

UNDERGROUND STRUCTURES SUBJECT TO AIR OVERPRESSURE<sup>a</sup>

---

Discussion by Paul I. Rongved, and G. S. Kovacs and R. T. Frankian

---

PAUL I. RONGVED,<sup>10</sup>—The authors have attempted to develop an analytical procedure for determining the damage to underground structures by pseudo-steady state air overpressure. Unfortunately, the assumptions made for the behavior of the soil are, in the opinion of the writer, not realistic, and consequently, the results arrived at have little if any validity.

To clarify the situation the following observations are made:

The structural behavior of an underground structure is a complex, inter-related action of the structure itself and the surrounding soil.

Engineers have not been able to produce one general analytic procedure that would solve all types of structural systems like slabs, beams, arches, shells, suspension structures, and so on.

To attempt to do something like that for a buried structure is even more difficult, but in essence this is what the author has attempted. This is believed to be entirely too ambitious; it should at least be deferred until well accepted theories for various specific buried structures have been developed.

Let us assume a uniform air overpressure varying with time applied to a horizontal ground surface of semi-infinite, elastic, homogenous soil. The vertical soil pressure under these conditions will increase with the amount of the air overpressure uniformly at any point in the soil. Because we have a uniformly applied overpressure over uniform soil here, and the sum of all vertical forces through all horizontal sections must be equal to zero at all times, the above statement becomes obvious. This merely means that if we apply a uniform overpressure, such as 100 psi at the surface, we will have a 100 psi increase in the vertical pressure at the surface of the soil, 10 ft, 100 ft or any other depth below the surface.

If we now assume that we have a buried structure in this soil, and the structure and its foundations have the same stiffness as the soil it replaced, the structure will receive the same amount of pressure as the soil had previously. If the structure or its foundations are harder or softer than the soil they replaced, the structure will receive, correspondingly, more or less pressure.

From these observations it is clear that our structure and its foundations should be softer than its surrounding soil. We may use a stiff structure with soft foundations or soft structure with stiff foundations or a soft structure with soft foundations. By the terms "soft" and "stiff" are meant a structure or foundation that give us a smaller or larger  $k$ -value (spring constant) than the  $k$ -value of the surrounding soil.

---

<sup>a</sup> August 1960, by E. T. Selig, K. E. McKee, and E. Vey (Proc. paper 2575).

<sup>10</sup> Partner, Strobel and Rongved, Cons. Engrs., New York, N. Y.

To further investigate the amount of the total load carried by the surrounding soil in case of a soft structure, foundation or both, the following observations are of great importance:

Most types of soil readily transmit compression forces, and can take considerably less shear forces, and practically no tension forces. Because of this, a soil mass cannot act like a beam or slab spanning a buried structure. The soil above a buried structure may carry its load in an infinite number of ways as long as it is in elastic equilibrium. Only after all possible ways of carrying the load have been exhausted will the soil reach a complete plastic equilibrium and ultimately fail.

Plastic equilibrium may be reached at earlier stages at individual points in the soil without necessarily causing the soil to reach a general plastic equilibrium.

If we can find any one structural system for the soil capable of carrying the load, still allowing it to remain in its elastic equilibrium, we know that its ultimate carrying capacity will be at least as great as the one we have found. It is, therefore, important to find the best suitable structural system for the soil.

This was recognized already by F. Engesser about 80 yr ago, when he talked about the arching effect of soil. Arching applies to soil over linear shaped structures. For soil over circular, rectangular, and similarly shaped structures one gets a number of two-way shell actions in soil. The shell systems in the soil that have the greatest carrying capacity determine the maximum carrying capacity of the soil.

A shell structure in its membrane condition has mainly compression forces. Soil can carry any amount of compression forces up to an equivalent of about  $1/K$  times the minimum side pressure exerted on the soil,  $K$  being the coefficient of earth pressure. This holds true for soil columns, soil arches, and soil shell structures as well.

Looking at the example used in the article under discussion, there is a cubicle structure 10 ft-by 10 ft-by 10 ft, buried so that the roof is 15 ft underground. No information was given on the stiffness of the foundations, but because the roof will have a deflection of 1 ft at its ultimate load, it can be classified as a soft structure.

One might consider the soil overlaying the structure as consisting of various structural types and elements. In the discussed article it was always assumed to be a stiff cube acting as a thick slab. One can, instead, choose concentric, spherical shells that will be closer to the optimum structural system. About ten shells, one on top of the other, approximately 1 ft thick each, can be arranged in the soil. The shells have a radius of about 7 ft to 9 ft.

Following through on the analytical computation for this chosen structural system, one sees that the carrying capacity of the soil is about at least three times greater than the value arrived at in the article discussed. This ratio of about 3-to-1, however, varies widely. In some cases the value may be considerably less than 1.

The preceding computations can be made either by using a known simplified, one degree of freedom, coupled dynamic design method, or by using a dynamic analysis with numerical integration with or without analog and digital computers. As a third alternative, an analytical computation could be made using a simple static-load design method, multiplied with an impact

factor similar to that used for impact loads on bridges, cranes, and so forth. The impact factor must, of course, be developed with dynamic methods or tests.

The reason for the increased bearing capacity of the soil when the shell method is used can easily be understood when it is kept in mind that the shell action in the soil creates horizontal components far in excess of those assumed to exist in the paper under discussion.

The shell theory outlined has the further great advantage that the carrying capacity of the soil can be shown as a function of the following items:

1. Shape, size, and strength of structure
2. Stiffness of the structure
3. Stiffness of the foundations of the structure
4. Depth, compaction, type, and geological history of the soil
5. Variation and duration of overpressure

As a result of this it can be shown that the dome and shell shaped underground structures induce far more carrying capacity in the overlaying soil than comparable flat-roofed structures.

It is impossible to know the exact sizes and types of weapons that can be used, the characteristics and duration of the blast wave might, therefore, vary widely. Accordingly, it is desirable to design underground shelters in such a way that they can withstand blast waves of various duration and distribution. This condition leads to generally stiffer structures with high buckling safety; however, to insure maximum load carrying participation of the soil above, the foundations should be designed for the proper spring constant. The spring constant for soils is not exactly known, but from laboratory experiments and field tests values may be selected that give reasonable results.

G. S. KOVACS,<sup>11</sup> A. M. ASCE and R. T. FRANKIAN,<sup>12</sup> A.M. ASCE.—This paper, that deals with a new field in which many engineering firms are engaged, could be enlarged upon by the authors in several aspects.

The impression is given that the structural element is assumed to have failed and then the forces that were developed in the soil are evaluated. The maximum pressures are developed for failure with a rigid structure. However, the yielding necessary to reduce the applied pressures to their minimum values may be less than that required for failure by the analysis. Therefore, the transient overpressure determined in the analysis may be greater than necessary for a proper analysis.

It should also be pointed out that there is a limiting depth of burial for any one structure, such that additional burial will not cause a further reduction in the overpressure felt by the structure. This limit is due to the formation of a ground arch, the height of which is a function of the size of the structure. In some cases, the height of the arch can be less than two times the width of a square structure.

Further justification would be desirable for the value of  $10^\circ$  given as the angle of internal friction for moist clays in Table 1. It appears that this was only necessary so that Eq. 21 would have significance. However, the use of an angle of internal friction for a saturated or moist clay can be very danger-

<sup>11</sup> Intermediate Engr., Bechtel Corp., Los Angeles, Calif.

<sup>12</sup> Project Engr., Bechtel Corp., Los Angeles, Calif.

ous for cases in which the clay would be loaded rapidly and insufficient time allowed for the excess pore-water pressure to be dissipated.

The meaning of the term used for ultimate resistance,  $P_m$ , is not entirely clear. It was presumed by the writers that this was the resistance to all loads (static plus dynamic). However, in the example problem the ultimate resistance was found insufficient to resist the static soil pressure prior to application of any dynamic load. Therefore, it must be assumed that the ultimate resistance ( $P_m$ ) is that required to withstand dynamic load alone and static forces are to be subtracted from the ultimate resistance as found by techniques of structural analysis.



ARCH DAM ANALYSIS WITH AN ELECTRIC ANALOG COMPUTER<sup>a</sup>

---

Discussion by Paul Baumann and Maurice L. Dickinson

---

PAUL BAUMANN,<sup>20</sup> F. ASCE.—The author has presented, in a simple and concise manner, the principles of electrical analogy applied to such statically complex structures as arch dams. The implication of this method of analysis, so far as the domain of the civil engineer is concerned, cannot escape attention as well as cogitation. Fortunately, the complicated as well as tedious analytical trial load method developed by civil engineers, with which the electrical analogy may successfully compete on an economic basis, can be greatly simplified by graphic statics so that respective competition would be less assured of success. One outstanding advantage must be conceded to the electrical analogy, namely the ease at which the effect of changes in assumptions as to loading by water, ice, earthquake, and temperature, or as to moduli of elasticity of dam and foundations, can be ascertained once the electrical "hookup" of the model has been completed.

Early in 1959 the writer was called upon by Leeds, Hill, and Jewett, Consulting Engineers in Los Angeles, California to participate in deliberations on the electrical analysis of the Blue Ridge arch dam in Arizona, that was described by the author. The wealth of information on some thirty-six different "cases," that is to say different assumptions and modifications, produced during the ten days the analog computer was occupied, was astounding. To accomplish the equivalent by the analytical trial-load method would require many times that length of time and would certainly exceed the actual cost of the electrical method of analysis that, it is understood, amounted to some \$25,000. Of course, in civil engineering practice the design of a dam of this size would not be subjected to any such elaborate variations in assumptions of loading, elastic properties, and structural details. Indeed, it is not so very long ago that much higher arch dams were designed by the "cylinder formula" based on a stress of perhaps 300 psi in a rigid arch barrel. Although these dams still stand, such design procedure must now be considered obsolete.

The author refers to tests on scale models of arch dams in Portugal that have gained due recognition by the engineering profession. Through his connection with Taiwan Power Company, as a member of its board of consultants, the writer has recently been apprised of the results of model tests conducted by the Société d'Équipement Industriel et de Laboratoires (SEIL) in Asnières, France on a high (760 ft ±) arch dam, known as Tachien Dam. Its design was prepared under contract by the engineering firm of Coyne and Bellier in Paris, France, who in turn arranged the model testing with SEIL. In studying the procedure used, it becomes at once apparent that not only does it resemble

---

<sup>a</sup> August 1960, by Richard H. Mac Neal (Proc. paper 2578).

<sup>20</sup> Cons. Engr., Sierra Madre, Calif.

that used at the Stevenson Creek dam, described by the author, but also that it has, at least in principle, much in common with the electrical "model" testing.

*Comparison Between Scale Model and Electrical Analysis.*—The scale factors used by SEIL were as follows:

$$\text{Scale of model, } S = \frac{(\text{Prototype})}{(\text{Model})} = 400$$

$$\text{Scale of loads, } T = \frac{(\text{Water})}{(\text{Mercury})} = 1/13.6$$

$$\text{Scale of stresses, } U = S \times T \frac{(\text{Prototype})}{(\text{Model})} = 29.4 \dots \dots (15)$$

$$\text{Scale of deflections, } V = S^2 \times T \times \frac{E_m}{E_p} = 482.4 \dots \dots (16)$$

in which  $E_m$  is the Young's Modulus of the model and  $E_p$  refers to the Young's Modulus of the prototype.

The material used for the model, some 23 in. in height was a mixture of plaster of paris, diatomite, and water so proportioned as to closely approximate Poisson's ratio of concrete and to have a modulus of elasticity that made it possible to measure strains and deformations with ease. For this purpose, 16 three-directional strain gages and deflection measuring points were installed on both the upstream and downstream faces. The model foundations were cast of the same material as the model dam. This differs from usual prototype conditions in that rock in place is likely to be more flexible than concrete. The respective discrepancy is, however, on the side of safety as the crown stresses in an arch dam increase with the increase in rigidity of the bed rock relative to that of concrete.

The model was initially over-dimensioned relative to the design drawings and upstream and downstream faces were gradually trimmed down by means of a specially installed cutting machine until the final, most satisfactory shape was established. A certain flexibility in assumptions, although not to the same extent as that pertaining to the electrical model, was thereby attained.

Contrary to the electrical analysis, no attempt was made, in the French model tests, to include the effect of gravity (that is weight) nor that of temperature changes. Hence, these effects had to be superposed on the "weightless" model of uniform room temperature by subsequent computations.

The reason given for omitting a scale of weights that could easily have been included in the computations based on structural similitude, namely because of the uncertainty as to the effect of construction procedure on the vertical weight distribution, is not too convincing to the writer. This, because the same uncertainty would seem to affect subsequent computations. The writer has reasons to believe that during construction of an arch dam the gravitational forces for each block between contraction joints are vertical and downward, and that magnitude and direction of these forces remain substantially unchanged after grouting of the joints on completion of the dam.

In the electrical analysis the effects due to gravity and temperature were directly ascertained by ingenious simulation as modestly described by the author. On the other hand the scale model was tested as a complete shell, strictly corresponding to the prototype, rather than a combination of straight, rigid, horizontal arch chords and vertical beams connected by bending-



resisting hinges. This articulation of an arch dam will no doubt lead to increasing error in the analysis of its elastic behavior as the number of hinges and intermittent chords and beams is decreased. As an absurd extreme one could visualize a single hinge at the crown section with rigid chords or struts between it and the abutments.

The writer feels that the distribution of load points between rigid chords and beams of an arched shell is a potential weakness of the electrical analysis that would be more or less pronounced depending on the number of load points and intermittent members. A comparison between tests on a scale model and an electrical model, each having the same number of load points and strain gages, respectively, and in precisely the same location, would be highly recommendable because it might furnish the answer to questions that could not be furnished otherwise.

MAURICE L. DICKINSON,<sup>21</sup> F. ASCE.—The significant and practical method for analyzing arch dams, presented in this paper is particularly useful for dams located in canyons with markedly unsymmetrical abutment outlines. For such dams analysis, by the trial load method programmed for a digital computer can become too complex for convenient use or practicable programming may require simplifying assumptions that could effect the validity of the results to an unknown, and possibly serious, degree.

As MacNeal points out, the operation of the computer is based on a mathematical analogy between the behavior of the electrical components of the model, and the behavior of an elastic framework representing the dam. The latter framework is sufficiently good representation of the dam for most design purposes. Although there is a mathematical correspondence between the electrical model and the elastic framework, the method described does not provide a solution of the generalized elastic equations. Thus, the method does not represent an end-point in the search for a complete solution to the problem of arch dam analysis.

One of the principal advantages of the electric analog is the fact that it essentially represents a reasonably valid elastic model of the dam. Once the electrical model has been set up, it permits easy step-by-step additions of the various forces and restraints, as well as rapid experimentation with varying boundary conditions. Consequently, the electric analog computer affords a convenient means of investigating and demonstrating the mechanics of arch dam behavior in a manner that is quite useful in evaluating the various effects and, consequently, in developing an economical and rational design.

On the other hand, in the practical use of the electric analog, the need to keep a considerable array of electrical components and equipment tied up until the analysis is complete requires careful planning of the study. It is not possible to refer back to the electric analog computer at a later date, as may readily be done with a digital computer, without incurring the cost of re-assembly of the electric analog. Thus, whereas some changes, such as the thickness of a particular arch ring, can be accommodated readily, changes in geometry of the structure must be planned in advance to avoid excessive standby time of the computer.

The facility with which various conditions of boundary restraint can be investigated by the electric analog leads to some important practical questions as to how such degrees of restraint can be built into an actual structure. The

<sup>21</sup> Chf. Hydr. Engr., Bechtel Corp., San Francisco, Calif.

design and performance of hinged and sliding joints in arch dam structures would be an interesting topic for further investigation.

Another subject that seems particularly adaptable to investigation by the electric analog computer is the secondary and more detailed analysis of special segregated portions of an arch structure, such as depressed spillway bays, large sluice openings, and the junction of the arch to a gravity thrust block.

RESTRAINED COLUMN<sup>a</sup>

Discussion by Donald S. Mansell

DONALD S. MANSELL.<sup>14</sup>—The author's paper is a logical development of the published work to which he makes reference, and in common with those authors he places severe limitations on the type of problem described. The writer believes that the waves  $y = \frac{M}{P} = f(x)$  can be used to solve a wider range of problems than those described in the paper under discussion.

A proof of the validity of the method used in deriving these waves, and in applying them, is given here, showing the general applicability of the results to compression members subject to any planar constraints at their ends including couples, shear and axial forces, and sway displacements.

Refer to the Fig. 9 and consider sagging moments to be positive.

$$y = y_1 - y_2 \dots\dots\dots (8)$$

$$F = -\frac{P}{L} (e_1 + e_2 - \Delta) \dots\dots\dots (9)$$

and

$$y_2 = e_1 + \frac{x}{L} (\Delta - e_1 - e_2) \dots\dots\dots (10)$$

That is,

$$M_a = -P (\Delta - y_1 - e_2) + F (L - x) \dots\dots\dots (11a)$$

$$M = +P (y_1 - y_2) = +P_y \dots\dots\dots (11b)$$

Now

$$\left. \begin{aligned} \frac{1}{R} &\approx -\frac{d^2 y_1}{dx^2}, \\ \frac{d^2 y_2}{dx^2} &= 0 \end{aligned} \right\} \dots\dots\dots (12)$$

Thus,

$$\frac{1}{R} = -\frac{d^2 (y_1 - y_2)}{dx^2} = -\frac{d^2 y}{dx^2} \dots\dots\dots (13)$$

However,

$$\frac{1}{R} = f_1(M) = f_1(Py) = f(y) \dots\dots\dots (14)$$

Thus,

$$\frac{d^2 y}{dx^2} + f(y) = 0 \dots\dots\dots (15)$$

<sup>a</sup> October 1960, by Morris, Ojalvo (Proc. paper 2615).

<sup>14</sup> Research Student, Univ. College of Swansea, Great Britain.

Thus, the deflected curve is represented by an exact differential equation if the thrust-line is used as abscissa, despite the presence of sway displacement. In other words the solution  $y = f(x)$  is independent of sway, that may be introduced into the problem simply as a rotation of axes.

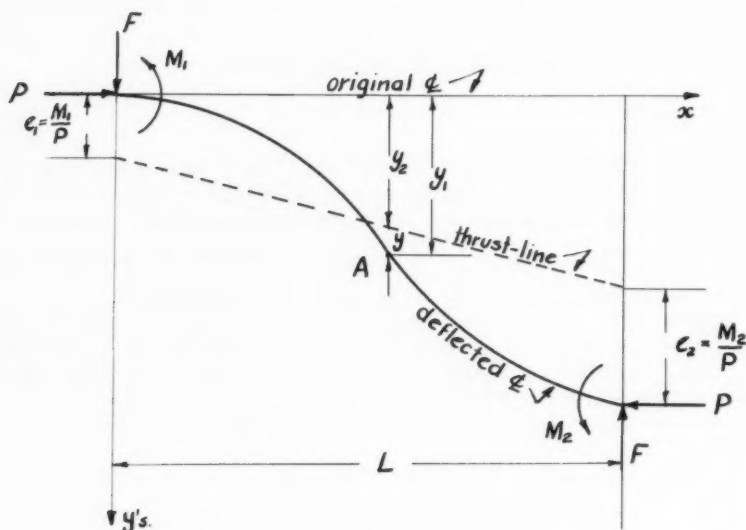


FIG. 9

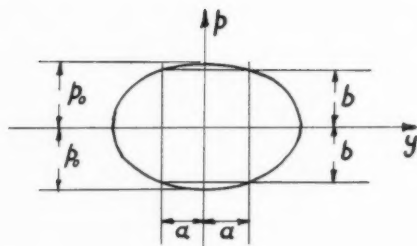


FIG. 10

It is possible to show that the general solution to Eq. 15 is a symmetric periodic wave if  $f(y)$  is single-valued, odd, and has positive slope. Providing unloading of yielded fibres does not occur, this condition is satisfactorily met by compression members composed of mild steel and some other structural materials. It is not necessary to solve the equation to demonstrate the form of the solution if the theory of limit cycles is used.

Integrating Eq. 15 once, we have

$$p \, dp = - f(y) \, dy, \dots\dots\dots (16)$$

in which

$$p = \frac{dy}{dx}$$

that is

$$\frac{p_y^2}{2} - \frac{p_o^2}{2} = - \int_0^y f(y) \, dy \dots\dots\dots (17)$$

Because  $f(y)$  is odd, and has positive slope,  $2 \int_0^y f(y) \, dy$  is always positive. Thus,

$$p_o^2 > 2 \int_0^y f(y) \, dy \dots\dots\dots (18)$$

For any value of  $y$ , for example,  $y = a$ ,

$$p_a^2 = p_o^2 - 2 \int_0^a f(y) \, dy = b^2 \dots\dots\dots (19)$$

Thus

$$p_a = \pm b \dots\dots\dots (20)$$

Because

$$\int_0^a f(y) \, dy = \int_0^{-a} f(y) \, dy \dots\dots\dots (21)$$

$$p_{-a} = \pm b \dots\dots\dots (22)$$

Therefore, the phase diagram  $p$  v.  $y$  is symmetrical about both  $p$  and  $y$  axes.

When  $y = 0$ ,

$$2 \int_0^y f(y) \, dy = 0, \dots\dots\dots (23)$$

thus

$$p_y^2 = p_o^2 \dots\dots\dots (24)$$

that is

$$p_o = p \, \max = - p \, \min. \dots\dots\dots (25)$$

Because  $\int_0^y f(y) \, dy$  is always positive, the equation

$$p_o^2 = 2 \int_0^y f(y) \, dy \dots\dots\dots (26)$$

always has two real roots. Thus,  $p_y$  has two zero points.

These conditions are uniquely determined because  $f(y)$  is single-valued, so the limit cycle is closed and symmetric, proving that  $y = f(x)$  is a symmetric periodic function.

The writer has programmed the integration of Eq. 15 for a digital computer. This included the computation of the increase in centroidal strain due to plasticity. In this way compatible values of axial thrust and deformation, with end couples and rotations, have been compiled for use in partially-plastic analysis of more complex structures; this includes triangulated trusses and structures subject to sway displacement.

The choice of boundary conditions is of some interest. Two of them are required for a complete solution of Eq. 15. The first, defining the particular

member of the family of waves may be the amplitude of either  $y$  or  $\frac{dy}{dx}$  or one of these functions at any known point, as mentioned by the author. The second depends on the problem considered (its symmetry and so on) and the proposed method of solution. The author selected the amplitude of  $\frac{dy}{dx}$  as the first boundary condition for reasons of convenience. However, a more cogent reason for this choice in a general solution may be seen from consideration of the integration process.

The elastic solution will serve as an illustration, although the conclusion is equally valid in the non-linear problem. The precise solution is

$$y = A \cos kx + B \sin kx \dots \dots \dots (27)$$

Choice of  $\left(\frac{dy}{dx}\right)_{\max} = \theta_0$  as boundary condition implies that  $A = 0$ . The numerical

integration process, being inexact, introduces small elements of  $A$  into the solution. However, because the cosine term decreases in this first quadrant the error is minimized.

But, if  $y_{\max}$  is chosen, the implication is that  $B = 0$ . Numerical error (such as rounding errors in a computer) then introduces elements of a sine term that increases throughout the integration whereas the correct cosine term decreases.

In the writer's experience with a digital computer integration from  $y_{\max}$  towards  $y = 0$  gave rise to errors in wavelength of the order of 3%, whereas, for the same step-length, integration in the opposite direction reduced the error to a very small fraction of 1%.

BEARING CAPACITY OF FLOATING ICE SHEETS<sup>a</sup>

---

Discussion by H. G. Hopkins  
(EMD, October, 1960)

---

H. G. HOPKINS.<sup>3</sup>—Some years ago the writer was concerned with problems of the stress analysis of aircraft runways, and hence was familiar with the work of the late H. M. Westergaard. During the period from 1952 to 1954, William Prager, F. ASCE and the writer as well as others, collaborated in the development of theories of plastic deformations in plates under transverse loads. The present approach, made on the basis of plasticity theory to problems of the bearing capacity of floating ice sheets, is most welcome. However, because of the writer's lack of familiarity with the more physical and practical engineering aspects of the situations involved, he is not in a position to comment extensively on the paper. A particularly important question that should be raised concerns the degree of realism in approximating the mechanical behavior of ice by that of a rigid, perfectly-plastic material. Under certain conditions, such a representation of mechanical behavior was known to be a useful one for mild steel, a highly ductile material. The same kind of approach had been proposed by K. W. Johansen for reinforced concrete; and now the author has proposed this approach for ice. In the development of the solutions of specific problems, it was of course necessary to choose a definite yield criterion, and here, for reasons of mathematical simplicity, that of Tresca had been taken. It would be valuable to undertake experimental studies of the yield strength of sheets of ice under combined loading conditions to determine the yield function as expressed in terms of principal bending moments. If it was shown to be sufficiently realistic, there could be theoretical advantages in working with Johansen's ('square') yield criterion in place of Tresca's.<sup>4</sup> In addition to laboratory experimental work, it was necessary to undertake field experimental work to provide adequate substantiation of any new theoretical approaches to such complex problems as those with which the author was here concerned.

---

<sup>a</sup> October, 1960 by G. G. Meyerhof (Proc. paper 2627).

<sup>3</sup> Armament Research and Development Establishment, Ft. Halstead, Sevenoaks, Kent, England.

<sup>4</sup> "Dynamic plastic deformations of simply-supported square plates," by A. D. Cox and L. W. Morland, *Journal of Mech. Phys. Solids*, 7, 1959, pp. 229-241.







# AMERICAN SOCIETY OF CIVIL ENGINEERS

OFFICE OF THE SOCIETY

## OFFICERS

President

CHARLES E. MCGEE

Vice-President

WILLIAM F. MANN

## MEMBERS

Executive Secretary

WILLIAM H. WISE

Assistant Secretary

WILLIAM F. MANN

Treasurer

WILLIAM F. MANN

## PROCEEDINGS OF THE SOCIETY

Editor

WILLIAM F. MANN

Editor

WILLIAM F. MANN

## PUBLICATIONS

Transactions

Proceedings

Journal

Report

Address

Publication

